CHEMICAL REVIEWS

REVIEW

pubs.acs.org/CR

Update 1 of: Computational Modeling Approaches to Structure−Function Analysis of G Protein-Coupled Receptors

Francesca Fanelli*,† and Pier G. De Benedetti‡

†Dulbecco Telethon Institute and ‡Department of Chemistry, University of Modena and Reggio Emilia, via Campi 183, 41125 Modena, Italy

This is a *Chemical Reviews* Perennial Review. The root paper of this title was published in *Chem. Rev.*, **2005**, *105*(9), 3297−3351, DOI: 10.1021/cr000095n; Published August 25, 2005. Updates to the text appear in red type.

CONTENTS

Received: December 17, 2010
Published: December 14, 2011

1. INTRODUCTION

Any aspect of cell activity is regulated by extracellular signals that are recognized, decoded, and transduced inside the cell via different classes of plasma membrane receptors.[1−3] G protein-coupled receptors (GPCRs) constitute the largest family of signal transduction membrane proteins, which mediate responses of a variety of bioactive molecules, including biogenic amines, amino acids, peptides, lipids, nucleotides, and proteins (reviewed in refs 1,4−7). As a result, GPCRs play a crucial role in many essential physiological processes as diverse as neurotransmission, cellular metabolism, secretion, cell growth, immune defense, and differentiation (reviewed in refs 1 and 4−7). They have also recently emerged as involved in tumor growth and metastasis as well as in the pathology of the Alzheimer's disease.[8−10] Not surprisingly, GPCRs are the most privileged targets for the drugs currently used in clinics and for the wealth of drug candidates that high throughput methods promise to deliver in the immediate future. This reflects not only the broadness of potential applications in all therapeutic fields but also the fact that GPCRs are by far the easiest targets that can be obtained through the synthesis of small organic molecules. In fact, they are naturally built to recognize a single structure among the widest variety of extracellular chemicals, and unlike many enzymes, they are exposed and reachable on the cell surface (reviewed in refs 1, 4−7, and 11).

Although varying considerably in molecular sizes, any GPCR polypeptide sequence contains seven hydrophobic α-helices that span the lipid bilayer and dictate the typical architecture of the macromolecule: seven transmembrane (TM) domains bundled up to form a polar internal tunnel and expose the N-terminus and three interconnecting loops, to the exterior, and the C-terminus with a matching number of loops, to the interior of the cell. This structural information, initially based on low resolution electron diffraction studies and on predictions from bioinformatics and molecular modeling,[12−15] was confirmed in June 2000 by the resolution of the ground-breaking crystal structure of bovine rhodopsin.[16] In many cases, ligands bind within the three-dimensional (3D) cavity of the TM bundle and form multiple connections with amino acid residues located in different domains. There is plenty of variation, however. In some cases the binding site is entirely located on a large and highly structured amino-terminal domain, as for glutamate[17] or glycoprotein hormone receptors (GPHR)[18] or the members of the secretin family (Reviewed in ref 19), or it involves both extracellular loops and residues in the transmembrane core, as often observed for neuropeptide receptors (reviewed in refs 1 and 4−7).

According to sequence analyses, GPCRs have been clustered in a number of families/classes.[4,20−23] The different classification systems include the A to F system,[23] the 1 to 5 system,[4] and the GRAFS system.[21] Thus, A (named 1 or rhodopsin in the 1 to 5 or the GRAFS system, respectively) is the rhodopsin-like class/family; B (or 2 or secretin) is the secretin-like class/family; C (3 or glutamate) is the metabotropic glutamate and pheromone class/family; D (or 4) is the fungal pheromone class/family;[24] E is the cAMP receptor class/family; and F (or 5 or frizzled) is the frizzled/smoothened family.[4,21,23] Family A receptors, the topic of this review article, are by far the largest and the most studied. The overall homology among all family A receptors is low and restricted to a small number of highly conserved key residues distributed in each of the seven helices.[4,21,23]

All GPCRs also share a common molecular strategy of signal transduction, to which they owe their name. Agonist binding promotes allosteric interactions between the receptor and one or more members of the family of heterotrimeric guanidine triphosphate (GTP) exchanging proteins or G proteins. These are specialized GTPases that act as signal transducers and broadcast the signal to a host of intracellular effectors, either enzymes, such as adenilyl cyclase, cGMP phosphodiesterase, and phospholipases, or ion channels, such as potassium and voltage gated calcium channels.[25−27] Some ligands can affect the intrinsic dynamics of a receptor by activating distinct G protein-mediated signaling pathways, a feature defined as "functional selectivity" (reviewed in ref 28).

Direct observation that GPCRs, including rhodopsin and the δ opioid receptor, can couple to G protein even in their inactive states comes from plasmon-waveguide resonance (PWR) spectroscopy, thus providing support to the hypothesis that receptors and G proteins are "constitutively coupled" or precoupled.[29,30] Evidence of receptor-G protein precoupling is emerging on a number of systems.[31−34]

G proteins account for the majority of signals that GPCRs can evoke into the cell. However, a multitude of relatively recent data shows that the signaling pattern of GPCRs is more dynamical than what was originally believed. On many occasions, that reflects the enhanced knowledge on the network of intracellular signaling pathways, in which G proteins are implicated. Thus, each GPCR can generate a secondary "wave" of signal transduction that essentially depends on the type of G protein α-subunits that are activated and, typically, involves signaling pathways, which are primary targets of growth-factor and cytokine receptors.[35] In others cases, however, there are clear indications that GPCRs can generate signals bypassing G protein intervention.[36] Although the exact mechanisms are not entirely elucidated, it is becoming increasingly apparent that direct receptor-receptor interactions, leading to a dimeric or multimeric quaternary structure, play a role in G protein-independent signaling.[36−38] The signaling and trafficking properties of GPCRs are often highly malleable depending on the cellular context. Such fine-tuning of GPCR function can be attributed in many cases to GPCR-interacting proteins (GIPs) that are differentially expressed in distinct cell types (reviewed in refs 39,40). In some cases GIPs directly mediate receptor signaling, whereas in other cases they act mainly as scaffolds to modulate G protein-mediated signaling.

Cells have counter-regulatory mechanisms that attenuate signaling by activated GPCRs (reviewed in refs 1 and 41). These mechanisms include acute desensitization involving GPCR-specific protein kinases and arrestins (homologous desensitization) and second messenger-activated protein kinases, such as protein kinases A and C (heterologous desensitization) (reviewed in refs 1,41, and 42). A combination of resonance energy transfer (RET) methods indicated that GPCR receptor kinase 2 remains associated to the receptor/G protein complex for longer periods than anticipated.[43] GPCRs can continue signaling after internalization together with their agonists (reviewed in ref 44). Signaling from inside the cell is persistent and appears to trigger specific downstream effects, which depend on the receptor subcellular localization (reviewed in ref 44).

The classical idea that GPCRs function as monomeric entities has been unsettled by the emerging concept of GPCR dimerization (reviewed in refs 45−61). Recent findings have indicated not only that many GPCRs exist as homodimers and heterodimers but also that their oligomeric assembly could have important functional roles. Several studies have shown that dimerization occurs early after biosynthesis, suggesting that it has a primary role in receptor maturation (reviewed in refs 52, 55, and 60). For many proteins, oligomeric assembly has an important function in endoplasmic reticulum (ER) quality control because it masks specific retention signals or hydrophobic patches that would otherwise retain the proteins in ER.[62] G protein coupling, downstream signaling, and regulatory processes, such as internalization, have also been shown to be influenced by the dimeric nature of the receptors (reviewed in refs 52 and 54). The question whether dimerization influences ligand-induced activation/regulation of GPCRs still remains to be answered. In fact, some studies suggest that ligand binding can regulate the dimer by either promoting or inhibiting its formation, whereas many others conclude that homodimerization and heterodimerization are constitutive processes that are not modulated by ligand binding (reviewed in ref 52). In any case, the structural data available strongly suggest that at least some GPCRs can form dimers in the absence of ligand stimulation. A clear evidence, in this respect, comes from atomic force microscopy (AFM) measurements, which showed that rhodopsin and opsin form a constitutive dimer in dark-adaptive retinal membrane.[53,63] Recent studies demonstrate that one receptor molecule is sufficient to activate a G protein and bind arrestin, thus suggesting that receptor self-association plays a biological role at different stages of GPCR functional cycle (reviewed in ref 64). However, evidence of asymmetric activation of GPCR dimers would imply that the minimal functional unit is two receptors and one heterotrimeric G protein.[65,66] Recent studies have suggested that heterodimerization could affect agonist-promoted GPCR endocytosis, a well-characterized process classically involved in signal attenuation (reviewed in ref 52). In the case of adenosine/dopamine and somatostatin/opioid receptors, the cointernalization was also associated with a cross-desensitization of the signaling activities (reviewed in ref 52). GPCR heterodimers may have an important impact in drug discovery.[67−77] Emerging studies indeed provide evidence for tissue-specific and disease-specific receptor heteromerization (reviewed in ref 75). This suggests that heteromers represent novel drug targets for the identification of selective compounds with potentially fewer side-effects. Furthermore, GPCR dimers may provide the necessary targets to increase the breadth and depth of receptors available for therapeutic interventions (reviewed in ref 69). Differential pharmacology, function, and regulation of GPCR heterodimers and heterooligomers suggest means to selectively target GPCRs in different tissues. They also hint that the mechanism of function of several pharmacological agents might be different in vivo than anticipated from simple ligand-screening programs that rely on heterologous expression of a single GPCR (reviewed in ref 67).

Thus, regulated protein−protein interactions are key features of many aspects of GPCR function and there is now increasing evidence for GPCRs acting as part of multicomponent units comprising a variety of signaling and scaffolding molecules, organized in supramolecular signaling assemblies (signalosomes or transducisomes).[1,2,78]

Usually with native GPCRs, activation is initiated by agonist binding. However, GPCRs can achieve the active states independently of agonists; that is, they can become constitutively active.[79,80] It is now evident that a number of native GPCRs exhibit constitutive signaling activity, but the role of agonist-independent activity in normal physiology is not known (reviewed in refs 81,82). Constitutively active GPCRs also are invaluable tools to discover the signal transduction pathways of the hundreds of orphan GPCRs, which are potential targets of novel drugs (reviewed in ref 83). On the other hand, a number of constitutively active GPCR mutants have been found, which are involved in the pathogenesis of human disease (reviewed in refs 41 and 84−86). Given the large number of GPCRs encoded within the human genome, additional examples of this pathogen mechanism are likely to be uncovered. Furthermore, the spectrum of diseases caused by constitutively active GPCRs is expanding to include diseases caused by infectious agents (reviewed in ref 41). A more complete elucidation of the roles of constitutively active GPCRs in human disease and an understanding, at the molecular level, of how these pathogenic GPCRs could be inactivated may allow rational development of specific compounds as therapeutic agents. Diseases are caused not only by constitutively active mutations ("gain-of-function" mutations) but also by mutations of an endogenous GPCR, which cause the receptor to lose the ability to bind agonist or to signal ("loss of function" mutations). A number of pathologies have been, hence, found to be related to mutations of GPCRs.[41,84,87,88] Most of these pathologies are related to obvious clinical manifestations, such as blindness, X-linked diabetes insipidus, and hypo- or hyperthyroidism, precocious puberty, obesity, cancer, etc. Some undiscovered mutations, providing nonobvious phenotypes, are also likely to be responsible for pathologies such as psychiatric or neurological disorders. Some inherited mutations may never be detected because they are incompatible with life.

Despite the enormous biomedical relevance of GPCRs, high resolution structural information on their active and inactive states is still lacking. Since 2007, the only GPCR whose structure had been resolved with atomic detail was rhodopsin in its dark state.[16,89−92] The five-year period 2007−2011 was marked by significant advances in structure determination of family A GPCRs, as the crystal structures of the: (a) β_2- and β_1-adrenergic receptors (ARs) bound to inverse agonists, antagonists, and partial and full agonists,[93−102] (b) A_{2A} adenosine receptor ($A_{2A}R$) bound to antagonists and agonists,[103−105] (c) squid rhodopsin in the dark state,[106] (d) constitutively active opsin apoprotein (Ops*) both free[107] and in complex with the eleven-residue C-terminal peptide from transducin (GtCT),[108] (e) constitutively active E113Q rhodopsin mutant bound to both all-*trans*-retinal and the GtCT peptide,[109] (f) metarhodopsin-II

Table 1. X-ray Structures of Family A GPCRs

accession ID	resolution (Å)	release date	molecular system	ref
			(Rhod)opsin	
1F88	2.80	2000−08−04	bovine rhodopsin with 11-*cis*-retinal	16
1HZX	2.80	2001−07−04	bovine rhodopsin with 11-*cis*-retinal	89
1L9H	2.60	2002−05−15	bovine rhodopsin with 11-*cis*-retinal	90
1GZM	2.65	2003−11−20	bovine rhodopsin with 11-*cis*-retinal	91
1U19	2.20	2004−10−12	bovine rhodopsin with 11-*cis*-retinal	92
2HPY	2.80	2006−08−22	bovine lumirhodopsin with all-*trans*-retinal	114
2G87	2.60	2006−09−02	bovine bathorhodopsin with all-*trans*-retinal	115
2I35	3.80	2006−10−17	bovine rhodopsin with 11-*cis*-retinal	116
2I36	4.10	2006−10−17	bovine rhodopsin with 11-*cis*-retinal[a]	116
2I37	4.15	2006−10−17	bovine rhodopsin with all-*trans*-retinal[a]	116
2J4Y	3.40	2007−09−25	mutant bovine rhodopsin with 11-*cis*-retinal	117
2PED	2.95	2007−10−30	bovine rhodopsin with 9-*cis*-retinal	118
2ZIY	3.70	2008−05−06	squid rhodopsin with 11-*cis*-retinal	119
2Z73	2.50	2008−05−13	squid rhodopsin with 11-*cis*-retinal	106
3CAP	2.90	2008−06−24	bovine opsin	107
3C9L	2.65	2008−08−05	bovine rhodopsin with 11-*cis*-retinal	120
3C9M	3.40	2008−08−05	bovine rhodopsin with 11-*cis*-retinal	120
3DQB	3.20	2008−09−23	bovine opsin in complex with GtCT	108
3PXO	3.00	2011−03−09	bovine MII with all-*trans*-retinal	110
3PQR	2.85	2011−03−09	bovine MII in complex with GtCT	110
2X72	3.00	2011−03−16	constitutively active bovine rhodopsin mutant bound to GtCt	109
			Nonopsin GPCRs	
2RH1	2.40	2007−10−30	human β_2AR with the inverse agonist carazolol	94
2R4R	3.40	2007−11−06	human β_2AR with the inverse agonist carazolol[a]	93
2R4S	3.40	2007−11−06	human β_2AR with the inverse agonist carazolol[a]	93
3D4S	2.80	2008−06−17	human β_2AR with the inverse agonist timolol	96
3NY8	2.84	2010−08−11	human β_2AR with the inverse agonist ICI 118,551	97
3NY9	2.84	2010−08−11	human β_2AR with a novel inverse agonist	97
3NYA	3.16	2010−08−11	human β_2AR with the antagonist alprenolol	97
3PDS	3.50	2011−01−12	human β_2AR with an irreversible agonist	101
3P0G	3.50	2011−01−19	nanobody-stabilized active state of the β_2AR	99
3SN6	3.20	2011−07−20	human β_2AR in complex with heterotrimeric Gs	100
2VT4	2.70	2008−06−24	turkey β_1AR with the antagonist cyanopindolol	95
2Y00	2.50	2011−01−12	turkey β_1AR with the partial agonist dobutamine	102
2Y02	2.60	2011−01−12	turkey β_1AR with the agonist carmoterol	102
2Y03	2.85	2011−01−12	turkey β_1AR with the agonist isoprenaline	102
2Y04	3.05	2011−01−12	turkey β_1AR with the partial agonist salbutamol	102
2Y01	2.60	2011−03−30	turkey β_1AR with the partial agonist dobutamine	102
2YCW	3.00	2011−06−01	turkey β_1AR with the antagonist carazolol	98
2YCX	3.25	2011−06−01	turkey β_1AR with the antagonist cyanopindolol	98
2YCZ	3.65	2011−06−01	turkey β_1AR with the antagonist iodocyanopindolol	98
2YCY	3.15	2011−06−08	turkey β_1AR with the antagonist cyanopindolol	98
3EML	2.60	2008−10−14	human A_{2A}R with the antagonist ZM241385	103
3QAK	2.71	2001−03−09	human A_{2A}R with the agonist UKA	105
2YDO	3.00	2011−05−18	human A_{2A}R with the agonist adenosine	104
2YDV	2.60	2011−05−18	human A_{2A}R with the agonist NECA	104
3OE0	2.90	2010−10−27	human CXCR4 with the peptide antagonist CVX15	111
3OE6	3.20	2010−10−27	human CXCR4 with the small ligand antagonist IT1t	111
3OE8	3.10	2010−10−27	human CXCR4 with the small ligand antagonist IT1t	111
3OE9	3.10	2010−10−27	human CXCR4 with the small ligand antagonist IT1t	111
3ODU	2.50	2010−10−27	human CXCR4 with the small ligand antagonist IT1t	111
3PBL	2.89	2010−11−03	human D_3R with the antagonist eticlopride	112

dx.doi.org/10.1021/cr100437t |*Chem. Rev.* 2011, 111, PR438–PR535

Table 1. Continued

accession ID	resolution (Å)	release date	molecular system	ref
3RZE	3.10	2011−06−15	human H_1R with the antagonist doxamine	113

[a] The resolution in the active site was insufficient to determinechromophore or ligand coordinates.

(Meta-II, MII) in its free and GtCT-bound forms,[110] (g) CXCR4 chemokine receptor bound to small-molecule and cyclic-peptide antagonists,[111] (h) D3 dopamine receptor (D_3R) in complex with the antagonist eticlopride,[112] and (i) H1 histamine receptor (H_1R) in complex with the antagonist doxapin[113] were released (see Table 1 for a summary of all GPCR structures released so far). Such an extraordinary crowding of structural information on GPCRs represents an advance in our understanding of the structural features of the inactive and active states, providing also tools for improving structure-based GPCR drug discovery strategies.

Yet, too many questions on GPCR function. Some of these are the following: Which is the precise structural basis of ligand specificity for a particular receptor, and how can the basic seven-helical structure be tuned to bind such a large and chemically diverse spectrum of ligands? Which are the molecular determinants of "functional selectivity"? Which is the precise molecular mechanism of ligand-dependent and ligand-independent GPCR activation? Which are the architectures of the different supramolecular assemblies of GPCRs? Which is the role of receptor dimerization/oligomerization in GPCR function? How is ligand- and mutation-induced chemical information transferred within a molecular network of GPCRs? Which are the G protein contact sites on the receptor and which is the stoichiometry of the receptor-G protein complexes? Which is the atomic pathway of signal transduction from the ligand-binding side on the receptor to the nucleotide-binding side of the G protein? Which are the structural bases of G protein-independent signaling displayed by many GPCRs? How do GPCRs dimers/oligomers and intracellular proteins organize themselves into a functional unit?

Experimental data obtained on chemically complex biosystems, like GPCRs, often contain more information than we need for a specific answer to a well conjectured hypothesis. Sound chemical/molecular models and data analysis techniques can help with decoding and describing intriguing experimental data. The advent of information and computer technology, hence, allowed for an intriguing integration between computational modeling and in vitro experiments.

The present work is aimed at critically reviewing the results of computational experiments, which have attempted, over the last two decades, to gain insights into different aspects of family A GPCR function.

2. STRUCTURAL FEATURES OF RHODOPSIN: THE FOUNDER OF FAMILY A GPCRS

2.1. Structural Models of the Dark State of Vertebrate Rhodopsin

Despite a growing appreciation of functional analogies between visual and hormonal signaling systems in the early 1980s, the discovery of the close structural relationship between rhodopsin and the β_2AR, and of the existence of a larger "superfamily" of such receptors, came as a total surprise.[6] Rhodopsin, thus, became the founder of family A GPCRs, which includes also the β_2AR, and the best source of high resolution information on the homologous receptors. Therefore, we thought it right to summarize herein the insights gained so far into the structural features of active and inactive states of the photoreceptor. These pieces of information have been, indeed, widely used in computational modeling of the homologous GPCRs

Rhodopsin is involved in the molecular transformation of light energy into a neuronal signal transmitted to the secondary neurons of the retina and ultimately to the brain.[16,121,122] In the case of rhodopsin, the signal is made up of two components: the bound chromophore, which undergoes cis−trans photoisomerization, and the trigger of such photoisomerization, a photon.[16] It has been recently inferred that the covalent bond between the chromophore and the opsin apoprotein is required for transmitting structural changes from the photoisomerized agonist to the receptor and that the covalent bond forcibly keeps the low affinity agonist in the receptor, resulting in a more efficient G protein activation.[123]

The first highly resolved structure of bovine rhodopsin, deposited in the Protein Data Bank (PDB: http://www.rcsb.org/pdb/) under the identifier 1F88, showed all major structural features as predicted from years of biochemical, biophysical, and bioinformatics studies on wild type and mutated proteins.[16] To date, a number of crystal structures of bovine rhodopsin have been released, which correspond to different states in the photoactivation cascade (Table 1). These include: (a) rhodopsin in the dark state,[16,89−92,116,120] (b) rhodopsin containing the non-native chromophore 9-*cis*-retinylidene (isorhodopsin) in the dark state,[124] (c) two early-photointermediates,[114,115] (d) a thermostabilized mutant in the dark state,[117] (e) a photoactivated deprotonated intermediate,[116] (f) the Ops* apoprotein both in its free state[107] and in complex with GtCT,[108] (g) the constitutively active E113Q rhodopsin mutant bound to all-*trans*-retinal and the GtCT peptide,[109] and (h) MII both in its free and GtCT-bound forms.[110]

Bovine rhodopsin contains 348 amino acids and folds into seven TM helices, varying in length from 19 to 34 residues, and one cytoplasmic helix, H8 (the letter "H" stands for helix). The seven TM domains contain a mix of canonical α- and 3.10-helices, and they possess a large number of kinks, twists, and bends (Figures 1 and 2). Further refinements have not reduced the number of these conformational anomalies.[89,90,92] Such anomalies are also present in the rhodopsin structures successively released.

In the rhodopsin structure, H1 is 44 Å long, it is tilted from the membrane normal, and it contains a bend, mostly due to the presence of P53(1.48). (The numbering in parentheses follows the arbitrary scheme by Ballesteros and Weinstein;[125] according to this scheme, every amino acid identifier starts with the helix number, followed by the position relative to a reference residue among the most conserved amino acid in that helix. That reference residue is arbitrarily assigned the number 50). H2 is tilted from the membrane normal about the same as H1, and it deviates from an ideal helix around G89(2.56) and G90(2.57). H3 is the longest (48 Å), the most tilted, and the most buried helix, bent at G120(3.35) and G121(3.36) and at S127(3.42).[16]

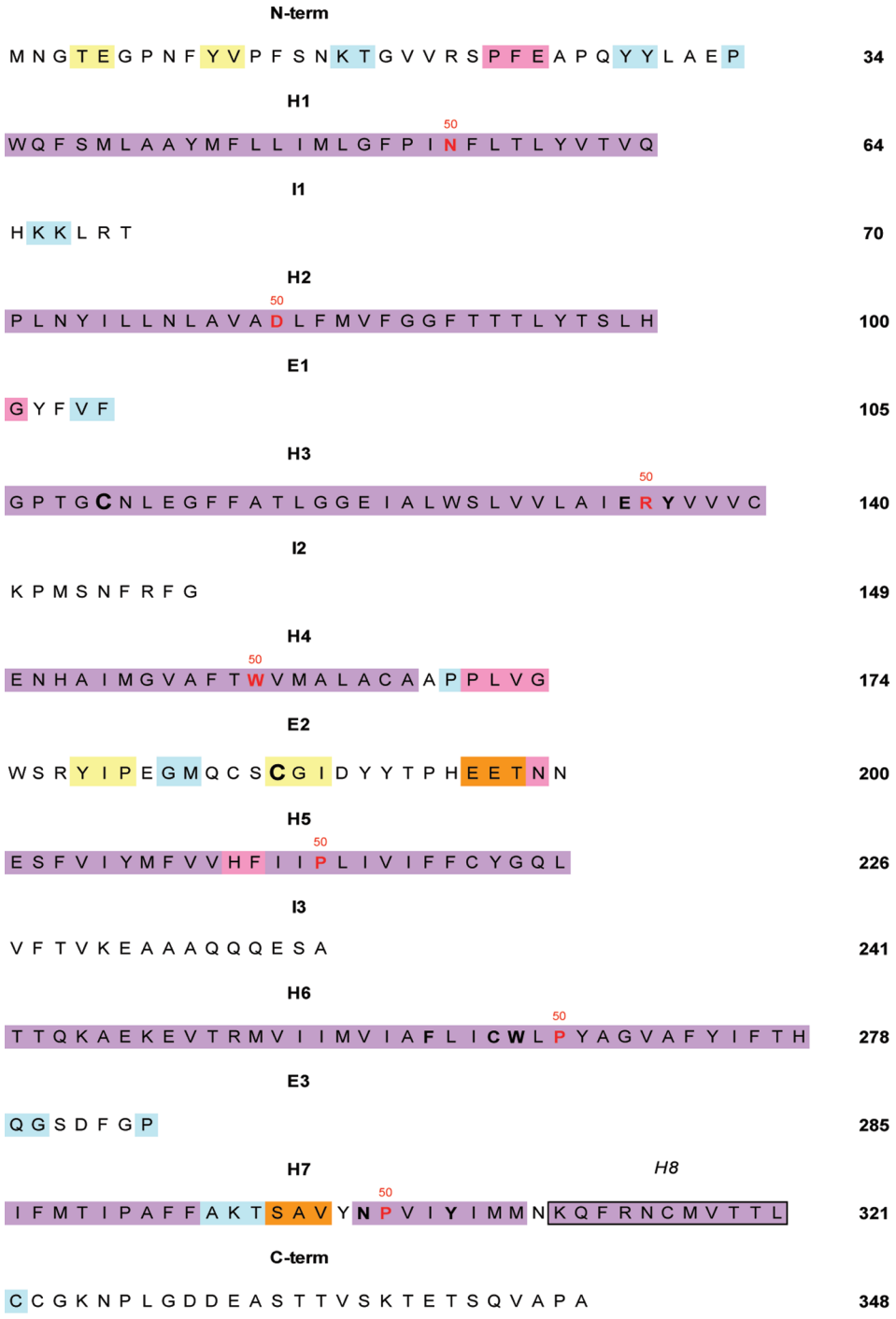

Figure 1. Amino acid sequence of bovine rhodopsin. Color highlights indicate the secondary structurecomputed on the latest structure (PDB code 1U19).[92] In detail, violet means canonical α-helices, and yellow stands for strand, whereas cyan, orange, and pink indicate, respectively, type 3-, 4-, and 5-turns. The most conserved amino acids in each helix are colored in red. These amino acids are at position 50 according to the arbitrary numbering scheme by Ballesteros and Weinstein.[125] Bold characters indicate the conserved members of the E/DRY, FxxCWxP, and NPxxY motifs in H3, H6, and H7, respectively. Boxed characters indicate the cytoplasmic H8.

The cytosolic extension of H3 is particularly important, because it contains the highly conserved E/DRY motif. In the rhodopsin structure, the arginine of this conserved motif, R135(3.50), is engaged in a double salt bridge with the adjacent glutamate, E134(3.49), and E247(6.30).[16] Both the E3.49−R3.50 and R3.50−E6.30 interactions are suggested to contribute to keep the photoreceptor and the homologous GPCRs in their inactive states, on the basis of the results of in vitro and computational studies[81,126−149] (see also the updated references in red). Currently, the R3.50−E6.30 salt bridge is widely termed "ionic lock". H4 is the shortest helix; it is almost perpendicular to the membrane and deviates from an ideal helix at its extracellular end, due to P170(4.59) and P171(4.60) (Figure 2). H5 is 35 Å long, it is tilted from the membrane normal, and it has two

dx.doi.org/10.1021/cr100437t |*Chem. Rev.* 2011, 111, PR438–PR535

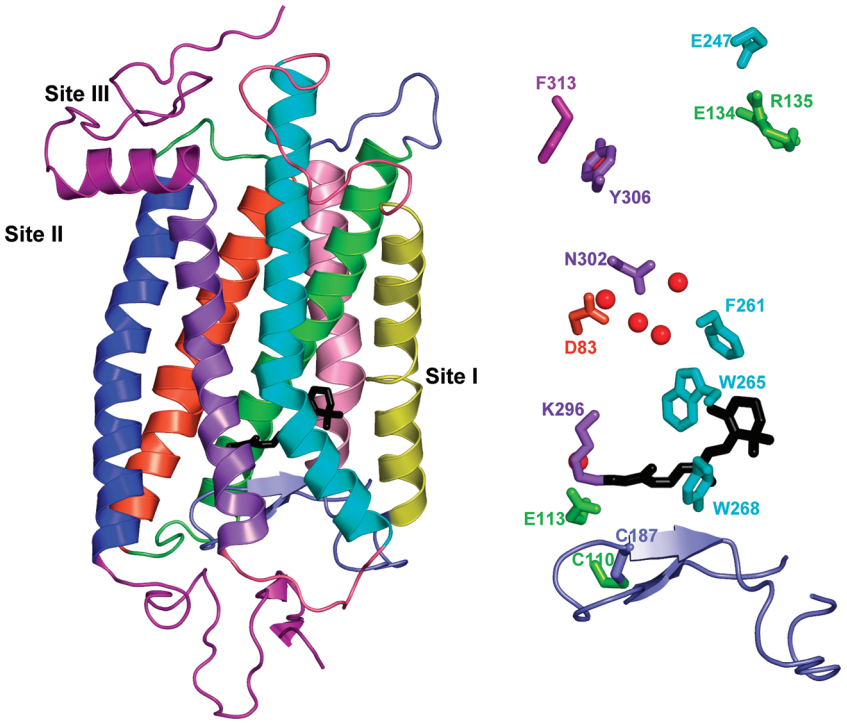

Figure 2. Side view, in a direction parallel to the membrane surface, of the rhodopsin structure encoded as 1U19.[92] On the left side, a cartoon representation of the whole structure is shown, including the 11-*cis*-retinal, represented by black sticks. On the right side, a stick representation of selected highly conserved amino acids in the seven-helix bundle and of C110(3.25) and of C187, which are engaged in a disulfide bridge, is shown. Red spheres represent the oxygen atoms of some of the water molecules resolved into the channel and close to the highly conserved amino acids in H2 and H7. A cartoon representation of E2 is also shown in the right panel. The intracellular side is at the top. H1, H2, H3, H4, H5, H6, and H7 are respectively colored in blue, orange, yellow−green, pink, yellow, cyan, and violet; the N- and C-termini, including H8, are in purple, I1 and E1 are in lime, I2 and E2 are in slate, and I3 and E3 are in salmon. Sites I, II, and III represent respectively the retinylidene binding pocket, the putative retinoid entrance site, and the putative retinoid exit site.[115] Drawings were done by means of the software PYMOL 0.97 (http://pymol.sourceforge.net/).

internal bends at residues F203(5.38) and H211(5.46) (Figure 2). H6 is the second longest helix. Its cytosolic half is almost perpendicular to the membrane plane, whereas its extracellular half is bent, because of P267(6.50), one of the most conserved residues in the rhodopsin family ofGPCRs.[13,14,150] H7 shows a considerable distortion and elongation in the region around the retinal attachment site K296(7.43) and contains two prolines, P291(7.38) and P303(7.50). The latter belongs to the highly conserved NPxxY motif (Figures 1 and 2). The tyrosine of this motif is involved in aromatic interactions with F313, a conserved residue in H8 (Figure 2). Recent experimental evidence suggest that the NPxxY$(x)_{5,6}$F and E/DRY motifs provide, in concert, a dual control of the activating structural changes in the photoreceptor.[151] In addition to these TM helices, another short helix in the cytoplasmic surface, termed H8, is located at the cytosolic end of H7 and it is almost perpendicular to the membrane normal (Figure 2).

The extracellular and intracellular regions of rhodopsin each consist of three interhelical loops (given the prefix E or I, for extracellular and intracellular, respectively) as well as of two tails (i.e., N-term and C-term, respectively).

A clear contrast exists concerning the packing of the intra- and extracellular domains; whereas the four extracellular domains associate significantly with each other, only a few interactions are observed among the cytoplasmic domains (Figure 2). The cytoplasmic loops are poorly determined in the structures. This is the region of the protein with the highest B-factors, and these loops are probably mobile in solution.[16] Residues missing from 1F88 are the stretches 236−240 in I3 and 331−333 in the C-term.

The extracellular domains of rhodopsin consist of a folded N-term, from residue 1 to 33, which overlays the rest of the loops (Figure 2). A β-hairpin in this domain interacts with a β-hairpin in E2, forming a β-sheet. E2 contains C187, which is involved in a disulfide bridge with C110(3.25) (Figure 2). Very recently, simulations of thermal unfolding of rhodopsin, by the recently developed floppy inclusion and rigid substructure topography (FIRST) method,[152] combined with fast mode analysis of rhodopsin, using the Gaussian network model,[153] identified the C110(3.25)−C187 disulfide bond and the retinal ligand binding pocket as part of a core region, which is assumed to be important for the formation and stability of folded rhodopsin.[154] This region was the most rigid one in rhodopsin. Experiments confirmed that 90% of the amino acids predicted by the FIRST method to be part of the core cause misfolding upon mutation.[154] The fundamental role of E2 in stabilizing the inactive state of the receptor has also been demonstrated for the complement factor 5a receptor (C5aR),[155] and it might serve a similar role in other GPCRs.[156]

The tight packing between the N-term and E2 and their secondary structure elements, as shown by the crystal structure, had not been predicted by bioinformatics approaches. Other unpredicted features were the irregularities in H1, H2, H3, and H5 and the short helix named H8 (Figure 2). The susceptibility of H7 to deviation from the canonical conformation had been instead already predicted prior to the release of the first crystalstructure.[157−159]

dx.doi.org/10.1021/cr100437t |*Chem. Rev.* 2011, 111, PR438–PR535

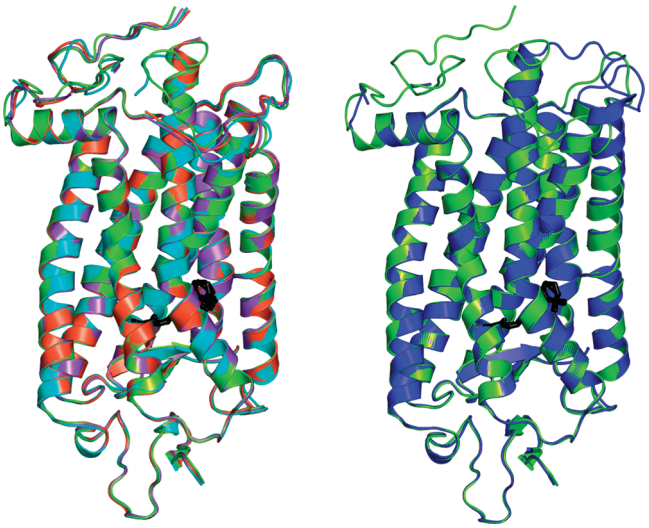

Figure 3. (left) Cartoons of the superimposed structures of 1U19 (yellow−green),[92] 1L9H (violet),[90] 1HZX (orange),[89] and 1F88 (cyan).[16] (right) Cartoons of the superimposed structures of 1U19 (yellow−green)[92] and 1GZM (blue).[91] The helix bundles are seen in a direction parallel to the membrane surface, with the intracellular side being at the top. Drawings were done by means of the software PYMOL 0.97 (http://pymol.sourceforge.net/).

Crystallographic refinement of the two molecules in the asymmetric unit generated the model of rhodopsin at 2.8 Å resolution, deposited in the PDB under the identifier 1HZX.[89] Differences between 1F88 and the refined 1HZX structures are located mainly in the cytosolic domains (Figure 3). The root-mean-square deviation (rmsd) between the Cα-atoms (i.e., Cα-rmsd) of 1F88 and 1HZX is equal to 1.05 Å. Major structural differences between 1F88 and 1HZX concern I3, which was rebuilt in 1HZX, lacking residues 236−240. In contrast, the extracellular loops and the chromophore were changed minimally. Furthermore, in 1HZX, additional amino acids in the C-tail (i.e., residues 328−330) are missing as compared to 1F88, whereas the amino acid stretch 334−348, which in 1F88 was filled with Ala residues, carries all the side chains in 1HZX.[89] Improved resolution was obtained concerning the successive structural models, 1L9H (2.6 Å resolution)[90] and 1U19 (2.2 Å).[92] 1L9H is changed to a much lesser extent when compared to 1HZX (i.e., the Cα-rmsd is 0.36 Å; Figure 3). No additional amino acids were added. The latest and most resolved rhodopsin structure, 1U19, completes the description of the protein backbone and is in general agreement with earlier diffraction studies.[16,89,90,92] The main differences between the 2.6 and 2.2 Å structural models essentially concern the completion of I3 and the C-term in the latter structure in addition to the consequent conformational differences in these cytosolic domains. The structures of the 11-*cis*-retinal chromophore and its binding site have been defined with greater precision than ever before in the 2.2 Å resolution structure, demonstrating a significant pretwist of the C11−C12 double bond, which is suggested to be critical for the function of rhodopsin.[92] The position of water molecules in 1L9H had already been defined with high precision.[90] In this respect, some of the highly conserved residues within family A GPCRs, including D83(2.50), N302(7.49), and Y306(7.53), are found to form binding sites for these water molecules (Figure 2). The latest structure by Okada and co-workers confirms the water molecule topography found in 1L9H but also adds new molecules, which leave no cavity in the protein.[92] When coupling radiolytic radical labeling with rapid H_2O^{18} solvent mixing, it was observed that no exchange of these structural waters with bulk solvent in either the ground state or the signaling states was capable of activation of the G protein.[160] Microsecond molecular dynamics (MD) simulations, however, predicted that substantial changes in internal hydratation play a key role in rhodopsin activation.[161]

The functional role of structural water molecules is being highlighted also for nonopsin GPCRs.[162−164]

Li et al. have resolved a rhodopsin structure at 2.65 Å (PDB code 1GZM),[91] by using untwinned native crystals in the space group *P*31, by molecular replacement from the 2.8 Å model solved in space group *P*41 (i.e., 1F88).[16] Like 1U19, 1GZM also resolves all the interhelical loops. The most significant main chain differences (i.e., Cα-rmsd above 1 Å) between 1GZM and 1U19 reside in I2, I3, and the C-terminal tail following H8. In detail, I2 has a similar "L-shape" in both structures but with a different orientation relative to the helix bundle. The difference may be described as a hinge movement about the junctions with the cytoplasmic ends of H3 and H4 (Figure 3). I3 and the cytoplasmic ends of H5 and H6 show the most striking difference between the two structures. In 1U19, H5 terminates at residue L226(5.61), following which the polypeptide chain re-enters the bilayer and is nonstructured between residues V227 and A241 (Figure 3, right). In contrast, in 1GZM, H5 extends to residue V230(5.65), and then the Cα-trace continues in a helixlike spiral path away from the membrane to Q236, where it changes direction to run parallel to the membrane and joins the cytoplasmic end of H6 at A241(6.24) (Figure 3, right). Differently from the case of 1U19, in 1GZM, the C-tail is disordered, except for a dipeptide suggested by the density in contact with I1.[91,92] Other differences between 1U19 and 1GZM concern the conformation of the retinal ring, which, in the latter, resembles the conformation held in the first structural model, 1F88.[16,91,92] Rhodopsin structure allowed for the design and structure determination of a mutant (PDB code 2J4Y), in which cysteine substitutions for N2 (in the N-term) and D282 (in E3) make a disulfide bridge.[117] The latter, while introducing only minor structural changes, increased the thermal stability of rhodopsin by 10 °C, probably by maintaining the β-sheet between N-term and E2 that shields the chromophore and contributes to the stability core of the protein.

2.2. Structural Models of Invertebtare Dark State Rhodopsin

Invertebrate phototransduction uses an inositol-1,4,5-trisphosphate signaling cascade in which photoactivated rhodopsin stimulates a Gq-type G protein. The same cascade is used by many GPCRs, indicating that invertebrate rhodopsin is a prototypical member. In 2008, the crystal structure of squid (*Todarodes pacificus*) rhodopsin bound to 11-*cis*-retinal, i.e., in its dark state, was released at 2.5 Å resolution (PDB code 2Z73) (Figure 4).[106] The structure is composed of seven TM helices (H1−H7) and two cytoplasmic helices (H8 and H9). The first eight helices show similar arrangements, irregularities, and kinks as compared to dark bovine rhodopsin (Figures 2 and 4). Also very similar is the β-hairpin structure of E2, which makes the gross of the retinal binding site. The disulfide bridge between C3.25 and C186 (corresponding to C187 in bovine rhodopsin) is conserved as well. Structural similarities between squid and

dx.doi.org/10.1021/cr100437t |*Chem. Rev.* 2011, 111, PR438–PR535

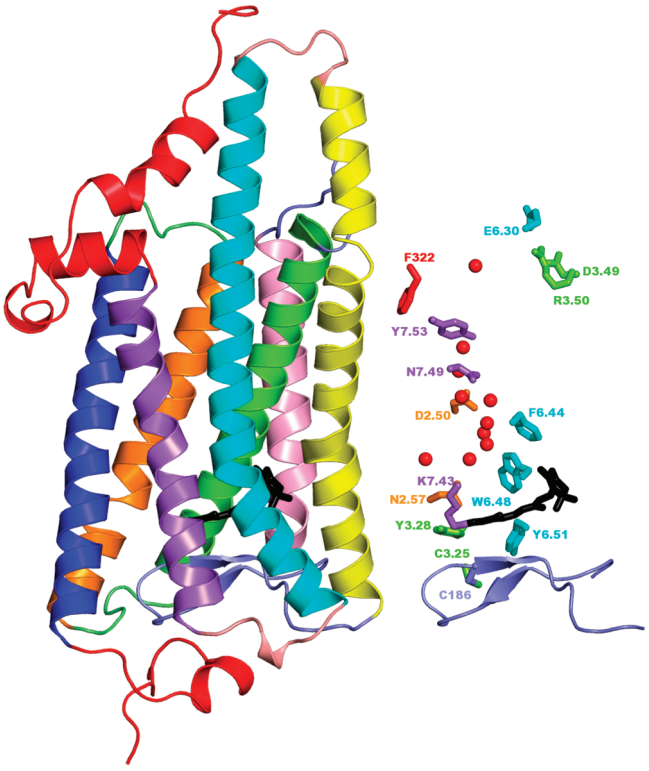

Figure 4. Crystal structure of squid rhodopsin. The receptor (PDB code 2Z73)[106] is seen in a direction parallel to the membrane surface, the cytosolic side being on top. On the left side, a cartoon representation of the whole structure is shown, including the 11-*cis*-retinal, represented by black sticks. On the right side, a stick representation of selected highly conserved amino acids in the seven-helix bundle and of C108(3.25) and of C186, which are engaged in a disulfide bridge, is shown. Red spheres represent the oxygen atoms of some of the water molecules resolved into the channel and close to the highly conserved amino acids in H2 and H7. A cartoon representation of E2 is also shown in the right panel. H1, H2, H3, H4, H5, H6, and H7 are, respectively, blue, orange, yellow−green, pink, yellow, cyan, and violet; the N- and C-termini, including H8, are red, I1 and E1 are lime, I2 and E2 are slate, and I3 and E3 are salmon.

bovine rhodopsin include also the interaction patterns of the highly conserved N1.50, D2.50, W4.50, F6.44, W6.48, the D/ER pair of the D/ERY motif, and N7.49 of the NPxxY motif (Figures 2 and 4). Major differences between the two structures include the 25 Å extensions of H5 and H6 into the cytosol. H5 is, indeed, divided into a membrane-embedded region and a medium-exposed region; owing to a flexible joint at Ser 226, the latter helical part has a large motional freedom. In contrast, H6 extends into the medium as a rigid spiral and its hydrophilic extension interacts with the C-terminal end of H9. Thus, a peculiar feature of squid rhodopsin structure, not shared with dark bovine rhodopsin, is the conformational rigidity of I3, which, together with the two cytoplasmic helices forms a rigid protrusion from the membrane surface (Figure 4). The squid rhodopsin structure determined at 3.7 Å resolution by another team (PDB code 2ZIY) holds 15 more amino acids in the C-tail, which make extensive interactions with I2, I3, H6, and H8.[119] This peculiar structure, which is not seen in bovine rhodopsin, is suggested to be crucial for the recognition of Gq-type G proteins.[106] Another unique feature of squid rhodopsin is a short 3_{10} helix formed in an interhelical loop between H8 and H9. This 3_{10} helix is dipped in the hydrophobic membrane region, whereas H8 is adhered to the hydrophilic surface of the lipid bilayer. Short 3_{10} helices are also found in the N-term and E3. The principal counterion of the protonated Schiff base (PSB) in the dark state is E180 in E2. Other remarkable peculiarities of squid rhodopsin structure are the H-bonding partners of the PSB, i.e., either the side chain carbonyl of N87(2.57) or the OH group of Y111(3.28), instead of E113(3.28) as in dark bovine rhodopsin (Figures 2 and 4). Furthermore, the conserved amino acids Y5.58 and Y7.53, are, respectively, directed toward R3.50 and far from F8.50, like in the crystal structure of Ops*.[107] This would be in line with the hypothesized precoupling of squid rhodopsin with GDP-bound heterotrimeric Gq.[106] Finally, squid rhodopsin possesses a large interhelical cavity that is filled by nine water molecules. Together with two highly conserved amino acids present the middle of this cavity (D80(2.50) and N311(7.49)), these water molecules form a long hydrogen-bonding network which extends from the retinal-binding pocket to a crevice of the cytoplasmic surface (Figure 4).[106] Quantum mechanical/molecular mechanical (QM/MM) calculations indicated that, although the presence of internal water molecules affect the structures near the Schiff base region, their impact on the absorption maximum is minimal.[165] Further QM/MM computations on bovine and squid rhodopsins compared the mechanism of molecular rearrangements, energy storage, and origin of the bathochromic shift accompanying the transformation of rhodopsin to bathorhodopsin in the two proteins.[166] It resulted that, following binding site relaxation during retinal isomerization, squid rhodopsin loses an amount of energy almost double the energy lost by bovine rhodopsin. Such a larger energy loss in squid rhodopsin was attributed to a flexible retinal binding site compared to the rigid retinal binding site of bovine rhodopsin.[166] Other comparisons between vertebrate and invertebrate rhodopsins relied also on comparative MD simulations, which suggested that differences in the H-bonding networks would cause differences in signal propagation from the retinal binding site to the G protein coupling regions.[167] Moreover, the electrostatic interactions between H6 and the cytosolic H9 would make squid rhodopsin less prone to undergoing structural changes upon photoactivation compared to bovine rhodopsin.[167]

2.3. Supramolecular Organization of Rhodopsin

Very recently, the presumed higher order oligomeric state in native membranes has been demonstrated for rhodopsin.[63,168] AFM experiments revealed the native arrangement of rhodopsin, which forms paracrystalline arrays of dimers in mouse disk membranes. Indeed, at higher magnification, almost all rhodopsin molecules are organized in rows of dimers, with a few monomers and some single rhodopsin pairs that have broken away from the rows.[63] These experimental evidence were challenged by Chabre and co-workers.[169] The criticisms of Chabre and co-workers were promptly addressed by the authors through additional experiments, which demonstrated also that, although activated rhodopsin monomer or dimers are capable of activating the G protein transducin, the activation process is much faster when rhodopsin exists as organized dimers.[170−173] Whether oligomerization of rhodopsin is a constitutive feature or an artifact is still in debate.[53,174,175]

On the basis of the AFM experiments, a semiempirical model of a higher order rhodopsin structure in native membranes was built (PDB code 1N3M, Figure 5).[176] Such an oligomeric model is made of repeats of the same monomeric unit. The latter was obtained by completing the structural model 1HZX,[89] by means of the MODELER program.[176,177] According to this supramolecular

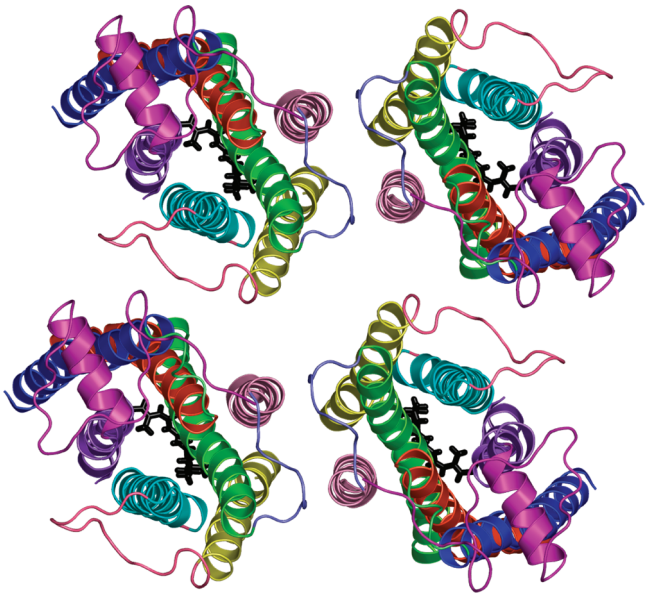

Figure 5. Cartoon representation of the semiempirical model of the rhodopsin tetramer 1N3M,[176] seen from the intracellular side in a direction perpendicular to the membrane surface. The extracellular loops are not shown. Color coding follows the same criteria as in Figure 2. Drawings were done by means of the software PYMOL 0.97 (http://pymol.sourceforge.net/).

model, two monomers of rhodopsin interact with each other at the extracellular (intradiscal) side (i.e., at E2, from both the monomers), at the cytoplasmic side (i.e., at I2 from both monomers), and also within H4 and H5 (Figure 5). On the basis of this model, the authors suggested that only the extracellular interactions involving E2 can transmit information about ligand binding from one receptor monomer to another because of the close proximity of E2 to the ligand binding pocket. Contacts between dimers involve I3 and both I1 and the C-tail (Figure 5). The latest structural model of rhodopsin, i.e., 1U19,[178] which differs from the monomer in 1N3M essentially for the conformation of the 228−244 amino acid stretch constituting I3, and for a portion of the C-tail (i.e., 323−335), can effectively substitute for the original monomers in 1N3M.[179] This model finds support in cysteine cross-linking experiments indicating that intermonomer interface in rhodopsin dimers would involve W175−W175 (in EL2) and Y206(5.41)−Y206(5.41) contacts.[180] Ciarkowski et al., very recently, proposed an alternative arrangement of the 1N3M monomers similarly compatible with the geometrical constraints from the AFM measurements[63] and judged by the authors more consistent with the mechanistic hypothesis of rhodopsin activation than the original organization in the 1N3M oligomer.[181] Rhodopsin crystals obtained under different experimental conditions showed further alternative dimeric architectures characterized by H1−H1 or H8−H8 contacts all compatible with the AFM images.[182] A similar architecture was also found for Ops*.[107]

Evidences for ordered alignment of squid rhodopsin in the membrane have also been derived from structure determinations by cryo-electron microscopy.[183] Consistent with previous findings from the projection map of squid rhodopsin, it appeared clear that the crystal lattice is formed by rows of rhodopsins with less protein−protein contacts between the rows. A different oligomerization model of rhodopsin arises from such studies, compared to the semiempirical model 1N3M.[176,183] In fact, docking the Cα-atoms of the structural model 1F88 into the 3D map of squid rhodopsin suggested that the contacts between adjacent rhodopsins along the lattice rows are made by H1, H8, H5, and I2. In detail, on the cytoplasmic side, positively charged amino acids in I2 or I3, of one monomer, would interact with negatively charged amino acids in the C-tail, of the other monomer.[183] Cross sections through the center of the membrane show contacts between H5 and H1, whereas interdimer contacts appear to be mediated by H4.[183]

Assuming that the dimeric/oligomeric state of rhodopsin is a constitutive feature of living cells, the functional role of oligomerization of the photoreceptor is still obscure. Functional characterization of rhodopsin monomers and dimers in detergents has recently demonstrated that monomeric rhodopsin can activate transducin, though the oligomeric form is moreactive.[171,173] This evidence seems to be in line with the idea that the receptor monomer holds the structural determinants for G protein activation and, in this respect, is the functional unit.[174,175] Recent advances from in vitro experiments strengthen this point, providing clear evidence not only that a monomeric rhodopsin is capable of full coupling to transducin[184,185] but also that only a single receptor in the nanodiscs containing two rhodopsins can interact with the G protein.[184]

Rhodopsin oligomerization may be essential for the ontogeny and/or desensitization of the photoreceptor and, hence, in the control of light signaling. Addressing these aspects may also have important implications in unraveling the molecular determinants of retinal degenerative diseases.

2.4. Insights into Rhodopsin Photobleaching from Spectroscopic Measurements and X-ray Crystallography

The high resolution structures of rhodopsin refer to the inactive state of the photoreceptor. Significant insights into the structural features of the active states were gained from spectroscopic and X-ray structure determinations (reviewed in refs 186−191).

Photochemical experiments allowed definition of the reaction coordinates of rhodopsinactivation.[192,193] Absorption of a photon provides rhodopsin with the energy to form the active state. Three phases of the activation process can be distinguished: (1) light-induced cis−trans isomerization of the retinal; (2) thermal relaxation of the retinal−protein complex; and (3) the late equilibria that are affected by the interaction of rhodopsin with the G protein (reviewed in refs 189,192, and 193).

2.4.1. Photoisomerization and Thermal Relaxation Stages. Photobleaching of rhodopsin involves different intermediates, identified by low temperature and time-resolved spectroscopic experiments (Figure 6).[193−197] Fourier transform infrared spectroscopy (FTIR) experiments suggest that D83(2.50) and E122(3.37) are both protonated in the dark rhodopsin state.[198] Following photon absorption and electronic excitation, fast isomerization of the chromophore leads to formation of bathorhodopsin (BATHO, 529 nm) (Figure 6) through photorhodopsin (PHOTO, 570 nm). This event, which utilizes two-thirds of the energy taken up by light absorption, would require 200 fs to occur. The reaction routes from rhodopsin to bathorhodopsin were investigated by the QM/MM theory.[199] In an elegant study, the coordinates mediating fast excited-state decay, the role of the electronic excited state in the isomerization, the structure of retinal in photorhodopsin, and the nature of the reaction coordinate leading to bathorhodopsin were inferred by femtosecond-stimulated Raman spectroscopy.[200]

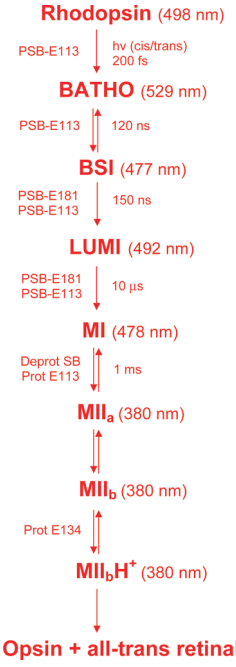

Figure 6. Rhodopsin photobleaching.

The latter produced time-resolved vibrational spectra of the molecular structures formed along the reaction coordinate.The findings from a recent study provide the most compelling evidence for the fact that rhodopsin reactivity is attributed to a conical intersection between the potential energy surfaces of the ground and excited electronic states, which enables the efficient and ultrafast conversion of photon energy into chemical energy.[201] BATHO is in equilibrium with the blue-shifted intermediate (BSI, 477 nm), which decays to lumirhodopsin (LUMI, 492 nm) in 150 ns. The BATHO to BSI transition only involves conformational changes of retinal, whereas the BATHO to LUMI transition is accompanied by a large motion of the β-ionone ring away from W265(6.48), which is in close proximity to the β-ionone ring in the dark and BATHO states. This is clearly shown by the X-ray crystallographic structures of BATHO and LUMI (PDB codes 2G87 and 2HPY, respectively), showing that the distorted all-*trans*-retinal in the BATHO structure relaxes by dislocation of the β-ionone ring in the LUMI intermediate along with displacements in the extracellular half of H3.[114,115] It has been also inferred that E181 (in E2) is charged in the BATHO state.[202] The LUMI undergoes a transition to metarhodopsin-I (META-I, MI, 478 nm) in 10 μs. A shift of the PSB from E113(3.28) to E181 (in E2) accompanies the transition from the dark to the MI state. It has been proposed that the switch is accomplished by transferring a proton from E113(3.28) to E181, through a structurally evolving H-bond network.[195] In the LUMI state, the PSB group has shifted away from E113(3.28) and the identity of a formal counterion has been lost because the negative charge becomes delocalized along the H-bond chain, which involves two water molecules and S186 in E2. Raman studies support the idea that LUMI is the transition state in the counterion-switching process, revealing that the H-bond of the Schiff base dramatically weakens in the BSI to LUMI transition before a more normal H-bond is formed with some residues in the LUMI to MI transition. The crystal structure of LUMI shows ~1 Å increase in distance between the nitrogen atom of the PSB and the carboxylate oxygen atoms of E113(3.28).[114] Finally, in the MI state, the Schiff base group has moved toward E181. Because the distance from the PSB to E181 in rhodopsin is only ~7 Å compared to ~3 Å for E113(3.28), only a modest conformational change that alters the spatial relationship between E2 and H3 is predicted to be required for the formation of the new salt bridge between E181 and the PSB in MI.[195] According to an alternative model, a change of the counterion from E113(3.28) to E181 during the transition from the dark state to MI would not require a protontransfer.[203] Both the negatively charged amino acids contribute to a complex counterion to the PSB, with E113(3.28) being the primary contributor in the dark and E181 being the predominant contributor in MI due to the rearrangement of the H-bonded network and of the PSB. E113(3.28) probably participates in such a complex counterion still in MI because it is the acceptor of the Schiff base proton in the transition to MII.[203] Very recently, density map of a photostationary state highly enriched in MI, to a resolution of 5.5 Å in the membrane plane, has been determined by electron crystallography.[204] The map shows density for H8, the cytoplasmic loops, the extracellular domains, all tryptophan residues, an ordered cholesterol molecule, and the β-ionone ring. Comparison of this map with the X-ray structures of the ground state reveals that MI formation does not involve large rigid-body helix movements, but there is a rearrangement close to the bend of H6, at the level of the retinal chromophore. This evidence suggests that there is no gradual buildup of the large conformational change known to accompany formation of MII, the signaling state capable of activating the G protein.[204] These results provide evidence for the first time that rhodopsin remains in a conformation similar to that of the ground state until late in the photobleaching process, the gross helix movements, and the conformational changes occurring in the MI to MII transition.[204] A recent investigation using genetically encoded infrared probes in rhodopsin, however, suggests that significant helix arrangements already occur in the MI state.[205] Indeed, it was proposed that retinal isomerization frees W265(6.48) and weakens the H3−H5 interaction, resulting in small tilt/rotation of H5 and H6.

2.4.2. The Signaling Active States. The transition from MI to MII would, indeed, occur in 1 ms. Formation of MII is also linked to proton uptake from the cytoplasm. The reaction depends on and probably involves the protonation of E134(3.49), a member of the highly conserved E/DRY motif.[193,206,207] In the dark state, this residue forms a salt bridge with the adjacent R135(3.50). Protonation of E134(3.49), which requires the presence of transducin,[207] would destabilize the charge-reinforced H-bond between E134(3.49) and R135(3.50), releasing an important constraint of the inactive state. This hypothesis is supported by the findings that a mutation eliminating the negative charge at E134(3.49) induces constitutive activity of theopsin.[126] Electron paramagnetic resonance (EPR) analyses of the cytoplasmic surface of the E134(3.49)Q constitutively active mutant showed a local conformational change around H3 and H7, whereas only a small change was seen in H6, which is suggested to undergo a dominant motion upon photoactivation.[208] These data suggest that the H6 motions induced by photoactivation are essentially triggered by the changes in the interaction pattern between the retinal and the opsin, following the cis−trans isomerization of the chromophore. Mutation of E134(3.49)

abolishes light-induced proton uptake but leaves the proton transfer to E113(3.28) unchanged,[209] suggesting that the two proton translocations can be decoupled, corresponding to the MII_a and MII_b states.[193,206] According to this model, the transition of MI to MII_a is accompanied by translocation of the Schiff base proton to E113(3.28).[193] In this stage, the *all-trans*-retinylidene group has the characteristics of a ligand agonist, in that it facilitates the MI−MIIa transition by elevation of the free energy (ΔG) of MI through a scaffold function for proton translocation.[210] Further insights into the MII_a formation from MI come from FTIR and UV−visible difference spectroscopy.[211] Besides the breakage of the ionic interaction between the Schiff base and E113(3.28), the MII_a substate appears characterized by structural changes in a conserved water-mediated hydrogen-bonded network involving N55(1.50), D83(2.50), and the NPxxY motif in H7.[211] These changes occur prior to other chromophore-induced changes that characterize MII_b formation, e.g., modifications in the H3-H5 network and outward movement of H6. It has been also demonstrated that the H-bonding network involving the conserved aspartate in H2 and the NPxxY motif are correlated with structural changes in the cytosolic H8.[212] MII_b formation requires also proton uptake from the cytoplasm, with a pH-dependent ΔG.[193] The positive enthalpy of MII formation indicates that molecular interactions built up in MI are lost upon transition to MII. To drive the conversion, the entropy and, thus, the overall disorder in the protein, must increase.[193] This observation would be consistent with the idea that formation of the active state is merely a release of constraints in the helix bundle, thus exposing cytoplasmic binding sites. Recent spectroscopic studies on rhodopsin in detergents allowed an extension of the MI↔MII_a↔MII_b to MI↔MII_a↔∓ MII_b↔MII_bH^+ equilibrium scheme, meaning that H6 motions, which cause the opening of a cytosolic crevice between H3 and H6 accompanying MII_b formation, culminate into the MII_bH^+ state following proton uptake from the cytosol.[213] The latter is likely due to a change in the pK_a of E134(3.49) of the E/DRY motif favored by H6 motions. In line with such a scheme, spectroscopic determinations in membranes confirmed that MII_b and MII_bH^+ share similar conformations although they differ in the protonation state of the conserved glutamate.[214] Protonation of E134(3.49) is essential for productive transducin recognition, which characterizes the MII_bH^+ state.[214,215] Using TM segments derived from H3 of bovine rhodopsin, it was shown that lipid−protein interactions play a key role in this cytosolic "proton switch".[215] Infrared and fluorescence spectroscopic pK_a determinations revealed that the E/DRY motif is an autonomous functional module coupling side chain neutralization to conformation and helix positioning.[215] Thus, the transitions associated with disruption of the PSB salt bridge and proton uptake from the cytosol are uncoupled under physiologic conditions. Disruption of the salt bridge between the PSB and its counterion is a structural prerequisite for the activating helix movements, whereas protonation of E134(3.49) is a thermodynamic requirement for shifting the conformational equilibrium to a completely active MII conformation.[214] It has been also inferred that proton uptake by E134(3.49) is not essential for binding to transducin but, rather, it is important for the release of GDP or the uptake of GTP.[216] Indeed, the MII state without proton uptake seems to bind transducin that has already released GDP (empty state).[216] Transient fluorescence spectroscopy determinations confirmed Schiff base deprotonation, structural change, and proton uptake as the sequence of events in rhodopsin photoactivation.[217]

Solid-state ^2H NMR relaxation experiments on the dark, MI, and MII states of bovine rhodopsin inferred a multiscale activation mechanism with a complex energy landscape, whereby the photonic energy is directed against E2 by the C13-methyl group, and toward H3 and H5 by the C5-methyl of the β-ionone ring.[218,219] Changes in retinal structure and dynamics would initiate activating fluctuations of H5 and H6 in the MI↔MII equilibrium of rhodopsin. The study suggests that the visual response is yelded by an ensemble of light-activated substates, which are the result of the entropy gain produced by photolysis of the inhibitory retinal lock.

2.4.3. MII Deactivation Process and the High Resolution Crystal Structure of Ops*. Initial deactivation of MII begins with the interaction of active rhodopsin with its receptor kinase, phosphorylation of the receptor, and a tight binding of arrestin to the still activated phosphorylated form of the receptor.[220,221] Full deactivation occurs when rhodopsin is regenerated. This requires the hydrolysis of the *all-trans*-retinylidene linkage and release of *all-trans*-retinal from the active site.[222,223] Critical steps include the nucleophilic the attack of water on the retinylidene bond within the hydrophobic binding site of rhodopsin and the diffusion of the hydrolyzed chromophore out of the binding pocket. Formation of opsin accompanies a significant increase in intrinsic tryptophan fluorescence after release of *all-trans*-retinal from the active site.[222,223] The retinal remains associated with opsin membranes and is converted by endogenous NADPH-dependent retinol dehydrogenase (RDH, reviewed in ref 192) to *all-trans*-retinol without further change in the intrinsic protein fluorescence. The RDH activity is suggested to exert an influence on the stability of the complex between arrestin and phosphorylated Meta II. In addition, during the Meta II decay, a storage form of rhodopsin, metarhodopsin III (Meta III, MIII) is generated. The formation of MIII can be triggered by blue light absorption in MII, passing through the anti-syn isomerization form or "reverted-Meta" intermediate MIII, and the subsequent reprotonation of the Schiff base.[197,224] Recently, it has been inferred that, in addition to the retinylidene pocket (site I), there are two other retinoid binding sites within opsin (Figure 2). Site II, involved in the uptake signal, is an entrance site, while site III is the exit site that is occupied when retinal remains bound after its release from site I.[225] Support for a retinal-channeling mechanism comes from the crystal structure of rhodopsin, which unveiled two putative hydrophobic binding sites in the cytosolic domains, i.e., close to the C-terminal end of H8 (site II) and on the solvent-exposed surface of the C-tail (site III) (Figure 2). The storage form is suggested to be characterized by the photolyzed *all-trans*-retinal bound in the exit site (site III). In this state, the retinal does not quench intrinsic tryptophan fluorescence. Opsin eventually returns to the ground state via a transiently formed opsin−11-*cis*-retinal complex, which contains both retinal isomers bound to site II and site III. RDH has access to its retinal substrate while bound to the site III of opsin.[225]

The activity of ligand-free opsin is equal to 10^{-6} of the activity of the *all-trans*-retinal-bound active MII state.[193,226] However, the 11-*cis*-retinal-bound rhodopsin ground state exhibits an even lower level of activity against transducin (Gt), suggesting that the 11-*cis*-retinal acts as an inverse agonist and imposes further structural constraints. Besides interactions with the chromophore, numerous intramolecular interactions are found in the crystal structure, which stabilize the ground state, and most of these are mediated by highly conserved residues inGPCRs.[150]

Lower pH enhances opsin activity, likely due to protonation of E134(3.49).[108,189] The residual activity of opsin can be explained by an active conformation (Ops*) in pH-dependent equilibrium with inactive opsin (reviewed in ref 189). The free energy gap

dx.doi.org/10.1021/cr100437t |*Chem. Rev.* 2011, 111, PR438–PR535

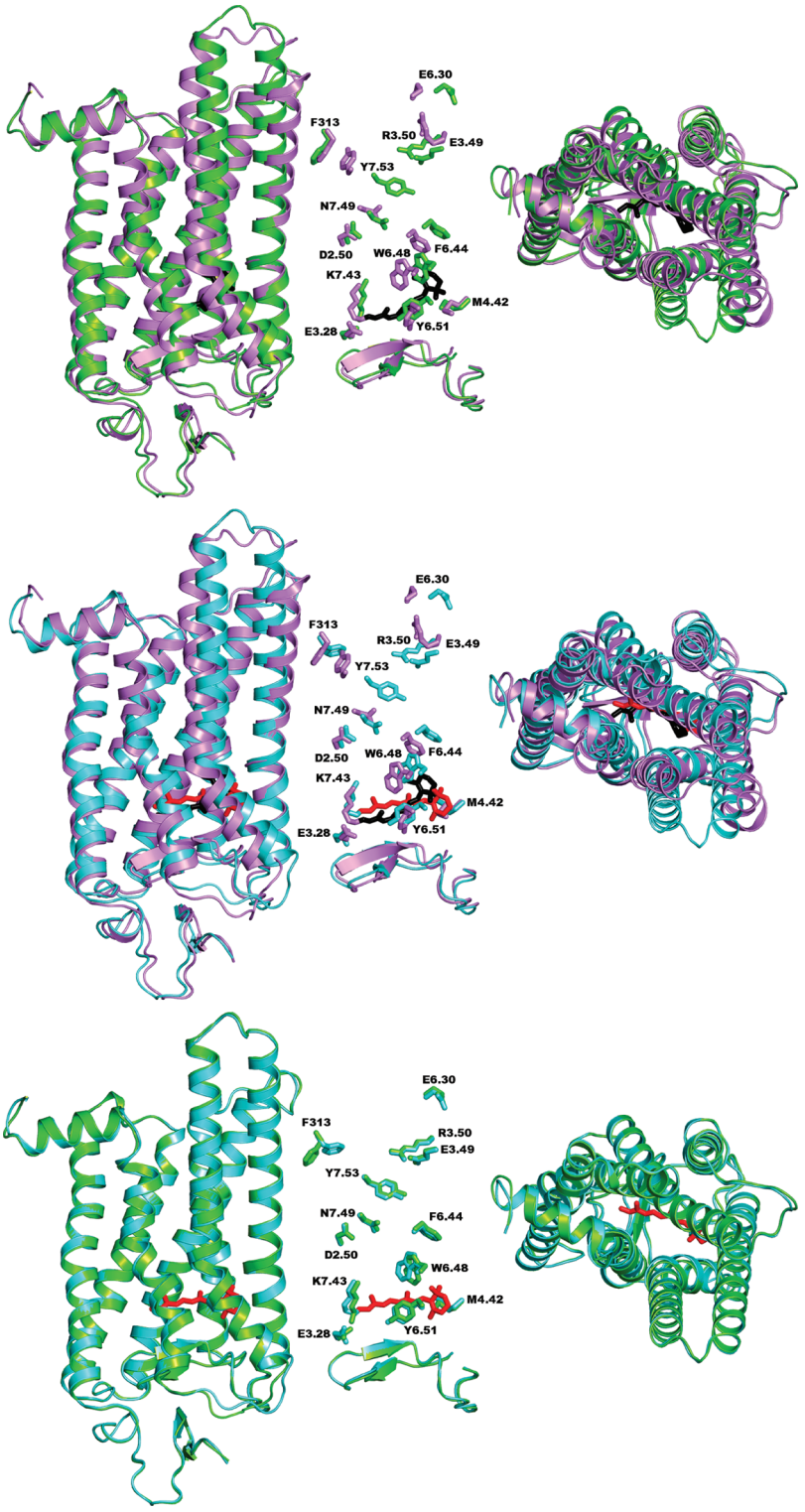

Figure 7. Structural comparisons of active and inactive (rhod)opsin structures. Cartoons of the superimposed structures of rhodopsin (PDB code 1GZM, violet),[91] Ops* (PDB code 3CAP, yellow−green),[107] and MII (PDB code 3PXO, aquamarine)[110] are shown. The helix bundles are seen both in a direction parallel to the membrane surface, with the intracellular side being at the top (left and middle panels) and from the cytosolic side in a direction perpendicular to the membrane surface (right panels). In the middle panels, the side chains of selected highly conserved and retinal binding site amino acids are shown; the E2 backbone is shown as well. 11-*cis*-Retinal and all-*trans*-retinal are shown as black and red sticks, respectively. The Cα-rmsd extended to all the equivalent atoms are, respectively, 2.38, 2.41, and 0.51 Å for the 1GZM−3CAP, 1GZM−3PXO, and 3CAP−3PXO structure pairs.

between MII and Ops* can be estimated as being approximately 5 kcal/mol, which can be assigned to the stabilizing effect of the all-trans-retinal agonist present in MII but not in Ops* (reviewed in ref 189).

dx.doi.org/10.1021/cr100437t |*Chem. Rev.* 2011, 111, PR438–PR535

Table 2

residues[a]	dark[b]	1U19[c]	light[d]	inter-Cα light[e]	2I37[f]	3CAP[g]	1LN6[h]	Gouldson[i]	1ov0[j]	1BOJ[k]
139−248	**12−14**	8.75	**23−25**	19.75	10.43	15.66	16.59	15.35	11.83	10.02
139−249	**15−20**	11.89	**15−20**	11.89	13.65	14.95	16.20	13.62	11.28	12.96
139−250	**15−20**	10.80	**12−14**	6.30	12.58	11.59	12.41	13.98	8.04	12.39
139−251	**12−14**	8.83	**23−25**	19.83	10.06	13.48	13.63	16.89	10.53	12.22
139−252	**15−20**	12.17	**23−25**	18.67	13.32	16.57	15.96	19.31	13.32	15.41

[a] Amino acids in bovine rhodopsin. [b] Distances (Å) between spin labels determined for dark rhodopsin (reviewed in ref 186). [c] Distances (Å) between the Cα-atoms measured in the crystal structure of dark rhodopsin (PDB code 1U19).[92] [d] Distances (Å) between spin labels determined light-activated rhodopsin (reviewed in ref 186). [e] Distances (Å) between the Cα-atoms estimated for light-activated rhodopsin, based upon the differences determined between spin labels and measured between the α-carbons in dark rhodopsin (1U19). [f] Distances (Å) between the Cα-atoms measured in the crystal structure of the photoactivated deprotonated intermediate of rhodopsin (PDB code 2I37).[116] [g] Distances (Å) between the Cα-atoms measured in the crystal structure of the constitutively active opsin (PDB code 3CAP).[107] [h] Distances (Å) between the Cα-atoms measured in the computational model 1LN6.[249,250] [i] Distances (Å) between the Cα-atoms measured in the computational model by Gouldson and co-workers.[251] [j] Distances (Å) between the Cα-atoms measured in the computational model 1OV0.[252] [k] Distances (Å) between the Cα-atoms measured in the computational model 1BOJ.[253]

The X-ray determination of the crystal structure of bovine Ops* (PDB code 3CAP) in 2008 represents a fundamental step in our understanding of ligand-independent GPCR activation.[107] Most of the structural features of dark bovine rhodopsin are retained in the Ops* structure (Figure 7). In detail, the "retinal plug", consisting in the four-stranded antiparallel β-sheet formed by the β-hairpins in the N-term and E2, is retained in Ops*. This strengthens the knowledge that these portions shield the chromophore from the extracellular environment both in the inactive and active states, thus participating in the stability core of the protein rather than in the exit/entrance route of retinal. In contrast to rhodopsin, the Ops* structure shows two openings in the retinal binding pocket: one between H1 and H7 (site A) and the other between the extracellular ends of H5 and H6 (site B).[108,227] These two openings hint at the different retinal entrance and exit routes which were proposed for retinal channeling in opsin.[225] A recent computational study by the same authors found a continuous channel that connects these two openings and comprises in its central part the retinal binding pocket. The authors propose two possible scenarios for the uptake of 11-*cis*- and the release of all-*trans*-retinal.[227] If the uptake gate of 11-*cis*-retinal is assigned to opening B, all-*trans*-retinal is likely to leave through the same gate. Alternatively, the uptake of 11-*cis*-retinal would occur through A and release of photolyzed all-trans-retinal through B.[227] The latter hypothesis finds support in the results of combined classical and random acceleration MD simulations.[228]

Within the stability core, the disulfide bridge between C110(3.25) and C187 in E2 is conserved as well. Also the H1−H4 portions undergo only marginal structural changes, compared to the dark state. On the same line, in both Ops* and rhodopsin, the P267(6.50)-induced kink divides H6 into two segments. Furthermore, H7 deviates most from a regular α-helical structure (as in rhodopsin) and shows an even more distinct S-shape. Other similarities between dark rhodopsin and Ops* include the length and orientation of H8.

Major structural differences between dark rhodopsin and Ops* essentially concern the cytosolic half of the H5−H7 portion. In particular, the N-terminal part of I3 adopts an α-helical structure (Figure 7). Therefore, H5 is 1.5−2.5 helical turns longer in Ops* than in rhodopsin, depending on the reference model. Furthermore, the cytoplasmic end of H5 is shifted by 2−3 Å toward H6. The whole H6 in Ops* is slightly displaced away from the center of the helix bundle (Figure 7). At the cytoplasmic end, H6 is tilted outward from the helix bundle by 6−7 Å with W265(6.48) as a pivot point. The cytoplasmic segment of H6 therefore comes closer to H5 so that it runs almost parallel to H5. The detachment of the cytosolic end of H6 from the cytosolic end of H3 in Ops* is smaller than predicted by earlier site-directed spin labeling (SDSL) experiments (Table 2, reviewed in ref 186) but consistent with recent high resolution distance mapping by double electron−electron resonance (DEER) spectroscopy.[229] These movements are associated with the breakage of both the salt bridge interactions found in dark rhodopsin between R135(3.50) and both D134(3.49) and E247(6.30) and the establishment of novel interactions by the triad of charged amino acids (Figure 8). In detail, (a) R135(3.50) engages interactions with the conserved Y223(5.58), tethering H5;(b) E247(6.30) flips over to interact with K231(5.66), thus stabilizing the H5 and H6 pair, and (c) E134(3.29) is positioned toward H2 and H4 and does not seem to undergo any specific interaction. It has been recently inferred that the establishment of the interaction between R135(3.50) and Y223(5.58) requires proton uptake to D134(3.49) to occur.[230]

The conformational change of R135(3.50), associated with the opening of a cytosolic crevice in between H3 and H6, is instrumental in maintaining the docking site for transducin, as shown by the crystallographic complex between Ops* and GtCT (PDB code 3DQB).[108] In line with our computational experiments on the constitutively active mutants of the GPHRs and the agonist-bound form of the thromboxane A_2 receptor (TXA_2R) (for review see refs 231−233), a major structural hallmark of the constitutive activity of Ops* is the ∼200 $Å^2$ increase in the solvent accessibility of selected amino acids in the neighborhood of R3.50, compared to the dark state (Figure 8). This evidence, together with the considerable similarity between unbound and Gt-bound structures of Ops*, indicate that Ops* has already all the structural requirements for transducin recognition and activation. The cytoplasmic end of H7 reorganizes in Ops* such that Y306(7.53) rotates to face into the helix bundle. It thereby blocks H6 from moving back toward H3 to adopt the conformation of rhodopsin. Solid-state NMR measurements of rhodopsin and MII investigating the intramolecular contacts around the E/DRY motif indicate that the interaction pattern of R3.50, Y5.58, and Y7.53 in MII are similar to those present in Ops* structure, supporting the idea that the latter is indeed an active state.[234]

Owing to Schiff base hydrolysis, MII is short-lived and difficult to crystallize. The Ops* crystals were recently soaked with all-*trans*-retinal, leading to the first crystal structure of the MII state, with Schiff base formation.[110] The structure, released both in its

dx.doi.org/10.1021/cr100437t |*Chem. Rev.* 2011, 111, PR438–PR535

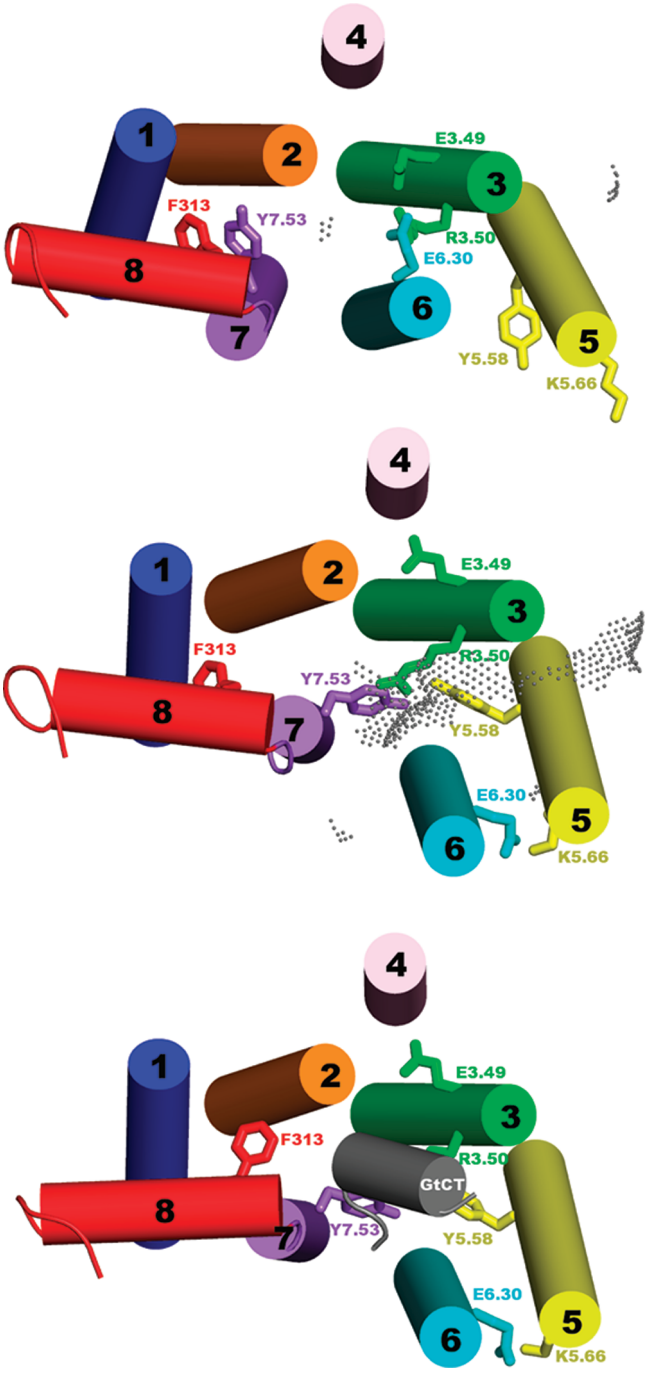

Figure 8. Cytosolic ends of dark rhodopsin (1GZM)[91] (top) as well as of Ops* in its free state (3CAP)[107] (center) and in complex with GtCT[108] (bottom). The structures are seen from the cytosolic side in a direction perpendicular to the membrane surface. Details of the interaction of selected conserved amino acids are shown in stick representation. Gray dots on dark rhodopsin and free Ops* are the solvent accessible surface computed over R135(3.50), V139(3.54), C140(3.55), L226(5.61) T229(5.64), V250(6.33), M253(6.36), V254(6.37), and M257(6.40). The solvent accessible surface area of such region in dark rhodopsin and free Ops* is 80 and 303 Å^2, respectively.

free state (PDB code 3PXO, 3.00 Å)[110] and in complex with the GtCT peptide (PDB code 3PQR, 2.85 Å),[110] is almost identical to the corresponding free and GtCT-bound states of Ops* (Figure 7). Ops* structure is also very similar to the crystal structure of the E113Q constitutively active rhodopsin mutant, resolved in complex with the GtCt peptide (PDB code 2X72, 3.00 Å).[109] The protein is in an active conformation that retains all-*trans*-retinal in the binding pocket after photoactivation and Schiff base hydrolisis. The Cα-rmsd between the 2X72 and 3DQB structures is 0.58 Å.

Collectively, the advances in structure determination of (rhod)opsins indicate that Ops* and MII, in spite of their differences in transducin-coupling efficiency, hold significant structural similarities. The crystal structure of the MII state would presumably represent the MII$_b$H$^+$ state.

2.5. Insights into Rhodopsin Activation from Cysteine Cross-Linking, SDSL, Scanning Accessibility, and NMR Determinations

Elegant cysteine cross-linking, SDSL, scanning accessibility, and NMR determinations on rhodopsin provided invaluable information on the structural rearrangements associated with MII formation. Indeed, the results of the experiments on the dark rhodopsin state were consistent with the rhodopsin structure, providing also a model for rhodopsin activation (see refs 186,189, and 229).

Cross-linking experiments aimed at inferring the structural changes in the retinal binding site, as induced by photoactivation, revealed a cross-link between retinal and A169(4.58) in the light-activated rhodopsin.[186,235] Since A169(4.58) in the crystal structure of rhodopsin faces outward from the helix bundle, such cross-linking is inconsistent with the retinal binding mode in the inactive state of rhodopsin. In fact, for the β-ionone ring of retinal to be linked to A169(4.58), the extracellular end of H3 should move away from the core of the helix bundle, and H4 and H7 should tilt or rotate to open a path between K296(7.43), which is covalently bound to retinal, and A169(4.58).[186,235] Insights into the configurational differences between dark and MII states in the retinal binding site come also from solid-state NMR determinations.[236−238] In detail, ^{13}C-labels on the retinal chromophore and specific ^{13}C-labels on tyrosine, glycine, serine, and threonine residues in the retinal binding site indicate that the essential aspects of the isomerization trajectory are a large rotation of the C20 methyl group toward E2, and a 4−5 Å translation of the retinal chromophore toward H5.[236] The observed shifts of the chromophore are predicted to trigger the motions of W265(6.48) accompanied by outward rotation of H6 using the conserved P267(6.50) as flexible hinge.[236] Changes in the interaction pattern of W265(6.48) upon rhodopsin activation are also indicated by changes in the chemical shifts of the ^{15}N-labeled tryptophan consistent with the indole nitrogens of W265(6.48) becoming less hydrogen bonded on going from dark rhodopsin to MII. NMR measurements also indicated breakages of the interhelical H-bonding interaction between E122(3.37) and H211(5.46) as a consequence of the establishment of intermolecular interactions with the β-ionone ring of the chromophore.[237] In contrast with the observations and conclusions of Patel et al., Spooner et al., on the basis of NMR determinations on ^{13}C-labeled C16 and C17 of retinal, concluded that the β-ionone ring becomes even more strongly restrained on activation.[238] Retaining the initial position on cis−trans isomerization, the chromophore ring would increase its steric interactions with the receptor, forcing the protein to adjust its structure around the ligand.[238]

NMR determinations also targeted the whole photoreceptor, providing the first evidence that activation of rhodopsin may involve differential dynamic properties of side chain versusback-bone atoms.[239] In fact, NMR studies of the α-^{15}N-lysine-labeled

receptor revealed large backbone motions in the inactive dark state. In contrast, indole side chain ^{15}N groups of tryptophans showed well resolved, equally intense NMR signals, suggesting restriction to a single specific conformation.[239] These results indicate that tryptophan side chains are more restricted in conformation than their backbone, suggesting that the indole side chain contacts, in part, contribute to restricting the conformation in a "locked" dark state, without fully restricting motional fluctuations in the overall molecule including the helix bundle itself.[239] Other high resolution information comes from solution and solid-state NMR spectroscopy of the intact mammalian photoreceptor rhodopsin in detergent micelles. These experiments suggest that the C-tail conformation observed in the crystal structure is no longer maintained upon phosphorylation, with the C-tail becoming disordered.[240]

A large number of intramolecular links, either cysteine disulfide bridges or Zn^{2+} chelated by substituted histidine side chains, were also engineered to connect the cytosolic ends of the helices, including H8. These cross-links were investigated in their ability to permit or inhibit activation (reviewed in ref 186). The observation that all the cross-links between H3 and H6 inhibit activation (dashed red lines in Figure 9) suggests that rhodopsin activation would require a change in the relative position of these two helices, most likely a separation of their cytoplasmic ends. In contrast, activation would require a change in the relative position of H3 and H5 without a significant separation. This was suggested by the findings that two inhibitory cross-links between these two helices were found close to activation permissive cross-links between the same helices (dashed green and red lines in Figure 9).[186] Cross-linking experiments also suggested that H3 might become less tilted upon activation, that is, more perpendicular to the plane of the membrane, causing its end to protrude more into the cytoplasm. Interestingly, one disulfide bond connecting residues 140(3.55) and 316 (in H8) was found only after photoactivation of rhodopsin (dashed yellow line in Figure 9).[241] This cross-link connected Cα-atoms that are 29 Å apart in the ground-state crystal structure, whereas the distance between Cα-atoms of disulfide-bonded cysteine residues is in the range 3.8−6.8 Å. One possibility is that light activation causes a significant conformational change that brings the two positions together.[186,241]

SDSL has been extensively used to explore the cytosolic domains of the photoreceptor.[186] This biophysical approach was used to assess the following changes induced by photoactivation: (a) changes in the hydrophobic/hydrophilic nature of the environment of the labeled amino acids, (b) changes in their solvent exposure, (c) changes in the distances between pairs of spin labels, and (d) increase in their mobility. Increases in the mobility of the targeted side chains were interpreted as increases in their solvent exposure. The estimated distances between the spin labels in dark rhodopsin and MII suggest that an increase in distance of more than 10 Å between the Cα-atoms of V139(3.54), on one hand, and those of K248(6.31) and T251(6.34), on the other one, would characterize the transition from dark to MII (Table 2).[186] Our conversion of interspin distances into inter-Cα-atom distances is based on the comparisons of the results of experimental determinations on dark rhodopsin with measurements on the crystal structure (Table 2). All together, the observed mobility changes suggest that activation opens a cleft on the cytoplasmic side of the helix bundle.[242−245] More specifically, the postulated rigid-body tilt or translation of H6, moving its cytoplasmic end out from the bundle, would

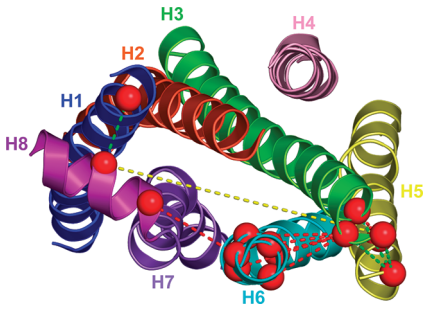

Figure 9. Cartoon representation of the seven-helix bundle and H8 of 1U19. The bundle is seen from the intracellular side in a direction perpendicular to the membrane surface. Red spheres indicate the α-carbons of the amino acids targeted by cysteine cross-linkingexperiments (reviewed in ref 186). Dashed red lines indicate inhibitory cross-links, and dashed green lines indicate cross-links compatible with activation, whereas the yellow dashed line indicates a cross-link that occurs only in light-activated rhodopsin (reviewed in ref 186). Drawings were done by means of the software PYMOL 0.97 (http://pymol.sourceforge.net/).

simultaneously increase exposure at the cytoplasmic end of H3 and decrease the exposure of some positions near the end of H5.[242−245] Mobility changes in the H1−I1−H2 region upon activation are relatively minor.[246] The results of SDSL determination in solution are qualitatively similar to SDSL determinations in phospholipid bilayer, the latter showing lower amplitude motions compared to the former.[247] Recently, DEER spectroscopy was used to determine distances and photoactivation-induced distance changes between pairs of nitroxide side chains introduced in helices at the cytoplasmic surface of rhodopsin, thus providing improved resolution into the helix movements associated with rhodopsin photoactivation.[229] For inactive rhodopsin, it was possible to find a globally minimized arrangement of nitroxide locations that simultaneously satisfies (a) the 1GZM crystal structure of dark rhodopsin, (b) the experimentally measured distance data, and (c) the known rotamers of the nitroxide side chain. A similar data analysis for activated rhodopsin yielded a new geometry consistent with a 5 Å outward movement of H6 and smaller movements involving H1, H7, and the C-terminal portion following H8.[229] Remarkably, the newly estimated outward movement of H6 is consistent with the Ops* structure, being smaller than estimated by earlier SDSL experiments (Table 2, reviewed in ref [186]), but larger than measured by comparing dark rhodopsin with the crystal structure of a photoactivated deprotonated intermediate of rhodopsin (PDB code 2I37, 4.15 Å).[116] The latter structure, indeed, shows no significant detachment of H6 from H3 compared to dark rhodopsin, as essentially marked by the distance between V139(3.54) and K248(6.31) (Table 2). This incongruence between the 2I37 structure and both SDSL and DEER determinations was interpreted as the crystal structure not corresponding to the functionally active conformation.[229] Collectively and considering also the structural features of Ops*, the outward displacement of H6 estimated from SDSL and DEER turns out to be a reliable hallmark of rhodopsin activation and not an artifact of the spectroscopic labeling technique.

SDSL has also been used to explore the role of the salt bridge between the protonated Schiff base at K296(7.43) and its counterion E113(3.28). In detail, molecular sensors were placed at selected positions in the cytosolic domains to monitor the structural changes in such domains triggered by the breakage of the salt bridge in the retinal binding site.[248] All together, the

dx.doi.org/10.1021/cr100437t |*Chem. Rev.* 2011, 111, PR438–PR535

results provide structural evidence that the salt bridge is a key constraint maintaining the resting state of the receptor and that disruption of the salt bridge is the cause, rather than a consequence, of the H6 motion that occurs upon activation.[248]

Further structural insights into the mechanism of rhodopsin photoactivation were gained from distance measurements using solid-state ^{13}C NMR spectroscopy between the retinal chromophore and the β2-strand in E2. These determinations showed that the loop is displaced from the retinal binding site upon activation and there is a rearrangement in the H-bonding networks that connect E2 with the extracellular ends of H4, H5, and H6.[254] NMR measurements further revealed that the structural changes in E2 are coupled to both motion of H5 and breaking of the "ionic lock" commonly thought to regulate activation. The displacement of E2 resulted not large because the H-bond involving E181 appeared to remain intact in MII. The authors interpreted the lack of E2 displacement in Ops* structure as the result of the absence of the retinal chromophore. Indeed, release of retinal from opsin was suggested to cause a rearrangement of the binding site residues and a shift back of E2 to its original position in dark rhodopsin.[254] In line with these results, a fragment complementation study indicated that E2 "mechanically" drives the conformational change of rhodopsin.[255] In spite of these observations, the crystal structures of (rhod)opsin released so far suggest that rhodopsin activation would not involve significant movements of E2.

2.6. Patchwork of Current Information on Rhodopsin Photoactivation

Up to MI, a state that is reached within a few microseconds, the activation remains near the retinal binding pocket and only minor structural changes occur in the more distant parts of the protein (reviewed in ref 189). With the formation of MI, the activation path reaches the level of the Meta intermediates (reviewed in ref 189). The spectrally identical MII substates MII_a, MII_b, and MII_bH^+ sequentially develop from one another until an equilibrium between all the states is reached after a few milliseconds. At physiological pH and temperature, MII_bH^+ accumulates in the reaction sequence (reviewed in ref 189). In the course of the Meta conversions, deprotonation of the retinal Schiff base and protonation of E113(3.28) of its complex counterion including E181 (step 1), motion of H6 (step 2), and proton uptake to E134(3.49) of the E/DRY motif (step 3) occur sequentially (reviewed in ref 189).

The spectroscopic data on rhodopsin photoactivation coupled with the high resolution structure of Ops* and MII now allow depiction of the sequence of rearrangements in the interhelical H-bonding networks, leading to the formation of the signaling states.[189,211,256,257] In this framework, multiple switches in rhodopsin activation were highlighted. The first movements of the TM helices are observed for MI, which has a lifetime of milliseconds. The side chain of W265(6.48) is released by isomerization of the chromophore and allows a small rotational movement of H6 and an additional tilt/rotational movement of H5 away from H3, which lead to a first set of rearrangements on the cytoplasmic receptor side. During these transitions, the interaction of the PSB with its complex counterion, consisting of E113(3.28) and E181, is altered. The main counterion function of E113(3.28) is gradually weakened, while that of E181 is strengthened. Deprotonation of the retinal Schiff base in the transition from MI to MII_a, which causes the breakage of the ionic interaction between the Schiff base and E113(3.28),[248] leads in the first place to structural changes in the water-mediated interhelical H-bonding network involving N55(1.50), D83(2.50), and the NPxxY motif in H7, which extends into the retinal binding site to W265(6.48). The transition from MII_a to MII_b is primarily characterized by a rearrangement of the H-bonding network involving E122(3.37), W126(3.41), and H211(5.46) following the shift of the retinal ring toward H5. The hallmark of the MII_a to MII_b transition is the outward tilt of H6, which contributes to form a solvent-exposed hydrophobic cleft for G protein binding.[108,245] The transition to MII_bH^+ involves uptake of a proton from the aqueous solvent and protonation of E134(3.49) of the ERY motif. This enthalpically favorable protonation step further stabilizes the active state of the photoreceptor in its native membrane environment. At some point during formation of the two MII_b intermediates, both salt bridges that involve R135(3.50) are lost, enabling the conserved arginine to engage in new intramolecular interactions with Y223(5.58) and Y306(7.53) as well as in intermolecular interactions with the C-term of transducin. The formation of R3.50 and Y5.58 interaction would occur after the transition to MII_bH^+.[230]

2.7. Computational Experiments on Rhodopsin

Rhodopsin is the GPCR with the highest number of high resolution information and as such it represents the privileged target of ever increasing computational experiments aimed at investigating different aspects of receptor function. Attempts to simulate the 11-*cis*-retinal excited-state motion as well as to make a quantitative evaluation of the isomerization coordinate and time scale are limited and very recent.[258,259] This contrasts with the ever increasing computational experiments based on atomistic or coarse-grained (CG) molecular mechanics force fields which attempted to infer processes that occur at larger time scales than photoisomerization (see here below for references).

2.7.1. Investigations of Retinal Dynamics and the Effects of the Environment on Dark Rhodopsin Structure.

The dynamics of retinal in dark rhodopsin was investigated through the analysis of a total of 23 independent 100 ns all-atom MD simulations of rhodopsin embedded into a lipid bilayer.[260] In agreement with the results of experimental solid-state ^2H NMR spectra,[261] the results of the study showed that, whereas the polyene chain is rigidly locked into a single twisted conformation, the β-ionone ring is mobile within its binding pocket, being able to rotate relative to the polyene chain.[260] Correlation analysis could identify the residues most critical to controlling mobility of retinal. In this respect, W6.48 was found to move away from the ionone ring prior to any conformational transition.

MD simulations on rhodopsin in an explicit membrane/water environment have attempted to investigate the conformational space around the native state of dark rhodopsin.[262] In detail, all-atom rhodopsin in a lipid/water environment was simulated for 15 ns. Different rhodopsin structures, including the incomplete A, C, and E chains of 1F88[16] and of 1HZX,[89] as well as a completed structure were used as input of calculations. Both the protonated and deprotonated forms of D83(2.50), E123(3.38), and H211(5.46) were probed. Simulations with and without internal water molecules were also carried out. Analysis was carried out over the last 5 ns trajectory. The computational study provided useful information on the membrane topology of the photoreceptor. A relevant outcome of this study is the finding that the cytoplasmic loops and the C-terminal tail, containing the G protein recognition and protein sorting sequences, exhibited high mobility, in marked contrast to the extracellular and transmembrane domains.[262] In fact, the average rmsd from the crystal structure during the last 5 ns of the 15 ns MD simulations

is 1.86 Å for all the Cα-atoms of the protein. In contrast, the C-terminal tail, I3, and I2 exhibited, respectively, Cα-RMSDs up to 13 Å, 9.0 Å and 5.0 Å, whereas the central parts of the TM helices revealed Cα-rmsd values as low as 0.5 Å. Also, H8 underwent significant motions. The local deviations from the crystal structure and fluctuation amplitudes revealed correspondences between flexible and functional domains of the protein.[262]

In an analogous study, the analysis of a 40 ns MD trajectory of dark rhodopsin in an explicit membrane/water environment highlighted changes in the water accessibility of I3 and the C-tail, likely driven by helix motion.[263] In an attempt to approach as much as possible the real composition of the retinal rod outer segment disk membranes, which are rich in polyunsaturated lipids and cholesterol, Pitman at al. embedded the rhodopsin molecule in a bilayer composed of a 2:2:1 mixture of 1-stearoyl-2-docosahexaenoylphosphatidylcholine (SDPC), 1-stearoyl-2-docosahexaenoylphosphatidylethanolamine (SDPE), and cholesterol (i.e., 1 protein, 49 SDPCs, 50 SDPEs, 24 cholesterols, and 7400 waters) and produced a 118 ns equilibrated MD trajectory in the NVE ensemble. Consistent with the observations from in vitro experiments, in silico experiments showed that the protein breaks the lateral and transverse symmetry of the bilayer. Lipids near the protein preferentially reorient such that the unsaturated chains interact with the protein, while the distribution of cholesterol in the membrane complements the variations in rhodopsin's transverse profile, thus suggesting that cholesterol stabilizes the dark state of the photoreceptor without interacting with the protein.[264] The same authors reported the results of three all-atom MD simulations, each at least 1.5 μs long, which predicted dramatic changes in internal hydration occurring during the formation of a putative MI photoactivated state.[161]

The effect of lipid composition on the structural features of rhodopsin was recently investigated by four 20 ns MD trajectories of different one-component lipid bilayers.[265] The results showed that lipids can modulate the structure of rhodopsin by affecting the tilt of the protein as a whole and the helix kink motions, but leaving unaltered helix-content and tilt.[265] On the other hand, the protein infers an ordering effect over the lipid bilayer. Furthermore, the analysis of lipid−protein interactions showed a greater sensitivity to the lipid environment of the cytosolic side of the protein compared to the extracellular one. The results of computations suggested also a role for the lipid composition in modulating the electrostatic lock at the cytoplasmic extensions of H3 and H6.[265] The structural effects of mutations on the components of such "ionic lock" were investigated by the same authors in a successive study.[266]

Computational experiments investigated also the effects of cholesterol on rhodopsin structure and dynamics by microsecond MD simulations of rhodopsin in explicit membrane.[267] The study highlighted three regions on rhodopsin exhibiting the highest cholesterol density throughout the trajectory: the extracellular end of H7, the intracellular parts of H1, H2, and H4, and the intracellular ends of the H2−H3 region.[267] Cholesterol was suggested to primarily affect the kinks in H1, H2, and H7, associated with rigid-body motions in the H1−H2−H7−H8 region. Ultimately the authors inferred a regulatory role of cholesterol in the structural rearrangements involved in GPCR function.[267]

These elegant studies prove an enormous effort to improve the reliability of the system, providing insights into the effects of lipids on receptor conformation. However, the reliability of the explicit lipid/water models remains undermined by the membrane-compartment dependence of lipid composition and lipid-receptor stoichiometry, in light of the ever-increasing evidence that GPCRs, including rhodopsin, exist as constitutive oligomers.[45−61,63]

Explicit membrane/water models make it even more difficult to detect, in the nanosecond time scale, the protein motions, which accompany MII formation. The latter event has been, indeed, demonstrated to occur in the millisecond time scale and may require the presence of transducin.[193,207] These limitations clearly emerge in recent computational attempts to simulate the active states of the photoreceptor.[268,269]

2.7.2. Computational Strategies to Predict/Investigate the MII State. Strategies to overcome the gap between time scale of the process and length of simulations included the employment of external forces[269] or restraints consisting in either interatomic distances from in vitro experiments,[249−251,270−273] or deformations derived from the anisotropic network model (ANM).[274,275] External forces were introduced in explicit membrane/water simulations to induce the clockwise rotation of H6 (when seen from the intracellular side), predicted to be associated with MII formation.[269] Experimental-derived distance restraints were, instead, employed by Yeagle and co-workers to transform a computational model of dark rhodopsin (PDB code 1JFP)[270] into MII (PDB code 1LN6) (Figure 10, left).[249,250,270] The model of dark rhodopsin, 1JFP, was obtained by combining NMR determinations of rhodopsin fragments with computational modeling.[270] The rmsd of the main chain atoms of amino acids 40−348 in 1JFP and in the latest rhodopsin structure (1U19)[92] is 7.3 Å. Such a deviation is still high, i.e., 5.7 Å, if only the seven TM domains are considered, as differences between rhodopsin structure and the computational model concern both the secondary structure elements and their packing. Both computational models of the inactive and active rhodopsin states, 1JFP and 1LN6, are of poor stereochemical quality, indicative of limitations in the modeling approach. Instead of using a computational model, Gouldson and co-workers employed the crystal structure of rhodopsin for restrained MD experiments.[251] Also in this case, restraints were derived by in vitro experiments on rhodopsin and homologous GPCRs.[251] The results of this study suggested that the main changes in the receptor conformation on activation involve H4, H5, H6, and H7. Such changes include (a) clockwise rotation of H4; (b) displacement of H6 away from H3, accomplished by a straightening of H6 itself; (c) increased flexibility in the intracellular half of H7; and (d) a general opening of the intracellular part of the structure (Figure 10, central panel).[251] A putative model of the MII rhodopsin state was built starting from the LUMI X-ray structure. The authors imposed two sets of distance restraints from in vitro experiments describing local and global motions.[272] In the first step, distance restraints describing local motions in the retinal binding site were applied through biased MD to an all-atom model. In the second step, distance restraints describing global motions were applied to an α-carbon elastic network model (ENM) of the rhodopsin structure resulting from MD simulations. The displacements of the ENM in response to the applied restraints provided a simplified representation of the global conformational changes that accompany the activation process. To finally gain an all-atom picture of such changes, biased MD was employed to force the model arising from the first step into the coarse grained ENM model. MD simulations were carried out in implicit membrane/water.[272]

dx.doi.org/10.1021/cr100437t |Chem. Rev. 2011, 111, PR438–PR535

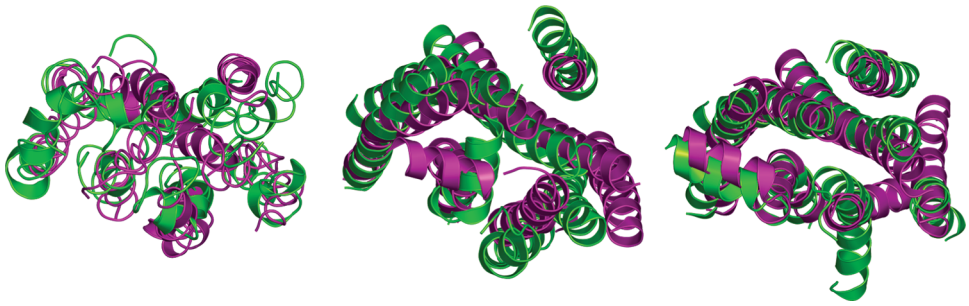

Figure 10. Cartoon representation of the seven-helix bundle and of H8 of computational models of the inactive (violet) and active (yellow−green) states of rhodopsin. In detail, on the left side, the models from Yeagle and co-workers deposited in the PDB as 1JFP (violet) and 1L6N (green) are shown;[249,250,270] in the central panel, the structures computed by Gouldson and co-workers are shown;[251] finally, in the right panel, the 1U19 structure (violet) is superimposed on the computational model of active rhodopsin, deposited in the PDB as 1OV0.[252] The helix bundles are seen from the intracellular side in a direction perpendicular to the membrane surface. Drawings were done by means of the software PYMOL 0.97 (http://pymol.sourceforge.net/).

The study could detect major changes in the loop regions, in H8, and in the cytosolic ends of H3, H4, H5, H6, and H7. The MII model showed changes in the interhelical network of H-bonding interactions, including the breakage of the "ionic lock".[272] A model of the MII state was also built by combining structural restraints provided by solid-state NMR measurements with MD simulations in an octane/water environment.[273] The simulations yielded a working model to investigate how photoisomerization of the 11-*cis*-retinylidene chromophore bound within the interior of rhodopsin is coupled to TM-helix motion and receptor activation. The study highlighted the role of multiple switches on the extracellular side of the protein as triggers of the structural changes that converge to disrupt the "ionic lock".[273] The global dynamics of rhodopsin that couples retinal isomerization to conformational changes in both the TM regions and the G protein binding sites was investigated by ANM-restrained MD in explicit membrane/water.[274] Consistent with a previous study by the same authors,[276] computational analysis highlighted a hinge site near the chromophore that facilitates the enhanced mobility of the cytoplasmic ends of H3, H4, H5, and H6 and their connecting loops. The redistribution of the interactions in the retinal binding site following the conversion to the all-trans form resulted in motions of H3 and H6 that propagate to their cytosolic ends.[274] The energy coupling between retinal binding site and G protein binding regions was investigated by equal-time correlations of the fluctuating interaction energy of residue pairs in MD trajectories.[277] Two highly conserved motifs, E/DRY and NPxxY, were found to have strong interaction correlation with retinal. Moreover, MD simulations with restraints on each TM helix indicated that the major signal-transduction pathway involves the interdigitating side chains of H6 and H7.[277]

In line with the attempts to overcome the computational and time-scale limitations in unforced and unrestrained simulations of rhodopsin activation in an explicit environment, Nikiforovich and Marshall recently presented the results of a computational approach aimed at generating the active state of rhodopsin.[252] The approach started with simplified energy calculations in an effort to find a set of sterically and energetically reasonable options for the TM helix arrangements with *all-trans*-retinal. Various 3D models of the TM helix packing found by computations were then compared to limited site-directed spin-labeling experimental data on rhodopsin activation, to identify the most plausible model of the TM helix bundle in the active state. The experimental data mainly used to drive model selection were light-induced changes in distances between spin labels in positions 139(3.54) and 248(6.31)−252(6.35) (Table 2).[252] In the next step, all non-TM structural elements (i.e., tails and loops) were reconstructed, and after the entire "MII" structure had been relaxed, all other currently available additional experimental data, both mutational and spectroscopic, on the structure of the MII state of rhodopsin were used to validate the resulting 3D model (PDB code 1OV0; Figure 10, right).[252] Contrary to what the authors say, the analysis of such a computational model does not reveal a striking agreement with site-directed spin-labeling experimental data. In fact, the distances between the Cα-atoms of V139(3.54), on one hand, and those of K248(6.31), T251(6.34), and R252(6.35), on the other one, in the computational model are respectively 11.83, 10.53, and 13.32 Å, whereas, according to the site-directed spin-labeling data, such distances should be about 19.75, 19.83, and 18.67 Å, respectively (Table 2).[186] Thus, the computational model does not show the predicted separation of the cytosolic extensions of H3 and H6, as compared to the dark state, and it should be taken with caution the author's proposal that such a computational model can be used as a template for modeling the active states of homologous GPCRs.[252] The same approach was successively used by the authors to model a number of constitutively active mutants of rhodopsin.[278]

In vacuo weighted masses MD was applied to a truncated form of the crystal structure of rhodopsin,[16] lacking all the nonprotein molecules, lacking all the intracellular and extracellular domains, except for E2, and holding the11-*trans*-retinal, to produce MII.[279] The structure averaged over the last 100 ps of a 1.2 ns equilibrated trajectory and minimized was considered consistent with the available experimental data and used as a template to achieve what the authors called an "in silico activated" form of the 5-HT$_{2A}$ receptor. Such a receptor model was then used for docking experiments with known activating ligands, without any further MD simulation.[279] An alternative approach to build rhodopsin's photointermediates lumirhodopsin, MI, and MII, starting from the crystal structure of the dark state, consisted of applying swings to selected TM domains according to in vitro experimental data coupled with optimizations by MD/energy minimizations.[280,281] The putative models of MI, MIb (opsin), MI$_{380}$, and MII were then used to construct the structural models of the putative inverse agonist-, antagonist-, partial agonist-, and full agonist-bound forms of aminergic GPCRs and, more recently, a nociceptin receptor.[282,283] We have concerns about the

dx.doi.org/10.1021/cr100437t |*Chem. Rev.* 2011, 111, PR438–PR535

approach employed to model the rhodopsin intermediates, as it is significantly biased by human intervention. We, therefore, are also concerned about the use of such rhodopsin intermediates as templates for modeling functionally different states of the homologous GPCRs.

The conformational changes occurring in MII formation starting from the dark state were also explored by means of the ligand-induced perturbations in the transmembrane rotational conformations (LITiCon) method.[284,285] This method involves a systematic spanning of the rotational orientation of the TM helices that are in the vicinity of the ligand for predicting the helical rotations that occur on ligand binding. The predicted ligand-stabilized receptor conformations are characterized by a simultaneous lowering of the ligand binding energy and a significant gain in interhelical and receptor−ligand hydrogen bonds. Thus, LITiCon identified which of the TM helices in direct contact with retinal would undergo conformational changes due to retinal isomerization.[284] The predicted ligand-stabilized receptor conformation was finally subjected to 30 ns MD simulations in explicit membrane/water.[284] The final model was found to correlate well with the experimentally observed conformational switches in rhodopsin and other class A GPCRs.[284] Attempts to infer possible activation pathways of rhodopsin were carried out by means of biased MD simulations.[286] The crystal structure of the photoactivated deprotonated state of rhodopsin and Ops* structure in the presence of 11-*trans*-retinal were employed as the starting and ending points. The authors reconstructed the system free-energy landscape along the predetermined transition trajectories using a path collective variable approach based on metadynamics. The study suggested that the two experimental end points may be connected by at least two different pathways, and that the conformational transition is populated by at least four metastable states of the receptor, characterized by a different amplitude of the outward movement of H6.[286]

Collectively, these computational experiments, consistent with advances from in vitro experiments and structure determinations,[189] highlight the E/DRY motif as the target of structural changes that lead to the formation of rhodopsin signaling state. Indeed, the substantially different computational models of activated rhodopsin share the breakage of the "ionic lock" between R135(3.50), of the E/DRY motif, and E247-(6.30).[250−252,266,272−274,276,284] The breakage of such an interhelical salt bridge has been suggested to be a feature of the active states of different family A GPCRs, by in vitro and computational experiments[131,132,134−139,142,145−148] (see also references in the red updates through the text).

2.7.3. Computational Experiments on Supramolecular Assemblies of Rhodopsin. A number of computational experiments focused on supramolecular assemblies of rhodopsin. In this respect, the semiempirical model of dimeric rhodopsin[176] was subjected to MD simulations and to the analyses of the essential motions.[287−289] These studies inferred the stability of the structural model,[287] and an asymmetry in the essential conformational spaces of the two monomers, which was interpreted as indicative of an allosteric modulation that could connect the monomers in a putative asymmetric activation mechanism.[288] The 1N3M rhodopsin model was also subjected to ENM deformations to investigate the effects of oligomerization on the normal modes of the receptor.[290] The study highlighted (a) significant perturbation of the normal modes of the rhodopsin protomer upon oligomerization, (b) increased intra-protomer positive correlation among TMs as well as between extracellular loops and TM regions, and (c) highest inter-residue positive correlation at the interfaces between protomers.[290] Neri and co-workers inferred a rather naive model of oligomerization-aided signal transduction by inducing photoisomerization in one monomer (i.e., subunit R*) and relieving structural changes in the G protein coupling portions of the other monomer in the dark state (i.e., subunit R).[289] According to this model, photoisomerization of retinal in the R* subunit causes changes at the dimer interface participated by H4. Interfacial structural changes are then transmitted to the cytosolic end of H3 in the R subunit by causing: (a) breakage of the "ionic lock", (b) subsequent outward movements of H6, and (c) opening of a cytosolic crevice for transducin recognition. The 1N3M oligomeric model of rhodopsin served also to develop a method for predicting mutational effects on the stability of GPCR dimers.[291]

CG molecular mechanics force fields are attractive approaches to gain mechanistic insights into long time scale processes and large biomolecular assemblies.[292−294] In this context, a CG molecular dynamics (CGMD) model was developed and used to investigate the molecular basis of how the physicochemical properties of the phospholipid bilayer affect self-assembly of visual rhodopsin.[292,293] The CGMD method is a mesoscopic simulation technique in which groups of atoms are mapped to particles on the basis of a four-to-one rule. This systematic reduction of the degrees of freedom allowed for computationally efficient calculation of the structure and dynamics of molecular assemblies for larger time and length scales than accessible to atomistic models, providing an unprecedented view of spontaneous protein assembly in biomembranes.[293] A further promising development combined structure-based (i.e., ENM) and physics-based (e.g., MARTINI force field) molecular force fields into a single representation (called ELNEDIN).[294] Rhodopsin has been used as well as a test case in the development of another CG model for protein simulations.[295]

2.7.4. Computational Screening of Pathogenic Rhodopsin Mutations. Rhodopsin, like other GPCRs and membrane proteins,[296] is particularly subjected to pathogenic missense mutations that affect folding or trafficking rather than protein function. These include rhodopsin mutations associated with retinitis pigmentosa (RP), a group of debilitating hereditary disorders that cause severe visual impairment in as many as 1.5 million patients worldwide.[87,297] The protein design FoldX algorithm was challenged in its ability to estimate the effects of the majority of the pathogenic rhodopsin mutations known so far on the stability of the protein.[298] The study provides a useful tool for coarse estimations of mutational effects, but it is inadequate to infer the structural determinants of such effects. We have recently undertaken in silico experiments to infer the structural effects of misfolding mutations associated with the autosomal dominant form of RP (ADRP), as well as to provide tools for in silico screening novel rhodopsin mutations.[299,300] In the most recent study, steered MD (SMD) simulations on nonameric rhodopsin were combined with protein structure network (PSN) analysis (by means of the Wordom software[301]) to compare the mechanical unfolding of wild type rhodopsin with that of selected ADRP-linked mutants.[300] In this framework, SMD simulations were instrumental in simulating the unfolding process, whereas PSN was used to infer the effects of mutations on the native fingerprint of the hyperlinked and most stable amino acids in the

structure network, i.e., hubs, that oppose resistance to connectivity loss in response to an external force.[300] The results of computational experiments provided a valuable framework to interpret the results of in vitro single-molecule force spectroscopy (SMFS) experiments on rhodopsin based on AFM.[302,303] Most importantly, the study revealed relevant intrinsic features that pertain to the structural network of rhodopsin. Rhodopsin fold is such that stable hubs essentially clusterize in the two poles of the helix bundle and along the main axes of H3 and H6. Such stable nodes are likely to play a role in protein folding and stability, as well as in the establishment of the intramolecular communication between extracellular and intracellular sides necessary to signal transduction.[300] The high concentration of hubs in the retinal binding site is consistent with computational studies that highlighted this receptor portion as a part of the stability core and a hinge site in the dynamics of the protein.[276,300,304] The distribution of highly connected nodes in the network reflects the existence of a diffuse intramolecular communication inside and between the two poles of the helix bundle, which makes pathogenic mutations share similar phenotypes irrespective of topological and physicochemical differences between them. Because of this communication, the considered ADRP-linked rhodopsin mutations share more or less marked abilities to impair selected hubs in the protein structure network, hitting in particular E2. The extent of this structural effect relates to the severity of the biochemical defect caused by mutation.[300] The ability to communicate with portions deputed to rhodopsin stability and function is what makes pathogenic mutation sites different from "neutral" mutation sites. In this respect, the amino acid location may have a priority over the amino acid typology as a determinant of the disease.

3. CRYSTAL STRUCTURES OF NONOPSIN GPCRS: β_2AR, β_1AR, A_{2A}R, CXCR4, D_3R, AND H_1R

3.1. Advances in X-ray GPCR Crystallography

Recent advances in GPCR crystallography led to the release in 2007 and 2008 of the first crystal structures of nonopsin GPCRs in their inactive states, i.e., the human β_2AR bound to the high-affinity inverse agonists carazolol (PDB codes 2R4R, 2R4S (3.40 Å), and 2RH1 (2.40 Å))[93,94] and timolol (PDB code 3D4S, 2.80 Å),[96] the turkey β_1AR bound to the antagonist cyanopindolol (PDB code 2VT4, 2.70 Å),[95] and the human A_{2A}R bound to the antagonist ZM241385 (ZMA) (PDB code 3EML, 2.6 Å)[103] (Table 1, Figures 11−13). Two other crystal structures of the cyanopindolol−β_1AR complex were released more recently (PDB codes 2YCX and 2YCY (3.25 Å and 3.15 Å, respectively)). Success in structure determination is due to strategies for improving the poor thermal and proteolytic stability, a common feature of nonopsin GPCRs.[305−307] Thermal stability was improved by introducing stabilizing ligands and stabilizing mutations (3D4S,[96,308] and 2VT4[95]), by adding lipids (2R4R/2R4S,[93] 2RH1[94] and 3EML[103]), and by reaching high salt concentration (3EML).[103] Strategies to enhance the proteolytic stability included truncation of disordered regions like the N- and C-terminals and replacement of I3 either with Fab, like in 2R4R and 2R4S,[93] or with T4 Lysozime (T4L), like in 2RH1, 3D4S, and 3EML.[94,96,103] Such replacements helped improve crystal contacts while eliminating the structurally instable loop. The T4L fusion strategy was adopted as well to solve the first crystal structures of a GPCR of the peptide subfamily, which were released in November 2010.[111] Three different constructs were, indeed, resolved, i.e., CXCR4−1, CXCR4−2, and CXCR4−3, differing in the precise T4L junction site, the position of the C-terminal truncation, and the presence of the T240(6.36)P mutation in CXCR4−3. All the constructs hold the L125(3.41)W stabilizing mutation and were cocrystallized with the isothiourea derivative IT1t antagonist (PDB codes 3OE6 (3.20 Å), 3OE8 (3.10 Å), and 3OE9 (3.10 Å) for CXCR4−1, CXCR4−2, and CXCR4−3, respectively). An alternative IT1t-bound form of the CXCR4−2 construct was resolved as well (PDB code 3ODU (2.50 Å)). The CXCR4−3 construct was cocrystallized also with the 16-amino acid cyclic peptide antagonist CVX15 (PDB code 3OE0 (2.90 Å)) (Figure 14).[111] Finally, the T4L stabilization strategy was also employed to resolve the structure of the D_3R and H_1R (Table 1, Figure 15).[112,113] For the D_3R, other stabilizing elements included the L119(3.41)W mutation and the complexation with the eticlopride antagonist, whereas, for the H_1R, additional stabilizing modifications concerned truncation of the first 19 amino acids.

The timolol−β_2AR complex exhibits a specific binding site for cholesterol between H2, H3, and H4. Sequence comparisons suggest that such site is conserved across multiple members of family A GPCRs.[96,309]

To assess the extent of ligand-induced conformational differences in β_2AR structures, the receptor was successively crystallized also in complex with two inverse agonists: ICI 118,551 (PDB code 3NY8, 2.80 Å), a recently discovered ligand (PDB code 3NY9, 2.80 Å), the antagonist alprenolol (PDB code 3NYA, 3.10 Å), and an irreversibly bound agonist (PDB code 3PDS, 3.50 Å).[97,101] The same experiments were carried out on the turkey β_1AR leading to the crystallographic complexes with functionally different ligands such as the antagonists carazolol (PDB code 2YCW, 3.00 Å) and iodocyanopindolol (PDB code 2YCZ), the partial agonists dobutamine (PDB codes 2Y00 and 2Y01 (2.50 Å and 2.60 Å, respectively)) and salbutamol (PDB code 2Y04, 3.05 Å),[102] as well as the full agonists carmoterol (PDB code 2Y02, 2.60 Å) and isoprenaline (PDB code 2Y03, 2.85 Å) (Figure 12).[98,102]

3.2. Structure Comparisons of Family A GPCRs

A number of reports have appeared, which discuss commonalties and differences among the different crystal structures.[306,309−312] Herein, we will make a comparison as well, highlighting correlations between sequence and structure conservations/divergences.

As expected from sequence comparisons, major similarities among bovine rhodopsin and the nonopsin GPCRs involve the 7TM helices. Structural conservation concerns also H8 for all GPCR structures except CXCR4. In fact, all the five CXCR4 structures lack such α-helix (Figures 2, 4,11−15). Structural similarities in the seven helices are reflected by the Cα-RMSDs, which for the inactive forms stay in the 1.56−2.72 Å range for pairwise comparisons of members of different subfamilies, whereas it lowers to 0.54 Å for the close homologues β_1AR and β_2AR (Table 3 and Figure 16). The whole-chain C_α-rmsd of the two βARs is 1.5 Å, the structural divergence being limited to I2. In fact, such a loop in the β_1AR holds an α-helix in its N-terminal half, pointing outward from the helix bundle, whereas in almost all the β_2AR structures solved so far, it is not structured and approaches the cytosolic end of H6 (Figures 11 and 15). A marker of these structural differences is also a tyrosine in the N-terminal half of the loop, which is conserved in the βARs, D_3R, and A_{2A}R. In β_2AR, this tyrosine makes van der Waals contacts with E6.30, whereas in β_1AR, A_{2A}R, and D_3R, it is involved in H-bond with D3.49 of the E/DRY motif. Curiously,

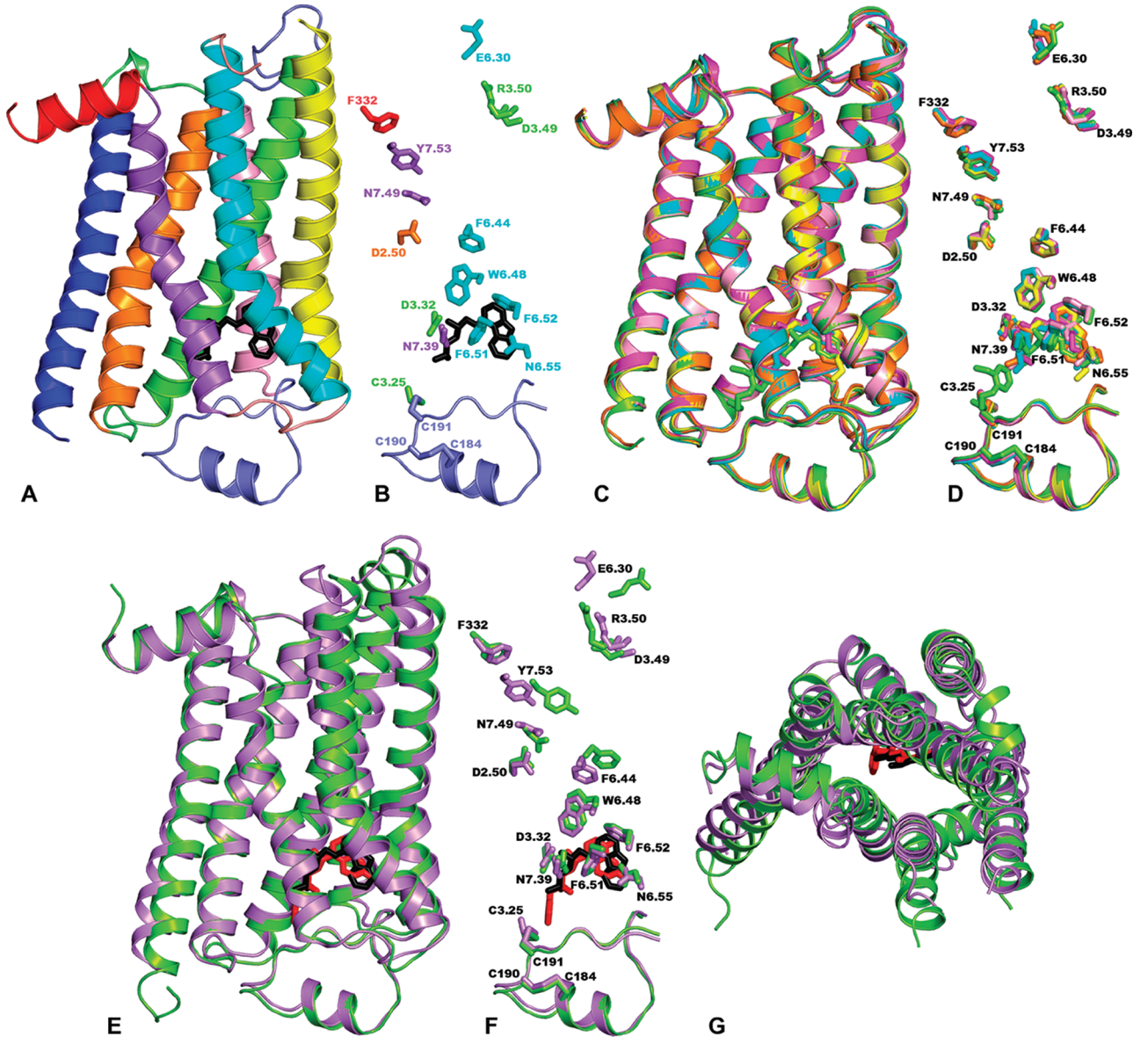

Figure 11. Crystal structures of the human β_2AR. In all panels except for G, the receptors are seen in a direction parallel to the membrane surface (the intracellular side being at the top). (A) The cartoon representation of the human β_2AR structure in complex with the inverse agonist carazolol (PDB code 2RH1)[94] is shown; the ligand is represented in black sticks. (B) The side chains of selected highly conserved amino acids, of the carazolol (black sticks) binding site amino acids, and of the E2 cysteines engaged in disulfide bridges are shown; the E2 backbone (represented in cartoons) is shown as well. (C) The cartoon representation of the superimposed structures of the β_2AR in complex with the inverse agonists carazolol (PDB code 2RH1, orange),[94] timolol (PDB code 3D4S, magenta),[97] ICI 118,551 (PDB code 3NY8, cyan),[97] and a recently discovered ligand (PDB code 3NY9, yellow),[97] with the antagonist alprenolol (PDB code 3NYA, pink),[97] and with an irreversibly bound agonist (PDB code 3PDS, yellow−green)[101] is shown; the ligands are represented in sticks. (D) Of the superimposed structures shown in (C), only selected details are shown (see the (B) description above). (E) The cartoon representation of the superimposed structures of β_2AR in its carazolol-bound (PDB code 2RH1, violet)[94] and a nanobody-stabilized BI-167107 agonist-bound (PDB code 3P0G, yellow−green)[99] states is shown; carazolol is black, whereas BI-167107 is red. (F) Of the superimposed structures shown in (E), only selected details are shown (see (B) description above). (G) Top view from the intracellular side of the two superimposed structures shown in (E). See the legend to Figure 4 for the color coding of the different receptor regions.

the agonist-bound forms of the β_2AR stabilized either by a G protein mimic or by Gs (PDB codes 3P0G and 3SN6, respectively) make two exceptions among the β_2AR structures because they hold the same α-helical segment in I2 present in β_1AR (Figure 11E−G).[99] Remarkably, similar to the β_1AR, in one of the two D_3R molecules present in the asymmetric unit of the crystal, I2 holds a 2.5-turn α-helix almost parallel to the membrane surface.[112]

Collectively, the βARs, D_3R, H_1R, and A_{2A}R are more similar between each other in the seven-helix bundle than rhodopsin and CXCR4 (Table 3). In line with the outcome of sequence comparisons,[150] the cytosolic halves of rhodopsin and non-opsin GPCRs are more similar than the extracellular ones; the latter, indeed, show significant structural differences (Figures 16 and 17).[313] Divergent features in the extracellular halves include a more pronounced tilt of H1 in the two βARs

dx.doi.org/10.1021/cr100437t |*Chem. Rev.* 2011, 111, PR438–PR535

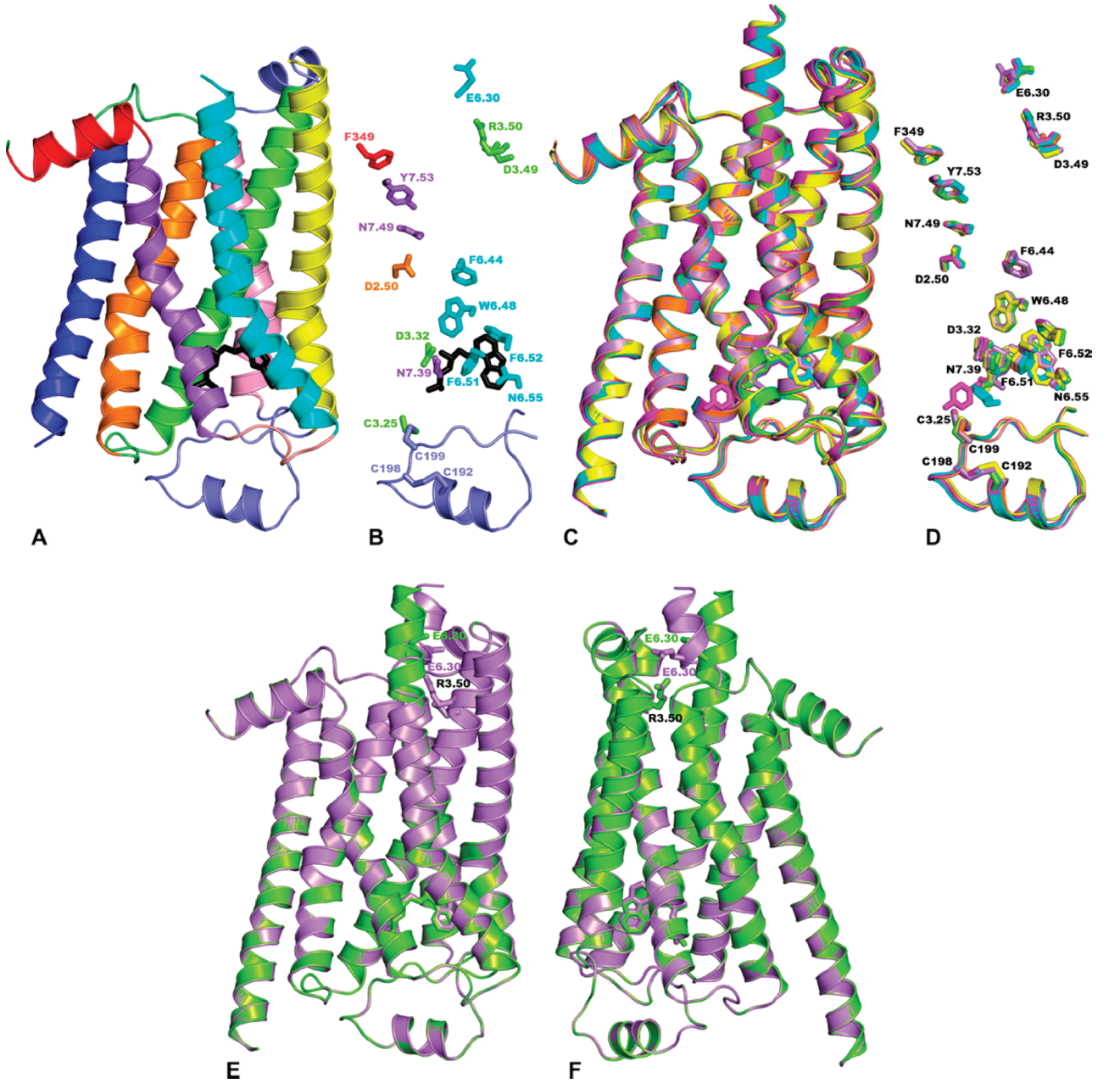

Figure 12. Crystal structures of the turkey β_1AR. The receptors are seen in a direction parallel to the membrane surface (the intracellular side being at the top). (A) The cartoon representation of the whole structure of the turkey β_1AR in complex with the antagonist cyanopindolol (PDB code 2VT4)[95] is shown; the antagonist is shown as well in black sticks. (B) The side chains of selected highly conserved amino acids, of the cyanopindolol (black sticks) binding site amino acids, and of the E2 cysteines engaged in disulfide bridges are shown; the E2 backbone (represented in cartoons) is shown as well. (C) A cartoon representation of the superimposed structures of the β_1AR in complex with the antagonists cyanopindolol (PDB code 2VT4, orange)[95] and carazolol (PDB code 2YCW, chain B, yellow),[98] with the agonists dobutamine (PDB code 2Y00, magenta),[102] carmoterol (PDB code 2Y02, cyan),[102] and isoprenaline (PDB code 2Y03, yellow−green),[102] and with the partial agonist salbutamol (PDB code 2Y04, violet)[102] are shown; the ligands are represented in sticks. (D) Of the superimposed structures shown in (C), only selected details are shown (see the (B) description above) and (E) and (F). Two cartoon views of the superimposed structures of the A (violet) and B (yellow−green) chains of the β_1AR bound to the antagonist carazolol (PDB code 2YCW)[98] are shown, together with the side chains of E3.49, R3.50, and E3.60; carazolol is shown in sticks as well. See also the legend to Figure 4 for the color coding of the different receptor regions.

compared to rhodopsin, A_{2A}R, and CXCR4. Furthermore, in the CXCR4: (a) H2 makes a tighter helical turn at P92(2.58) resulting in ∼120° rotation of its extracellular end compared to the other GPCRs; (b) both the intracellular and extracellular tips of H4 in CXCR4 substantially deviate (∼5 Å and ∼3 Å, respectively) from their consensus positions in other GPCRs; (c) the extracellular ends of H5 and H7 in CXCR4 are about one and two-turn longer, respectively, than in other GPCRs; and (d) H6 is shifted by ∼3 Å in CXCR4 relative to β_2AR and A_{2A}R. Other significant differences in the extracellular regions concern E2. In this respect, the β-hairpin in such loop is no longer present in the βARs, A_{2A}R, D_3R, and H_1R. Different

dx.doi.org/10.1021/cr100437t |*Chem. Rev.* 2011, 111, PR438–PR535

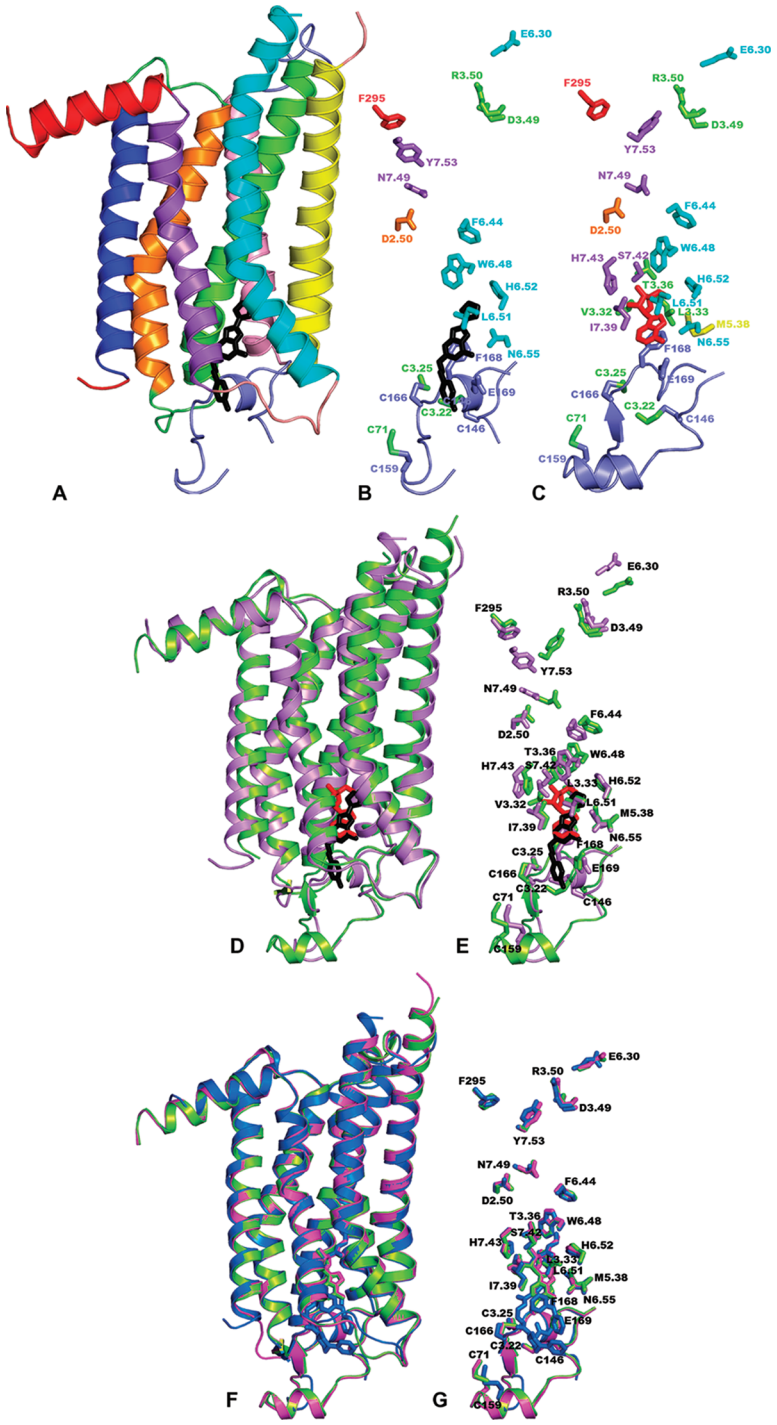

Figure 13. Crystal structures of the human $A_{2A}R$. The receptors are seen in a direction parallel to the membrane surface (the intracellular side being at the top). (A) A cartoon representation of the whole structure of the human $A_{2A}R$ in complex with the antagonist ZMA (PDB code 3EML)[103] is shown; the ligand is shown in sticks. In (B,C), selected side chains and the E2 backbone (represented in cartoons) extracted, respectively, from the complexes with the antagonist ZMA (PDB code 3EML)[103] and the agonist adenosine (PDB code 2YDO)[104] are shown. The selected side chains concern highly conserved amino acids, the E2 cysteines engaged in disulfide bridges, and the amino acids involved in interaction with ZMA (black sticks) and adenosine (red sticks). (D,E) Superimposed structures of the $A_{2A}R$ in complex with the antagonist ZMA (black sticks) (PDB code 3EML, violet)[103] and the agonist adenosine (red sticks) (PDB code 2YDO violet);[104] for an explanation of (D,E), see the legend to (A) and (B,C), respectively. (F,G) Superimposed structures of the $A_{2A}R$ in complex with the agonists adenosine (PDB code 2YDO, yellow−green),[104] NECA (PDB code 2YDV, magenta),[104] and UKA (PDB code 3QAK, blue);[105] for an explanation of (F,G), see the legend to (A) and (B,C), respectively. See also the legend to Figure 4 for the color codingof the different receptor regions.

from rhodopsin, in these receptors E2 does not occlude the ligand binding site (Figure 17). In more detail, in the βARs, E2 holds a two-turn α-helical segment in its N-terminal half which is exposed to the solvent, whereas the C-terminal half is in

dx.doi.org/10.1021/cr100437t |*Chem. Rev.* 2011, 111, PR438–PR535

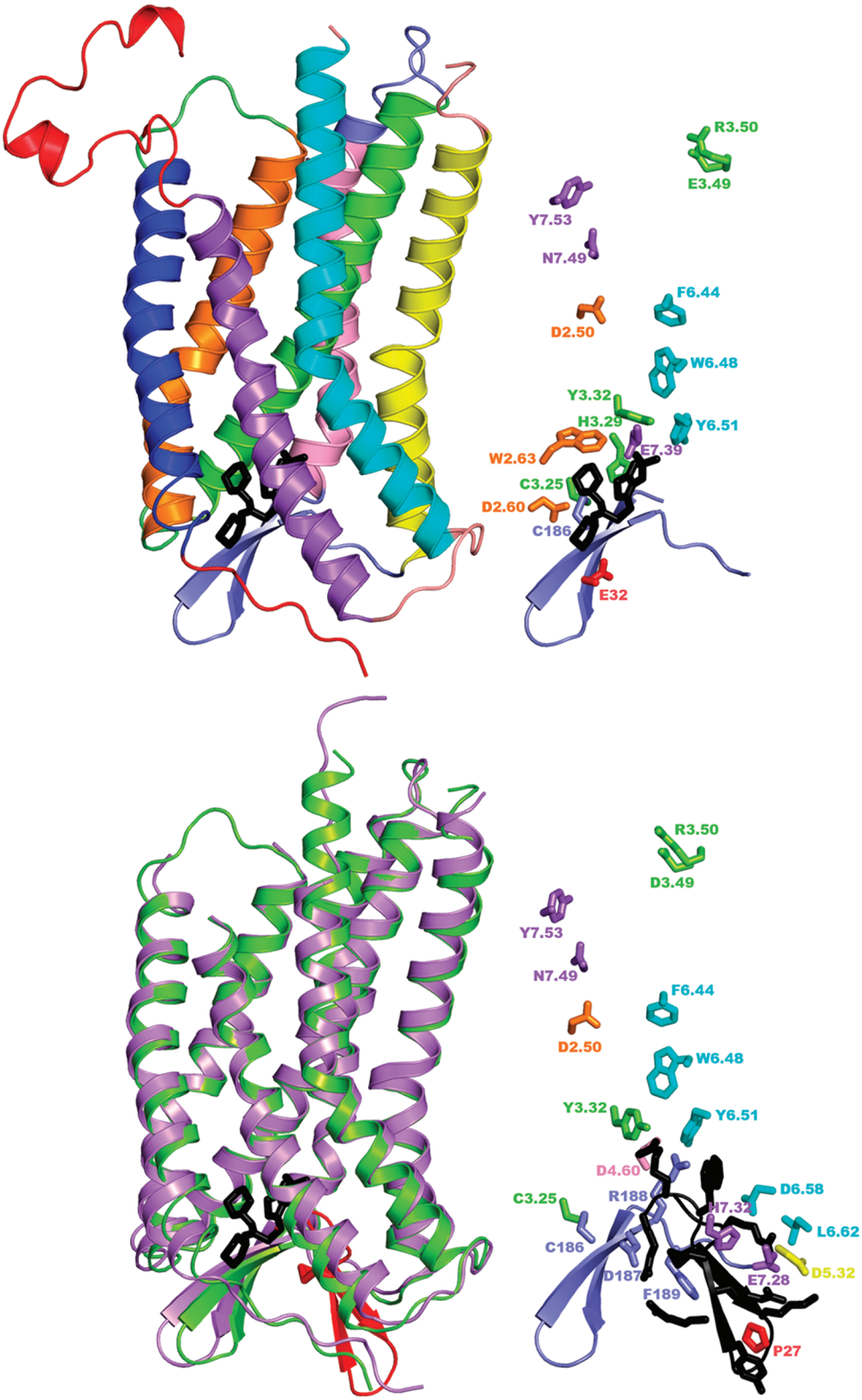

Figure 14. Crystal structures of the human CXCR4. The receptors are seen in a direction parallel to the membrane surface (the intracellular side being at the top). In the left panels, the whole receptor structures are shown. In detail, in the top left panel, the complex with the antagonist IT1t is shown colored according to the different receptor portions (see the legend to Figure 4 for the color coding). In the bottom left panel, the complexes with the small molecule IT1t (PDB code 3ODU)[111] and the cyclic peptide CVX15 (PDB code 3OE0)[111] are superimposed. In this respect, the receptor in complex with IT1t is yellow−green, whereas that in complex with CVX15 is violet; the antagonists IT1t and CVX15 are black and red, respectively. In the right panels, only the side chains of selected highly conserved amino acids, of the IT1t (top) and CVX15 (bottom) binding site amino acids, and of the E2 cysteines engaged in disulfide bridges are shown; the E2 backbone is shown as well. In these images, the ligands are black and only selected side chains of CVX15 are shown.

dx.doi.org/10.1021/cr100437t |*Chem. Rev.* 2011, 111, PR438–PR535

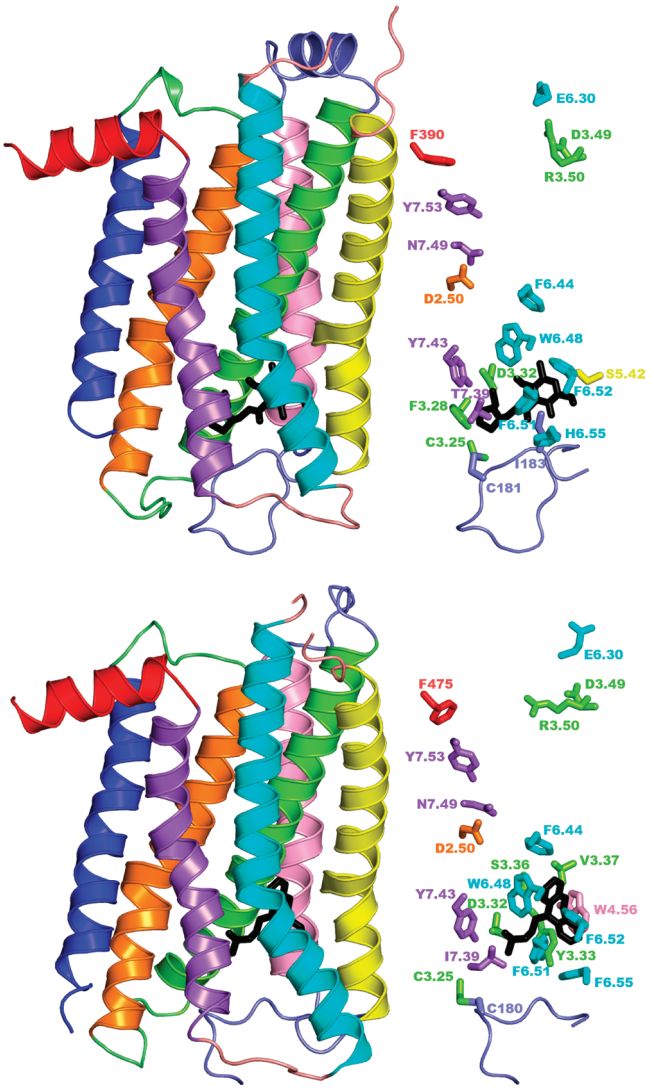

Figure 15. Crystal structures of the human D_3R and H_1R. In the top two panels, the D_3R structure in complex with the antagonist eticlopride is shown (PDB code 3PBL),[112] whereas the two bottom panels show the H_1R structure in complex with the antagonist doxepin (PDB code 3RZE).[113] The receptors are seen in a direction parallel to the membrane surface (the intracellular side being at the top). In the left panels, the whole receptor structures are shown, whereas in the right panels, only the side chains of selected highly conserved amino acids, of the eticlopride and doxepin (black sticks) binding site amino acids, and of the E2 cysteines engaged in disulfide bridges are shown; the E2 backbone is shown as well. See the legend to Figure 4 for the color coding of the different receptor regions.

random coil conformation and participates in ligand binding (Figures 11 and 17B). In the βARs, the loop is further stabilized by two disulfide bridges: one is intraloop between C184 and C190, whereas the other, in the C-terminal portion, is between C190 and the conserved C3.25 (Figures 11 and 12). In the first crystal structure of the $A_{2A}R$, E2 is incomplete (Figures 13 and 17F). The loop is, however, complete in the more recent crystallographic complexes between the $A_{2A}R$ and the agonists adenosine and NECA (PDB codes 2YDO and 2YDV (3.00 Å and 2.60 Å, respectively); Figures 13 and 17G).[104] In these structures, the loop holds a two-turn α-helix in the 151−158 portion as well as a β-strand in the 163−165 portion; the latter forms a β-sheet with the 70−72 β-strand in E1 (Figures 13 and 17G). Moreover, the loop holds three disulfide bridges between C146 and C74 (3.22), C159 and C71 (in E1), and C166 and the conserved C77(3.25). In the D_3R, E2 is much shorter than in the βARs and lacks any α-helical segment (Figure 15). However, the portion of E2 in the D_3R that contributes to the ligand binding pocket (i.e., residues 182−185) is structurally similar to the corresponding portion in the βARs. In the H_1R, the resolved portion of E2, which is incomplete in the crystal structure released so far, does not hold secondary structure elements (Figures 15 and 17D,E). Finally, in the CXCR4 structures, similar to rhodopsin, E2 folds in a β-hairpin. However, different from rhodopsin, such a β-hairpin is arranged so as to allow access to the ligand binding site, which is larger, more open, and located closer to the extracellular surface, compared to the other GPCR structures (Figures 11−15 and 17). In all nonopsin GPCR structures, the conserved disulfide bridge involving C3.25 falls in the C-terminal portion of E2, whereas in the bovine and squid rhodopsin structures, it falls almost in the middle of the loop.

In the CXCR4 structure, an additional disulfide bridge is formed between C28 in the N-term and C274 in E3, whereas $A_{2A}R$, D_3R, and H_1R share an additional intraloop disulfide bridge in E3.

In summary, in contrast to rhodopsin, in which the extracellular regions form a compact folded unit, in nonopsin GPCRs, these regions make limited contacts between each other (Figure 17); moreover, the N-term seems to be an element of structural instability for nonopsin GPCRs, rather than a part of the stability core like in (rhod)opsins. These data are in line with the hypothesis that the extracellular region of the βARs has evolved to allow access to the ligand binding site.[309]

As for the ligand−receptor binding modes, as expected, the salt bridge between the protonated nitrogen atom of the ligands and D3.32 is shared by all the crystallographic complexes involving the GPCRs of the amine subfamily (Figures 11, 12, and 15).

Table 3. Sequence Percent Identity Compared with Cα-RMSDs (Å)[a]

	1U19	3CAP	2HR1	2VT4	3EML	3ODU	3PBL	3RZE
bovine rhodopsin (1U19)	100% 0.00 Å	100% 2.03 Å	22% 1.95 Å	21% 2.01 Å	23% 2.30 Å	23% 2.36 Å	29% 1.68 Å	20% 1.98 Å
bovine opsin (3CAP)		100% 0.0 Å	22% 2.25 Å	21% 2.39 Å	23% 2.58 Å	23% 2.75 Å	29% 2.32 Å	20% 2.14 Å
human β_2AR (2RH1)			100% 0.0 Å	68% 0.54 Å	35% 1.95 Å	26% 2.60 Å	40% 1.37 Å	38% 1.53 Å
turkey β_1AR (2VT4)				100% 0.0 Å	38% 2.00 Å	26% 2.72 Å	37% 1.40 Å	38% 1.71 Å
human $A_{2A}R$ (3EML)					100% 0.0 Å	22% 2.71 Å	34% 1.56 Å	35% 2.04 Å
human CXCR4 (3ODU)						100% 0.0 Å	25% 2.15 Å	27% 2.25 Å
human D_3R (3PBL)							100% 0.0 Å	36% 1.40 Å
human H_1R (3RZE)								100% 0.00 Å

[a] Sequence identities concern the aligned seven helices, i.e., the following segments (numbered according to the numbering scheme by Ballesteros and Weinstein): 1.33−1.59, 2.38−2.66, 3.22−3.45, 4.39−4.62, 5.36−5.61, 6.30−6.60, and 7.32−7.53. Cα-RMSDs (Å) were computed on the same amino acid segments. Pairwise comparisons involving theD_3R structure start from 1.35 as the amino acids 1.33 and 1.34 were not resolved.

dx.doi.org/10.1021/cr100437t |*Chem. Rev.* 2011, 111, PR438–PR535

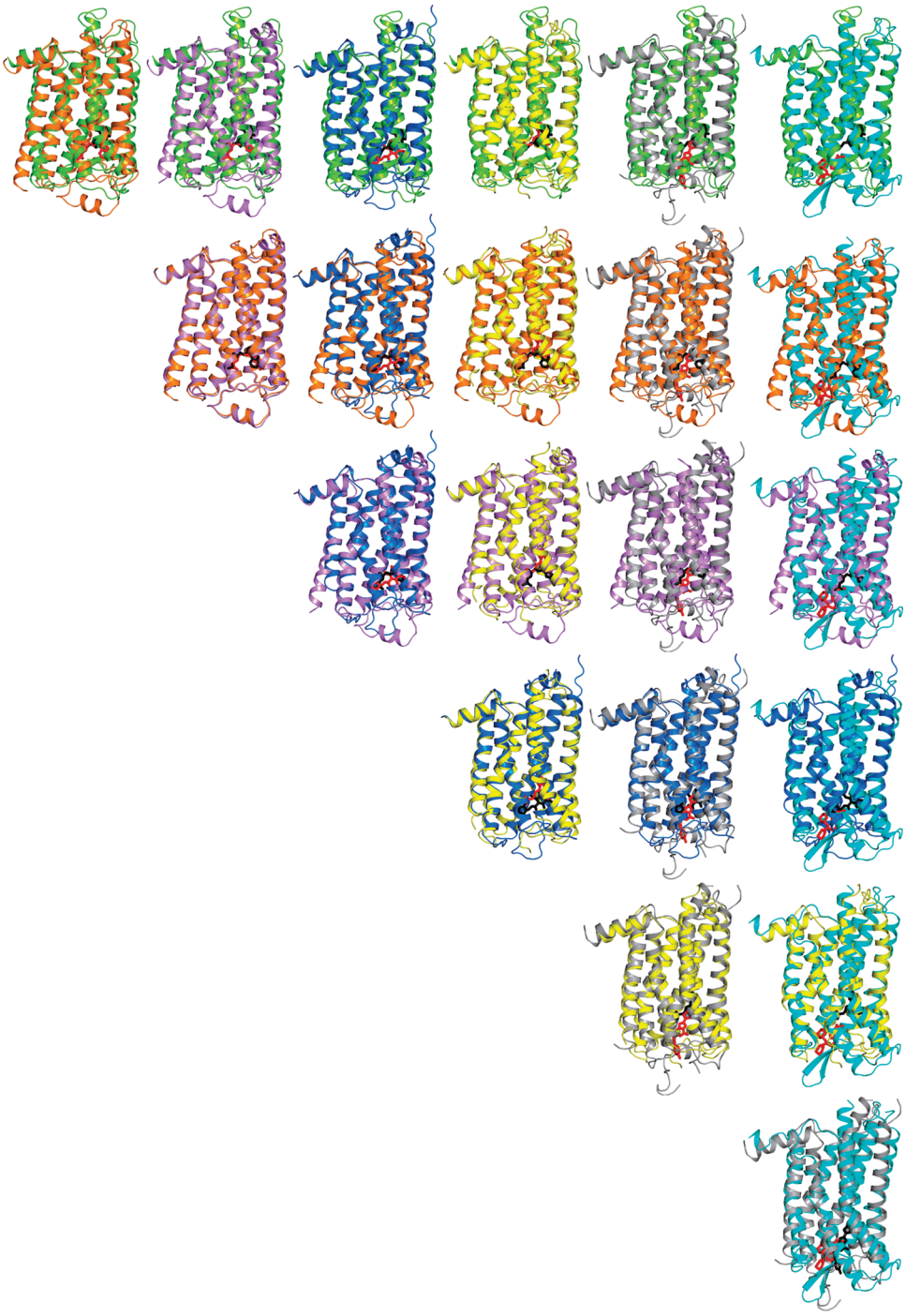

Figure 16. Comparisons of selected GPCR crystal structures. The pairwise structural superimpositions of rhodopsin (PDB code 1U19, yellow−green),[92] β_2AR (PDB code 2RH1, orange),[94] β_1AR (PDB code 2VT4, violet),[95] D_3R (PDB code 3PBL, blue),[112] H_1R (PDB code 3RZ3, yellow),[113] A_{2A}R (PDB code 3EML, gray),[103] and CXCR4 (PDB code 3ODU, cyan)[111] are shown. The structural models are seen in a direction parallel to the membrane surface, the intracellular side being at the top. Rigid body fit concerned the Cα-atoms of the seven helices, i.e., the following segments (numbered according to the numbering scheme by Ballesteros and Weinstein): 1.33−1.59 (1.35−1.59 for D_3R), 2.38−2.66, 3.22−3.45, 4.39−4.62; 5.36−5.61, 6.30−6.60, and 7.32−7.53. For each superimposed pair, the ligand bound to the fixed protein is black, whereas that bound to the mobile protein is red.

Structure comparisons of the different β_1AR and β_2AR complexes show that the ligand binding site of these receptors can accommodate with very minor local structural rearrangements compounds holding different chemical and pharmacological properties (Figures 11C,D and 12C,D). Moreover, the ligand binding sites of the two ARs are the same (Figure 16). They involve amino acid side chains from H3, H5, H6, H7 and, to a lower extent, E2. The aliphatic chain of the βAR ligands overlaps with the C9−C11 atoms of retinal; in contrast, the extreme heterocyclic moiety shared by all the βAR ligands is more shifted toward the extracellular side compared to the β-ionone ring of retinal, therefore, it does not interact with the conserved W6.48 (Figures 11 and 12). In general, such a moiety makes van der Waals

dx.doi.org/10.1021/cr100437t |*Chem. Rev.* 2011, 111, PR438–PR535

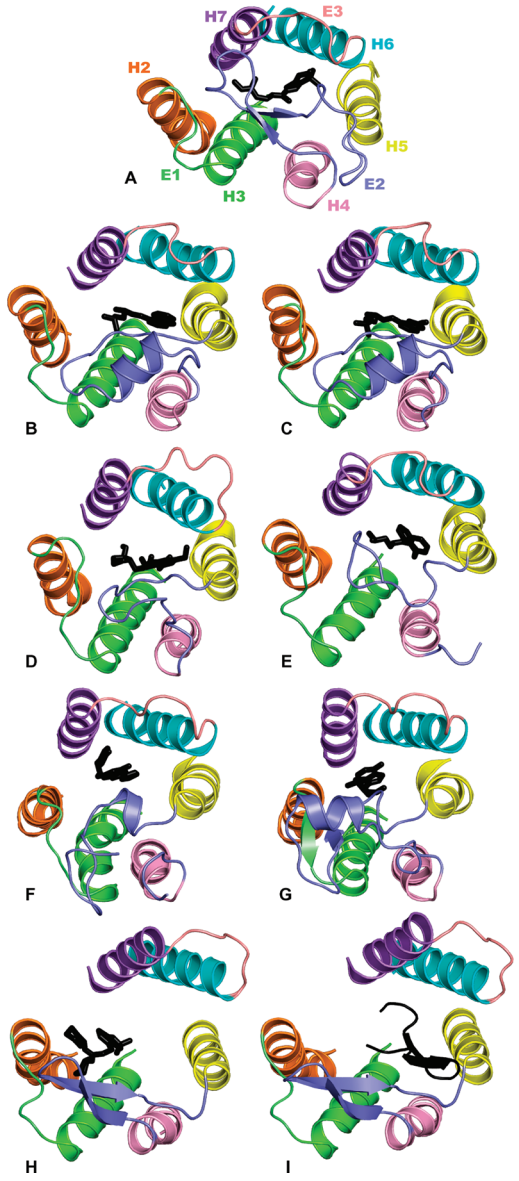

Figure 17. Extracellular regions of selected GPCRs. The receptors are seen from the extracellular side in a direction perpendicular to the membrane surface. The following crystallographic complexes are shown: (A) rhodopsin bound to 11-*cis*-retinal (PDB code 1U19),[92] (B) β_2AR bound to the partial agonist carazolol (PDB code 2RH1),[94] (C) β_1AR bound to the antagonist cyanopindolol (PDB code 2VT4),[95] (D) D_3R bound to the antagonist eticlopride (PDB code 3PBL),[112] (E) H_1R bound to the antagonist doxepin (PDB code 3RZ3),[113] (F) A_{2A}R bound to the antagonist ZMA (PDB code 3EML),[103] (G) A_{2A}R bound to the agonist adenosine (PDB code 2YDO),[104] (H) CXCR4 bound to the small antagonist IT1t (PDB code 3ODU),[111] and (I) CXCR4 bound to the cyclic peptide CVX15 (PDB code 3OE0).[111] Only the extracellular halves of the helices bridged by E1, E2, and E3 are shown. Ligands are represented as blue sticks.

interactions with Y5.38, S5.42, S5.46, and F6.52 as well as van der Waals or H-bonding interactions with N6.55. The latter is conserved in the A_{2A}R, playing a relevant role in ligand binding (Figure 13). Of the three binding side serines in H5 conserved in those GPCRs that recognize catecholamines, S5.42 seems to be the one deputed to make signaling-productive H-bond(s) with the βAR agonists.

As expected, the binding site of eticlopride in the D_3R is very similar to those of the βARs (Figures 11, 12, 15, and 16). In contrast, the H_1R antagonist doxepin overlaps with retinal, being more internalized compared to the βAR and D_3R ligands (Figures 11, 12, 15, and 16). The tricyclic extremity of such ligand, indeed, interacts with W6.48, similar to the β-ionone ring of retinal (Figures 2, 15, and 16).

Whereas the main axis of retinal as well as of the βAR, D_3R, and H_1R ligands is almost parallel to the membrane surface, that of the A_{2A}R antagonist and agonists is almost perpendicular to the membrane surface (Figures 2, 4, 11−13, and 16). Collectively, the A_{2A}R ligands are more shifted toward the extracellular side compared to the ligands of rhodopsin, βARs, D_3R, and H_1R. Structure-driven site directed mutagenesis of the A_{2A}R suggested that F168(5.29), E169(5.30), N253(6.55), and L249(6.51) play a central role in coordinating the bicyclic core present in both agonists and antagonists.[314] Comparisons of adenosine receptor sequences from different species led to prediction that the interactions that determine subtype selectivity reside in the more divergent "lower" region (i.e., more extracellular, according to our graphics representations) of the binding cavity, while the "upper" part of the binding cavity is conserved across the adenosine receptor subtypes.[314] Consistent with these inferences, the crystallographic structures show that, whereas the common bicyclic core of functionally different A_{2A}R ligands docks in the same site and in the same mode, the variable extremities make different contacts with the extracellular loops (Figure 13).[103−105]

Different from the binding modes of rhodopsin, βAR, D_3R, H_1R, and A_{2A}R ligands, in the CXCR4, the IT1t ligand occupies a part of the pocket defined by side chains from H1, H2, H3, and H7, making no contacts with H4, H5, and H6 (Figure 14). The nitrogens of the symmetrical isothiourea group are both protonated, one of them (N4) forming a salt bridge with the D97(2.63). An alternative salt bridge involving the N3 nitrogen cannot be precluded.[111] Both cyclohexane rings fit into small subpockets and so make hydrophobic contacts with the CXCR4. Connected by a short flexible linker, the imidazothiazole ring system is the only part of the ligand that contacts H7, in particular through the formation of a salt bridge between the protonated imidazothiazole N1 and E288(7.39) (Figure 14). In the CXCR4−3−CVX15 complex, the bulky 16-residue ligand fills most of the binding-pocket volume (Figure 14). The peptide forms a disulfide-stabilized (Cys4 to Cys13) β-hairpin, with D−P8-P9 at the tip of the turn exposed to the extracellular milieu. The N-terminal part of the CVX15 backbone (i.e., from R1 to C4) forms H-bonds with the backbone of the residues D187−Y190 in E2, adding a partial third strand to the E2 β-hairpin. The core-specific interactions are formed by two arginines at the peptide N-term: (a) R1, which makes polar interactions with D187, and (b) R2, which interacts with T117(3.33) and D171(4.60) and may form an additional H-bond with H113(3.29), depending on its protonation state. Another arginine, R14, makes a salt bridge with D262(6.58). Finally, the C-terminal D-proline is buried in the pocket next to the N-term of the peptide and so makes a water-mediated interaction with the side chain of D288(7.39). The small-molecule and peptide ligand binding sites substantially overlap with minor conformational changes in the receptor structures (Figure 14).

Collectively, interhelix packing interactions in the extracellular halves of the helix bundle differ among the GPCRs solved so far, whereas those in the intracellular halves are more similar as they involve a number of highly conserved amino acids like N1.50, D2.50,

W4.50, Y5.58, F6.44, W6.45, N7.45, and the members of the E/DRY and NPxxY motifs. The βARs, D_3R, H_1R, and $A_{2A}R$ share some similarities in the highly conserved amino acids, which differ from rhodopsin. First of all, in these nonopsin GPCRs: (a) an asparagine substitutes for the serine found in rhodopsin at position 7.45; (b) similar to squid rhodopsin, Ops*,[107] MII,[110] and the constitutively active E113Q rhodopsin mutant,[109] Y5.58 is directed toward the helix bundle instead of the membrane like in dark bovine rhodopsin; and (c) the Y7.53−F8.50 pair points toward H2 instead of H1 (Figures 2, 11−13, 15). The CXCR4 shows some structural singularities concerning the highly conserved amino acids in the cytosolic halves. These include the presence of a histidine at position 7.45 and the lack of interaction between Y7.53 and the phenylalanine of the NPxxY(x)$5_{,6}$F conserved motif.

3.3. Structural Features of the Inactive and Active States: The E/DRY Motif and the Arrangements of the Cytosolic Regions

As stated above, the crystal structures of the inactive and signaling active states of rhodopsin show clear differences in the cytosolic regions, including the interaction pattern of the E/DRY arginine.[107,109,110,122] Indeed, the double salt bridge found in dark rhodopsin between R3.50 and both E3.49 and E3.60 is broken in the active forms, and this is associated with a significant outward motion of H6 and the opening of a cytosolic crevice instrumental for transducin binding (Figures 7 and 8).

Different from rhodopsin, which remains the only "native" ligand-bound GPCR structure determined to date, the crystal structures of nonopsin GPCRs cocrystallized so far with functionally different ligands show significant ambiguities concerning the structural hallmarks of the inactive and active states. This may be due, at least in part, to possible artifacts linked to the stabilization strategies as well as to the intrinsic instabilities of the active states. As an example, it has been hypothesized that the crystal structure of the β_2AR represents an active-like state due to the increased basal activity by the T4L, not completely dropped by the inverse agonist.[305,315−317]

As for the features of the inactive states, i.e., inferred from the structures co-crystallized with antagonists or inverse agonists, the D3.40−R3.50 salt bridge is shared by all the structures solved so far except for the H_1R−doxapin complex. In contrast, the interhelical salt bridge with E6.30, the "ionic lock", is present only in the D_3R−eticlopride complex (Figure 15)[112] as well as in selected chains of very recent crystallographic structures of the β_1AR in complex with the antagonists cyanopindolol, iodocianopindolol, and carazolol.[98] In detail, the "ionic lock" is present in both chains of the β_1AR−cyanopindolol crystals (PDB code 2YCX, 3.25 Å), whereas it is present only in chain A of the β_1AR−carazolol crystals (PDB code 2YCW, 3.00 Å; Figure 12E, F) and in chain B of the β_1AR−iodocyanopindolol crystals (PDB code 2YCZ, 3.65 Å). The presence of such lock in selected chains of the β_1AR crystals is favored by a bent of the cytosolic end of H6 toward H3, which has been interpreted as a distinct conformational state of the antagonist-bound forms of the receptor (Figure 12E,F).[98] However, even in the bent state, the distance between R3.50 and E6.30 is longer and the electrostatic interaction is consequently weaker than in the dark rhodopsin structure; this feature was supposed to be related to the higher basal activity of the β_1AR compared to rhodopsin.[98]

The lack of the "ionic lock" in most of the antagonist-bound forms of nonopsin GPCRs as well as in the CXCR4 structures, in which a lysine substitutes for the glutamate/aspartate at position 6.30, opened the question whether such lock is really a feature of the inactive states and a switch of activation in these receptors. Collectively, sequence comparisons,[150] structure determination of selected nonopsin GPCRs,[93−96,103,111] and recent in vitro experiments on rhodopsin converge on the indication that the E/D3.49−R3.50 salt bridge is a more important switch of GPCR activation than the interhelical R3.50−E/D6.30 interaction. Early computational experiments on the 5-HT_{1A} serotonin receptor, indeed, showed that in the empty form of the receptor, the D3.49−R3.50 intra-DRY salt bridge is more stable than the "ionic lock", as the former was persistent during the whole simulation time, whereas the latter was alternately lost and gained.[138] Recent MD simulations on the crystal structures of the β_1AR and β_2AR[318−321] as well as of the $A_{2A}R$[322−324] suggest that the "ionic lock" reforms during the simulation time. However, sufficiently long simulations on the β_2AR show that it reforms and breaks,[318,320] suggesting the existence of equilibrium states characterized by the presence and the absence of the lock. The probability of occurrence of the "ionic lock" was computed in the carazolol, timolol, and the agonist-bound states of β_2AR by means of the side chain reassignment program SCREAM.[325325] The study showed that both the carazolol- and timolol-bound forms hold a finite population of side chain conformations with the "ionic lock".

In summary, whereas the R3.50−E6.30 salt bridge is a feature of selected inactive states, the intra-E/DRY ion pair is likely a common feature to the majority of the inactive states visited by the receptor structure. This remarks the role of such interaction, but not of the "ionic lock", as a universal marker of the inactive states.

The agonist-bound forms of nonopsin the GPCRs show even higher inconsistencies compared to the antagonist-bound ones. This is particularly true for the β_1ARs bound to the agonists carmoterol and isoprenaline, which are quite similar to the antagonist-bound forms (i.e., the Cα-RMSDs between the 2VT4 structure and 2Y00, 2Y02, and 2Y03 is 0.65, 0.71, and 0.67 Å, respectively; Figure 12C,D). The same holds for the β_2AR bound to the antagonist alprenolol and to an irreversibly bound agonist (i.e., the Cα-rmsd between the 3NYA and 3PDS structures is 0.63 Å). These significant similarities between antagonist- and agonist-bound structures suggest that the latter do not represent the signaling active states of the βARs. This hypothesis is supported by the fact that the cocrystallization with a camelid antibody fragment (nanobody, NB80) showing G protein-like behavior toward the β_2AR (PDB code 3P0G) was necessary to stabilize the BI-167107 agonist-bound active state of the β_2AR.[99] Indeed, in the agonist−β_2AR−NB80 ternary complex, the nanobody docks in between the cytosolic extensions of H3 and H6, favoring an outward displacement of H6 in line with the one observed in the Ops* structure (Figures 7 and 11E−G). An even higher H6 displacement is observed in the more recent crystal structure of the agonist−β_2AR−Gs complex (PDB code 3SN6, 3.20 Å). We recall that such displacement is absent in the agonist−β_2AR complex (Figure 11). The G protein mimic propensity of NB80 is consistent with the evidence that its binding site in the β_2AR overlaps with that of the Gs C-terminus (GsCt)[100] In the complexes with NB80 or Gs, different from all the other ligand-bound forms of the β_2AR, the intra-DRY salt bridge is weakened because R3.50 is involved in interaction with the nanobody or the G protein. This would suggest that neutralization of D3.49, as in Ops*, and/or intermolecular-interaction with a G protein or a G protein mimic, like the nanobody, is necessary to destabilize such a strong intrahelix interaction. In line with this inference, all the agonist-bound forms of the A_2AR retain the D3.49−R3.50 interaction found in the antagonist-bound structure (Figure 13B,C,E,G). Peculiar to these structure is the approaching of the cytosolic half of H7 to H3 (marked by the

interaction between Y7.53 and R3.50) and the reciprocal approaching of the cytosolic halves of H5 and H6 (Figure 13D,E).

Collectively, the advancements in the crystal structures of non-opsin GPCRs strengthen the role of the intra-E/DRY salt bridge as a marker of the inactive states, highlighting the frailty of the "ionic lock". The cocrystallization with G protein or G protein-like proteins seems to be necessary to get high resolution information on the signaling active states of these receptors.

4. COMPUTATIONAL APPROACHES TO GPCR MODEL BUILDING

4.1. GPCR Databases, Web Servers, and Sequence-Based Predictors

Modeling of GPCRs has enormously profited from the availability of molecular class-specific databases capable of dealing with highly heterogeneous data on these receptors. The G protein-coupled receptor database (GPCRDB; http://www.gpcr.org/7tm/) is a molecular-specific information system (MSIS) for GPCRs aimed at the collection and dissemination of GPCR related data.[326−329] It holds sequences, mutant data, and ligand binding constants as primary experimental data. Mutation data within the GPCRDB (http://www.gpcr.org/7tm/mutation/) are automatically extracted from the scientific literature.[330] In detail, the mutation data extracted from the literature are validated by plausibility filters and integrated into the corresponding molecular class-specific information system, where they are combined with structural and sequence information already stored in the database.[330] The GPCRDB is linked to the SWISS-PROT protein sequence database (http://www.expasy.ch/sprot/sprot-top.html), to the Olfactory Receptor DataBase (http://senselab.med.yale.edu/senselab/ORDB/), specializing in olfactory receptors, and to the GRAP and tinyGRAP mutant databases.[331] The GRAP database allows searches for specific amino acid substitutions in specific proteins within user-specified groups of receptors.[332−335] The database also contains searchable information on quantitative ligand-binding data and qualitative descriptions of the effect of the mutation on agonist binding and signal transduction. The GRAP database has not been updated recently. Mutant database development moved on to the tinyGRAP database, which holds only the most basic information on the receptor type, literature reference, and mutant type (http://www.cmbi.ru.nl/tinygrap/credits/).[332−335]

Computationally derived data such as multiple sequence alignments, 3D models, phylogenetic trees, and two-dimensional (2D) visualization tools are added to the GPCRDB to enhance the database usefulness. The GPCRDB is also linked to a fingerprint database that determines if a given query sequence belongs to one of the characterized superfamilies, families, or receptor subtypes (http://www.biochem.ucl.ac.uk/bsm/dbbrowser/GPCR/). Another bioinformatics tool useful for GPCR modeling through the GPCRDB is the Viseur program, which allows one to interactively visualize and/or modify amino acid sequences, TM areas, alignments, models, and results of mutagenesis experiments in an integrated environment.[336] The GPCRDB is also linked to the SWISS-MODEL server for the automated modeling of the TM helix bundle of GPCRs (http://swissmodel.expasy.org//SWISS-MODEL.html).[337] Very recently, the developers of the GPCRDB have created the MSIS for GPCR Interacting Partners (G proteins and RAMPs), the GPCRIPDB (http://www.gpcr.org/GPCRIP/). Since recently, the GPCRDB is linked also to the GPCR-Oligomerization Knowledge Base (GPCR-OKB). GPCR-OKB is a system that supports browsing and searching for GPCR oligomer data (http://www.gpcr-okb.org).[338,339] Another link to the GPCRDB is the natural variants (NaVa) database (http://nava.liacs.nl) that integrates data on natural variants in human GPCRs from online databases, the scientific literature, and patents.[340]

The SSFA-GPHR database (http://www.ssfa-gphr.de/) provides a comprehensive set of mutation data for the GPHR.[341] Moreover, it provides a platform for comparison and investigation of these homologous receptors and helps in understanding protein malfunctions associated with several diseases.

In the context of GPCR classification, a number of predictors proved high accuracy.[342−347] Among them, a support vector machine (SVM)-based method, GPCRpred, has recently been developed for predicting families and subfamilies of GPCRs from the dipeptide composition of proteins.[342] The method classified GPCRs and non-GPCRs with an accuracy of 99.5% when evaluated using 5-fold cross-validation. The method is also able to accurately classify GPCRs. A server for recognition and classification of GPCRs based on multiclass SVMs has been set up at http://www.imtech.res.in/raghava/gpcrpred.[342] The other web-server predictor is GPCR-CA (http://218.65.61.89:8080/bioinfo/GPCR-CA), where "CA" stands for "cellular automaton".[344] GPCR-CA is a two-layer predictor: the first layer prediction engine serves to identify a query protein as GPCR or non-GPCR; if the protein is a GPCR, the process automatically continues with the second-layer prediction engine to further identify the type among the following six functional classes: (a) rhodopsin-like, (b) secretin-like, (c) metabotropic/glutamate/pheromone; (d) fungal pheromone, (e) cAMP receptor, and (f) frizzled/smoothened family. The overall success rates by the predictor for the first and second layers are over 91% and 83%, respectively. Finally, a three-layer SVM-based predictor of GPCR classes has been recently presented as being more accurate than GPCRpred and GPCR-CA.[345] A hidden Markov model (HMM) of GPCR (GPCRHMM) sequences was generated to detect remote homologues.[347] The method was benchmarked to profile HMMs and generic TM detectors on sets of known GPCRs and non-GPCRs. GPCRHMM model was used to search for novel members of the GPCR superfamily in five proteomes, overall detecting 120 sequences that lack annotation and are potentially novel GPCRs. The GPCRHMM server is available at http://gpcrhmm.cgb.ki.se.[347] Other recent GPCR classification methods are based on principal component analysis (PCA) and can be accessed via WEB server (http://www1.spms.ntu.edu.sg/~chenxin/PCA_GPCR).[346] The GPCR-MPredictor is a web predictor that can efficiently classify GPCRs at five levels (http://111.68.99.218/gpcr-mpredictor/).[348] The first level determines whether a protein sequence is a GPCR or a nonGPCR. If the predicted sequence is a GPCR, then it is further classified into family, subsubfamily, and subtype levels.

A list of the URLs for sequence-based classification of GPCRs is also provided and critically discussed in ref 349.

A translational web-application is now available (http://www.ssfa-gphr.de)[350] that facilitates the interactive linkage of functional and structural data on naturally occurring gain- or loss-of-function mutations, with focus on the human GPHRs, for which a huge number of mutations are known to cause diseases. Functional data are converted into relational percentage values, allowing the comparison and classification of data from different GPHR subtypes and different experimental approaches.[350]

A database extremely useful for the study of G protein−GPCR interactions (Human-gpDB) has recently been set up with a

Table 4. GPCR Databases and Servers

name	URL	ref
	Databases	
GPCRDB	http://www.gpcr.org/7tm/	326−329
	http://www.gpcr.org/7tm/mutation/	330
	http://www.cmbi.ru.nl/tinygrap/credits/	332−335
GPCR pattern recognition	http://www.biochem.ucl.ac.uk/bsm/dbbrowser/GPCR/	
GPCRIPDB	http://www.gpcr.org/GPCRIP/	
GPCR-OKB	http://www.gpcr-okb.org/	338,339
NaVa	http://nava.liacs.nl/	340
GPHR database	http://www.ssfa-gphr.de/	350
human-gpDB	http://bioinformatics.biol.uoa.gr/human_gpdb/	351,352
reactome	http://www.reactome.org/	354
RINGdb	http://ringdb.csie.ncu.edu.tw/ringdb/	355
GLIDA	http://gdds.pharm.kyoto-u.ac.jp:8081/glida	356
GPCRRD	http://zhanglab.ccmb.med.umich.edu/GPCRRD	362
GRIPDB	http://grip.cbrc.jp/GDB/index.html	353
SSFA-GPHR	http://www.ssfa-gphr.de/	341
	Servers	
GPCRpred	http://www.imtech.res.in/raghava/gpcrpred	342
GPCR-CA	http://218.65.61.89:8080/bioinfo/GPCR-CA	344
GPCRHMM	http://gpcrhmm.cgb.ki.se	347
PCA_GPCR	http://www1.spms.ntu.edu.sg/~chenxin/PCA_GPCR	346
SNAP	http://cubic.bioc.columbia.edu/services/SNAP/	360
GPCR-SSFE	http://www.ssfa-7tmr.de/ssfe/	363
GPCR-MPredictor	http://111.68.99.218/gpcr-mpredictor/	348

focus on G proteins and their coupling specificity with GPCRs (http://bioinformatics.biol.uoa.gr/human_gpdb/).[351,352]

The G protein-coupled Receptor Interaction Partners DataBase (GRIPDB) provides information about GPCR oligomerization (http://grip.cbrc.jp/GDB/index.html).[353] The entries in the database are divided into two sections: (i) "experiment information" section and (ii) "prediction information" section. The "experiment information" section contains (a) experimentally indentified GPCR oligomers and their annotations, and (b) experimentally suggested interfaces for the oligomerization. The experimentally suggested or computationally predicted interfaces are displayed by 3D graphics, using GPCRs with available coordinates.

The human biological pathways and processes are collected into the reactome open-source freely available database (http://www.reactome.org).[354] Within this database, the reactome GPCR pathway provides a template for the orthology-based inference of GPCR reactions for diverse model organism species, and can be overlaid with protein−protein interaction and gene expression data sets to facilitate overrepresentation studies and other forms of pathway analysis.

RINGdb is a novel integrated biological database that provides comprehensive and organized information on Regulators of G protein signaling (RGSs) and GPCRs (http://ringdb.csie.ncu.edu.tw/ringdb/).[355] It contains information on mutations, tissue distributions, protein−protein interactions, diseases/disorders and other features, and offers various userfriendly query functions to answer different questions on the possible relationship between RGS and GPCRs as well as on their contribution to disease processes.

GPCR-LIgand Database (GLIDA) (http://gdds.pharm.kyoto-u.ac.jp:8081/glida) is a novel public GPCR-related chemical genomic database that is primarily focused on the correlation of information between GPCRs and their ligands.[356] It provides correlation data between GPCRs and their ligands, along with chemical information on the ligands, as well as access information to the various web databases regarding GPCRs. GLIDA includes structure similarity search functions for the GPCRs and for their ligands, being able to provide correlation maps linking the searched homologous GPCRs (or ligands) with their ligands (or GPCRs), useful tools for drug design efforts.

A recent study presented a classification of GPCRs that is purely based on their ligands, complementing sequence-based phylogenetic classifications of these receptors.[357] Targets were hierarchically classified into phylogenetic trees, for both sequence space and ligand (substructure) space. The study highlighted potential cross-reactivity of GPCR ligands and was suggested as useful for the design of new ligands with the desired activity profiles. The method proved to have drug design and GPCR deorphanization potentials.[357]

In a chemogenomic analysis, the alignment of 369 TM sequences of nonolfactory GPCRs led to the identification of 30 conserved residues supposed to line the ligand binding cavity of ground-state receptors.[358] A TM cavity could be found for all investigated GPCRs with physicochemical properties matching that of their cognate ligands, which permits to easily detect key residues that drive ligand selectivity or promiscuity. Along this line, the ss-TEA method makes an entropy-based identification of receptor-specific ligand binding residues from a multiple sequence alignment of class A GPCRs.[359] The method is also available online via GPCRDB at http://www.gpcr.org/7tm/.

Single nucleotide polymorphisms (SNPs) represent a very large portion of all genetic variations. SNPs are either "neutral" in the sense that the resulting point-mutated protein is not functionally discernible from the wild-type, or they are "non-neutral" in that the mutant and wild-type differ in function.[360] A challenge in GPCR research is discriminating non-neutral SNPs, which may have pathologic effects, from wild type-like SNPs. A neural network-based method, SNAPs, was developed, which uses in silico derived protein information (e.g., secondary structure, conservation, solvent accessibility, etc.) to predict the functionality of mutated proteins.[360] SNAP needs only sequence information as an input, but benefits from functional and structural annotations, if available. In a cross-validation test on over 80000 mutants, SNAP identified 80% of the non-neutral substitutions at 77% accuracy and 76% of the neutral substitutions at 80% accuracy. The method was challenged in an in silico mutagenesis study on the human melanocortin 4 receptor (hMC4R), which is particularly susceptible to spontaneous mutations many of which implicated in obesity.[361] The study consisted in a complete in silico mutagenesis experiment to assess all possible non-native point mutants in the entire hMC4R protein (332 residues). The authors compiled a mutability score

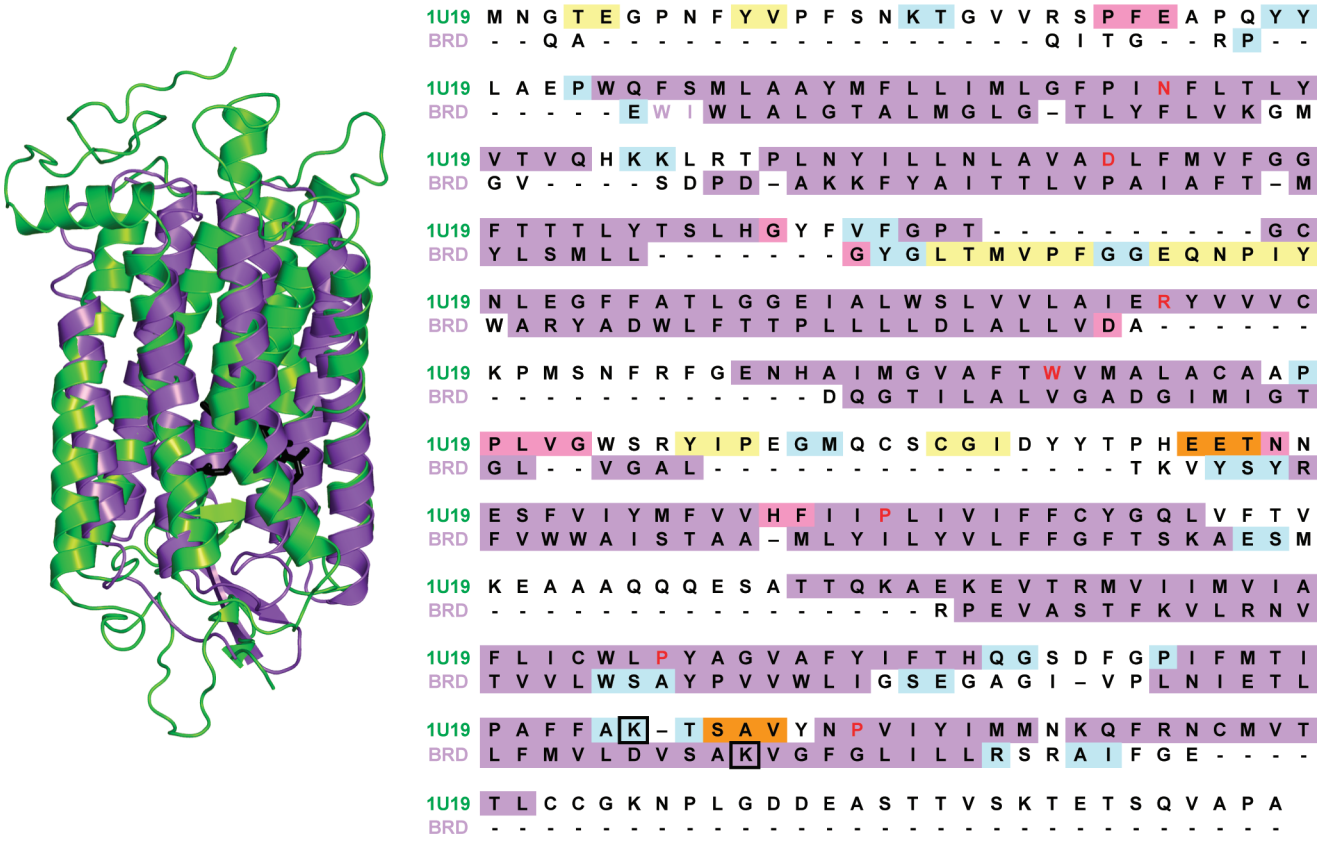

Figure 18. (left) Cartoons of the superimposed structures of rhodopsin (1U19, in yellow−green)[92] and of BRD (PDB code 1BRR, violet).[422] The retinal molecules are also shown by black sticks. (right) Sequence alignment which results from the α-carbon atom fit shown on the left side. In this alignment, color highlights indicate the secondary structure computed on the superimposed crystal structures of the two proteins. In detail, violet means canonical α-helices, and yellow stands for strand, whereas cyan, orange, and pink indicate respectively types 3-, 4-, and 5-turns. Black boxes enclose the lysine residues covalently linked to retinal in both the photoreceptors. As for the rhodopsin sequence, the most conserved amino acids in each TM helix are colored in red. Drawings were done by means of the software PYMOL 0.97 (http://pymol.sourceforge.net/).

that reflects the degree to which a particular residue is likely to be functionally important. The results were generally consistent with available in vitro experimental annotations and led to prediction of 12 functionally important amino acids in hMC4R not yet validated by in vitro experiments. SNAPs is available as a WEB server at http://cubic.bioc.columbia.edu/services/SNAP/.

The G Protein-Coupled Receptor Spatial Restraint Database (GPCRRD) (http://zhanglab.ccmb.med.umich.edu/GPCRRD/) was designed to systematically collect all experimental restraints (including residue orientation, contact and distance maps) available from the literature and primary GPCR resources using an automated text mining algorithm combined with manual validation.[362] The main purpose is to assist GPCR 3D structure modeling and function annotation. The current data set contains thousands of spatial restraints from mutagenesis, disulfide-mapping distances, electron cryomicroscopy and FTIR spectroscopy experiments.

The GPCR-SSFE database (http://www.ssfa-7tmr.de/ssfe/) stores the template predictions, sequence alignments, identified sequence and structure motifs, and homology models for 5025 family A GPCRs.[363] Users can browse the GPCR data set according to their pharmacological classification or search for results using a UniProt entry name. It is also possible for a user to submit a GPCR sequence that is not contained in the database for analysis and comparative model building. The models can be viewed using a Jmol applet and are also available for download along with the alignments.

All the URLs presented in this section are listed in Table 4.

4.2. Comparative Modeling Using the Bacteriorhodopsin Structure as a Template

A high resolution structure of the light-driven proton pump from *Halobacterium halobium* bacteriorhodopsin (BRD) has been available since 1990.[364] Since BRD possesses seven TM α-helices and binds the retinal chromophore, it has been considered a bacterial homologue of vertebrate rhodopsin. Reports concerning comparative modeling of GPCRs using the BRD structure as a template have appeared in the years that preceded the release of the first electron density 2D map of rhodopsin,[12,365−375] in the years between the releases of the first 2D and the first 3D electron density maps of rhodopsin,[12,15,376−398] in the years between the releases of the 3D map and of the crystal structure of rhodopsin,[16,399−406] and even in the years after the release of the rhodopsin crystal structure.[407−410] However, BRD is a proton pump, is not coupled to a G protein, and does not even display remote sequence similarity with any GPCR. Two hypotheses were made to demonstrate the existence of a link between GPCRs andBRD.[411,412] One of these hypotheses was formulated by Pardo and co-workers, who suggested that the sequence homology in the helical region of BRD and GPCRs would be greater if the sequential ordering of the helices is ignored.[411] The authors, hence, proposed a mismatch of the helices, in which BRD H2, H3, H4, H5, H6, and H7 matched, respectively, with GPCR H4, H5, H6, H1, H2, and H3. Such a mismatch between BRD and GPCR sequences was suggested to

dx.doi.org/10.1021/cr100437t |*Chem. Rev.* 2011, 111, PR438–PR535

be caused by an exon shuffling event that occurred during the evolution of GPCRs and BRD from a common ancestor.[411] The second hypothesis suggests that H5, H6, and H7 originated from H1, H2, and H3 as a result of ancestral gene duplication, leading to homologies between helices H1, H2, and H3 in BRD and helices H5, H6, and H7 in GPCRs.[412] An alternative helix-mismatching alignment between GPCRs and BRD was obtained by Metzger and co-workers, and this made the authors trust comparative modeling based upon the BRD structure.[413] The authors, indeed, built a model of the κ opioid receptor, which has been used in computational experiments until recently.[404,408,414,415] Sequence analysis studies led, however, to the conclusion that there is no significant evidence for similarities between BRD and GPCR, regardless of the ordering of the helices, and that, hence, BRD cannot be used as a template for comparative modeling of GPCRs.[416] These conclusions found strong support in the evidence from the first 2D electron density map of rhodopsin at 9 Å resolution, which showed clear differences from the electron density map of BRD resolved at comparable resolution.[12] These structural evidence, combined with the information from alignments of a significant number of GPCR sequences, suggested that GPCRs share a common architecture of the seven helices that differs from that of BRD, strongly underscoring the drawbacks in the use of BRD as a template for the construction of molecular models of GPCRs.[13]

Comparisons of the high resolution structures of BRD and rhodopsin,[92] in fact, confirmed the marked structural dissimilarities between the two photoreceptors, in line with the evidence from the low resolution electron density maps.[12] Indeed, the seven helices differ in length and location of the breakages. Furthermore, loops and tails are completely different in length, amino acid composition, and structure. In line with these data, the sequence alignment obtained from the superimposition of rhodopsin and BRD structures shows mismatches in the seven helices, concerning also the lysines in H7, which are covalently bound to the retinal chromophore in both the photoreceptors (Figure 18). Along the same line, the highly conserved amino acid motifs characterizing family A GPCRs (colored in red in Figures 1 and 18) are not present in BRD. This suggests that, even if proteins may share the same fold even in the absence of any sequencesimilarity,[417,418] BRD is not the proper template for modeling family A GPCRs, including rhodopsin. On the basis of these considerations, any attempt to overcome the drawbacks of using BRD as a template, by first modeling rhodopsin on BRD, then the β_2AR on the rhodopsin model, and finally the target receptor on the β_2AR model, is likely to fail.[384,386−388,394,410] Critical comparisons between a B_2 bradykinin receptor achieved through this approach and a model based upon the rhodopsin structure were, however, unable to distinguish a preference for one of the two models.[410] This could be due to the low resolution of the data employed for evaluating the models. In more recent works, the authors adjusted their original BRD-based models to incorporate high resolution structural information on rhodopsin.[419−421]

In summary, due to the lack of functional, sequence, and structural similarity between rhodopsin and BRD, comparative modeling of GPCRs by using the BRD structure as a template is likely to produce unreliable models and there is no way to change the alignment so as to improve the model. Despite this evidence, BRD has been used as a template for achieving 3D models of GPCRs until very recently and it was even concluded that the receptor model based upon the BRD structure is more consistent with site-directed mutagenesis data than the model based on the crystal structure of rhodopsin.[409] This exceptional conclusion may reflect the inadequacy of low resolution site-directed mutagenesis data for evaluating the reliability of atomistic models.

4.3. Ab Initio Modeling of GPCRs

Because of the lack of a proper homologous template for comparative modeling of GPCRs, various ab initio approaches have been developed for computational modeling of GPCRs (reviewed also in ref 423).

Very early ab initio modeling experiments on the D_2 dopamine, β_2-adrenergic, and 5-HT_2 serotonin receptors led to predictions of either clockwise (when viewed from the extracellular side) or nonsequential helix-packing arrangements, inconsistent with both the BRD and rhodopsin structures.[424−428] Lybrand and co-workers were the most enthusiastic in pursuing their ab initio "clockwise" model.[425,429−434] Their computational modeling approach is summarized as follows. The seven α-helices are built in a canonical conformation, oriented approximately perpendicular to the plane of the bilayer in a continuous bundle arrangement and bundled together, in a way that hydrophobic residues are exposed to the lipids. Then the loops are modeled by restrained MD and added to the helix bundle. Topological and physical properties and low resolution information from site-directed mutagenesis and biophysical studies are used as constraints for helping to reduce the number of helix-bundle candidate structures from about 1500 to only 10−20 structures.[425,429] These best candidate structures are then subjected to energy minimization and MD refinement, leading to the final selection of only one structure, based upon the available experimental data. In the first study, the clockwise helix arrangement was proposed as the most reliable, whereas in successive studies it was always flanked by the "counterclockwise" model.[425,429−434] The necessity of probing both the alternative arrangements was dictated by the author's judgment that the available experimental data were inadequate to drive selection of the proper stereochemistry and that, at least for the β_2AR, the clockwise model appeared to better explain ligand selectivity data.[429] Despite the indications in support of the "counterclockwise model", inferred from computational[13,14,158] and in vitro experiments on several GPCRs,[435−438] the authors recognized the inconsistency of the "clockwise" model only when the first crystal structure of rhodopsin was released.[434] They, however, pursued their ab initio approach, until very recently.[439−442]

One of the most successful approaches to GPCR-structure prediction was that used by Baldwin and co-workers, which consisted of integrating the information from sequence analyses with that from the 3D electron density map of frog rhodopsin and that from biochemical and biophysical experiments on the members of the rhodopsin family.[13,14] This approach led to the building of a Cα-atom model of the seven-helix bundle of rhodopsin and a Cα-atom template for comparative modeling of GPCRs.[14] Retrospective analysis validates Baldwin's model of rhodopsin, as the Cα-rmsd between rhodopsin structure (i.e., 1U19) and the model is 2.96 Å (Figure 19, left). This deviation is due, at least in part, to the regularity of the seven helices in the model, which is different from the crystal structure (Figure 19, left). Indeed, the only helix bend correctly predicted by Baldwin's study was the kink at P267(6.50). The results of Baldwin'sstudies[13,14] and the electron density 2D and 3D maps of rhodopsin[12,15] have been milestones and invaluable sources of information for GPCR modeling in the years that preceded,[443−484] and even in those that followed, the release of the crystal structure of rhodopsin.[485−498] The Baldwin template was used since very recently in a study intended for probing

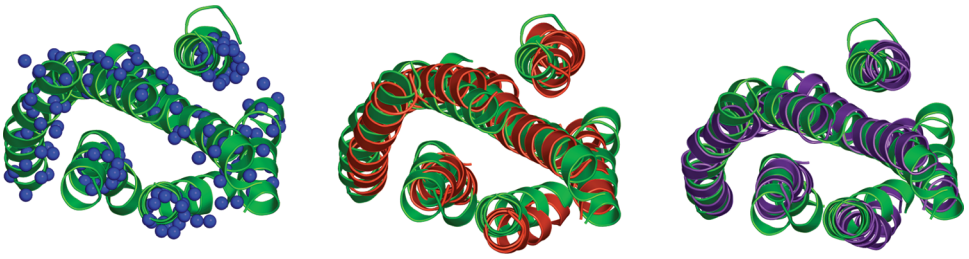

Figure 19. Cartoon representation of the seven-helix bundle and of H8 of the rhodopsin structure 1U19 (yellow−green)[92] superimposed on the computational models by Baldwin and co-workers (left side, in blue),[14] by Herzyk and Hubbard (central panel, in orange),[500] and by Pogozheva and co-workers (right side, in violet).[253] The helix bundles are seen from the intracellular side in a direction perpendicular to the membrane surface. Superimposition between rhodopsin and each of the three computational models has been done on the α-carbons of the following amino acid stretches: 38−63, 71−95, 111−140, 151−175, 204−223, 250−274, and 288−310. The Cα-RMSDs resulting from the three matches shown in the left, central, and right panels are respectively 2.96, 2.91, and 2.68 Å. Drawings were done by means of the software PYMOL 0.97 (http://pymol.sourceforge.net/).

a modification of the Profiles-3D software, REPIMPS. The latter validates and predicts the rotational orientation and vertical position of helices within the helix bundle of individual GPCRs based on the physicochemical properties of amino acids and the surrounding environment. 3D models were built for TM helical segments of 493 GPCRs based on the Baldwin template, and the models were then scored using REPIMPS and Profiles-3D. The compatibility scores increased significantly using REPIMPS because it takes into account the physicochemical properties of the (lipid) environment surrounding the helix bundle. The arrangement of helices in the helix bundle of the 493 models was then altered systematically by rotating the individual helices. For most GPCRs in the set, changes in the rotational position of one or more helices resulted in significant improvement in the compatibility scores. The predicted model of bovine rhodopsin showed a 3.31 Å rmsd from its crystal structure for 198 Cα-atom pairs.[499]

The helical wheel projection models, which were inferred from an earlier Baldwin study,[13] represented the background of our ab initio building of the seven-helix bundles of several GPCRs of the rhodopsin family.[501] The study consisted of probing different helix arrangements by MD and then selecting the average arrangement more consistent with Baldwin's helical wheel projection model and the 2D electron density map of bovine rhodopsin at 9 Å resolution.[12,13,501] These computational experiments, which highlighted the highly conserved polar amino acids as drivers of the helix packing through H-bonding networks, constituted the first step of an iterative procedure, consisting of progressive domain additions and modifications in the receptor model, to incorporate the ever-increasing experimental evidence on rhodopsin and the homologous GPCRs.[502] The preferential targets of the approach were the α_{1b}-adrenergic receptor (α_{1b}AR), the M_1- and M_3-muscarinic receptors, the oxytocin receptor (OTR), and the luteinizing hormone receptor (LHR).[127,128,130,502−513] The last updates of the ab initio models of these receptors held the structural information derived from the electron micrographs of 3D frog rhodopsin crystals[15] and from the last GPCR sequence analysis from Baldwin and co-workers.[14,130,502,510−513]

Weinstein and Ballesteros proposed an ab initio approach to GPCR model building based upon the integration of information about the primary, secondary, and tertiary structural properties of GPCRs as well as inferences from the experimental probing and biophysical analysis of TM proteins.[125]

Alkorta and Loew employed an ab initio approach to model rhodopsin and the δ opioid receptor, consisting of different steps, including (a) multiple sequence alignment, (b) calculation of a variability profile of the aligned sequences, (c) use of the variability profile to identify the boundaries of the TM regions, (d) prediction of their secondary structure, (e) helix bundling, (f) predictions of side chain conformations, and (g) structure refinement.[514,515] Helix packing into a bundle was based on the assumption that helices are packed in a sequential order and in antiparallel fashion except for H1 and H7, that they are all canonical, and that they are all perpendicular to the putative membrane surface.[514,515]

Donnelly and co-workers reported a 3D model of a GPCR based on the helix arrangement observed in the projection structure of rhodopsin.[516,517] The model was created using a method that detects helical periodicity in sequence alignments, using amino acid substitution data derived from protein structures. The method, which also compares the relative directions of the conserved and hydrophobic faces, was first tested on BRD and proved to be successful at orientating the helices. As the method detects the outside face of each helix, the positions of charged residues on this face were used to detect the points at which these helices contact the more polar regions of the phospholipid headgroup/aqueous interface. The projection structure of rhodopsin and the connectivity predicted by Baldwin were also considered in the model building.[516,517] The Cα-rmsd between the rhodopsin model obtained through this approach and available at the GPCRDB (http://www.gpcr.org/7tm) and the rhodopsin structure (i.e., 1U19) is 6.89 Å.

Herzyk and Hubbard developed a rule-based automated method for modeling the structure of the seven TM helices of family A GPCRs.[500] With this method, the structures are generated by using a simulated annealing Monte Carlo (MC) procedure that positions and orients rigid helices to satisfy structural restraints. The restraints are derived from analysis of experimental information from biophysical studies (including electron density maps) on native and mutant proteins, from analysis of the sequences of related proteins, and from theoretical consideration of protein structure. The four main steps in this approach are as follows: (a) analysis of the available experimental and theoretical data to derive geometrical restraints, (b) employment of a protein representation adequate for applying the restraints, (c) construction of a penalty function that efficiently penalizes violations of the restraints, and (d) optimization of the penalty function to find a family of structures that best satisfies the restraints. The method was first validated by generating a model of BRD, characterized by a Cα-rmsd of 1.87 Å, from the structure determined by electron microscopy.[364] Calculations were then carried out by using experimental and theoretical

dx.doi.org/10.1021/cr100437t |*Chem. Rev.* 2011, 111, PR438–PR535

information available for bovine rhodopsin to assign the helices to a projection density map[12,13] and to produce a rhodopsin model useful as a template for comparative modeling of homologous GPCRs.[500] The Cα-rmsd between the TM model of rhodopsin, generated by such a method and available at http://www.gpcr.org/7tm, and the crystal structure of rhodopsin (i.e., 1U19) is 2.91 Å (Figure 19, center). These results validate the approach by Herzyk and Hubbard in its ability to predict the architecture of TM α-helical proteins. Even if the seven helices in the computational model are shorter than those in the rhodopsin structure and are all canonical, the topography of the highly conserved amino acids is quite conserved in the computational model and in the crystal structure. The rhodopsin model by Herzyk and Hubbard has been used as a template for modeling several homologous GPCRs.[518−520] Moreover, this automated approach, implemented in the program PANDA, was used to achieve computational models of different GPCRs of the rhodopsin family, including the melanocortin-1 receptor (MC1-R).[519]

Peitsch and co-workers developed the automated protein modeling server, SWISS-MODEL.[521] With this approach, models are constructed in a two-stage process. In the first stage, the seven TM helices are represented as being idealized and rigid. Structural restraints derived from theoretical and experimental data are then used to fit the helices together. A penalty function is used to measure any violations to the structural restraints. This penalty function is then globally optimized using a MC simulated annealing procedure to generate an optimal model. In the second stage, the optimal model is converted into a full-atom model by the ProMod package.[337] The Cα-rmsd between the rhodopsin model generated by such an automated method and the rhodopsin structure (i.e., 1U19) is 4.52 Å. The SWISS-MODEL server has been widely used to build GPCR models aimed at mapping the ligand binding sites.[522−526]

An elegant and successful approach was that employed by Mosberg's team to predict the architecture of the seven-helix bundle of several GPCRs of the rhodopsin family.[253,527,528] This approach, based on the use of distance restraints, as in calculations of protein structures from NMR spectroscopy data, consists of iterative distance geometry refinements of an approximate initial receptor model, using an evolving system of H-bonds. The rationale for identifying the required constraints is based on the presence of numerous polar residues in the TM hydrophobic α-helices of GPCRs and on the knowledge that polar side chains of proteins buried from water have a strong tendency to form H-bonds.[253] In TM α-helices, backbone peptide groups are already paired, whereas the polar side chains must interact with each other to form intra- or interhelical H-bonds. The H-bonding pairs can be identified from the analysis of sequence alignments as polar residues in TM segments, which appear and disappear in a correlated manner, and by using approximate receptor models to exclude all spatially distant residues from the list of possible correlations. H-bonds thus identified can be applied as distance restraints for the packing of the TM α-helices using the distance geometry algorithm. In detail, the approach consists of the following stages: (a) construction of the initial "crude" receptor model using electromicroscopy and a few site-directed mutagenesis and cross-linking data; (b) calculation of the average seven-helix bundle model for rhodopsin-like GPCRs, by using an iterative distance geometry refinement of the initial model with an evolving system of interhelical side chain H-bonds formed by various GPCRs and collectively applied as distance constraints; and (c) distance geometry calculations of the TM domain of the target receptor from its own H-bonds and using the "average" GPCR model to restrain the relative positions of the helices.[253] The approach was used to build a model of rhodopsin and of 26 rhodopsin-like GPCRs, including the opioid receptors.[253,527,528] Retrospective analysis supports the validity of the approach, as the Cα-rmsd between the rhodopsin model (PDB code 1BOK) and the rhodopsin structure (i.e., 1U19) is 2.68 Å (Figure 19, right). The model 1BOK was used as a template to achieve computational models of the oxytocin and vasopressin receptors.[529]

Another good prediction by Pogozheva and co-workers was that E2 of the opioid receptors would assume a β-hairpin structure that would partially cover the ligand binding cavity between H3 and H7, coming from H4 toward H3 and returning back to H5.[527] The predicted loop also adopts a nonregular structure at its N- and C-terminal extremities. A significant sequence similarity exists concerning this loop between the opioid receptors and rhodopsin, thus suggesting structure similarity. In the rhodopsin structure, E2 adopts a structure similar to that predicted by Pogozheva and co-workers.[16,527] The authors also inferred that both branches of the loop forming a U-like shape are too short to form any additional α-helices.[527] Collectively, these structure predictions, which are expected to be correct in light of the significant sequence similarity concerning E2 between rhodopsin and the κ opioid receptor, disagree with predictions by Paterlini and co-workers[530] and by NMR structure determination on the isolated E2 of the κ opioid receptor.[530] Pogozheva and co-workers employed their distance geometry-based approach also for predicting the structure of MII.[320] Inconsistent with the evidence from in vitro experiments (reviewed in ref 186), the model of the active state of rhodopsin, deposited in the PDB as 1BOJ, does not show any significant deviation in the backbone conformation as compared with the model of the dark state (PDB code 1BOK), obtained by the same approach (Table 1). Thus, the method appears inadequate for predicting the active state of the photoreceptor and the predicted MII model should not be used as a template for modeling the active states of homologous GPCRs, as recently reported.[531]

A program for packing the TM helices of GPCRs from the electron density map of rhodopsin, named BUNDLE, was also proposed.[532,533] The approach consisted of the following steps: (a) location of the centers of the helices according to the low resolution electron density map; (b) calculation of the tilt angle of each helix on the basis of the elliptical shape observed by each helix in the map; (c) definition of a local coordinate system for each of the helices; (d) packing of the helices in an antiparallel orientation; (e) rotation of each helix through the helical axis in such a way that its hydrophobic moment points in the same direction of the bisector formed between three consecutive helices in the bundle; (f) rotation of each helix through an axis perpendicular to the helical one to assign a proper tilt; and (g) translation of each helix to its center deduced from the projection map.

A different approach, based upon the integration of sequence analysis and computational molecular modeling, has been very recently proposed to build TM α-helix bundles from low resolution electron density maps.[534] The approach is based on the observation that, typically, the lipid-exposed faces of TM proteins are evolutionarily more variable and less charged than the core. On the basis of this rule, the authors developed score functions and automated methods for orienting TM helices, for which locations and tilt angles have been determined using cryo-electron microscopy data (cryo-EM). The method was

parametrized with the aim of retrieving the native structure of BRD from among near- and far-from-native templates. It was then tested on proteins that differ from BRD in their sequences, architectures, and functions, such as the acetylcholine receptor and rhodopsin. The predicted structures were within 1.5−3.5 Å of the native state in all cases. In particular, for rhodopsin, the Cα-rmsd between the highest scored conformation and the native state was 1.5 Å.[534] These encouraging results led to the conclusion that such a computational method can be used in conjunction with cryo-EM data to obtain approximate model structures of TM domains of proteins, for which a sufficiently heterogeneous set of homologues is available (reviewed in refs 535,536). Staying in the context of EM-driven structure predictions of α-helical membrane proteins, two computational approaches were more recently proposed by Kovacs and co-workers[537] and Lindert and co-workers.[538] The latter proposed a promising structure-prediction algorithm "EM-Fold" that resolves ambiguities in density rod connectivity by placing predicted α-helices into the density rods and adding missing backbone coordinates in loop regions. In a benchmark of 11 mainly α-helical proteins of known structure a native-like model was identified in eight cases (rmsd 3.9−7.9 Å).[538]

The MembStruk protocol for predicting structures of GPCRs has been recently proposed.[285,539−547] Such a quite elaborate protocol consists of the following steps: (1) prediction of the TM regions; (2) construction and optimization of individual helices; (3) assembly of the seven-helical TM bundle; (4) coarse grain optimization of the TM bundle; and (5) addition of interhelical loops and optimization of the full structure. Step 1 is accomplished by means of the TM2NDS program that determines the TM regions in GPCRs using hydropathicity analysis, combined with input from multisequence profiles. In step 2, the canonical right-handed α-helices are then built with extended side chains and subjected to torsion angle optimization. In step 3, each helical axis is oriented according to the 7.5 Å electron density map of bovine rhodopsin.[548] The hydrophobic moments of the optimized helical bundle are aligned so that the net hydrophobic moment of each helix would be pointing outward toward the membrane from the center of mass. Step 4 consists of coarse-grain rotations of the helical orientations, starting with the directions of the net hydrophobic moment of each helix from step 3. Each helix is rotated through a grid of rotation angles about its helical axis. The total energy of this helix in the field of all of the other helices (fixed) is minimized using conjugate gradients. After finding the optimum configuration for each specific helix, a second cycle is initiated (seven such optimizations) and continued until the energy converges. Layers of explicit lipid molecules (52 molecules of dilauroylphosphatidylcholine lipid) are then added and optimized with the current configuration of the seven helices. Then, to achieve proper packing of the TM helices, the seven helix-bilayer complex is further optimized with rigid-body MD of the seven helices and lipid for 100 ps. In step 5, following the rigid-body dynamics, loops are added to the helices by using the WHATIF software.[549] The possible disulfide bridges are added. Then, addition of the side chains for all of the residues is carried out, followed by a full-atom MD optimization of the structure, with the explicit lipids. The protocol has been benchmarked on the BRD and rhodopsin structures.[540] As for rhodopsin, the rmsd in coordinates (CRMS) of the α-carbons in the predicted structure of the photoreceptor for the residues in the TM domains is 3.1 Å compared with the crystal structure with a resolution of 2.8 Å (PDB code 1F88).[540] Including the loops, the overall CRMS is 8.3 Å.[540] Following a rather convoluted strategy, a computational model of the $5HT_{2B}$ serotonin receptor was achieved[550] by using as templates either the electrondensity map of frog rhodopsin[548] or the MembStruk-derived models of two remotely related GPCRs.[543,545] The best $5HT_{2B}$ model was then mutated to build the $5HT_{2C}$ subtype.[550] Complexes between the two receptor models and selected ligands were also predicted. The MembStruk protocol was also used for predicting a β_2AR model and combined with the LITiCon method.[551] In this respect, the structural features of the β_2AR conformations stabilized by five different ligands (i.e., a full agonist (norepinephrine), a partial agonist (salbutamol), a weak partial agonist (dopamine), a very weak agonist (catechol), and the ICI-115881 inverse agonist) were found to correlate with the functional behavior of the ligands. Moreover, virtual ligand screening on the norepinephrine-stabilized receptor conformation showed an enrichment of 38% compared to the ligand unbound receptor conformation.[551] The LITiCon method was also used to map the differences in a MembStruk-build model of the CXCR4 stabilized by four moncyclam and one bicyclam antagonists.[552]

An improved version of MembStruk, the GPCR ensemble of structures in membrane bilayer environment (GEnSeMBLE) method, was proposed that predicts the ensemble of low-energy conformational states for a GPCR.[553] The method was challenged at the Critical Assessment of GPCR Structure Modeling and Docking (CAGSMD), i.e., "GPCR Dock 2008", in structure prediction of the A_{2A}R in complex with ZMA.[554] The whole-chain and TM 1−7 Cα-RMSDs between predicted and crystal structures were 4.3 and 2.5 Å, respectively, whereas the ligand rmsd was 5.0 Å.[554] The GEnSeMBLE method was also used to predict the structures of agonist- and antagonist-bound A_3 adenosine receptor (A_3R).[555]

Another ab initio modeling approach for packing TM helical bundles, called PREDICT, has been recently developed.[556,557] Without relying on sequence similarity to any other protein of known structure, the algorithm predicts the native 3D conformation of a protein using only its amino acid sequence and the physicochemical properties of the membrane environment. The concept of structural "decoys" is employed, consisting of generating many alternative possible conformations and optimizing them simultaneously to ensure that the algorithm identifies the correct structure without risk of ending up trapped at a local minimum. The core of PREDICT consists of two main steps: generation of decoys, followed by optimization and scoring of the decoys. In the first step, the program automatically produces hundreds to thousands of possible TM conformations (decoys). In this step, a coarse 2D grid search is conducted over the receptor conformational space, followed by initial optimization of the hydrophobic moments and protein−protein interactions in each decoy conformation, and generation of the initial 3D structures. In the second step, all the decoys are optimized and the most stable structures are identified according to the PREDICT energy function. The final model is further optimized using MD simulations and virtual complexation with a known ligand. The PREDICT algorithm was used to create an all-atom model of bovine rhodopsin that was further optimized using 300 ps of MD simulation without the retinal. The Cα-rmsd between the retinal-bound TM model of rhodopsin and the crystal structure was 2.9 Å.[556]

Very recently, a two-step approach to assemble the TM helices of integral membrane proteins, including rhodopsin, has been

presented.[558] In the first step, the conformational space of membrane protein folds matching a set of distance constraints is explored to provide initial structures for local conformational searches.[558] In step 2, the helical bundles from step 1 are refined using a Monte Carlo simulated annealing (MCSA) protocol designated for local minimization of an empirical structure-based penalty function. Applying this method to the seven rhodopsin helices, by using 27 distance constraints from biophysical experiments on the photoreceptor, reduced the approximately 7.0×10^{11} possible bundle configurations to 87 helical bundles with Cα-rmsd ranging from 4.3 to 9.5 Å. After MCSA refinement, the bundle with the lowest penalty function (i.e., with a penalty function of 3.3) had a Cα-rmsd from the known structure of 4.1 Å. It was, however, noticed that the best nativelike bundle, i.e., with a Cα-rmsd of 3.2 Å, was characterized by a penalty function of 1003.3. It was, therefore, concluded that stopping the refinement when the penalty function is between 1000 and 2000 would be worthy and more effective for seven-helix bundles.[558]

Nikiforovich and co-workers developed an approach to computer modeling of 7TM proteins validated on the experimental X-ray structure of BRD.[559] Within this approach, packing is achieved by minimizing the sum of all intrahelical and interhelical interatomic energies in the multidimensional space of parameters; the latter include "global" parameters (those related to movements of individual helices as rigid bodies, namely translations along the coordinate axes *X*, *Y*, *Z*, and rotations around these axes T*x*, T*y*, and T*z*) and "local" parameters (i.e., the dihedral angles of the side chains for all helices). The approach was used to attempt computational modeling of constitutive activation as well as to rationalize an observed functional impairment of the angiotensin 1 receptor (AT_1R).[560,561] In these case studies, the "global" starting point for assembling the TM bundle of the receptor was the X-ray structure of dark rhodopsin.

A dual-scale approach was developed to predict the native TM structures of retinal proteins (RPs) including bovine rhodopsin by combining coarse grained Monte Carlo (CGMC) simulations and all-atom (AA) MD simulations. The molecular system consisted of the 7TM helices represented as rigid cylinders and the retinal molecule bound to H7. Loop constraints were imposed between the helices, based upon the loop lengths evaluated from the protein sequences. For rhodopsin, the main-chain rmsd from the X-ray structure was 5.54 Å.[562] The approach was also used to infer the structural features of a constitutively active form of the C5a receptor.[563]

A computational method based on sequence conservation patterns was proposed, which is capable of generating native-like structural models for simple TM-helix bundle proteins. The only requirement for the method is the availability of more than 30 homologous sequences for an accurate extraction of sequence-conservation patterns.[564] The prediction method first computes a number of representative well-packed conformations for each pair of contacting TM helices, and then a library of tertiary folds is generated by overlapping the TM helices of the representative conformations. This library is scored using sequence conservation patterns, and a subsequent clustering analysis yields five final models. The Cα-rmsd between the best predicted model of rhodopsin and the crystal structure is 5.2 Å.[564]

In a high prediction challenge, the threading assembly refinement (TASSER) method was used to generate structure predictions for all 907 putative GPCRs in the human genome.[565] On the basis of a benchmarked confidence score, approximately 820 predicted models were supposed to have the correct folds. The majority of GPCR models share the characteristic 7TM helix topology, whereas 45 ORFs are predicted to have different structures. All predicted GPCR models are freely available for noncommercial users on the Web site (http://cssb.biology.gatech.edu/skolnick/files/gpcr/gpcr.html). A retrospective analysis of the models of the β_2AR and the A_{2A}R downloaded from the server confirms that high-throughput modeling of the entire GPCR sequence is not feasible at the moment. The whole Cα-rmsd (i.e., concerning the resolved portions of the β_2AR and of the A_{2A}R) between best predicted model and crystal structure are 4.88 and 4.76 Å, respectively. All the extracellular intraloop disulfide bridges as well as the α-helical portion of E2 in the β_2AR structure are not predicted by the method. Along this line, the huge N-term, I3, and C-term, absent in the crystal structure of the β_2AR, and the C-term, absent in the structure of the A_{2A}R, hold improbable structures in the predicted models also because they penetrate the putative membrane. Finally, the best of the five available models for each receptor is closer to rhodopsin

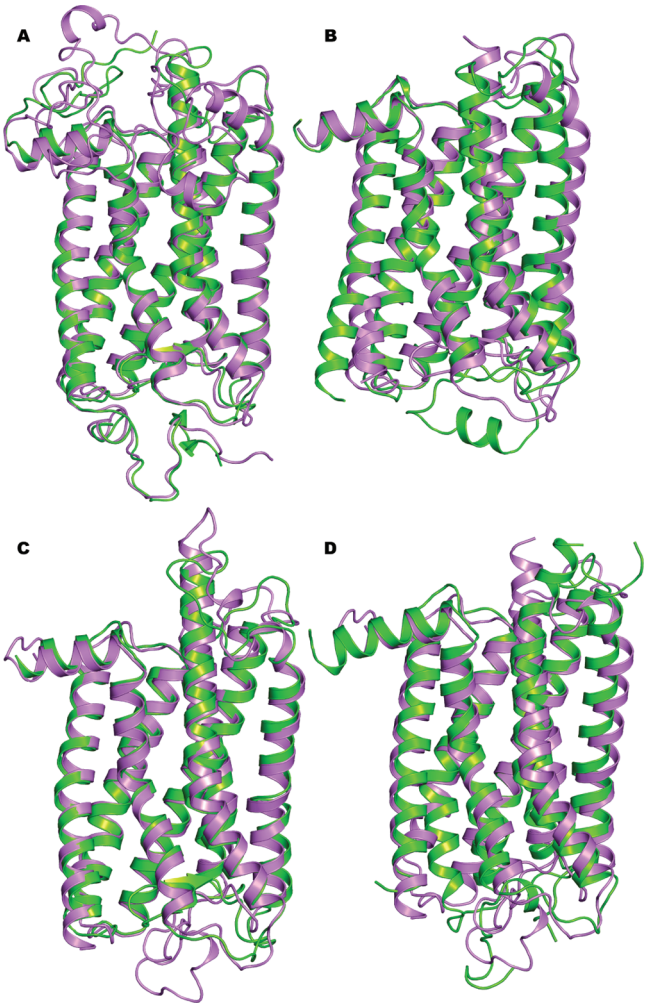

Figure 20. Structural comparisons between TASSER-predicted models and X-ray structures. In (A,B) the predicted model of the β_2AR (violet) is pairwise superimposed to the crystal structures of rhodopsin and of the β_2AR, respectively (both green). In (C,D) the predicted model of the A_{2A}R (violet) is pairwise superimposed to the crystal structures of rhodopsin and of the A_{2A}R, respectively (both green).

dx.doi.org/10.1021/cr100437t |*Chem. Rev.* 2011, 111, PR438–PR535

structure than to the crystal structure of itself. Indeed, the Cα-rmsd between the β_2AR model and the crystal structures of rhodopsin and β_2AR are 1.35 and 1.99 Å, respectively, whereas that between the predicted models of the A_{2A}R and the crystal structures of rhodopsin and A_{2A}R are 1.65 and 2.37 Å, respectively (Figure 20). This is due to the fact that the threading method implemented in TASSER individuated rhodopsin as a template for the two nonopsin GPCRs.

Most of the methods described above, which all require some input from structural determinations such as electron density maps or from biophysical and biochemical experiments, have proven to be effective in predicting the architectures of the seven TM helices in rhodopsin. Some of these methods have been invaluable in the years that preceded the release of the high resolution structure of rhodopsin. In fact, the models of the TM domains of rhodopsin achieved by these approaches, in particular Baldwin's Cα-atom model, have been used as templates in most of the comparative modeling studies done from 1993 to 2004. Hence, electron microscopy data on bovine and frog rhodopsin have been the main experimental foundation for ab initio and comparative modeling of GPCRs over one decade.

Ab initio approaches still remain the only possible strategy for structure prediction of those α-helical membrane proteins for which the high resolution structures of either a homologous or an analogous protein is not available, which is not anymore the case of GPCRs. Indeed, the latest critical assessments of GPCR structural models, i.e., "GPCR Dock 2010", showed the better performance of comparative modeling than the MembStruk ab initio modeling operated by the same investigators in predicting the structural models of the D_3R and CXCR4.[566]

4.4. The Functional Microdomain Approach to GPCR Modeling

In the years 1997−2005, an approach consisting of extensive conformational searches was presented, based on simulated annealing MC runs with the conformational memories (CM) method or MD simulations on isolated receptor domains, either a helix or a loop. This was done to overcome limitations inherent in both the low resolution level of site-directed mutagenesis results and computational modeling of the whole receptor structure.[129,131,159,567−579] The assumption of the approach is that GPCRs are made of structural microdomains characterized by discrete function and, hence, treatable as independent units. In this context, extensive calculations on such microdomains are assumed to provide a reliable picture of the microdomain itself in the context of the whole receptor molecule.[572]

The approach was used to investigate different aspects of GPCR function and to interpret the results of in vitro experiments. In particular, it was used to predict the conformational behavior of H7 in the 5-HT_{2A} serotonin receptor.[159] In detail, two different initial models of H7 of the receptor were built: one incorporating the structural features of the (N/D)P motif inferred from a database search and the other holding a regular Pro-kink. The two structures were used as starting points for two identical sets of CM simulations. For the simulations, H7 was divided into three regions: (1) an entirely flexible region (A7.47−N7.49); (2) two flanking semiflexible regions (i.e., S7.45−S7.46 and P7.50−Y7.53) where the φ and ψ dihedral angles were constrained ±20° around the values −63.0 and −41.6, respectively; and (3) the intracellular and extracellular ends that were kept fixed. The CM procedure consisted of four steps: in step 1, a classical Metropolis MC simulation was performed in torsion space at 10000 K for 1000000 steps, collecting 64 structures. In step 2, a simulated annealing from 10000 to 582 K was performed on both sets of 64 structures, providing two separate sets of dihedral angle maps. In step 3, two biased Metropolis MC simulations were done using the set of populations obtained from all data. At each biased Metropolis MC step, three randomly selected dihedral angles were assigned a new value, by using a biased temperature annealing method, leading to two collections of 100 structures. The fourth step consisted of cluster analysis of the two sets of 100 structures. The main outcome of this study was that the conserved N/DPxxY motif in this helix is the major determinant for deviation of H7 from ideal helicity.[159]

CM simulations of isolated TM helices of the D2 dopamine receptor (D_2R) were extensively used to rationalize the results of the substituted-cysteine accessibility method applied to H2, H4, and H6 of the D_2R.[131,569,570,574] Moreover, CM simulations of H6 done in combination with in vitro experiments were instrumental in inferring the helix motions associated with activation of the β_2AR and the 5HT_{2A} receptor.[131,136,567,568,575]

MC simulations on the isolated H3 of the gonadothropin-releasing hormone receptor (GnRH), in combination with in vitro site-directed mutagenesis experiments, highlighted the intrahelix charge-reinforced H-bond between D3.49 and R3.50, of the E/DRY motif, as a feature of the inactive state of the receptor. Interpreting the results of computations in the context of a TM model of the GnRH receptor led to the speculation that, in the active states, the E/DRY arginine would lose the interaction with the adjacent aspartate, establishing new interactions with the highly conserved D2.50.[129]

A similar computational approach was employed to infer the structure/dynamics differences between the wild type and a mutated form of I2 of the 5-HT_{2C} receptor, which might correlate with the lower basal activity of the mutant. Computations revealed differences in the conformational space explored by the two different forms of I2, and it was speculated that this would imply differences in G protein recognition.[576]

CM calculations on isolated H6 of the CB1 cannabinoid receptor highlighted the conformational behavior of the highly conserved W6.48 as responsible for the functional state of the receptor.[579] The results of computations suggested that the presence of the constitutive activity in the CB1 receptor was due to the absence of aromatic amino acids at positions i-4 (i.e., F6.44) and i+3 (i.e., F6.51) with respect to W6.48. This would provide W6.48 with higher conformational mobility, with a W6.48 trans χ_1 preferred. The χ_1 g+ → trans transition has been indicated to be linked to rhodopsin activation by spectroscopic studies.[580] In rhodopsin, the presence of F6.44 and F6.51, forming an aromatic cluster with W6.48, would restrict the conformational freedom of the conserved tryptophan, thus contributing to the lack of constitutive activity in the photoreceptor. It was also inferred that the W6.48 χ_1 g+ → trans transition is correlated with the degree of kinking of H6, with the bending being smaller with W6.48 χ_1 trans, thus suggesting that H6 straightens upon activation.[579] The inferences of these computational experiments were found consistent with similar calculations on H6 of the β_2AR.[575] Interpreting the results of CM simulations on H6 in the context of a TM model of the CB1 receptor based upon the rhodopsin structure led to the hypothesis that F3.36 χ_1 trans helped maintain W6.48 χ_1 g+, hence stabilizing the inactive state of the receptor. It was, thus, suggested that the W6.48/F3.36 interaction may act as the "toggle switch" for CB1 activation, with W6.48 χ_1 g+/F3.36 χ_1 trans representing the inactive state and W6.48 χ_1 trans/F3.36 χ_1

dx.doi.org/10.1021/cr100437t |Chem. Rev. 2011, 111, PR438–PR535

g+ representing the active state of the CB1 receptor.[579] The CM method was also used to provide an explanation for the apparent deviation from the ideal helicity of H2 in the CB2 receptor.[581] Computational modeling pinpointed S2.54 as the location responsible for possible conformational differences concerning H2 between CB2 and rhodopsin.[581] The functional microdomain approach was used as well to explore endocannabinoid recognition by H6 of the CB1 receptor embedded into phospholipid bilayer.[582]

MD simulations of model α-helices in a nonpolar environment were done to investigate the structural effect of the TXP motif in H2 of the CCR5 chemokine receptor and, hence, rationalize the functional effects of mutating this motif.[573] A similar approach was used to compare the dynamic behavior of H3 holding the rhodopsin sequence with that of the same helix with the 5-HT_{1A} sequence.[578] The results of simulations on the isolated helix in a hydrophobic environment were interpreted in the context of the rhodopsin structure, and it was inferred that the 5-HT_{1A} H3 tends to bend toward H5, whereas the rhodopsin H3 does not. This structural/dynamic divergence, which would allow H3 and H5 to be properly bridged by the cationic neurotransmitter serotonin, was attributed to the presence of the conserved C(3.36)T(3.37) motif, a feature of cationic neurotransmitter GPCRs and not of rhodopsin.[578]

We find interesting the use of an extensive conformational sampling method to infer the structure/dynamics features of helices, which carry conserved amino acids known to play important structural/functional roles. One must, however, be cautious in interpreting the results of simulations on isolated helices or loops in the context of the whole helix bundle. In fact, the degrees of freedom and the dynamics of an isolated helix or loop may be significantly different from those of the same helix or loop in the folded protein. Along the same lines, the inferences on interhelical interaction patterns based upon extensive simulations on a single helix inserted, a posteriori, in a low resolved static model of the receptor risk being too speculative. In summary, we think that extensive simulations on isolated receptor domains can provide useful information, unless the information involves receptor domains not included in the simulation.

4.5. Comparative Modeling of GPCRs

4.5.1. Suitability of Rhodopsin Structure as a Template.

In the years that preceded the release of the first crystal structure of rhodopsin,[16] both comparative and ab initio modeling approaches strongly relied on information from low resolution electron density maps of rhodopsin[12,15] and on the results of sequence analyses predicting that the members of family A share the same architecture of the seven helices.[13,14] Paradoxically, as soon as the structural information on rhodopsin reached atomic detail, several papers were published raising the question whether and to which extent the other members of the rhodopsin family share with rhodopsin the structure and the mechanism of functioning.[150,572,583−586] This repeated and not yet definitely addressed question originates from the low sequence similarities among the members of family A. The length of GPCRs from family A, in fact, may vary between less than 300 and more than 900 amino acid residues, with the majority of receptors having a length around 310−470 residues.[150]

Sequence analysis suggested that family A GPCRs could share the same arrangement of the seven helices, also due to the presence of a few but significantly conserved residues and motifs in each of the seven helices.[13,14,150] The amino acids, which resulted in having 80−100% conservation from a recent study on the alignment of 270 members of family A, are N1.50, L2.46, D2.50, C3.25, E/D3.49, R3.50, W4.50, F6.44, W/F6.48, P6.50, P7.50, and Y7.53 (Figure 1).[150] In detail, the analyses of the frequencies of individual amino acids in particular positions of the seven helices revealed that H1, in addition to the invariant asparagine, N1.50, holds G1.49, L1.52, and V1.53 that are highly conserved (68, 60, and 66%, respectively). In several cases, basic residues are found at the beginning of H1 and at the end of H2, possibly stabilizing the interaction of these helices with phospholipids. Frequently, a proline residue is at the beginning of H2, likely without perturbing the helical structure (Figure 1). H2, in addition to the almost invariant D2.50, has six conserved aromatic/hydrophobic residues toward the cytoplasmic surface, while residues toward the extracellular domain are more divergent.[150] H3 is characterized by the presence of highly conserved amino acids at its extracellular and intracellular ends, i.e., C3.25 and the E/DRY motif, respectively. This cysteine in the rhodopsin structure forms a disulfide bond with cysteine residue 187 of E2, and its very high conservation (90%) is suggestive of disulfide bridge conservation between position 3.25 in H3 and a variable position in E2 of family A GPCRs. This inference is being validated by the crystal structures of the nonopsin GPCRs recently determined.[93−97,99−105,111−113] Interestingly, with few exceptions, the residue immediately following C3.25 corresponds to the ligand type for the receptor. If the residue is basic, the ligand for the receptor is most likely a peptide (34% K, 19% R). If it is acidic (D, E), it is a biogenic amine.[150] The highly conserved residues at the cytosolic extension of H3 are E/D3.49 and R3.50 (86% and 96% conservation, respectively) of the E/DRY motif (Figures 1 and 2). H4 contains invariant aromatic residues, mostly tryptophan. H5 contains two aromatic residues, F5.47 and Y5.58, which are common in GPCRs (70 and 77%, respectively). As for H6, the highly conserved aromatic amino acids F6.44 and W5.48, together with P6.50, constitute the FxxCWxP functionally important motif (Figure 1). Interestingly, the glutamate/aspartate at position 6.30, suggested to be involved in stabilizing the inactive state of rhodopsin and other homologous GPCRs, [131,132,134−139,142,145−148] (see also references in the red updates through the text) has a low conservation (32%), being mainly a feature of rhodopsin, the amine, and some nonpeptide subfamilies. Three highly conserved amino acids in H7, i.e., N7.49, P7.50, and Y7.53, form the functionally important NPxxY motif, where x's are mostly hydrophobic L, V, and I residues (Figure 1).

Mapping the structural information from biochemical experiments on GPCRs of family A (reviewed in refs 186 and 572) into the rhodopsin structure led to the predictions that several of the highly unusual structural features of rhodopsin are also present in amine GPCRs, despite the absence of amino acids that might have been thought to be critical to the adoption of these features.[572] These conclusions were based on the hypothesis that different amino acids or alternate microdomains can support similar deviations from regular α-helical structure, thereby resulting in similar tertiary structure. This phenomenon has been defined as "structural mimicry", in other words a mechanism by which a common ancestor could diverge sufficiently to develop the selectivity necessary to interact with diverse signals, while still maintaining a similar overall fold.[572]

The availability of the high resolution structure of rhodopsin made it also possible to extend the prediction of structural commonalties between rhodopsin and the homologous GPCRs

to the intracellular and extracellular domains.[150] Combining the information from sequence analysis with the structure of bovine rhodopsin, the beginning and ending of the N- and C-termini and of the three extracellular and intracellular loops were predicted for all the 270 aligned receptors. The study predicted that the amino acid length of the N-terminal region is highly variable, containing from as little as four to as many as over 50 amino acid residues in length.[150] Among the three extracellular loops, E1 has the most consistent loop size; in fact, 144 GPCRs have the same number of amino acids in E1 as rhodopsin (i.e., 5 amino acids, Figure 1), whereas, in the remaining members, this loop ranges from only three amino acids to as many as 18 amino acids. The other two extracellular loops (E2 and E3) have more variable sizes. Similarly to the extracellular loops, the intracellular loops can vary in size, with the most conserved loops being I1 and I2. There are 198 GPCRs that have the same number of amino acids in I1 as rhodopsin (i.e., 6 amino acids, Figure 1), whereas the remaining members of family A have either five or seven amino acids. For I2, over 150 receptors have a loop size of 10−12 amino acids (i.e., 11 amino acids in rhodopsin, Figure 1). I3 and the C-terminus have the highest variations in amino acid lengths among all the considered GPCRs.[150] Indeed, sequence conservation in the C-term concerns the first 15 amino acids, which in all the resolved structures but the CXCR4 fold in an α-helix parallel to the membrane surface. Such an eight helix has been predicted to be shared by all family A GPCRs,[587] and the very recent crystal structures of the CXCR4 would represent the first exceptions.

Collectively, the results of in vitro experiments aimed at structurally probing GPCRs of family A[186,572] and those of sequence analyses[14,150] suggest that comparative modeling of the seven-helix bundle of GPCRs using rhodopsin structure as a template is likely to produce reliable results, and this has been, indeed, the assumption of high throughput computational modeling experiments, very recently reported, which targeted the TM domains of 235 GPCRs.[588]

It is, however, possible that the beginning and ending of a TM helix may vary among the members of different subfamilies. Therefore, in those cases in which a given helix in the target receptor is expected to be longer than the corresponding one in the rhodopsin structure, extra α-helix restraints could be required while modeling the target receptor. Predictions of the beginning and ending of each helix are difficult but essential to characterize the nonstructured parts of the individual intracellular and extracellular domains and, hence, to estimate the potential structural similarity in such domains between the target receptor and the rhodopsin structure. Difficulties are, indeed, expected to reside in modeling such hydrophilic domains, which vary both in amino acid composition and in length. In this respect, we have estimated whether each of the extracellular and intracellular domains in 163 selected GPCRs of family A can be modeled using the corresponding domain in the rhodopsin structure as a template. We have considered the human sequences of 163 members of family A, including 35 amine, 79 peptide, 3 hormone, 11 olfactory, 8 prostanoid, 9 nucleotide, 2 cannabinoid, 1 platelet activating factor, 1 gonadotropin-releasing hormone, 3 thyrotropin-releasing hormone and secretagogue, 4 melatonin, 5 lysosphingolipid, and 2 leucotriene B4 receptors. The evaluation has been based on sequence alignments between rhodopsin and one or more members of a given subfamily. For each receptor, a pairwise sequence alignment with rhodopsin has finally been obtained, which has been manually adjusted to incorporate additional information, including the results of multiple sequence alignments. As stated above, the intracellular and extracellular domains are characterized by lack of sequence similarity among the members of the rhodopsin family and rhodopsin. However, initial models of such regions, based upon the rhodopsin structure, can be achieved in those cases in which there is a significant similarity in length and there is absence of extra-disulfide bridges and/or extra-structured segments. Since our reference program for comparative modeling is MODELER, which is based on the satisfaction of stereochemical restraints,[177] we have also estimated those cases in which extra α-helical restraints would be needed to impose an α-helical conformation to insertions in the target receptor proximal to the N- or C-terms of each TM helix. In these cases, deletions in the template structure would be needed as well, at the junctions between the tail/loop and the helix. As for the extracellular domains, the N-term, in a few cases, including the glycoprotein hormone, the endothelin, and the proteinase-activated-like subfamilies, in which it is significantly longer than that of rhodopsin, structural restraints are unlikely to be transferred from the rhodopsin structure to the target receptor. As for the glycoprotein hormone receptor subfamily, the N-term is predicted and demonstrated to fold into a regular structure;[18,140,589−594] thus, it must be modeled separately and then incorporated into an ad hoc modified rhodopsin template to achieve the receptor model. E1 can almost always be modeled on the basis of the rhodopsin structure; exceptions include the glycoprotein hormone receptor subfamily, whose E1 is significantly longer than that of rhodopsin. In these cases, E1 modeling should be attempted following energy-based ab initio approaches, such as that implemented in the MODELER program.[139,595] Energy-based computational protocols for ab initio modeling of GPCR loops are being developed.[596−602] Alternatively, attempts to model the exceeding sequence as an extracellular extension of H2 and/or H3 should be done, by adding extra-α-helical restraints during comparative modeling, following deletion of one or two amino acids at the helix/loops junction in the template structure. As for E2, in all the rhodopsin structures released so far, the first 18 amino acids in this loop (i.e., the segment 174−191) form a β-hairpin whose second strand begins with a conserved cysteine, C187, which is involved in a disulfide bridge with the highly conserved cysteine at position 3.25 (Figures 1 and 2).[16,89−92] At least one cysteine is found in E2 of the homologous GPCRs. This is suggestive of the disulfide bridge between C3.25 and a variable cysteine in E2 being shared by family A GPCRs, as supported by the crystal structure of nonopsin GPCRs.[93−97,99−105,111−113] In selected sequences within the peptide, prostanoid, and hormone subfamilies, matches with the rhodopsin's β-hairpin can be achieved with a few insertions and/or deletions, allowing C187 to align with a cysteine residue in the target GPCR. However, retrospective analysis of the CXCR4 structure shows that although the E2 of both rhodopsin and CXCR4 folds in a β-hairpin, they differ significantly in structure and arrangement. For the other subfamilies, sequence alignments with E2 of rhodopsin are not feasible; moreover, there is significant variability even among close homologues. The members of the amine subfamily are exemplar in this respect. Among them, only the βARs hold two additional cysteines with respect to the C3.25-linked cysteine that is the most C-terminally located. In the βAR structures, the two additional cysteines in E2 are involved in an intraloop bridge. Consistent with structure determinations of βARs and D_3R,[93−97,99−102,112] reasonable sequence alignments between the six-amino acid C-terminal fragment of βAR E2 (i.e., starting from the C3.25-linked cysteine) and the corresponding sequences of the α_1ARs or the dopamine receptors can be used for comparative modeling.[603] In these receptors, the portion that precedes the

C-terminal cysteine has to be modeled by ab initio approaches.[603] Another example of high E2 sequence variability among close homologues concerns the purine subfamily, in which only the $A_{2A}R$ and $A_{2B}R$ subtypes hold at least two additional cysteines in the loop. Thus, structure predictions of E2 by comparative modeling may be difficult even for close homologues of the actual templates.[604]

As for E3, it can be comparatively modeled for the amine subfamily, whereas, for the peptide subfamily, in which such a loop is predicted to be longer than that of rhodopsin, it is frequently difficult to achieve on the basis of the rhodopsin structure. In this respect, the rhodopsin structure can be used as a template only if the required insertions can be modeled as one/two-turn extensions of H6 and/or H7 and not as part of the loop. In those cases, extensions of H6 and/or H7 could be eventually achieved during comparative modeling by applying extra α-helical restraints to the target amino acid segment. This would require deletion of one or two amino acids at the helix/loops junction in the template structure. Retrospective analysis shows that the crystal structures of the CXCR4 of the peptide GPCR subfamily are indeed characterized by one- and two-turn extensions of the extracellular ends of H6 and H7, respectively.[111]

As for the intracellular domains, I1 and I2 can almost always be modeled on the basis of the rhodopsin structure. In contrast, comparative modeling of I3 based upon the rhodopsin structure is not possible for many GPCRs, in particular for the amine subfamily. In fact, in this case, I3 is significantly longer as compared to that of rhodopsin, and it is also predicted to hold elements of secondary structure and, hence, a fold. Structure predictions of these huge loops could be attempted by alternative approaches such as sequence similarity search or fold recognition to find homologous or analogous structures useful as templates for the target loop. This would lead to the building of chimeric rhodopsin templates in which rhodopsin's I3 has been replaced by the corresponding loop of the target receptor in the predicted fold.[502,605] As recently shown by the crystal structure of the Gq-coupled squid rhodopsin,[106,119] and the NMR structure of the Gs-coupled vasopressin V2 receptor (V_2R) (PDB code 2JX4),[606] I3 can form a rigid helical column as a result of the cytosolic protrusion of H5 and H6; the unstructured part of the loop that connects the two helices is quite short. If significant sequence similarity exists between the I3 of the target and that of either squid rhodopsin or V_2R, the latter can be used as a fragment template. Alternatively, lengthening of the cytosolic extremities of H5 and H6 may be attempted by applying external α-helical restraints; the bridge between the two helices should be then modeled by ab initio approaches.[607] In contrast to the case of the amine GPCR subfamily, for the remaining subfamilies, there may occur two situations: (a) the loop can be modeled on the basis of that of rhodopsin, eventually introducing one or two α-helix turns at the N-term of H6, as reported for subtypes 1 and 2 of the melanin-concentrating hormone receptor (MCHR1 and MCHR2);[608] (b) I3 is significantly shorter than that of rhodopsin, and its modeling should be attempted following energy-based ab initio approaches, such as that implemented in the MODELER program[139,595] (see refs 560,596−599,609−613 as examples of alternative computational protocols), or a database loop search; and (c) I3 is significantly longer than that of rhodopsin, and it should be built separately, as seen above for the amine subfamily. As for case (a), it should be considered that profound disagreement is found between the $P4_1$ (1U19)[92] and $P3_1$ (1GZM)[91] rhodopsin structures concerning the ending of H5, the beginning of H6, and the structure of their interconnecting loop. Such mismatch would require probing both the two different rhodopsin structures as templates. As for case (c), this situation occurs only in a minority of cases, including the vasopressin-like subfamily.[130,141]

For almost all GPCRs, the C-tail cannot be entirely modeled on the basis of the rhodopsin structure. In general, the N-terminal portion of the C-tail, including the structurally conserved H8, can often be achieved, differently from the C-terminal half. In a few cases, the C-tail is predicted to fold in a regular structure and it should be modeled on the basis of alternative templates and then merged into an ad hoc modified rhodopsin template.[605]

In summary, comparative modeling of the entire sequences of GPCRs, based upon the rhodopsin structure, is largely far from being trivial. We have estimated that full automated modeling of an entire GPCR sequence is never feasible but rather human intervention is always necessary for modifying ad hoc the rhodopsin template, for introducing extra restraints (e.g., incorporating information from secondary structure predictions and/or disulfide linkages), or for ab initio modeling of selected domains, or for adding fragments inferred from fold recognition. Moreover, the models produced by the MODELER program should be considered as the starting points of further energy refinements and MD simulations. Average structures produced by such calculations show RMSDs (in the TM domains) from the rhodopsin structure more reliable than those of the models prior to calculations.[132,614] In fact, the structure deviation, in terms of main-chain RMSDs, for pairs of protein which, such as rhodopsin and the homologous GPCRs, are ∼22−24% identical, is expected to be close to 2 Å instead of 0 Å, as is the case of the initial receptor model produced by MODELER.[615]

An alternative approach to the comparative modeling based on the satisfaction of restraints is the one based on the assembly of fragments, like the approach recently employed to model the human ghrelin receptor (hGHS-R).[616] In this respect, the starting model of hGHS-R was achieved by: (a) fragmenting the amino acid sequence in 15 segments, (b) modeling each segment separately by comparative modeling, and (c) assembling the fragments by using the rhodopsin structure as a template.[616]

4.5.2. New Perspective in Comparative Modeling of GPCRs from the Advances in Structure Determinations. The very recent availability of the crystal structure of squid rhodopsin[106] and of six nonopsin GPCRs in complex with functionally different ligands,[93−97,99−105,111−113] now imposes selection of the proper template for comparative modeling (see also refs 617,618) by careful sequence comparisons, which is a crucial step in comparative modeling.[619] Selection of the proper template is trivial if the target is a close homologue of one of the available templates, as recently demonstrated.[620] According to a recent investigation, the optimal templates for nonorphan non-olfactory human class A GPCR would be SSR5, SSR4, or CXCR2.[617] As for the question whether the use of multiple templates provide most accurate GPCR models than single templates, the same study showed that the low sequence similarity among the available templates hampers the effectiveness of their combined usage. It was, indeed, estimated that, to effectively test the ability of multiple template modeling to impact the accuracy of GPCR homology models for docking studies, additional GPCR crystal structures in the 35−65% sequence identity range are needed, which can serve as templates.[617]

At the moment, the crystal structure of close homologues are available only for a few GPCRs. This status urges the need to find

strategies aimed at improving the quality of structure predictions such as combining comparative and ab initio modeling.[621−625] Sequence-based methods aimed at predicting residue−residue contacts such as those based on covariation analysis have been proposed, which could eventually improve comparative models of GPCRs and detect functional sites such as those intended for ligand binding.[626] A new approach to refining protein structure models was proposed that focuses sampling on regions most likely to contain errors, while allowing the whole structure to relax in a physically realistic all-atom force field.[622] In applications to models produced using NMR data and to comparative models based on distant structural homologues, the method proved to significantly improve the accuracy of the structures in terms of both backbone conformations and placement of core side chains. The approach has been used at the "GPCR Dock 2008" assessment for refining regions of theA_{2A}R poorly aligned with either the β_1AR or the β_2AR templates.[554] The whole-chain and TM 1−7 Cα-RMSDs between predicted and crystal structure were 3.5 and 2.1 Å, respectively, whereas the ligand rmsd was 5.8 Å.[554] Another protocol (foldGPCR) to model the structural divergence between template and target in the TM helices was recently developed.[624] The protocol is based on predicted conserved inter-residue contacts between template and target and exploits an all-atom implicit membrane force field. The placement of the ligand in the binding pocket is guided by biochemical data. The foldGPCR protocol is implemented by a stepwise hierarchical approach, in which the TM-helical bundle and the ligand are assembled by simulated annealing trials in the first step, and the receptor−ligand complex is refined with replica exchange sampling in the second step. The protocol was applied to model the human β_2AR bound to carazolol, using contacts derived from the template structure of bovine rhodopsin. The protocol was able to predict helix backbone irregularities and helix−helix packing interactions that distinguish rhodopsin from β_2AR.[624] Other refinement strategies of comparative models of GPCRs rely on the application of low frequency normal modes.[625] The latter are used to generate an ensemble of alternative models for ligand docking. The ensemble of ligand−receptor complexes are hence filtered based upon the information from in vitro experiments. Finally, the model is refined in the presence of the ligand. The approach was used to generate models of the antagonist-bound form of H3 histamine receptor (H_3R). Model validations were based on the outcome of virtual screening and structure−activity relationship (SAR) data on H_3R antagonists.[625] Methods to GPCR model refinement include also an approach aimed at expanding those ligand binding sites, which are too small to accommodate known ligands.[623] It is a systematic method that refines the active sites by a pressure-guided MD simulation that introduces perturbations in the backbone atoms in addition to side-chain adjustments. The method was validated on two test cases: (a) docking of retinal into an MD-relaxed structure of opsin, and (b) docking of known ligands into a comparative model of the CCR2 receptor. In both cases, the MD expansion algorithm made it possible to dock the ligands in poses that agree with the crystal structure or mutagenesis data.[623]

Two of the top three groups in the "GPCR Dock 2008" assessment of GPCR structural models[554] employed a so-called ligand-guided backbone ensemble receptor optimization (LiBERO) approach, in which structure−activity relationship information for representative series of ZMA analogues was used to predict the binding site and optimize the receptor conformation. In general, the ligand-guided approaches are based on the generation of multiple conformations of the target receptor and ranking of conformations according to their performance in virtual ligand screening-enrichment for known ligands in a random decoy set. LiBERO was recently used to predict the complexes between a number of adenosine receptor subtypes and selected antagonists.[627] Advances in the LiBERO approach include the incorporation of significant variations of the protein backbone by using either MC sampling or elastic network-normal-mode analysis (EN-NMA) techniques.[628]

Despite the difficulties in using the available high resolution structures as templates for modeling the homologous GPCRs, we think that, at the moment, comparative modeling remains preferable to the most effective ab initio approaches, and it has, indeed, been widely used since the year 2000[132,134,135,137−140,142,251,279,577,588,593,596,605,608,629−703] (see also references in the red updates through the text).

As expected, the first and the second assessments of GPCR structural models, i.e., "GPCR Dock 2008" and "GPCR Dock 2010" confirmed that the higher the sequence identity between template and target, the higher the accuracy of structure predictions.[554,566] Indeed, the modeling accuracy for the three GPCR targets evaluated so far decreases in the order $D_3R > A_{2A}R$ > CXCR4, which follows the order of corresponding target-template phylogenetic distances.[554,566]

In conclusion, comparative modeling of GPCRs as well as of other membrane proteins[704] is still hampered by the limited amount of high-resolution structures, which urges the need to develop effective strategies that mix comparative modeling of the portions that align well with the template(s) with ab initio modeling of sequence-divergent portions. The need to improve the effectiveness of comparative modeling is imperative for structure-based drug design (see also refs 554,628,705).

A significant aid to structure prediction protocols will derive by an amplification of the spectrum of crystal structures, possibly covering the principal subfamilies. This is, indeed, the short-term goal of the GPCR network of investigators who are involved in high-throughput crystallization of GPCRs (http://gpcr.scripps.edu/index.html).

5. COMPUTATIONAL EXPERIMENTS ON FAMILY A GPCRS

5.1. Thermodynamic Models of GPCR Function

Until 1995, GPCR ligands were classified as antagonists, and full or partial agonists, depending on whether they produce null, full, or partial stimulus upon binding to the receptor, respectively.[706] However, recent advances in receptor theory and experimental technology for ligand screening led to the discovery of many additional types of receptor ligands.[80,706] Some of these are (a) inverse agonists, which inhibit constitutive activity of GPCR systems (i.e., agonist-independent spontaneous activity that emanates from the system itself) or, in other words, ligands that display negative efficacy; (b) allosteric agonists, which function as agonists by interacting with a site distinct from that of the endogenous agonist (usually a nonpeptide ligand for a peptide receptor), i.e., the orthosteric site;[706,707] (c) allosteric modulators, i.e., ligands that bind to an allosteric site and modulate the binding and/or signaling of an orthosteric ligand; they can positively or negatively affect either the affinity, the efficacy or both the affinity and efficacy of the orthosteric ligand;[706−717] (d) dualsteric or bitopic hybrid ligands, which bind to both the

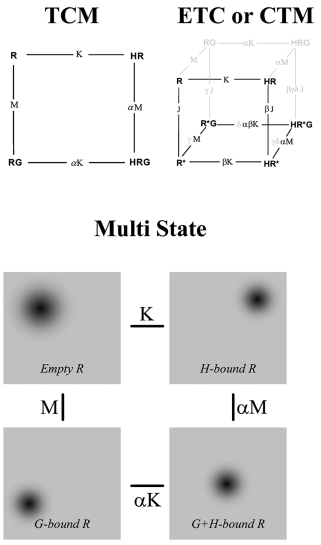

Figure 21. Representation of thermodynamic models of GPCR interactions. In the ternary complex model (TCM), the receptor is assumed to hold four ligation states: empty, G protein (G)-bound, ligand (H)-bound, and bound to both ligand and G protein. Two unconditional equilibrium constants (K, M) and one equilibrium coupling constant (α) describe the entire equilibrium between the possible ligation states. α describes the reciprocal effect that ligand and G protein impart on each other's binding. In the extended (or cubic) ternary complex model (ETC or CTM), the active and inactive states of the receptor (R* and R) are explicitly included in the equilibrium scheme. An additional equilibrium constant J governs the unconditional isomerization equilibrium of the receptor (R−R*). As in the case of the ternary complex scheme, greek letters represent the coupling constants between relevant equilibria. Note that δ is a "second-order" constant stating the reciprocity of the three chemical events occurring in the receptor (two ligand binding processes and the isomerization). The dark paths and the associated species indicate how the model simplifies if we assume that there is no binding of G to the R form of the receptor (which represents ETC). The picture of the multistate model is a schematic representation of the model, where the receptor is assumed to have an unlimited number of states in equilibrium with each other and representing the entire conformational space of the receptor (schematized as gray squares in the picture). A macroscopic state of the receptor is defined as a probability distribution over this conformational space. This probability distribution, schematized as a fuzzy spot in the conformational space, is subjected to change depending on the ligation state of the receptor. Again, the receptor has four ligation states and the equilibrium between them is governed by three macroscopic equilibrium constants (K, M, α), as in the TCM. In this case, however, the macroscopic constants are determined by the relationship between the probability distributions that the receptor assumes at different ligation states. For example, the allosteric constant α results from the discrepancy between the probability distributions that arise when the receptor is empty, G protein-bound, or ligand-bound.

orthosteric and allosteric binding sites with the potential to enhance subtype selectivity.[716,718]

Concepts regarding the mechanisms by which drugs activate receptors to produce biological and physiological response have progressed beyond considering the receptor as a simple on−off switch (reviewed in refs 706,719). Current evidence suggests that the idea that agonists produce only varying degrees of receptor activation is obsolete and must be reconciled with data showing that agonist efficacy, i.e., the ability of a molecule to produce some observable physiological response, has texture as well as magnitude. Thus, GPCR ligands can block a system's constitutive response (inverse agonists), behave as positive and inverse agonists on the same receptor (protean agonists), and differ in the stimulus pattern they produce in physiological systems (ligand-selective agonists). The underlying general mechanism for this seemingly diverse array of activities is the same, namely, ligand-dependent changes in the conformational states of the receptor (reviewed in refs 706,719).

GPCRs are allosteric proteins designed by nature to transmit extracellular signals to the intracellular milieu of the cell. They accomplish this task by changing their interaction with large intracellular proteins (G proteins) upon binding of extracellular ligands. The most general model that formulates this ligand-mediated process is the ternary complex model (TCM) (Figure 21).[720,721] According to this view, the interactions of ligand (H), G protein (G), and receptor (R) can be described by the equilibrium scheme shown in Figure 21, where K and M are the unconditional affinities for the formation of ligand−receptor and G protein−receptor complexes, respectively, and α represents the reciprocal effect that ligand and G protein impart on the binding of each other when they form the ternary complex (HRG) (Figure 21). It measures the standard free energy transferred from the binding of ligand to the binding of G protein (or vice versa). The equivalence between ligand efficacy and α is obvious: α greater than, equal to, or less than 1 means that the ligand enhances, leaves unchanged, or reduces the tendency of R to bind G; thus, it has positive (agonist), null (neutral antagonist), or negative (inverse agonist) efficacy, respectively. Efficacy defined by α depends on H and R but also on G. Therefore, the scheme is extendible to describe the interaction of R with G_1, G_2, ..., G_n, which yields α_1, α_2, ..., α_n for the same ligand. This means that a given ligand H interacting with the same receptor R will have different efficacies when R binds to different types of G proteins. Note also that the receptor and G protein influence each other and they can interact even in the absence of agonist ligands. The system can be forced to produce a response by changing the stoichiometry of the reactants, namely, R and G. Thus, the constitutive activity (as defined by elevated levels of [RG]) can be increased by raising the receptor concentration or by increasing the concentration of G protein. Another way in which constitutive activity can be produced is through alteration of M. Although this idea summarizes the entire phenomenology mentioned above, it addresses the question of ligand-induced conformational change only implicitly; changes in the conformational state of the receptor are hidden in the parameter α, and the model does not specify their nature but only their consequences on the interactions of H and G with R.

The extended ternary complex (ETC)[722] or cubic ternary complex (CTM)models,[723−725] which are based on the same thermodynamic principles as the TCM, consider the active (R*) and inactive (R) conformational states of the receptor explicitly (Figure 21). Those conformations of the receptor that hold an arrangement in the cytosolic domains that can activate the G protein are referred to as the "active state", and those that do not are referred to as the "inactive state". Accordingly, the two conformations R and R* exist in equilibrium with each other, which is governed by an "allosteric constant" (denoted as J and defined as [R*]/[R]). Under normal circumstances, J is a unique molecular constant for a given receptor (i.e., the energy barrier to formation of spontaneous active states for some receptors is lower than it is for others), but experimental methods such as the removal of sodium ions[726,727] or point mutation (reviewed in refs

41,81,84,85) can affect *J* and make receptors more constitutively active. In principle, agonists can induce response by causing enrichment of the active state by selectively binding to R*. Under these circumstances, efficacy is a matter of the quantity of the active state produced by the agonist. More generally, selective affinity of ligands for various receptor conformations will change the overall distribution of the species in the GPCR ensemble and, thus, either induce or inhibit response. This is the basic mechanism of ligand efficacy and the basis for the molecular nature of inverse, protean, and ligand-selective agonism according to the allosteric models such as the ETC and CTM models (Figure 21; reviewed in refs 706,719). There is no theoretical constraint on the number of active states of the receptor. Even though the ETC and CTC models have both been referred to as "two-state" models, this is a misnomer in that there is the capability within both to be multistate models (reviewed in refs 706,719).

In light of the ever-increasing evidence of GPCR dimerization/oligomerization, thermodynamics models have been recently proposed to account for either the lack of cooperative ligand binding or the presence of negative or positive cooperative binding generated by the crosstalk between protomers within a dimer/oligomer (reviewed in refs 53,728,729).

It is now clear that efficacy cannot be considered as a strictly receptor-based ligand property, but rather a function of the entire GPCR system, involving both the receptor and its cellular environment (reviewed in refs [719,730]). GPCRs have an extremely wide spectrum of behaviors, which include pleiotropic coupling (i.e., the ability to activate more than one type of G protein), dimerization, oligomerization, internalization, desensitization, and interaction with other numerous cellular coupling proteins (reviewed in refs 719,730). Studies of these behaviors indicate that some molecules can induce some of these effects but not others and that, occasionally, a drug might not produce an overt physiological response but might, nevertheless, change receptor behavior and, hence, have efficacy. This issue includes the concepts of "stimulus trafficking", "biased agonism", and "functional selectivity", which are the bases of "collateral efficacy".[28,731−737] So, there are different "efficacies" for different behaviors beyond the activation of G proteins. The question is whether a general molecular mechanism can account for all of these expressions of efficacy. One approach to describing the numerous other manifestations of efficacy that do not necessarily produce a cellular response is to consider receptor proteins in terms of ensemble theory.[719,738,739] This theory is based on the fact that receptors exist as collections of ensembles of numerous conformations. In this respect, the probabilistic multistate model that assumes an unlimited number of conformational states for the receptor predicts that the relationships between conformational states and protein function are stochastic rather than deterministic as the allosteric models imply (i.e., the multistate model in Figure 21). The latter statement amounts to the idea that the active state of the receptor cannot be attributed to individual conformational states, but rather to an ensemble of the states in the conformational space of the receptor. Each ensemble is associated with a given function such as G protein activation, interaction with cellular proteins, dimerization/oligomerization, etc. At any given instant, the various conformations in an ensemble can be represented as a Gaussian distribution, and there could be intersecting ensembles for a range of GPCR behaviors (see ref 739 for a more detailed discussion of the idea).

Ligands influence receptor behavior through selective affinity for the various conformations in the receptor reference ensemble. Although some ligands will bind preferentially to some receptor conformations over others, the weighted average affinity that a ligand has for a receptor ensemble is known as the "macroaffinity" of the ligand for the receptor, that is the concentration of ligand that is bound to 50% of the receptors at any one instant.[719] Even if common in vitro experiments are inadequate to address the question whether ligands select or induce various receptor conformations, the restructuring of a collection of receptor conformations through selective binding affinities emphasizes the idea that affinity is not a passive phenomenon, whereby a ligand simply binds to a protein but does not change it.[719] Both ligand and receptor are dynamics entities. Their selective interaction is governed by dynamic cooperative events encoded in their molecular structure and described by statistical thermodynamics. The idea that ligands, whatever their efficacy is, may alter receptor conformational states appears to be supported by fluorescence spectroscopy experiments on the β_2AR[740−742] and on the human leukotriene B_4 receptor.[743] Fluorescence spectroscopy studies aimed at monitoring catecholamine-induced conformational changes in purified β_2AR provided evidence for a multistep process of agonist binding where contacts between the receptor and key moieties on the agonist stabilize a succession of conformational states with distinct cellular functions (reviewed in refs 744,745).[746,747]

The huge complexity of the GPCR-mediated signaling would benefit from system biology-based modeling[748−751] better if integrated with molecular structure/dynamics information.

5.2. Computational Modeling of Mutation-Induced Active States

We have pioneered the use of computational modeling to infer the structural features of the agonist-independent active states of different GPCRs. [81,127,128,130,132,134,135,139,142,145,146,148,510−513,614,752−754] For review, see also refs 231−233.

The first studies were done on an ab initio model of the α_{1b}AR holding all the domains but the N-term, I3, and the C-tail.[127,128] The idea was that comparing the structure/dynamics features of the wild type α_{1b}AR with those of receptor mutants, characterized by different degrees of constitutive activity or inability to activate the G protein, would help identify some of the molecular changes correlated with the transition from R to R*, independently of the presence of agonist.[127,128]

The computational approach consisted of generating a large number of average configurations following MD simulations of the wild type and the mutated forms of a common input structure. A comparative analysis of such average arrangements was then carried out, focusing on a few but significant structural features, which were shared in common by the majority of the mutant structures with similar functionality and which made the difference between active and nonactive forms. This strategy is thought to overcome, at least in part, the drawbacks related to the low resolution of the computational models and the approximations and simplifications in the computational setup.

Simulations were carried out in vacuo, using a distance-dependent dielectric and intrahelix distance restraints between the backbone oxygen and nitrogen atoms of all amino acids in the helix, except for prolines. The application of these intrahelical distance restraints, developed in early computational simulations of the packing arrangements of seven-helix bundles,[501] was instrumental in (a) reducing the system degrees of freedom, (b) inferring the structure/dynamics role of prolines, and (c) letting the helices move as rigid bodies, consistent with the

experimental evidence on rhodopsin activation.[755] A fundamental step in this approach is the choice of the input structure and of the computational conditions that produced divergent average behaviors for the active and nonactive receptor forms, consistent with the experimental information available thus far.

Computational modeling of all the 19 possible substitutions for A293(6.34) in the α_{1b}AR, characterized by variable levels of constitutive activity,[756] highlighted the role of the E/DRY conserved motif in regulating the agonist-independent receptor transition from the inactive to the active receptor states.[127] In the inactive states, represented by the wild type and the nonactive A293(6.34) mutants, R143(3.50), of the conserved E/DRY motif, was found engaged in H-bonding and van der Waals attractive interactions with the amino acids of a highly conserved polar pocket in the cytosolic halves of H2 and H7. These studies were, therefore, suggestive of an H-bonding network of conserved amino acids as a constitutive structural feature of the nonactive receptor states, consistent with the results of previous computations on more simplified models of the same receptor.[503,504] The release of the H-bonding network involving R143(3.50) and the cluster of conserved polar amino acids was found to be the common feature to all the constitutively active mutants (CAMs) at A293(6.34).[127] Computer simulations suggested also a potential mechanism of regulation of GPCR function via changes in the protonation state of the aspartate of the E/DRY motif, with the protonated form being associated with the active states.[127] This hypothesis was inferred from the observation that protonation of D142(3.49) conferred to the α_{1b}AR the same average structural features shown by the highly active mutants of A293(6.34). The idea that protonation of D3.49 was the perturbation rather than mutation able to trigger agonist-independent active states of wild type α_{1b}AR was also supported by the results of in silico mutagenesis showing that replacements of D142(3.49) with neutral amino acids would give the structural features of the active states to the receptor.[127,128] Predictions of computational modeling were validated by the experimental findings that the irreversible reprotonation, following mutation, of D142(3.49) led to constitutively active forms of the α_{1b}AR.[127,128] In this respect, the D142(3.49)A mutant was the first example in the literature of computational design of a constitutively active GPCR mutant.[127] The hypothesis that reprotonation of the aspartate/glutamate of the E/DRY motif could favor the active states was successively strengthened by in vitro and in silico experiments on the GnRH and μ opioid receptors.[129,133] In line with these evidence and consistent with the knowledge that the homologous glutamate in rhodopsin is involved in proton uptake from the cytosol (reviewed in refs 189,193), very recent pK_a calculations on the crystal structure of rhodopsin proved the susceptibility of E134(3.49) to undergo significant pK_a shifts and, hence, change its prototropic state depending on its environment.[757]

Upgrading and complicating the α_{1b}AR model, to incorporate advances in structural determination of rhodopsin, strengthened the hypothesis that the E/DRY motif might play a role in maintaining the inactive state of the receptor, while introducing novel structural hallmarks of the active and nonactive states, such as the degree of solvent accessibility of selected cytosolic domains, including I2, I3, and the cytosolic extensions of H3 and H6. These domains, in fact, underwent solvent exposure on going from the nonactive to the active receptor forms and were, hence, suggested to hold potential recognition points for the G protein.[502,510,511] These results found consistency with the results of the automatic docking simulation of the wild type α_{1b}AR and two CAMs (i.e., D142(3.49)A and A293(6.34)E) with different heterotrimeric G proteins.[510,511]

The same computational approach was used to build an agonist-independent activation model of the human LHR,[512] which is particularly susceptible to spontaneous pathogenic activating and loss-of-function mutations.[84,85,231] The studies of Lin and co-workers and by Fanelli represented the first attempts reported in the literature aimed at inferring the molecular determinants of mutation-induced activation of the LHR.[457,512] The LHR model by Lin et al., limited to the TM domains, which were packed by fitting the peaks in the 9 Å electron density map of bovine rhodopsin, suggested that single activating mutations perturb the specific interactions of H6 with H5 and H7, either by disrupting the hydrophobic packing between H5 and H6 or by weakening the H-bonds between H6 and H7.[457] In the study by Fanelli, MD simulations were carried out on the wild type and on the majority of the spontaneous active and nonactive LHR mutants known thus far.[512] Similarly to the case of the α_{1b}AR, the mutation-induced active states of the LHR shared the release of the charge-reinforced H-bonding interactions involving the conserved arginine of the E/DRY/W motif in the wild type form and the opening of a crevice between I2 and I3.[512] The latter effect was found to be properly accounted for by the solvent accessible surface area of W465(3.51), of the E/DRY/W motif (i.e., $SAS_{W3.51}$). This index was indeed found to be close to 0.0 Å^2 in the nonactive forms and above 32.0 Å^2 in the active ones. The $SAS_{W3.51}$ index, together with the distance between D405(2.50) and R464(3.50), was used for predicting the functional behavior (i.e., active or nonactive) of 48 novel LHR mutants, constituting the first attempt in the literature of in silico functional screening of GPCR mutants.[512]

Computational modeling of both mutation- and agonist-induced activation of the human OTR also suggested the weakening of the interaction pattern of the E/DRY/C arginine and the opening of a cytosolic crevice as features of the active receptor states.[130]

As soon as the first crystal structure of rhodopsin was released, computational modeling of agonist-independent activation was carried out on novel models of the α_{1b}AR, LHR, and OTR, which were achieved by comparative modeling, using the rhodopsin structure as a template.[132,134,135,139,141,142,145,146,148,614,752,753]

As for the α_{1b}AR, MD simulations of more than 100 single and double mutants of the receptor, done in parallel with in vitro experiments, made possible the definition of virtual structures, representatives of the agonist-independent active and nonactive states, both for the ab initio and homology models.[132,134] The virtual structure of the ground state was obtained by making an average over the average structures of the wild type and of the receptor mutants showing a wild type-like phenotype, whereas the virtual structure representative of the active state was obtained by making an average over the average structures of the most active α_{1b}AR mutants.[132,134] Critical comparison between the "ground state" models achieved by ab initio and comparative modeling highlighted overall similarities in the length and arrangement of the TM helices.[132] Both the ab initio and, perhaps better, the homology models predicted that the majority of amino acids susceptible to activating mutations [D142(3.49), Y144(3.51), V137(3.44), R143(3.50), E289(6.30), and A293(6.34)] belong or are close to the interface between the cytosolic extensions of H3 and H6. A common feature to all these

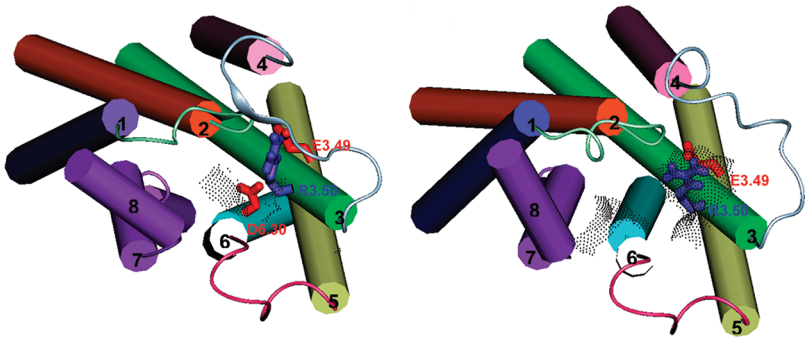

Figure 22. Average minimized structures of the wild type LHR (left) and of the D564(6.30)G constitutively active mutant (right).[135,139] The receptors are seen from the intracellular side in a direction perpendicular to the membrane surface. The seven helices are represented by cylinders, whereas the three intracellular loops are represented by thin ribbons. Theextracellular loops are not shown. H1, H2, H3, H4, H5, H6, and H7 are respectively colored in blue, orange, green, pink, yellow, light-blue, and violet, whereas I1, I2, and I3 are respectively colored in light-green, gray, and purple. The amino acid stretch corresponding to rhodopsin's H8 is colored in violet as well. The side chains of E463(3.49), R464(3.50), and D564(6.30) are represented by sticks and colored according to their polarities. The composite solvent accessible surfaces computed over the amino acids R464(3.50), T467(3.53), I468(3.54), and K563(6.29) are also shown, represented by gray dots.

residues is that they contribute to the environment of R143(3.50) of the E/DRY motif on H3. Critical comparisons also highlighted differences in the amino acids which participate in the H3/H6 interface and, thus, constitute the environment of R143(3.50) of the DRY motif. In the homology model, R143(3.50) makes a charge reinforced H-bond with both the adjacent D142(3.49) and E289(6.30) and, hence, D142(3.49) is suggested to exert a constraint on the motion of R143(3.50) through a charge-reinforced H-bond rather than through long-range electrostatic interactions as suggested by the ab initio model.[132] A feature of the inactive state within the homology model, not shared with the previous ab initio model because of slightly different rotation of H6, is the charge-reinforced H-bond between the E/DRY arginine and E289(6.30), predicted to be an additional constraint to the R143(3.50) motion and a link between the cytosolic extensions of H3 and H6. For both the ab initio and the comparative models, the virtual structures representative of the active state are characterized by the weakening of the charge-reinforced H-bonds involving R143(3.50) in the inactive state.[132,134] The hypothesis, raised by the homology model, that both D142(3.49) and E289(6.30) contribute to stabilize the inactive state of the α_{1b}AR found support in the results of in vitro experiments, which showed that replacing either D142(3.49) or E289(6.30) with a neutral or a cationic amino acid that would break the salt bridge with R143(3.50) leads to agonist-independent receptor activation.[127,128,132,134] An equivalent role of the E/DRY arginine, as important switch of mutation-induced receptor activation, has been inferred by very recent computations on OTR.[141]

Our hypothesis that the R3.50−E6.30 salt bridge would be a feature of receptor inactive states lost in the active ones appeared in two publications, one in 2001[132] and the other in 2002.[134] The first publication came out the same year of the very highly cited publication by Ballesteros and co-workers, which launched the universally adopted term "ionic lock" to indicate the R3.50−E6.30 salt bridge. The role of the charge-reinforced H-bond between R3.50 and E6.30 in maintaining the inactive states of GPCRs has been overemphasized by a number of computational and in vitro experiments[131,132,134−139,142,145−148] (see also references in the red updates throughout the text). However, the significantly lower conservation of the glutamate/aspartate at position 6.30 (i.e., 32%) compared to the glutamate/aspartate at 3.49 (i.e., 86%)[75] makes its potential role valid only for a few GPCRs. Computations on the μ opioid receptor,[758] on the MCHRs,[608] and on OTR[141] suggested that, in the absence of a conserved glutamate/aspartate at position 6.30, other amino acids in the cytosolic extension of H6 may contribute to create H-bonding interactions with the E/DRY arginine. These amino acids include T6.34, for the μ opioid receptor,[758] T6.30, for MCHR1,[608] and T6.33, for OTR.[141] Collectively, the low conservation of E6.30 in family A GPCRs, the recent crystal structures of the inactive states of nonopsin GPCRs,[93−96,103] and in vitro data on rhodopsin[759] suggest that, of the two salt bridges involving R3.50, the interhelical one is expected to not characterize all the inactive receptor states. In contrast, the intra-E/DRY salt bridge should be considered as an universal switch of GPCR activation.

As for the LHR, simulations on the novel homology model of most of the spontaneous pathogenic activating and inactivating mutations discovered so far strengthened the role of the second and third intracellular loops and of the cytosolic extensions of H3 and H6 as the targets of the structural modifications induced by the different spontaneous activating mutations.[135,139,142,614,752,753] Indeed, the average minimized structures of the constitutively active mutants share the increase in solvent accessibility of selected amino acids at the cytosolic interface between H3 and H6. This effect, already observed in the previous ab initio model, is properly described by the solvent accessible surface area (SAS) computed over selected amino acids, including the E/DRY arginine. Such a computational index proved to be an effective hallmark of the functional receptor state, being lower than 50 Å^2 in the inactive forms and higher than 50 Å^2 in the active ones (Figure 22).[135,139,614] It was, therefore, successfully challenged in its ability to predict the functional behavior (i.e., active and nonactive) of a large number of artificial mutants of the LHR.[135,139,142] Another feature of the most active LHR mutants was the weakening of either one or both the charge-reinforced H-bonding interactions found in the wild type between R464(3.50) of the E/DRY/W motif and both E463(3.49) and D564(6.30) (Figure 22). The correlation between weakening of such interactions and an increase in the basal receptor activity has been proposed also for the thyrotropin receptor (TSHR).[140] However, according to our computational models, the interaction pattern of the E/DRY/W motif is a less effective hallmark of the functional state of LHR than the SAS index.[135,139,142] These inferences were stressed by more recent computations on the

other two members of the GPHR subfamily, i.e., the follicle stimulating hormone receptor (FSHR) and TSHR.[146,148] In this respect, the comparative analysis of equivalent mutants in LHR and FSHR suggested that the mechanisms through which homologous mutations increase the basal activity of the LHR and the FSHR are substantially similar. This is particularly true for the strongest CAMs. We speculated that disparate properties of the LHR vs FSHR active mutants may be due to differences in shape and electrostatics features of the solvent-exposed cytosolic receptor regions involved in the receptor−G protein interface, rather than to differences in the nature of the local perturbation at the mutation site, or in the way local perturbation is transferred to the putative G protein binding regions.[148] In a recent paper, the importance of the SAS index as a hallmark of the functional receptor state was correlated with the G protein recognition properties of the receptor.[145] In this respect, in vitro and in silico mutational experiments on the LHR targeting the cytosolic extensions of H3, H5, and H6, as well as I2 and I3, could differentiate the hot spots in the intramolecular communication involving the activating mutation sites from the hot spots in the intermolecular communication between receptor and G protein. The hot spots in the intermolecular communication are few and include most of the amino acids found to contribute to the SAS index in early computational experiments on different LHR models (reviewed in ref 233).[145] These results corroborate the hypothesis that the cytosolic receptor portions that undergo solvent exposure triggered by activating mutations participate in the receptor−G protein interface.[145] The latter include the highly conserved E/DRY arginine that, therefore, is expected to be a receptor recognition point for the G protein (i.e., Gs) rather than a switch of receptor activation. The inferences from the study suggested a novel way to consider CAMs, i.e., receptor states characterized by improved complementarity for the G protein.[145] Thus, activating mutations of the GPHRs, in spite of the topological and physicochemical differences between them, seem to share the ability to communicate with the cytosolic extensions of H3 and H6, where they induce the opening of a crevice recognized by the C-term of the G protein α-subunit. These results find support in the crystal structures of Ops* and MII both in their free state and in complex with GtCt,[107,108,110] as well as in the more recent complex between agonist-bound β_2AR and nucleotide-free Gs heterotrimer.[100] The computational model of the LHR-Gs interface has been very recently refined following docking simulations between GDP-bound heterotrimeric Gs and a novel model of the D564G LHR CAM based upon the crystal structure of Ops*.[607]

In a recent study, we looked at the structural models of inactive and constitutively active LHR forms in terms of structure networks, in which each amino acid constitutes a node, and in terms of communication paths between intracellular and extracellular nodes.[754] The analyses allowed the identification of key amino acids that are part of the regulatory network responsible for propagating communication between the extracellular and intracellular poles of the receptor. Another novelty in the study compared to our previous works on the LHR is that the constitutively active LHR mutant originates from MD simulations on a structural model based upon Ops* structure. We found that the number of hubs and link-involving hubs in the wild type is higher compared to the two CAMs, D6.30G and D6.44H, consistent with the demonstrated lower stability of the active GPCR forms compared to the inactive ones. The study suggested also that constitutive activation of the LHR is associated with an increase in the number of intramolecular communication paths, indicative of augmented information flow between the two poles of the helix bundle. Thus, in the CAMs, a reduction in highly connected amino acids seems to be associated with enhanced intramolecular communication.[754] Highly conserved amino acids in the rhodopsin family GPCRs were predicted to participate in the protein structural stability as they acted as stable hubs both in the inactive and active states. Moreover, they behaved as the most frequent nodes in the communication paths between the extracellular and intracellular sides in both functional states, with emphasis on the active one. In this respect, nonconservative loss-of-function mutations of these amino acids were predicted to impair the most relevant way of communication between activating mutations sites or the hormone-binding domain and G protein recognition regions.[754]

In summary, the extensive in vitro and computational experiments on substantially different GPCRs, such as the α_{1b}AR, LHR, FSHR, TSHR, and OTR, allowed us to infer hypotheses on the requirements for a GPCR site to be susceptible to activating mutations, highlighting commonalties and differences among the distinct mutation sites. One inference from computations was that, despite the topological and structural differences between them, the activating mutation sites are structurally connected with peculiar portions of the cytosolic domains, including the E/DRY motif. Such a highly conserved stretch of amino acids is particularly susceptible to undergo structural modifications in response to activating mutations. In fact, activating mutations tend to weaken the ground state interactions of R143(3.50) and increase the solvent accessibility of selected amino acids at the cytosolic extensions of H3 and H6, which are likely binding sites for the G protein.[100,108,110,145,607] Calculations show that this structural effect is mediated by highly conserved polar amino acids in the seven-helix bundle. Whether the main role of the E/DRY arginine is to maintain the inactive state of the receptor or to recognize the G protein is not clearly understood and may depend on the receptor system (critically analyzed in refs 143,760). For some GPCRs, such as the α_{1b}AR,[513] OTR,[130] and the novel receptor ORF74-EHV2,[144] in which the ad hoc engineered or spontaneous absence of the E/DRY arginine is associated with constitutive activity that is abolished in the presence of the DR pair, the main role of the conserved arginine might be to maintain the inactive state of the receptor and drive receptor isomerization into different functional states (reviewed also in ref 143). On the other hand, combined in vitro and computational experiments on LHR-Gs coupling[145,607] together with the advances in crystallographic determinations of Ops* and MII in complex with GtCt,[108,110] as well as of β_{2A}R in complex with heterotrimeric Gs[100] suggest that R3.50 participates in G protein recognition.[108,145]

Critical comparisons of the interpretative and predictive abilities of the previous ab initio and novel homology models of the α_{1b}AR, LHR, and OTR seem to suggest that the homology models can be considered advancements over the previous ab initio models, which have, however, been extremely useful for developing the computational approach. However, these conclusions are essentially based on low resolution experimental data, which are not properly adequate for validating atomistic models. Therefore, perhaps it would be better to say that homology models are expected to be more reliable than the ab initio ones (at least in the portions where significant sequence similarity exists between template and target proteins), on the basis of the results of critical assessments of protein structure prediction methods.[761]

The major problems with in vacuo simulations, such as those that we have carried out to study mutation-induced GPCR activation, are associated with the rough evaluation of the electrostatic energies, including the dielectric constants that represent the effect of the protein environment. One consequence of the lack of the proper screening effect of the solvent is an overall overestimation of the water-exposed salt bridges and charge-reinforced H-bonding interactions. However, active and nonactive receptor forms have been simulated by using the same computational setup. Therefore, the selective breakage or formation of electrostatic interactions with changes in the functional receptor state may be indicative of a significant effect. Along the same line, the inferences from in vacuo simulations were recently corroborated by MD simulations on mutation- and ligand-induced activation of OTR, by using the IMM1 implicit membrane/water model[762] without any intrahelical distance restraints, as well as more recently on mutation-induced activation of the GPHRs,[145,146,148,754] and ligand-induced activation of the TXA_2R[147] by using the GBSW implicit membrane/water model.[763] Convergence was, indeed, found between in vacuo and implicit membrane/water computations, concerning the structural peculiarities of the inactive and active forms of the receptor.[141,145−148,754] This may be due to the fact that the structural hallmarks of the inactive and active states preferentially involve the helix bundle rather than the loops, which have lower resolution and are more sensitive to differences in the electrostatic models than the seven helices. In this respect, consistency between the two different electrostatic models has been found although the implicit representation of the protein environment provides a better screening effect than in vacuo simulation.

The strength of our computational approach is that it relies on an extensive comparative analysis, which is aimed at inferring similarities/differences within the same approximations. One of the main inferences of this comparative approach is that a receptor exists in different active states that, however, share a few key structural features, which presumably determine the macroscopic functional receptor state. This inference is in line with the ensemble theory.[719,738,739]

As for computational experiments by other researchers, recent investigations employed computational models of H_1 histamine, 5-HT_4 serotonin, and δ opioid receptors as a structural context to interpret in vitro-observed constitutive activities of selected receptor mutants.[764−767] The receptor models were achieved by using the crystal structures of rhodopsin, or the β_2AR, or Ops* as templates. The analyses of local perturbations in the mutation sites highlighted selected intramolecular interactions made either by D3.49, W6.48, or N7.49 as switches of receptor transitions toward different active states. In line with these computational experiments, a comparative study on the inactive (based upon dark rhodopsin structure) and active (based on Ops* structure) state models of the TSHR suggested that, whereas the inactive state is constrained by a core set of polar interactions among H2, H3, H6, and H7, the active state conformation is stabilized mainly by nonpolar interactions between H5 and H6.[767]

Full-atom normal mode analysis (NMA) was employed to investigate the functional dynamics of the ghrelin receptor ($GHS\text{-}R_{1a}$).[768] In this respect, NMA was applied to an energy minimized structural model based upon the crystal structure of the β_2AR and extracted from a 8 ns equilibrated MD trajectory in explicit water/membrane. Homology models of the $GHS\text{-}R_{1a}$ based upon the rhodopsin and Ops* structures were employed as representatives of the inactive and active states, respectively. The results of the study suggested that the constitutive activation of the unbound receptor can be mostly described by only one of the lowest frequencies normal modes (mode 16). Such normal mode was, indeed, able to describe both the transitions from the β_2AR-based model to the rhodopsin-based model, and, in the opposite direction, to the opsin-based model. The mode was found to agree with the helix-motions, the increase in solvent accessibility of the ERY motif, and the flip of W6.48, commonly associated with GPCR activation.[768]

MD simulations served to infer potential differences in the intrinsic dynamics of the thyrotropin releasing hormone receptors 1 and 2 (TRH-R1 and TRH-R2), potentially related to the higher basal activity of TRH-R2 compared to the other subtype. The study highlighted the involvement of W6.48 in the signaling process and a relation between basal activity and conformational changes in H5.[769]

5.3. Computational Modeling of Ligand−Receptor Interactions

Heterogeneity in the functional properties of GPCR ligands is nothing compared to the heterogeneity in their structural features. Indeed they comprise small molecules, such as ions, organic compounds, amino acids, nucleotides, and lipids, or large ones, such as peptides, proteins, and even viral particles.[1,4−7] Chemical diversity on the ligand side corresponds to diversity in the receptor binding site and, hence, in the ligand−receptor interaction modes, as also highlighted by in vitro mutagenesis and biochemical experiments.[1,4−7] According to an oversimplified and broad view, small organic ligands are thought to bind into the TM portions of the helix bundle, whereas peptide compounds would dock primarily into the extracellular loops. The latter situation is particularly true for glycoprotein hormone receptors, for which the N-terminal domains have been predicted as being highly structured and holding the major recognition points for their natural agonists.[140,589−593] The very recently released crystal structure of the follicle-stimulating hormone (FSH) in complex with the ectodomain (i.e., the N-term) of the FSH receptor confirmed structure predictions that the major receptor binding site for the hormone is a portion of the N-term, holding a leucine-rich repeat (LRR) topology.[18] However, in the crystal structure, the LRR topology belongs to the class β,[18] rather than to the class $\alpha-\beta$ as predicted by early studies.[140,589−591,593] This has been confirmed by the recent crystal structure of the thyroid-stimulating hormone (TSH) in complex with a thyroid-stimulating autoantibody.[594]

Most of the computational experiments done so far on GPCRs concerned ligand binding site identification and predictions of the ligand interaction modes for either qualitative or quantitative structure−affinity/selectivity relationships and drug design (reviewed also in refs 423,770−782). In contrast, very few computational studies have been aimed at investigating the structural changes induced by agonists into receptor portions more or less distal from the ligand binding site.[130,138,141,147,158,426,473,478,489,492,503,504,509,511,608,783−793] The results of these studies are reviewed in a separate section.

The literature is full of examples of more or less sophisticated computational approaches aimed at achieving interaction models between GPCRs and their ligands. Attempts to unravel the mechanism of ligand entry into the putative binding site have been done by a few computational experiments, based upon either Brownian dynamics[794] or MD coupled with quasi-harmonic analysis.[462] In the first case, Brownian dynamics on a model of the extracellular domain of the β_2AR suggested that helical

movement must accompany movements of the extracellular loops to allow the ligand to pass through.[794] The second case concerns computational experiments on a model of the extracellular loops of the thyrotropin-releasing hormone (TRH) receptor (TRHR).[462] The static analysis based on curvature and electrostatic potential on the surface of TRHR suggested the formation of an initial recognition site between TRH and the surface of its receptor. A quasi-harmonic analysis of the vibrations of the extracellular loops suggested that the low frequency motions of the loops could aid the ligand to access its transmembrane binding pocket. It was, hence, suggested that all small ligands may bind sequentially to the TM pocket by first interacting with the surface binding site and then may be guided into the transmembrane binding pocket by fluctuations in the extracellular loops.[462]

Microsecond MD simulations in explicit membrane/water led to hypothesize that a classical cannabinoid would enter through a lipid pathway involving the TM interface between H6 and H7.[795] The LigPath algorithm was recently used to scan the potential energy surface of the binding process of dimeric histaprodifen, a partial agonist at H_1R, to a H_1R model based upon the crystal structure of rhodopsin.[796] The difficulties in simulating the ligand entry into the receptor binding site are also linked to indetermination in the arrangements of the extracellular loops, which are expected to play a relevant role in ligand recognition. Before the release of the crystal structures of nonopsin GPCRs, the extracellular domains were predicted to form a tightly bound canopy that makes ligand entry difficult. This is evident in the crystal structures of rhodopsin, in which the N-terminal tail forms a very compact β-sheet structure with E2, thus completely shielding the retinal chromophore from the extracellular environment. Such an arrangement of the extracellular domains, if conserved in a number of homologous GPCRs, suggests that dramatic conformational changes should occur to let the ligand enter the receptor binding site, or that interhelical locations may constitute the entrance. For rhodopsin, a potential entrance site for the chromophore has been, indeed, hypothesized to reside in the cytosolic domains (i.e., site II in Figure 2).[225] Two recent investigations agree on the hypothesis that the uptake of 11-*cis*-retinal would occur through a site in between H1 and H7, whereas the release of photolyzed all-trans-retinal would occur through a site in between H5 and H6.[227,228] However, this feature must be unique to rhodopsin and not to the homologous GPCRs, which recognize ligands from the extracellular side as also suggested by the recent crystal structures of nonopsin GPCRs, which show significant accessibility of the ligand binding sites from the extracellular medium (Figure 17). The recently determined crystal structure of the human β_2AR provides an excellent structural basis to explore ligand binding and dissociation process. On the basis of such structure, the random acceleration molecular dynamics (RAMD) simulation method served to explore ligand exit from the receptor, and to infer a putative entry site.[797] Simulations showed that the extracellular opening on the receptor surface is the most frequently observed egress point, whereas the cleft formed by the hydrophobic bridge between E2 and H7 as well as H1, H3, and H7 on the extracellular surface likely serves as a more specific ligand-entry site.[797]

Thus, almost all the intermolecular-interaction models reported so far were achieved following either manual or automatic docking of the ligand into the putative binding site of the target receptor model. Given the enormous number of reports on the matter, we prefer to broadly classify and quote them according to the approach used to bundle the TM helices, i.e., (a) by ab initio approaches strongly based on the 2D electron density maps of rhodopsin[527,539,543−545,798−804] or on the integration between 2D and 3D electron density maps of rhodopsin and inferences of Baldwin's analysis[130,158,444,446−450,452−454,456,461,464,466,468−473,475−484,486−498,506−509,511] or (b) by comparative modeling, employing either BRD[365,366,368,370−373,375−395,397−399,402,403,405−407,409,410,414,415,702,805−814] or ab initio models of rhodopsin,[518−520,531] or, since very recently, the crystal structure of bovine rhodopsin as a template.[138,141,279,530,577,593,608,630,631,634,637,639−655,658,660−672,676−683,685−699,701,702,781,783,795,815−928] Alternative approaches consisted of modifying helix-bundle models previously achieved using BRD as a template to incorporate the available structural information on rhodopsin, i.e., the cryo-microscopy 3D map,[15] the outcomes of Baldwin's study,[14] and the crystal structure.[16,419−421,811−813,929,930] A number of computational modeling studies on the GPCR ligand binding sites are also reviewed in refs 423,770−776 . Since the release of the crystal structures of Ops* and nonopsin GPCRs, comparative modeling of the homologous GPCRs is being done, by using either one structure or combinations of the available structures as templates.[603,781,910,912,916,922−924,931−965] A number of binding site-targeting computational experiments are being done as well on the crystal structures of nonopsin GPCRs.[97,314,315,791,797,966−979]

Differences in the modeling approaches, however, concerned not only the ways of packing the TM helices but also the criteria for determining the beginning and ending of each TM domain, the absence or the more or less complete inclusion of the extracellular and intracellular domains, and the ways of modeling such hydrophilic domains. Differences also concerned the energy refinements of the ligand and the receptor before and after docking. In fact, a few steps of energy minimization or MD simulations were employed either to achieve the input receptor structure for manual or automatic docking or to produce the final ligand−receptor complex. Extremely variable computational setups were employed. Differences resided in the force field; the more or less implicit treatment of the hydrogen atoms; the protonation state of titratable amino acids or of ligand functional groups; the approaches for choosing the proper ligand conformation and charge distribution; the ways of capping the terminal amino acids; the ways of approximating the lipid/water environment; the ways of truncating the nonbonded potentials; the employment or not of intramolecular and intermolecular restraints; the type of restraints and the ways of applying them; the algorithms used for energy minimizations; the number of minimization steps; the molecular simulation methods (e.g., simple MD or mixed Monte Carlo−stochastic dynamics (MC-SD)); the integration steps; the length and organization of the different simulation stages (i.e., heating, equilibration, and production phases); the simulation ensemble; etc. A significant number of cases also exist in which no energy refinement has been done before and after the ligand−receptor docking. Overall, the receptor systems were subjected to short MD simulation time periods, which only in a few cases exceeded 500 ps (i.e., refs 138,139,141,473,487,488,510,512,608,648,655,659,675,677,682−685,690,691,698,699,783,980 among the articles on the free and/or ligand-bound receptor forms reviewed in this article). In some cases, the lengths of MD simulations were exceedingly short (i.e., 250−500 ps unrestrained production phases) for the molecular systems under study (i.e., all-atoms TM-receptor model in explicit methane[658,817,818,981] or lipid/water[692,696,982]). Simulation time is, however, becoming ever increasingly longer over the last years (reviewed in ref 983 as well as in the updated (red) parts of the text).

Despite the enormous diversity in the computational approaches to GPCR modeling, it frequently happened that substantially different models of the same ligand−receptor complex were found consistent with the available experimental data, independently of the accuracy and reliability of the computational model. This is a consequence of the low resolution of the experimental data, such as the results of site-directed mutagenesis experiments, which were generally used both to drive the computational experiments and to evaluate the reliability of the models. In this respect, it is not surprising, for example, that an early model and a recent significantly different model of the melanin-concentrating hormone (MCH) interacting at its target receptor were both consistent with site-directed mutagenesis data.[405,608] In fact, the ligand−receptor interaction, suggested to be crucial for the MCH binding (i.e., the charge-reinforced H-bond between Arg11 of the hormone and D3.32 of the receptor), was present in both the models regardless of the different stereochemistries of the complexes.[405,608] It is noteworthy that the early model included only the TM helices in a BRD-like architecture and the extracellular loops.[405] In contrast, the novel model was achieved by using the crystal structure of rhodopsin as a template and included all the domains but the C-tail.[608] The relevant differences between the two models originate also by the fact that the early model was simply subjected to a few steps of energy minimization, whereas the novel one was the product of a large series of MD simulations.[405,608] This example, that is quite representative of the many ones reported in the literature, suggests that the results of site-directed mutagenesis experiments are inadequate to assess or improve the stereochemical quality of an atomistic model. Significant insight into mapping the ligand−receptor interactions could be provided by photoaffinity labeling and FRET experiments, which could estimate spatial proximity between photolabile residues within a ligand and its receptor.[430,433,434,439,442,984,985] The resolution level of the information inferred by such approaches, although higher than that achieved by common in vitro site-directed mutagenesis experiments, is, however, still not high enough for help in assessing the stereochemical quality of atomistic models. This is clearly demonstrated by a novel report, showing that two substantially different models of E2 in the human NK1 receptor, one obtained by comparative modeling, using the crystal structure of rhodopsin as a template, and the other achieved by NMR determinations on the isolated peptide, both were consistent with distance estimations by photoaffinity labeling experiments.[637]

Computational models of GPCRs, which do not incorporate structural information from the high resolution structure of rhodopsin, have been useful in driving and interpreting the results of low resolution experiments. However, their indetermination is too high for de novo drug design purposes, which would require knowledge of the exact stereochemistry of the ligand binding site. This is particularly true for the interaction models involving huge peptide ligands, which are expected to establish more contact points with the receptor, as compared to small cationic compounds, and many of these contacts are predicted to involve the extracellular loops, whose conformation and architecture are ill-defined in the majority of the computational models not based upon the rhodopsin structure. The best examples of lead optimization based on 3D models of GPCRs relied on robust and extensive SAR analyses on highly informative sets of compounds, such as, for example, the ligands of the adenosine receptors.[773]

The recent availability of the crystal structures of nonopsin GPCRs opens unprecedented opportunities to effectively challenging structure-based drug design approaches and improving the reliability of comparative models especially for close homologues[566] (reviewed also in refs 310,986−990). In this respect, mapping the surfaces of the crystal structures of β_1ARs and β_2ARs revealed distinct pockets formed at both solvent-exposed and lipid-exposed cavities, which may constitute potentially druggable allosteric sites.[976] In this respect, we are confident that comparative modeling would produce more reliable results than NMR determinations on the isolates peptides, as largely demonstrated by the inconsistency between the cytosolic domains of rhodopsin determined by NMR and those in the crystal structures.[92,991−994]

Once different starting configurations of the ligand−receptor complexes fulfilling the ligand−receptor shape and electrostatic complementarities and the key interaction requirements from the experimental data have been obtained, these must necessarily be subjected to molecular simulation protocols aimed at finding suitable different local minima of the potential energy surface. This has to be done independently of the functional state of the considered ligand (i.e., full, partial, inverse agonist, neutral antagonist, etc.), essentially because GPCRs exist in different conformational states already in their empty forms and the shape of their potential energy surface changes on the basis of the structural features of the interacting ligands. An intriguing inference from recent docking simulations between agonists and antagonists and different GPCRs, including the 5-HT$_{1A}$ serotonin receptor, MCHR1, and MCHR2 and OTR, is that the same ligand, depending on its interaction modes, can generate different average configurations of the same receptor. These configurations differ from those of the empty receptor forms. On the other hand, comparing a large number of average configurations obtained for the different agonist− and antagonist−receptor complexes, following different computational protocols, it has been possible to infer similarities in the interaction modes of the different agonists at their cognate receptors.[138,141,608] The receptor sites, in which most of such similarities occur, essentially concern selected positions in the extracellular halves of H3, H5, and H6 (Figure 23). Computational modeling of the agonist-bound forms of the 5-HT$_{1A}$, MCH, and OT receptors suggests that these receptor portions hold the key contact points for the ligand moieties responsible for the efficacy.[138,141,608] These receptor essential contact points overlap, at least in part, with those which have been recently proposed to constitute conserved GPCR binding pockets recognized by "privileged structures".[661] The term "privileged structures" indicates an ensemble of structural motifs, shared in common by ligands, which bind different receptors, in other words, "a single molecular framework able to provide ligands for diverse receptors".[661,772] We have shown that the combination of rhodopsin-based receptor models with extensive comparative MD simulations could be able to find such privileged structures even in large peptide ligands such as MCH and OT.[141,608] These results would have been hard to achieve with static models. In our opinion, the most promising approaches to the search for a linkage between ligand−receptor atomistic models and biological responses (i.e., affinity, selectivity, and efficacy) will be those based on ever increasingly accurate and effective configurational sampling methods.

5.3.1. Computational Approaches to Virtual Screening of GPCR Ligands. *5.3.1.2. Definition of Structural Descriptors for*

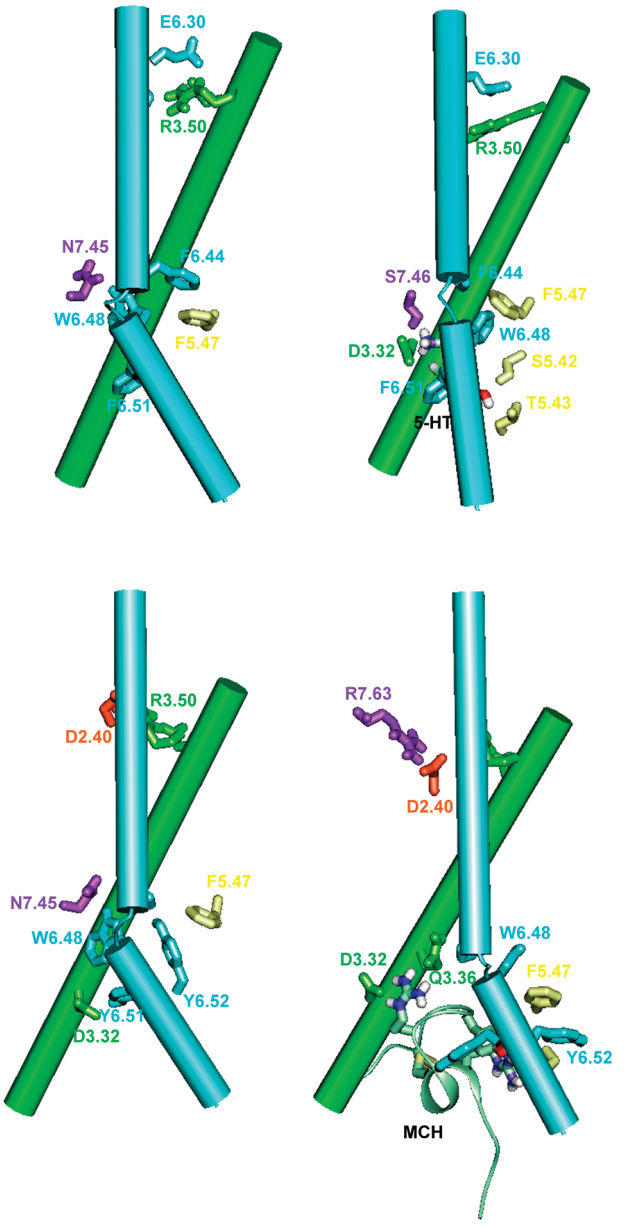

Figure 23. (top) Structures of the empty (left panel) and of the 5-HT-bound (right panel) forms of the 5-HT_{1A} receptor averaged over the 1000 structures collected during the last 500 ps of a selected 2 ns trajectory and minimized.[138] (bottom) Structures of the free (left panel) and MCH-bound (right panel) forms of the MCHR1 averaged over the 200 structures collected during the last 100 ps of a 2 ns trajectory and minimized.[608] The models are viewed in a direction parallel to the membrane surface, with the cytosolic side being at the top. Only H3 and H6 are shown, represented by cylinders. Details of the interactions made by R3.50, by the agonists, and by the members of the aromatic cluster in H6 are shown. The amino acid side chains are colored according to their location (i.e., the helix they belong to), following the color coding described in the legend to Figure 22. 5-HT and MCH are colored by atom type. 5-HT is represented by sticks (top right), whereas MCH is represented by cartoons (bottom right).

Estimating Ligand Affinity and Efficacy. A challenging task in computational modeling of GPCRs is to define intermolecular-interaction descriptors and computational protocols, which could be used for virtual functional screening (reviewed also in ref 995). The effectiveness of these computational descriptors will rely on the reliability of the ligand−receptor complex, on the accuracy of the computational protocols, and on the availability of highly informative training sets of compounds with accurately determined biological responses. Pioneers in this respect have been computational experiments aimed at defining intermolecular-interaction descriptors on the ligand−receptor complexes, which could correlate linearly with biological data such as binding affinities or efficacies (reviewed also in refs 996−998).[377,378,448,503,507−509,644,999] In this respect, an intermolecular-interaction descriptor, somewhat related to the binding energy and, hence, called BE, was used to rationalize and predict the binding affinities and selectivities of different GPCR ligands.[370,378,448,508,644] Such a descriptor, which ill-defines all the entropic effects, is computed on the ligand−receptor energy-minimized complexes according to the following formula: BE = IE + E_R + E_L, where IE is theligand−receptor interaction energy (i.e., the total energy of the ligand−receptor complex minus the energy of the ligand and the receptor in thecomplex) and E_R and E_L are the distortion energies of the receptor and of the ligand, respectively, calculated as the differences between the energies of the bound and of the free optimized molecular forms. Fora series of selective and nonselective antagonists of the α_{1a}, α_{1b}, and α_{1d}AR subtypes, consistency was found between the affinity/selectivity predictions by the intermolecular-interaction descriptor BE[508] and those by a ligand-based approach, i.e., the supermolecule approach (reviewed also in refs 996−998).[1000−1002] The supermolecule approach assumes that the volume obtained by superimposing the most structurally different ligands showing the highest affinities for the same receptor (supermolecule) might reflect the overall shape and conformational flexibility of the high affinity receptor binding site. Therefore, size and shape descriptors can bedefined ad hoc (that is, on a specific molecular series and in connection with a specific bioactivity) with respect to the supermolecule, and this constitutes the main advantage overmolecular descriptors defined and performed for a single structure and a single conformation. The most effective indices in this respect were V_{in} and V_{out}, which are respectively the intersection and the outer van der Waals volumes of the ligand considered with respect to the volume of the reference supermolecule, and V_{dif}, which is computed according to the following formula: $V_{dif} = (V_{in} - V_{out})/V_{sup}$, where V_{sup} is the molecular volume of the reference supermolecule. According to the definition of size and shape descriptors, higher affinitiesare realized by maximizing V_{in} and minimizing V_{out}.[1000−1002]

Convergence was found concerning the inferences from the ligand−receptor interaction models and from the supermolecule approach.[508,1000−1002] It was, in fact, inferred that, while the protonated nitrogen atom is an essential pharmacophoric element for the long-range electrostatic recognition and productive interaction with the aspartate of the α_1AR binding site, its contribution to the interaction energy is relevant but almost constant.[508] In contrast, short-range forces modulate both ligand affinity and selectivity. Thus, the modulation of the binding affinity by a widen oncongeneric series of α_1AR ligands can be described and explained by the variation of the ligand size−shape features that are related to the short-range acting forces. In this respect, the intermolecular-interaction descriptor, BE, is rather independent of the reliability of the ligand−receptor complexes.

Assuming that differences in entropic and solvation/desolvation terms are small within aseries of structurally similar ligands, Shim et al. approximated the binding free energy of a series of CB1 ligands to the interaction energy. The latter is the total

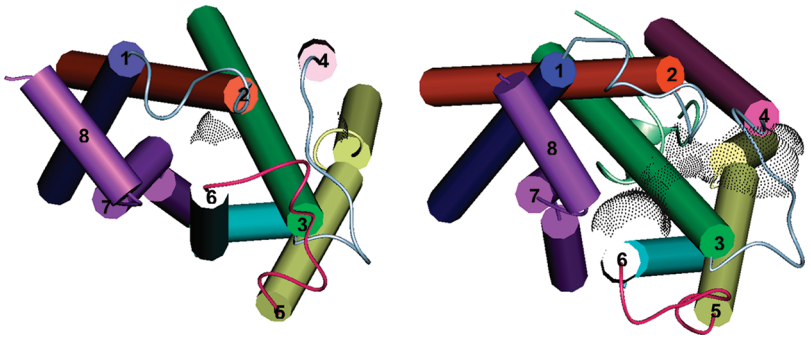

Figure 24. Structures of the empty (left) and MCH-bound (right) forms of MCHR1, averaged over the 200 structures collected during the last 100 ps of the selected 2 ns trajectories and minimized.[608] The extracellular loops are not shown. H1, H2, H3, H4, H5, H6, and H7 are respectively colored in blue, orange, green, pink, yellow, light-blue, and violet, whereas I1, I2, and I3 are respectively colored in light-green, gray, and purple. The amino acid stretch corresponding to rhodopsin's H8 is colored in violet as well. The hormone is colored by atom type. The structures are seen from the intracellular side in a direction perpendicular to the membrane surface. The solvent accessible surface computed over N76(2.37), R141(3.50), K153 (in I2), I247(6.26), and T251(6.30) is shown represented by gray dots.[608]

energy of the ligand−CB1 complexes minus the energies of the unbound ligand and receptor forms.[657] This index was used to evaluate the best binding conformations for a seriesof nonclassical CB1 agonists.[657]

Very recently, an intermolecular-interaction descriptor has been proposed for its qualitative agreement with the in vitro binding affinity data concerning selected GPCR ligands.[539,799,800] This descriptor, which merely relies on the ligand energetics, being the difference between the potential energy of the free solvated and the receptor-bound forms of the ligand, has been proposed as potentially useful for in silico screening.[539,799,800] The AutoDock 3.0.3 scoring function computed on the ligand−receptor complexes was, instead, employed as computational binding free energy in linear correlations with the in vitro-determined binding affinities of CCR5 antagonists.[681]

One of the first attempts to build computational models for in silico functional screening of GPCR ligands is represented by computational experiments on 34 functionally different ligands (i.e., antagonists as well as partial and full agonists of the M_1-muscarinic receptor).[377] In this respect, the percent of the van der Waals contribution (IE_{VDW}%) or the percent of the summation over the H-bonding and electrostatic contributions (IE_{HB+EL}%) to the total interaction energy of the ligand−receptor complexes proved effectiveness in predicting the functional behavior of the targeted ligands.[377] In fact, the IE_{HB+EL}% index was below or close to 20% (IE_{VDW}% above or close to 80%) for antagonists, above 30% (IE_{VDW}% below or close to 70%) for full agonists, and between the previous two values for partial agonists.[377] These computational indices were successfully challenged in their ability to predict the functionality of novel muscarinic ligands docked into an upgraded model of the human M_1-muscarinic receptor.[507] Thus, these intermolecular-interaction descriptors appeared effective, independently of the stereochemistry of the ligand−receptor complexes. This may be due, at least in part, to the fact that they are correlated with intrinsic properties of the ligands such as the size−shape and the propensity to perform H-bonding interactions. In fact, for the same training set of compounds, considered in the same bioactive prototropic forms, it was also possible to definemolecular orbital (MO) derived descriptors, such as the electrophilic superdelocalizability, or size−shape descriptors computed through the "supermolecule approach", which correlated linearly with the ligand efficacy, though less efficiently than the intermolecular-interaction descriptors.[999,1003]

A computational protocol, based upon extensive comparative MD simulations of the free as well as agonist- and antagonist-bound forms of MCHR1 and MCHR2, was recently proposed, which may be used for virtual functional screening of MCHR ligands.[608] This approach relies on size−shape descriptors computed on the average minimized structures representative of the different functional states of the receptor. In detail, the SAS computed over selected amino acids in the cytosolic domains proved to be a good hallmark of the functional receptor state, being close to 0 $Å^2$ in the nonactive states (i.e., empty and antagonist-bound forms) and significantly above 100 $Å^2$ in the active states (i.e., agonist-bound forms)(Figure 24). The amino acids employed for SAS calculations were defined ad hoc for each of the two MCHR subtypes. The predictive ability of the SAS indices was challenged on mutant forms of the hormone obtained by in silico alanine-scanning mutagenesis of all the 19 amino acids of the hormone, except for the two cysteines involved in a disulfide bridge.[608] A truncated form of the hormone, lacking the last three amino acids, was also considered. In detail, each modified form of the hormone was docked in both the MCHR1 and MCHR2 exactly in the same orientationand conformation selected as input for the wild type MCH. Docking was followed by MDsimulations, according to the same computational protocol employed for the wild type MCH and for the antagonist, leading to the calculation of the SAS index. Consistency between in silico-predicted and in vitro-determined functionalities was obtained, as the SAS indices were below 100 $Å^2$ only for the MCH mutants with impaired functionality.[608] Interestingly, for both the MCHR subtypes, the SAS indices correctly predicted that deleting the last three amino acids of the hormone does not cause any impairment in functionality.[608] This, we think, is an encouraging example of in silico functional screening based upon a computational descriptor of allosteric structural modifications in distal cytosolic domains as induced by critical intermolecular interactions in the extracellular half of the receptor.

5.3.1.3. Virtual Screening of Compound Libraries.

Automated docking-based approaches are being ever increasingly used to screen libraries of compounds against computational models or, until very recently, selected crystal structures of GPCRs; the major goal is to discover new leads.

The AutoDock 3.0 scoring function was employed in virtual screening of $P2Y_1$ ligands.[820] The receptor model, which comprised only the TM domains, was achieved by fitting each helix into the corresponding one of the rhodopsin structure.[1004] A database of 500 compounds was screened. Of the 30 top-ranked compounds, 21were selected for in vitro functional screening. Twelve compounds were, finally, identified as agonists or antagonists of the $P2Y_1$ receptor.[820]

Combinations of the scores provided by different docking algorithms have been recently used by an in silico screening study aimed at finding lead compounds for target GPCRs.[646] In detail, Bissantz and co-workers constructed "antagonist-bound" molecular models of three human GPCRs (dopamine D3, acetylcholine M_1-muscarinic, and vasopressin V_{1a} receptors).[646] These models were achieved by manual docking of a known antagonist into a homology model (based upon the crystal structure of rhodopsin) of its cognate receptor, followed by energy minimization. Removing the ligand atoms from the minimized complexes finally yielded, for each of the three receptors, one set of coordinates of what the authors considered to be representative of the "antagonist-bound state".[646] The three models were evaluated in terms of their ability to identify known antagonists seeded into a database of randomly chosen "druglike"compounds. A virtual screening procedure based upon the combination of different docking algorithms in association with seven scoring functions was used.[646] Consensus scoring was then applied to generate small subsets (hit lists) comprising only the top scorers common to two or three scoring lists. Agonist ligands were also considered in a separate study. Different agonist-bound GPCR models were built to account for the knowledge that the "activated states" of GPCRs are conformationally more flexible than the antagonist-bound inactive states. Two agonist-bound models were built for each receptor following the same refinement procedure as that used for the antagonist-bound models, but using full agonists rather than antagonists for receptor refinement, merely based upon energy minimization.[646] The conclusions drawn from this study are that rhodopsin-based models are suitable for virtual screening, since known antagonists seeded in the test databases could be distinguished from randomly chosen molecules. However, such models are not accurate enough for retrieving known agonists.[646] Better suited for agonist screening is a knowledge- and pharmacophore-based modeling procedure that might partly simulate the conformational changes occurring in the active site during receptor activation.[646] The authors speculated that receptor coordinates generated by such a new procedure are suitable for agonist screening and that two alternative strategies relying on different sets of receptor coordinates are needed for the virtual screening of GPCR ligands, depending on whether they are agonist or antagonists. We agree with the author's idea that for antagonist and agonist screening it is better to use, respectively, antagonist- and agonist-bound states of the target receptor. A simple energy minimization is, however, not sufficient to explore the configurational space of the ligand-bound states, whatever the functional behavior of the ligand is. Thus, despite the apparent success of the virtual screening done on static receptor models, we would expect that an exhaustive sampling of the complexes between selected ligands and the receptor, leading to the extraction of one or more representative average configurations of the empty receptor, would improve the results of the screening.

Recently, ab initio computational models of GPCRs, generated by the PREDICT method, have been used for in silico screening.[556,1005] Also in this case, virtual screening was performed on the receptor coordinates extracted from a refined complex with an ad hoc selected antagonist. This strategy is instrumental in overcoming the drawback that all high throughput docking procedures must use a rigid protein structure, which would impair the results of in silico screening. To generate the ligand−receptor complex for virtual screening, a potent small-molecule ligand is placed inside the binding pocket in an initial orientation that agrees with proposed key interactions in the site. To overcome the bias introduced by the imposed initial orientation, a free-energy-perturbation-like simulation is done on the ligand−receptor complex to allow the ligand to reorient itself in the site in response to specific ligand−protein interactions. Screening of the compound library against the receptor models is then performed with the DOCK4.0 software,[1006] employing a special screening and scoring protocol.[1005] At the end of the docking process, the compounds are sorted on the basis of their best docking score. The effectiveness of the virtual screening is estimated by the following two measures: "enrichment factor", which is related to the common measure of "hit rate", and "coverage." An enrichment factor measures the success of virtual screening relative to random screening (which is equivalent to experimental high throughput screening) by comparing the virtual screening hit rate with the hit rate of random screening. A hit rate is the fraction of active compounds found in the screening library by whatever method. The other parameter, "coverage", is defined as the number of active compounds M^q that are included within the top q percent of the ranked library vs the total number of active compounds in that library M: $\text{coverage}^q = M^q/M$.

The approach was first tested on the D2, NK1, and NPY Y1 receptors, by enriching the random libraries of known ligands of these receptors, followed by blind screening.[556,1005] As for testing, coverage was 85%, 80%, and 50% for D2, NK1, and NPY Y1, respectively. The blind screening targeting the D_2, $5\text{-}HT_{1A}$, $5\text{-}HT_4$, and CCR3 receptors always found hits with a binding affinity $< 5\ \mu M$ with hit rates of up to 21%. Thus, in general, the assays validated the quality of the hits as lead compounds for drug discovery. We think that these encouraging results of virtual screening would be significantly improved by increasing the resolution of the structural information incorporated while modeling the receptor. So far, the highest resolution information on the members of the rhodopsin family can be inferred from the crystal structure of rhodopsin. Contrarily to what the authors state, we believe that careful comparative modeling aimed at extracting as much stereochemical restraints as possible from the rhodopsin structure, possibly including the extracellular and intracellular domains, would provide more reliable starting models of GPCRs than the most effective ab initio modeling approaches currently available.[556,1005] In this respect, the authors' statement that their ab initio models are better than those based upon the rhodopsin structure only because they are in better agreement with site-directed mutagenesis data is not acceptable, since the resolution level of site-directed mutagenesis data is low and cannot be used to evaluate the stereochemical quality of atomistic models. Furthermore, the extracellular loops, completely neglected in the ab initio models by the authors, are expected to play a meaningful role in recognizing a significant number of GPCRs' ligands.

Virtual screening by means of ligand−receptor docking was also used by Gouldson et al. to determine whether the inactive model of the β_2AR showed preference for antagonists, while the restraint-based active model showed preference for agonists.[251] The models were

challenged by 172 GPCR ligands, 50% of which were adrenergic ligands. The binding site was primed for docking by interactively docking norepinephrine or *S*-propanolol into the active or inactive models, respectively, minimizing, running MD simulations for 100 ps, and then carrying out a final minimization. High performance of the active-state model in retrieving agonists was shown.[251]

Evers and Klebe developed the MOBILE (modeling binding sites including ligand information explicitly) approach to build GPCR models suitable for virtual screening.[672,1007] With this approach, the information from a selected ligand binding is added as additional restraints during comparative modeling by MODELER.[672,1007] A final model is then chosen from the individual models that best explain the observed ligand binding. Combining the information from the 3D receptor model and the analysis of known NK1 receptor antagonists, a pharmacophore model was deduced, which was used for 2D and 3D database searches.[672] The hits from such searches were docked into the modeled binding pocket of the NK1 receptor, leading to the final selection of seven compounds for the biochemical testing, including one in the submicromolar range. A similar approach was also employed to virtual screening of α_{1a}AR antagonists.[824] In this case, the receptor model was achieved by using a modified version of the MOBILE approach, consisting of the following steps: (a) a ligand is docked into an ensemble of homology models of the target proteins; (b) refinement of the models is done by considering explicitly the interactions with a selected ligand; (c) finally, the best models in terms of intermolecular interactions are selected and assigned side chain conformers from a set of selected models, followed by energy optimization of the entire complex. The finally selected model was used for virtual screening by docking a database of 22950 compounds resulting from the application of a series of hierarchical filters, which also included fulfillment of the Catalyst-generated pharmacophore requirements.[824,1008] The top-scoring 300 compounds were, hence, subjected to cluster analysis, and 80 were sent to in vitro testing of binding affinities. Thirty-seven compounds revealed K_i values better than 10 μM, and the most active compound had a 1.4 nM affinity. We do not think that biasing the results of comparative modeling by low resolution information on the binding properties of a selected compound leads to more reliable receptor models. We rather think that giving the receptor the fingerprints of a lead compound is exclusively instrumental in ligand−receptor docking-based virtual screening that would not be possible otherwise. A modified version of the MOBILE approach was used in a recent study by Klabunde and co-workers, based upon the observation that most family A GPCRs share a small-molecule binding site located in the outer part of the 7TM bundle.[937] The authors developed an automated method to build sequence-derived 3D pharmacophore models capturing the key elements for addressing this binding site by a small-molecule ligand. They generated structure-based pharmacophore models from 10 homology models and 3 X-ray structures of receptor−ligand complexes. These 13 pharmacophores were dissected into 35 different single-feature pharmacophore elements, each associated with a sequence motif or chemoprint, describing its molecular interaction partner(s) in the receptor. Subsequently, the protein sequences of 270 GPCRs were searched for the presence of chemoprints and the appropriate single-feature pharmacophores were assembled into three- to seven-feature 3D-pharmacophore models for each human family A GPCR. These models can be used for virtual screening and for the design of subfamily-directed libraries. A case study demonstrated the successful application of the approach for the identification of potent agonists for the complement component 3a receptor 1 by virtual screening.

The strategy of priming the putative receptor binding pocket with a known antagonist was also employed in a computational study on a CB2 receptor model based upon the crystal structure of rhodopsin.[881] The model of the ligand−receptor complex, refined by MD simulations, was validated by FlexX-Pharm docking against a testing compound database that contains known antagonists. Furthermore, a consensus scoring (CScore) function algorithm was established to rank the ligand docking poses into the receptor. The study indicated that the known antagonists seeded in the testing database can be distinguished from a significant amount of randomly chosen molecules. On the same line, the putative ligand binding site of a rhodopsin-based model of the CCR5 chemokine receptor was refined to accommodate a set of five known nonpeptide antagonists.[882] The structural model was, hence, used to screen a library of 1.6 million commercially available compounds by means of two different docking programs, i.e., Gold2.0[1009] and Surflex1.1.[1010] The screening yielded a hit list of 59 compounds, out of which 10 exhibited a detectable binding affinity to the CCR5 receptor with most binders showing agonist activity.

A structure-based virtual screening was conducted on a ligand-supported homology model of the human H4 histamine receptor (H_4R) based upon the crystal structure of rhodopsin.[908] More than 8.7 million ligand 3D structures derived from different vendor databases were investigated by docking into the H_4R binding site using FlexX. A total of 255 selected compounds were tested by radioligand binding assay, and 16 of them possessed significant binding. Several novel scaffolds were identified as potentially useful for developing selective H_4R ligands.

Ligand-based and receptor-based virtual screening were compared each other in a study on HIV-entry inhibitors for the CXCR4 and CCR5.[893] Receptor-based screening consisted in ligand docking into structural models of the two receptors achieved by using the crystal structure of bovine rhodopsin as a template. For ligand-based virtual screening, several shape-based and property-based molecular comparison approaches were probed, using high-affinity ligands as query molecules. The ligand-based and receptor-based approaches were compared by virtually screening a library of 602 known CXCR4 and CCR5 inhibitors and 4700 presumably inactive molecules. For each receptor, the library was queried using known binders, and the enrichment factors and diversity of the resulting hit lists were analyzed. Overall, ligand-based shape-matching searches yielded higher enrichments than receptor-based docking, especially for CXCR4.

A promising computational approach for binding-site identification and in silico screening of GPCRs with a potential to be used to "deorphanize" orphan GPCRs was recently developed and tested on bovine rhodopsin and BRD.[1011] The methodology, based on the Internal Coordinate Mechanics (ICM) program, was validated inaccurately identifying the ligand-binding pocket of the two TM proteins. Furthermore, ICM flexible docking with and without the loop regions accurately predicted the binding geometry of retinal. The authors also demonstrated that the native ligand can be identified by flexible docking and scoring in 1.5% and 0.2% (for rhodopsin and for bacteriorhodopsin, respectively) of the best scoring compounds from two different types of compound databases. Finally, it was also demonstrated that, even if the side chain positions in the rhodopsin binding pocket are entirely wrong, their correct conformation can be fully

restored with high accuracy (0.28 Å) through ICM global optimization with and without the ligand present.[1011] These binding site adjustments are critical for flexible docking of new ligands to known structures or for docking to GPCR models based upon the rhodopsin structure. Of course, the effectiveness of the approach in virtual screening ofGPCR ligands is expected to strongly depend on the accuracy of the GPCR model. More recently, the virtual screening by the ICM program followed a ligand-steered homology modeling approach to find ligands of MCHR1. The receptor structure was achieved by comparative modeling, by using the crystal structure of rhodopsin as a template. Six novel chemotypes were identified as low-micromolar affinity antagonist.[906]

A combination of 3D pharmacophore search and high-throughput docking (by means of the Glide software)[1012] was used to identify new ligands for the free fatty acid receptor 1 (FFAR1), previously named GPR-40.[909] Virtual screening of 2.6 million compounds resulted in identification of 15 compounds active at FFAR1 either as full agonists, partial agonists, or pure antagonists.

A virtual screening approach aimed at reducing the effects of the low resolution of receptor models was used to find novel ligands of the TRH-R1.[907] A structural model of the complex between THR and TRH1-R1 was employed to generate a receptor-based pharmacophore describing the interaction potential of the TRH-R1 binding pocket. One million commercially available compounds from the ZINC database of diverse drug-like compounds were screened using the FlexSearch protocol (Unity). A subgroup of 100 compounds was selected, leading to the experimental identification of five structurally diverse antagonists of the TRH-R1 and TRH-R2.[907]

β_2AR states induced by functionally different ligands, i.e., full, partial, and inverse agonists were subjected to virtual screening with a test set of 10147 compounds, by means of the docking software GLIDE.[325] The results of the study showed that: (a) a receptor model optimized for agonists produces enhanced enrichment of agonists compared to antagonists; (b) a receptor model optimized for a functionally specific partial agonist produces enhanced enrichment for partial agonists compared to full agonists; (c) the norepinephrine-stabilized conformation causes the enrichment of agonists rather than inverse agonists, whereas the reverse is true for the carazolol-bound crystal structure; and (d) the salbutamol-stabilized model leads to a significantly higher enrichment for noncatechol agonists compared to the norepinephrine-stabilized model.[325]

Virtual screening of more than 130000 lead-like compounds on a computational model of GPR17 led to the discovery of five novel and chemically diverse full and partial agonists of the receptor.[955]

Retrospective screening of more than 9400 compounds, including 182 known ligands was used to validate a computational model of the active state of the 5-HT_{2A} serotonin receptor. The latter was achieved by comparative modeling, by using the crystal structures of the β_2AR and of the Ops*−GtCt complex as templates. The final model was achieved by docking both an agonist and a peptide from the C-term of Gq and then running SMD simulations. The latter were coupled with the application of a number of intermolecular and receptor−intramolecular distance constraints favoring the formation of selected H-bonds.[960]

Virtual screening was also used to assess the validity of the agonist binding site in a computational model of the β_2AR based upon the crystal structure of Ops*.[961] The outcome was that the model is selective for βAR agonists over other GPCR ligands, for (*R*)- over (*S*)-β-hydroxy agonists, and for β2-selective agonists over β1-selective agonists.

A combination of virtual and cell-based screening provided a useful tool for identifying pharmacologic chaperones for the P23H ADRP-linked rhodopsin mutant.[1013] Virtual screening consisted in automated docking (i.e., by DOCK 5.1) of 24000 drug-like small molecules into the crystal structure of dark rhodopsin. The study individuated both weak and potent pharmacological chaperones. In this respect, the β-ionone was easily identified by the high-throughput screening. It strongly inhibited rhodopsin formation and, when incubated in cells expressing P23H opsin, resulted in a 2.5-fold rescue of P23H opsin. The screen also identified compound NSC45012 as a weak inhibitor of opsin regeneration and resulted in a 40% rescue of the mutant opsin. The level of rescue correlated well with the extent of inhibition.

Recent advances in X-ray crystallography of pharmacologically relevant GPCRs provide more templates for improving comparative receptor models (reviewed also in ref 987) Moreover, they offer unprecedented opportunities to evaluate the advantages and limitations inherent in a structure-based approach to drug discovery.[566]

Approximately 1 million commercially available "lead-like" molecules were docked by means of the DOCK3.5.54 program against the β_2AR structure.[968,988] On testing of 25 high-ranking molecules, six were active with binding affinities <4 mM, with the best molecule binding with a K_i of 9 nM (95% confidence interval 7−10 nM); 5 of these molecules were inverse agonists.

The crystal structure of the β_2AR was also used to evaluate the applicability of ligand-based and structure-based models to quantitative affinity predictions and virtual screenings of receptor ligands.[975] In all cases, the bioactive conformation of each ligand was derived from molecular docking onto the crystal structure of the receptor. It resulted that, for ranking the affinity of closely related analogues when a training set is available, a ligand-based consensus model seems to be the best choice, while the structure-based score seems the best alternative in the absence of a training set. Consensus predictions by different models were more robust than those from individual models.

Other studies, aimed at examining the viability of the crystal structure of the β_2AR for computer-aided drug design, inferred that the docking model was able to (a) reproduce the binding mode of the cocrystallized ligand carazolol; (b) predict compelling binding modes for known antagonists; (c) extract known antagonists from high throughput docking studies; and (d) find diverse chemical leads that differ from historic β-antagonist motifs.[966,967]

Receptor−ligand cross-docking experiments revealed that a single β_2AR complex can be suitable for the docking of a range of antagonists and inverse agonists, but they indicated also that additional ligand−receptor structures may be useful to further improve performance of in silico docking or lead-optimization in drug design.[97]

The crystal structure of the A_{2A}R was used as well as a target of docking studies.[970,972,986,970] In this respect, molecular docking by means of DOCK3.5.54 was used to screen a 1.4 million-compound database against the X-ray structure. A number of high ranking and previously unknown compounds (20 compounds) were then subjected to in vitro testing. Of these, 35% showed substantial activity with affinities between 200 nM and 9 μM. For the most potent of these new inhibitors, over 50-fold

specificity was observed for the $A_{2A}R$ versus the related A_1 and A_3 subtypes. Despite the bias of commercial compound libraries toward GPCR-like chemotypes, many of the most potent ligands were novel and dissimilar from known ligands.

The suitability of virtual screening to drug discovery was proved also by a study, in which more than 4 million commercially available "drug-like" and "lead-like" compounds were docked against the $A_{2A}R$ structure.[972] Out of 56 high ranking compounds tested in $A_{2A}R$ binding assays, 23 showed affinities under 10 μM, and two compounds had affinities under 60 nM. The identified hits represent at least 9 different chemical scaffolds and are characterized by very high ligand efficiency (0.3−0.5 kcal/mol per heavy atom). Significant $A_{2A}R$ antagonist activities were confirmed for 10 out of 13 ligands tested in functional assays.

The "GPCR Dock 2010" suggests that fully automatic solutions for docking to modeled GPCRs remain out of reach. Indeed, although most predictions involved extensive computation, expert knowledge of the subject area, information from site directed mutagenesis, and chemical intuition remained the main determinants of success in the distant homology cases.[566] In spite of these inferences, the examples reported above together with a recent study[1014] seem to support the applicability of docking-based virtual screening not only to high resolution crystal structures but also to lower resolution computational models of GPCRs.

5.4. Computational Modeling of Ligand-Induced/Stabilized Active States

The few computational experiments reported in the literature, aimed at simulating the active and nonactive states of GPCRs induced/stabilized by agonists or antagonists, respectively, have been essentially based on comparative analyses of the average structures derived from MD simulations of the free and agonist- and antagonist-bound forms of the target receptor.[130,138,141,158,426,473,478,489,492,503,504,509,511,608,783,1015] Ligands were manually or automatically docked either into the input or the average structure of the receptor, driven by the available indications from in vitro experiments. Comparisons of the MD trajectories of free, antagonist- and/or agonist-bound forms is a strategy still adopted to infer structural/dynamics differences between inactive and active receptor states.[147,789,793]

Early studies include that by Zhang and Weinstein on the TM domains of the 5-HT_{2A} serotonin receptor.[426] MD simulations of the interactions between the 5-HT_{2A} receptor and ligands of different pharmacological efficacies suggested that the binding of a full agonist, but not an antagonist, produces a marked structural change at the cytosolic ends of H5 and H6. MD trajectories showed that the secondary structure of the TM domains of the receptor is well maintained, whereas the conformational changes involve mainly the relative translations and rotations of the helices in the bundle. An algorithm was, hence, developed for improving the analysis of the ligand-induced domain motions over the different MD trajectories obtained for the 5-HT_{2A} receptor.[1016]

The β_2AR was the target of the computational experiments by Gouldson and co-workers, who docked agonists, antagonists, and partial agonists into a receptor model achieved by using Baldwin's α-carbon model as a template and ran MD simulations over a period of 500 ps.[158] The major structural changes were found to occur in the intracellular halves of H5 and H6. The agonist-induced structural changes to H5 and H6 were thought to be large enough to induce a conformational change in I3. An alternative hypothesis inferred by computations was that the change in the tilt of these helices might enhance the formation of a H5,H6-dimer due to the formation of a more optimal helix packing at the dimer interface. Indeed, in the unbound receptor, H5 and H6 were found to be essentially perpendicular to the membrane. However, after the agonist-induced structural changes, the tilt of these helices had changed by approximately 20°.[158]

Sylte and co-workers performed MD simulations on agonist- and antagonist-bound forms of the NPY Y_1 receptor.[478] Packing of the energy-minimized structure of each TM helix was driven by the inferences from the first Baldwin study.[13] All the intracellular and extracellular domains were, then, included in a conformation assigned by MD simulations. The main inferences from this study were that the agonist NPY induces motions of H5 and H6, whereas the antagonist BIBP3226 does not.[478] The same team repeated similar computational experiments on the 5-HT_{1A} receptor, drawing overlapping conclusions with their previous study on the NPY Y_1receptor.[478,492] The initial receptor structure was achieved by modeling the helix bundle on Baldwin's Cα-atom model, taking the N-term structure from an earlier model, and using a database loop search to achieve the three extracellular loops as well as I1, I2, and the C-tail.[492] The free as well as full agonist-, partial agonist-, and antagonist-bound forms of the receptor were subjected to comparative MD simulations. In the simulations, the agonist induced larger conformational changes in H3 and H6 compared to the other helices, whereas the main conformational differences between the agonist- and antagonist-bound receptor forms essentially resided in H5 and H6. During the simulations, all the ligands constrained helix movements, compared to the case of the empty receptor form.[492] In a more recent study, following docking and MD simulations of a number of ligands characterized by different functionalities at pre- and postsynaptic 5-HT_{1A} receptors into an updated model of the 5-HT_{1A} receptor, the authors speculated that presynaptic antagonistic behavior is connected to large movements of H7, whereas presynaptic agonistic behavior is associated with large displacements of H2 and small displacements of H7. Moreover, postsynaptic partial agonist behavior would be connected to large displacements of H4 and H5, which, instead, would show a small displacement following interaction with postsynaptic antagonists.[783]

Over the last 15 years, we have done extensive studies aimed at investigating the propagation of the structural modifications from the ligand binding site to distal receptor domains, following the docking of selected agonists and antagonists into their cognate receptors.[130,138,141,147,503,504,509,511,608] Targets of our study have been different members of family A, including the α_{1b}AR, M_3-muscarinic receptor, OTR, 5-HT_{1A} serotonin receptor, MCHR1, and MCHR2 as well as the $TX_{A2}R$.[130,138,141,147,503,504,509,511,608]

The computational approach was essentially the same as that employed to infer the structural differences between mutation-induced active and nonactive receptor states, the only difference being the perturbation introduced in the initial model, i.e., ligand docking, in one case, and point mutation, in the other. The computational approach consisted of manual docking of selected agonists and antagonists into the putative binding sites of the average minimized receptor structures, in early studies, or, more recently, in the input receptor structure derived by MODELER refinements, followed by comparative MD simulations. Manual docking was driven, at least in part, by the available indications of site-directed mutagenesis experiments. The receptor models employed in early studies were achieved by ab initio

modeling,[130,504,509,511] whereas those employed in the latest studies were achieved by comparative modeling, using the crystal structure of rhodopsin as a template.[138,141,147,608]

Early computational experiments focused on the α_{1b}AR and on the M_3-muscarinic receptors lacking the extracellular and intracellular domains.[503,504] First, the average minimized structures of the free receptor were analyzed to identify the hydrogen bonding interactions involving the most conserved polar amino acids. Successively, analyses of the antagonist- and agonist-bound receptor forms were done, focusing on the ligand-induced perturbation in such a H-bonding network. For both the receptors, antagonists substantially preserved, whereas agonists perturbed, the H-bonding network found in the empty forms. By different binding modes and different dynamics mechanisms, the different agonists induced, as a final result, the movement of R3.50 of the E/DRY motif out from a highly conserved polar pocket, possibly exposing this residue ready for interaction with the G protein. This model was in agreement with the hypotheses by Oliveira and co-workers.[1017] MD simulations on more complex ab initio receptor models (i.e., carrying the extracellular and intracellular domains) of the α_{1b}AR and of OTR indicated as well the fully conserved arginine as the target of the structural modifications induced by agonists.[130,511] These studies suggested also that agonist-triggered helix movements would induce the opening of a solvent accessible crevice involving I2, I3, and the cytosolic extensions of H3 and H6.[130,511]

Further insight was achieved by applying the same computational approach to models of the 5-HT_{1A} serotonin receptor, OTR, MCHR1, MCHR2, and TXA_2R built by comparative modeling, using the crystal structure of rhodopsin as a template.[138,141,147,608] The entire sequence of TXA_2R was modeled, whereas the models of OTR and MCHRs included all the intracellular and extracellular domains but not the C-tail, and the model of the 5-HT_{1A} included all the domains but not the N-terminus and the huge I3. The inferences from the latest studies relied on more extensive MD simulations than the previous ones. Indeed, the approach consisted of comparative analyses of a large number of short (100 ps) and relatively long (up to 2 ns) MD trajectories, probing different starting structures as well as different intrahelical (for the empty receptor form) and intermolecular (for the ligand-bound forms) distance restraints. For the empty receptor form, the criteria for selecting the short trajectory that could be worth prolonging included the stereochemical quality of the average minimized structures and their degree of similarity to the rhodopsin structure. Despite the differences between previous and latest approaches and between the receptor systems under study, hallmarks of the ligand-induced active and nonactive forms of the receptors were found to involve R3.50, the arginine of the E/DRY motif, and the cytosolic extensions of H3 and H6. In fact, for the agonist-bound (i.e., active state) and the antagonist-bound (i.e., nonactive state) forms, the establishment of crucial intermolecular interactions (as suggested by the experimental evidence) was found, respectively, concurrent with destabilization and reinforcement of the intramolecular interactions involving the E/DRY arginine in the empty receptor forms.[138,141,147,608] Therefore, the choice of the ligand−receptor complexes, which better fulfill the intermolecular-interaction requirements, implies selecting divergent interaction patterns of the E/DRY motif in the agonist-bound (active) and antagonist-bound (nonactive) forms.

A common inference from the comparative analysis of the four substantially different receptors was that the agonist-bound forms share the release of all or some of the charge-reinforced H-bonds involving R3.50 in the empty receptor. The aspartate/glutamate at position 3.49 is one of the arginine partners in the empty and antagonist-bound states (i.e., inactive states) of all the three receptors, whereas E6.30 is the other partner of R3.50 only in the 5-HT_{1A} receptor (Figure 23) and in TXA_2R. In fact, in the empty and antagonist-bound forms of the 5-HT_{1A} receptor, both the D133(3.49)−R134(3.50) and R134(3.50)−E340(6.30) interactions are almost persistent during the 2 ns time of the MD simulation.[138] However, in the empty form, the intrahelical salt bridge is more stable than the interhelical one, as the former is conserved during the whole 2 ns simulation, whereas the latter is alternately lost and gained.[138] The loss of the H-bonding contribution to this interhelical interaction is always concurrent with the establishment of another H-bonding interaction between the E/DRY arginine and T343(6.33). Also for TXA_2R, the double salt bridge between R3.50 and both E3.49 and E6.30, represents a structural hallmark of the empty receptor fom.[147] In empty OTR, the lack of a glutamate at 6.30 is compensated by T273(6.33), which is involved in H-bonds with the E/DRY arginine in the second half of the most representative 1 ns trajectories.[141] In contrast, in both the empty forms of the MCHR1 and MCHR2 subtypes, which both lack an anionic amino acid at 6.30, the E/DRY arginine in the inactive forms is engaged in interhelical salt bridge interactions with an aspartate at position 2.40 and, only for MCHR1, in H-bonding interaction with T251(6.30) (Figure 23).[608]

Interestingly, for the 5-HT_{1A} receptor, the analysis of an extensive number of different MD trajectories suggested that the interactions with three relevant amino acids of the putative ligand binding site, in the extracellular half of the helix bundle, are essential for both the agonists (i.e., serotonin and (R)-8-OH-DPAT) to destabilize the salt bridge interactions that, in the empty and antagonist-bound receptor forms, involve the E/DRY arginine. These amino acids are (a) D3.32, which recognizes the protonated nitrogen atom of the ligand, (b) S5.42, which interacts with the indole or tetralin hydroxy groups of the ligands, and (c) F6.51, which interacts with the indole or tetralin ring of the ligands. The occurrence of the latter interaction relies on the establishment of the first two. Interestingly, the establishment of a double H-bonding connection between the agonist serotonin and both S5.42 and T5.43 is concurrent with the highest degree of destabilization of both the salt bridges involving the E/DRY arginine.[138] An interesting suggestion inferred from comparative MD simulations of the 5-HT_{1A} receptor and MCHRs, which differ both in amino acid composition and in the natural agonist (i.e., a small biogenic amine for the 5-HT_{1A} and a huge cyclic peptide for the two MCHRs), is that the essential requirements for the agonist to perturb the peculiar features of the inactive receptor forms are to accomplish charge-reinforced H-bonds with the binding site aspartate and to make van der Waals attractive interactions with one or more members of the aromatic cluster in H6 (Figure 23).[138,608] These interactions involve essentially two out of the 19 amino acids, which constitute MCH. In this scenario, the few critical interactions needed for the huge MCH or for the small serotonin to transfer the chemical information from the extracellular to the intracellular domains of their target receptors are overlapping (Figure 23). This hypothesis has been strengthened by the results of simulations of the OT-OTR complexes, suggesting that the few critical intermolecular interactions include that between Tyr2 of the agonist and F291(6.51) of the aromatic cluster in H6.[141] On the same line, for TXA_2R, the

establishment of the H-bonds between the carboxyl and hydroxyl groups of the U-46619 agonist and R295(7.40) and S201(5.43), respectively, of the receptor was suggested to trigger the local perturbations that promote the active state.[147]

Thus, for all the four different GPCRs, the agonist-induced chemical information transfer from the extracellular to the cytosolic domains (i.e., vertical information transfer) appears to be mediated by a cluster of aromatic amino acids in H6, i.e., formed by F6.44, W6.48, and F6.51, following the ligand interaction with selected amino acids in the extracellular half of the receptor.[138,141,147,608] In detail, the interaction between the aromatic ring of the agonist and F6.51 of the aromatic cluster induces a conformational change of W6.48, which loses its original H-bonding interaction with N7.45 and moves from H7 toward H5, consistent with the results of UV determination on rhodopsin (Figure 23).[580] These changes are concurrent with a significant reduction in the bend at the highly conserved P6.50, as compared to the empty and the antagonist-bound receptor forms, consistent with the results of conformational sampling on the isolated H6 of the β_2AR and the CB1 receptor and restrained MD simulations on an almost complete model of the β_2AR.[251,575,579] These results also agree with the computer simulation- and experiment-based hypothesis that GPCR activation would significantly diminish the kink at P6.50.[571] The straightening of H6 is one of the features of the agonist-bound forms correlated with weakening of the interactions made by R3.50, of the E/DRY motif. Another common feature to the agonist-bound forms of the simulated receptors is the release of the interaction found in the inactive forms between Y7.53, of the NPxxY motif, and a conserved phenylalanine in H8. This is particularly true for the computational models of the two MCHRs, whose agonist-bound forms are characterized by the approaching of H8 to the cytosolic extension of H3.[608] Although this structural change may be due to an overestimation of the electrostatic interactions due to the absence of the screening effect of water, it is also true that the approaching of H8 to the cytosolic extension of H3 is a feature of the active forms of MCHRs and not of the nonactive ones. Active and nonactive forms of both receptors have been simulated by using the same computational setup.[608] These structural changes, suggestive of increased flexibility of H7 and H8, are consistent with the experimental evidence that a disulfide bridge is allowed to form between the amino acids at positions 7.63 and 3.55 in the light-activated states of rhodopsin and not in the dark state.[241] Other structural changes in the cytosolic domains, which are concurrent with the establishment of the few critical interactions between MCH or the U-46619 agonist and their cognate receptors, include the opening of a solvent accessible crevice involving the second intracellular loop and the cytosolic extensions of H2, H3, and H6. This structural change is properly described by the solvent accessible surface area computed over selected amino acids, including the arginine of the E/DRY motif. This index, which was significantly lower than 100 Å^2 in the empty and antagonist-bound receptor forms and significantly higher than 100 Å^2 in the agonist-bound receptor forms, proved effectiveness as a hallmark of the functional receptor state (i.e., active ornonactive)[147,608] and suitability for virtual functional screening of novel MCH ligands (Figure 24).[608]

Agonist binding induces significant changes in the arrangements of the extracellular ends of the helices and in the conformation/orientation of the N-terminus and E2, the latter being strongly involved in interaction with the peptide agonists OT and MCH and with the nonpeptide U-46619 TXA_2R agonist.[141,147,608] The high extent of the structural differences in the putative agonist binding site between free and agonist-bound receptor forms suggests that the role of agonists cannot be limited to a conformation selection but it should also include the triggering of relevant structural changes, unlikely to occur spontaneously in the empty receptor form. The same is true for the antagonist-bound receptor forms. Of course, these inferences should be taken with caution given the indeterminations in the extracellular and intracellular domains of the receptor models and the approximations of the computational approach. The computational experiments on the TXA_2R suggest that the communication between the agonist-binding site and the cytosolic extensions of H3, H5, and H6, is two-way, in the sense that the establishment of a few privileged interactions between the agonist and the receptor is associated with changes in the interaction pattern and solvent accessibility of selected amino acids in the cytosolic domains. Vice versa, a perturbation in the cytosolic domains, like valine substitution for R130(3.50), is associated with a change in the reciprocal orientation of the extracellular halves of H3, H4, H5, and H6 that participate in the agonist binding site.[147]

Collectively, the results of our computational experiments highlight the existence of microswitches in GPCR activation consistent with inferences of in vitro experiments.[1018,1019]

The hypothesis of the intrahelix salt bridge interaction between D/E3.49 and R3.50 of the E/DRY motif as the target of the structural perturbation induced selectively by agonists and not by antagonists was challenged in computational experiments on the free as well as the agonist- and antagonist-bound forms of the δ, κ, and μ subtypes of the mouse opioid receptors.[473] The receptor models were limited to the TM helices, which were packed using the Baldwin's Cα-atom model as a template.[14] MD simulations of the empty forms of all the three opioid receptor subtypes proved the stability of the intrahelix salt bridge between the two charged members of the E/DRY motif. For the δ opioid subtype, selected energy-minimized complexes with an agonist, etorphine, and an antagonist, naltrexone, were prepared in the putative "inactive" and "active" states, differing, respectively, in the presence or absence of the D3.49−R3.50 salt bridge. The four complexes were then subjected to a 1 ns MD simulation, and the outcome of the study was that, starting from the "inactive" form, the charge-reinforced H-bond between D3.39 and R3.50 is maintained over the whole simulation time, independently of the functionality of the bound ligand. In contrast, starting from the "active" form, the antagonist is able to restore the D3.49−R3.50 interaction, whereas the agonist does not.[473] It was also inferred that the agonist produces larger structural effects on H1, H3, and H6, whereas the antagonist induces larger effects on H4.[473] The E/DRY motif resulted to be the target of the structural changes induced either by activating mutation or by agonist in a combined in silico and in vitro study on the cholecystokinin 2 receptor (CCK_2R).[785] Recent in vitro and in silico experiments on the AT_1R suggested that receptor activation involves an anticlockwise rotation (seen from the extracellular side) and a shift of H7 into the ligand binding pocket.[790] This motion would be hindered by an inverse agonist.

Disruption of an intramolecular salt bridge between D170(3.32), the key recognition receptor point of amine ligands, and K379(7.36) was suggested to be the primary event leading to the α_{1d}AR activation.[489] This hypothesis, in agreement with the

results of in vitro experiments on the α_{1b}AR,[1020] was inferred from a computational model of the α_{1d}AR, holding the TM helices, arranged according to Baldwin's model, and the three extracellular loops.[489] According to this model, the inactive state of the receptor would be stabilized by the D170(3.32)−K379-(7.36) ionic lock and would move spontaneously into an active state, following the switch of the anionic partner of K379(7.36) from D170(3.32) to E375 (in E3). The active state of the receptor would be, hence, stabilized by the agonist, which would anchor to D170(3.32) of the receptor, through its protonated nitrogen atom. This model would provide an interpretation, with atomic detail, for the hypothesis of agonist selection of pre-existent active receptor states. However, an inconsistency in the mechanistic hypothesis concerns the antagonist-bound state that, similarly to the agonist-bound state, lacks the crucial ionic lock, though being inactive. The inferences of such a computational study could be misled by the low resolution of the computational model. In fact, models of the α_1AR subtypes, based upon the crystal structure of rhodopsin, suggest that K7.36 would be more likely involved in an interhelical salt bridge with E2.65 instead of D3.32.[668] The structural relationship between E2.65 and K7.36 is also supported by their tendency to mutate in a correlated manner. In fact, in the 5-HT$_{1A}$ receptor, E2.65 and K7.36 are respectively replaced by a glutamine and an alanine.[668] The hypothesis of a potential role of D3.32 in stabilizing an inactive receptor state through an interhelical salt bridge is, hence, not supported by computational models based upon the high resolution structure of rhodopsin and has also been recently challenged by in vitro experiments on the 5-HT$_{2A}$ receptor.[482] Perhaps, upgrading the receptor model according to the advances in the determination of the rhodopsin structure would have led the authors to different conclusions.

The employment of a set of "activating" distance constraints, derived from the experimental studies of different GPCRs in the active conformation, was used to derive active state models of the μ and δ opioid receptors from the crystal structure of inactive rhodopsin.[819,826] These models were used to build the complex with agonists.[819,826] We expect that the reliability of these active state receptor models strongly depends on the specificity, quality, and resolution level of the experimental data employed as additional distance constraints to induce a structural divergence from the rhodopsin template. Distance restrained MD simulations were used as well to model the inactive and active states of the H$_1$R.[787] The study highlighted the aromatic amino acids F6.44 and W6.48 as switches of receptor activation coupled with the linearization of the proline-induced kink in H6. A conformational change in the side chain of W6.48 was also found as the major switch in the agonist-induced conformational changes of the A$_3$R following 13 ns MD simulations in explicit membrane.[784] In a rather convoluted computational study on CCK$_2$R activation, an active state of the CCK$_2$R was achieved by simulating for 1 ns in explicit membrane a complex with the CCK agonist followed by removal of the ligand.[786] The latter had been docked into a receptor binding site previously primed by CCK4 through in vacuo steered MD simulations based on distance constraints.[786] On the other hand, an inactive state was achieved by subjecting to 750 ps of equilibrated MD simulations the homology model of the receptor based upon dark rhodopsin. Comparisons between the average structures of the "refined" inactive and active states served to individuate the intramolecular interactions, which would stabilize either one of the two states, whereas targeted MD simulations served to simulate the conversion from the inactive to the putative active state.[786] The most significant structural changes associated with such conversion were: (a) a rearrangement of the interaction network around W6.48, (b) a clockwise rotation of H6 when seen from the extracellular side, and (c) a tilt of the extracellular end of the helix toward H3. Movements of H6 were found to be coordinated with rotation of H5 and upper motions of H7.

In an original approach, mechanistic hypotheses on the agonist-induced activation of CCK$_1$R were inferred by simulating the inactivation process. In this respect, the complex between CCK$_1$R and the CCK9 agonist served as a paradigm of an active conformation.[788] Assuming microreversibility, the initial step toward the inactivation of the CCK$_1$R was modeled using free energy calculations, whereby the ligand is removed from the binding pocket. However accurate the reproduction of the experimental affinity constant, this simulation was thought to only represent an embryonic stage of the inactivation process. Starting from the apo receptor, 0.1 μs MD trajectory was generated, bereft of experimental biases. Hydration was found intimately related to the isomerization of the highly conserved residue W6.48, which in the active state obstructs the crevice, thereby preventing water leakage. The latter would otherwise trigger the disruption of an ionic lock between H2 and H3 involving the E/DRY motif.[788]

The crystal structure of the β_2AR was used to investigate the modulation of the potential energy landscape of receptor by ligands with different efficacies (i.e., two full agonists, two partial agonists, and an inverse agonist) by the LITiCon coarse grain method.[285,325,737] As already stated above in the text, the latter involves a systematic conformational spanning of the receptor TM helices followed by energy minimization and ligand redocking in each sampled conformation. The binding energy landscape for the inverse agonist carazolol was such that the ligand-stabilized state was located in a deep energy well with high barriers to access the agonist-stabilized states. On the other hand, the binding energy landscapes of the agonist-bound states (norepinephrine- and epinephrine-bound) were characterized by a broad potential well of energetically favored states, showing a favorable energy channel connecting the carazolol-bound conformational state to the norepinephrine- or the epinephrine-bound state. This was interpreted as a receptor ability to sample the inverse agonist states when bound to norepinephrine and as a receptor trapping into an inactive state when bound to carazolol. More subtle differences in the energy landscapes were found between full agonists and partial agonists. The receptor states induced by functionally different ligands showed differences in the interaction patterns of selected amino acids including the arginine of the E/DRY motif, which was found involved in almost persistent interaction with E6.30 in the carazolol-bound state but not in the agonist-bound ones, in line with previous computational experiments on the homologous GPCRs (referenced above in this section) as well as with the crystal structures of dark rhodopsin, Ops*, and MII.[99,100,107,108,122] The agonist-induced active states were also found to be characterized by an increase in solvent accessibility of selected cytosolic portions again in line with the hallmarks of mutation- and agonist-induced active states inferred by our extensive computational experiments (referenced in the text above) as well as with the crystal structures of Ops*, MII, and β_2AR in complex with either NB80 or Gs.[99,100,107,108] An MC sampling was also used to derive the activation pathways for several agonists and partial agonists.[325] The calculated pathways for

the full agonists start with an energy downhill step that leads to a stable intermediate followed by a barrier crossing, which in turn leads to the active state upon breaking an interhelical hydrogen bond between H5 and H6. In a successive study, the receptor conformations sampled along the activation pathway using the MC scheme were clustered and used as starting conformations for the fine-grained MD simulations.[1021] It was found that the ligand-free receptor samples an extensive conformational space that includes a breathing of the orthosteric ligand binding site and a shear motion of H5 and H6 against the other helices. The shear motion resulted similar to the reorganization of the intracellular regions of H3, H5, and H6. The binding of the agonist norepinephrine or the partial agonist salbutamol led to the selection of a subset of conformations comprising active and inactive state conformations, while the inverse agonist carazolol could select only inactive-state conformations.[1021]

A combination of NMR spectroscopy and computational modeling of the β_2AR suggested that the extracellular ends of H6 and H7 move on activation.[792] According to the proposed active state model, an inward movement at the extracellular end of H6 would permit the known interaction between N6.55 and the chiral β-hydroxyl of the formoterol agonist. This motion would be simultaneous to an outward motion at the intracellular end of H6 toward H5. The H6 motion was suggested to necessitate a lateral displacement of H7 that reorients the K7.32-D192 salt bridge, which attenuates with activation. Remarkably, NMR spectroscopy indicated the existence of three distinct conformations of the β_2AR extracellular surface: one for an unliganded receptor or a neutral antagonist, one for an inverse agonist, and one for an agonist. These conformations correspond to distinct functional behaviors.[792] Thus, small-molecule drugs that bind within the TM core and exhibit different efficacies toward G protein activation (agonist, neutral antagonist, and inverse agonist) also stabilize distinct conformations of the extracellular surface. The study demonstrated a conformational coupling between the extracellular surface and the orthosteric binding site, showing that drugs targeting this diverse surface work as allosteric modulators with high subtype selectivity. In general, solution- and solid-state NMR approaches are revealing high potential in studying GPCR−ligand interactions that are vital for drug discovery.[1022]

A computational study on the crystal structure of the β_2AR showed that while the carazolol pocket captured in the β_2AR crystal structure accommodates (*S*)-isoproterenol and other agonists without steric clashes, a finite movement of the flexible extracellular part of H5 could further improve the calculated binding affinities for agonists.[791] The study highlighted systematic differences in the capacity of partial, full, and inverse agonists to induce H5 tilt in the β_2AR model, suggesting a potential role of H5 as a conformational "rheostat" involved in the whole spectrum of β_2AR responses to small molecule signals.

Evidence for distinct structural changes induced by full and inverse agonists comes also from in situ disulfide cross-linking experiments on the M_3-muscarinic acetylcholine receptor.[1023,1024] In this respect, it was predicted that the cytoplasmic end of H6 undergoes a rotational movement (and perhaps a partial unfolding) becoming closer to the corresponding segment of H5. According to the study, the cytoplasmic portion of H7 is predicted to move closer to the corresponding region of H1, also accompanied by a rotational movement and/or a partial unfolding. Furthermore, the N-terminal portion of H8 is expected to move away from the cytoplasmic end of H1, whereas in the inverse agonist-bound states, it appears to move closer to H1. Collectively, agonist-induced activation was reported to open a cytosolic cleft characterized by the increase in solvent accessibility of different helices including H3, H6, and H7. This is consistent with the results of our computational experiments (referenced in the text above and reviewed in ref 233) as well as with the crystal structures of Ops*, MII, and β_2AR in complex with either NB80 or Gs.[99,100,107,108]

The combined inferences from computational and in vitro experiments seem to suggest that an "extended conformational selection model"[1025] that embraces a repertoire of selection and adjustment processes is more suitable to describe the binding of functionally different ligands to GPCRs rather than either the "induced fit" or "conformation selection" models that can be considered as extremes of a complex process such as molecular recognition.

6. GPCR OLIGOMERIZATION

6.1. Role of Dimerization/Oligomerization in GPCR Function

GPCRs have classically been assumed to exist and function as monomeric entities, and the paradigms of ligand binding and signal transduction were based on this hypothesis.

It is often said that, unlike growth factor and cytokine receptors, GPCRs were believed to exist as monomeric proteins in the membrane, and the likelihood that they could form dimers was refuted by the majority of investigators. It is more fair to say that oligomerization among GPCRs was considered a tedious topic. In fact, data suggesting that GPCRs can oligomerize were presented recurrently over the years, but no evidence was ever found that such a physical interaction could be vital for GPCRs' function. The fundamental questions about GPCRs were focused on the mechanisms of interaction with agonists and G proteins. Whether that occurred between individual or gregarious partners was a matter of secondary importance. What suddenly stirred general interest on oligomerization was evidence showing that direct receptor−receptor interactions can rescue functional activity in complementation experiments. As shown by Maggio and co-workers, pairs of GPCR chimeras or truncated fragments, which were inactive when individually expressed, regained binding and signaling activity if coexpressed in the same membrane.[1026,1027] On this line, using mouse LHR as a model GPCR, it was demonstrated that transgenic mice coexpressing binding-deficient and signaling-deficient forms of LHR can reestablish normal LH actions through intermolecular functional complementation of the mutant receptors in the absence of functional wild type receptors.[1028] This, per se, did not identify which role oligomerization plays in GPCR function, but it definitely demonstrated that receptor−receptor interaction could affect the agonist binding pocket and the G protein interacting interface of GPCRs, as importantly, perhaps, as the intramolecular interactions that directly drive receptor activation. The study on mouse LHR, indeed, provides in vivo evidence for the physiological relevance of intermolecular cooperation in GPCR signaling.[1028]

Following early findings by Maggio and co-workers, studies on GPCR dimerization have been appearing at a steadily increasing pace.[45−54,56−61,68,70,74,1029−1040] Although their existence is now largely accepted, their functional importance remains more enigmatic and in some cases even controversial (reviewed in refs 45−54,174,1041). These conclusions can also be inferred from the recent review article by Terrillon and Bouvier, concerning the

state of the art in our understanding of the role of dimerization of GPCRs in the five different steps of their half-life cycle, i.e., ontogeny, ligand-promoted regulation, pharmacological diversity, signal transduction, and internalization.[52]

As for ontogeny, GPCRs of family C were the most generous so far in yielding clues on the possible role of oligomerization. $GABABR_1$ and $GABABR_2$ receptors represent an emblematic case (reviewed in ref 1042). Each of the two genes makes an incompetent GPCR protein, as the first is not properly glycosylated or inserted in the membrane, and the second has no signaling activity. However, when both are expressed in the same cells, which physiologically occurs in brain neurons,[1043,1044] they make a functional GABA responsive heterodimer.[1043−1046] The structural requirement in this case was identified in the C-terminus, where there are recognized sequences prone to make coiled−coil interactions.[1047] That is in contrast with another member of family C receptors, the glutamate receptor type 1, where dimerization occurs in the N-terminus.[1048] This large "flytrap" domain has structural similarity to the glutamate binding domain of glutamate receptor channels, where they, in fact, form stable oligomeric forms.[4] Although the examples above seem "special" cases, evidence that GPCRs dimerize in order to act as molecular chaperones, i.e., to catalyze their own folding and transport to the cell surface, was also found for family A GPCRs, such as the V_2 vasopressin receptors[1049,1050] and the chemokine receptor CCR5.[1051] See also ref 55 for a review. A recent study provides evidence for homodimerization/oligomerization of the $5\text{-}HT_{2C}$ receptor in the endoplasmic reticulum (ER) and Golgi of intact living cells, and suggests that dimer/oligomer formation is a naturally occurring step in $5\text{-}HT_{2C}$ serotonin receptor maturation and processing.[1052]

A role for dimerization in GPCR ontogeny does not exclude the possibility that, once the receptor has reached the cell surface, its oligomeric state could be dynamically regulated by ligand. Experiments based on fluorescence resonance energy transfer (FRET) and bioluminescence energy transfer (BRET) reveal that many GPCRs exist as oligomers, or at least as closely packed clusters, in the membranes of living cells.[45−52,1029,1036,1053−1055] Fluorescence spectroscopy approaches allowed to detect pyrenzepine-induced dimerization of the M_1-muscarinic receptor,[1056] as well as ligand regulation of the quaternary organization of cell surface M_3-muscarinic receptor.[1057] Coupling RET to protein-fragment complementation assays (PCAs), also known as bimolecular fluorescence/luminescence complementation (BiFC/BiLC), now allows protein interactions to be detected in the context of living cells.[1058] The methodology was used to monitor drug-modulated hetero-oligomerization of $A_{2A}R$ and D_2R in living neuronal cells.[1059] Moreover, the combination of FRET and BiFC showed that at least three $A_{2A}Rs$ assemble into higher order oligomers at the plasma membrane.[1060]

However, as to the question of functional relevance, they have contributed very little insight, so far. In fact, since the majority of such studies show that agonist binding does not significantly change the optical signal, it appears that GPCRs are constitutive dimers and that this supramolecular organization is not perturbed by the state of activation of the protein. Thus, according to a number of FRET and BRET determinations, neither enhancement nor disruption of the dimeric state seems to be necessary for receptor-mediated activation of G protein. Yet, that may be a glaring case in which nothing tells something, because, by the same token, there is no available evidence to refute the possibility that a dimeric GPCR is an obligatory structure for engaging a productive interaction with the G protein heterotrimer. Indeed, structural and biochemical evidence suggest that the binding surface of the G protein trimer can accommodate the twin footprints of a dimeric GPCR,[1061,1062] although the same observation can be interpreted as an indication that the cytosolic region of a single GPCR can undergo large conformational changes upon interaction with the G protein.[1063] Very recently, elegant experiments consisting of a combination of mass spectrometry after chemical cross-linking and neutron scattering in solution have unambiguously established that the complex formed between the purified, activated leukotriene B_4 receptor BLT1 and $Gi_{\alpha 2\beta 1\gamma 2}$ corresponds to a pentameric assembly of one dimeric receptor and one heterotrimeric G protein.[1064] A successive study on a stabilized and purified heterodimer of BLT1 indicated that although ligand binding to one protomer in the heterodimer is associated with cross-conformational changes, a trans-activation mechanism where the ligand-free subunit would trigger GDP/GTP exchange is unfeasible.[1065]

A recent study demonstrated the importance of G protein in the maintenance and regulation of human somatostatin receptor dimers.[1066] A functional complementation study enabling control on the components of a signaling unit indicated that for the D_2R the minimal signaling unit is two receptors and one G protein.[65] However, for a number of GPCRs, in vitro evidence shows that one receptor molecule is sufficient to activate a G protein and bind arrestin[1067] (reviewed in ref 64). Indeed, rhodopsin,[184,1068] the β_2AR,[1069] and the neurokinin-1 receptor[1070] activate their cognate G proteins in the monomeric form. Moreover, supramolecular organization of rhodopsin,[184] neurotensin 1 (NTS1)[1071] receptor, and leukotriene BLT2[1072] receptor reduce G protein coupling. For the $5\text{-}HT_4$ serotonin receptor, it was recently shown that activation of one protomer in a dimer is sufficient to stimulate G proteins.[1073] However, coupling efficiency was two times higher when both protomers were activated. Expression of combinations of 5-HT4 receptors, in which both protomers were able to bind to agonists but only one could couple to G proteins, suggested that upon agonist occupancy, protomers did not independently couple to G proteins but rather that only one G protein was activated.

Oligomerization may be a strategy to diversify and extend the signaling properties that are intrinsic in each individual receptor gene (reviewed also in refs 1061,1074,1075). Opioid receptors have been extensively studied in this regard.[1076−1078] It was shown that coexpressed δ and κ receptors can generate a different binding pattern and synergistic effects on MAP-kinase.[1079] Similarly, mixes of μ and δ receptors gain special signaling and binding properties if jointly expressed.[1080] A recent study demonstrated differential response to morphine by the oligomeric state of μ in the presence of δ opioid receptors.[1081] It was found that the μ subtype exists primarily as a dimer that will oligomerize with δ into tetramers, and morphine promotes the dissociation of these tetramers.Thus, it is possible that the complex combination of opioid receptor subtypes generated by studies in the precloning era and never matched by the genes that were actually found is explained by the fact that such receptors differ in signaling properties when they exist in homomeric or heteromeric form.[1076,1077] Similar results have been presented for many other receptor types and suggest a general trend.[45,48,52] Supramolecular arrays containing mixtures of different receptors may constitute specialized signaling patches of the plasma membrane, and their differential distribution in cell regions may have fundamental roles in fine-tuning the complex signaling

networks of the central nervous system. This phenomenon, if true, poses a daunting challenge but also new opportunities in the design of new drugs. On this line, a recent study demonstrated that the heterodimerization between the 5-HT_{2A} serotonin receptors and the metabotropic glutamate receptors (mGluR) may be involved in the altered cortical processes of schizophrenia, providing a promising new target for the treatment of psychosis.[77] The study predicted also H4−H5 contacts between the two receptors. Physiological relevance has been recently demonstrated also for the heterodimerization of the Gq-coupled AT_1R and the Gi-coupled CB1 receptor.[76] Thus, allosterism across GPCR homo- or heteromers, whether dimers or higher order oligomers, can be considered as an additional topographical landscape that has to be considered pharmacologically to open new perspectives toward novel therapeutic approaches.[1082] However, the question whether there are allosteric interactions across the receptor−receptor interface of a heterodimer that modulate the binding properties of the heterodimer components and thereby change their pharmacology still awaits an unequivocal answer.[1083] Collectively, allosteric communication across dimers and the related asymmetric/symmetric activation may have implications in multiple signaling pathways.[65,66,1084,1085] In this respect, a study on the BLT1 receptor highlighted asymmetric conformational changes in the receptor dimer only in the presence of the G protein, suggesting that the interaction of the G protein with the receptor dimer prevents a symmetric functioning of the dimer.[1086] On the same line, in vitro evidence on the D_2R showed that a functional unit made of two receptors and one G protein is maximally activated by agonist binding to a single protomer, suggestive of an asymmetrically activated dimer.[65] Inverse agonist binding to the second protomer as well as constitutive activation of the second protomer blunts signaling. On the basis of these data, the authors concluded that the functionality of a GPCR dimer can be modulated by the activity state of the second protomer.[65]

One signaling pathway, in which oligomerization may be a crucial player, is G protein-independent signaling of GPCRs to mitogen-activated protein kinases. Arrestins, a family of proteins that were previously thought to be exclusively devoted to disconnect receptors from G proteins,[42] are now known to act also as recruiting adaptors that divert GPCR signaling toward intermediate kinases such as ERK1, ERK2, and others.[37,38] Recent AFM experiments on rhodopsin indicate that the photoreceptor forms dimers in the plasma membrane, with cytosolic protrusions that are located 3.7 nm apart.[63] This distance matches that of two evident grooves that are present in the crystal structure of arrestin.[63,176] This would suggest that GPCRs must be in dimeric form to bind arrestin. Very recent in vitro experiments, based on complementation of individually nonfunctional GPCRs, support this hypothesis, providing evidence that binding of β-arrestin-1 to M_3-muscarinic receptors requires paired stimulation of two receptor components within the same receptor dimer.[54,1087,1088] The consequences of arrestin-mediated signaling in vivo are not entirely understood yet, but studies of opioid effects in mice bearing deletions of arrestin genes suggest that arrestin signaling may be important for the control of tolerance and dependence.[1089,1090]

Although a number of recent studies unambiguously demonstrate that one receptor molecule is sufficient to activate a G protein and bind arrestin (reviewed in ref 64), the stoichiometry of the receptor−G protein functional unit still remains an open question.[1091] It has been also proposed that GPCR oligomerization may provide the structural basis for organizing distinct cell compartments along the plasma membrane where different extracellular signals may be perceived and discriminated.[1092] In the case of rhodopsin, it has been also postulated that oligomerization would serve to exclude rhodopsin molecules from phototransduction, a mechanism of adaptation.[1093]

The molecular organization of the ternary complex involving melatonin 1 receptor (MT_1), Gi protein, and RGS20 was monitored in its basal and activated states by BRET between probes inserted at multiple sites of the complex.[1094] The study allowed inference of a model wherein one Gi and one RGS20 protein bind to distinct protomers of MT_1 dimers in a preassociated complex that rearranges upon agonist activation. The study highlights the advantage of GPCRs organized as dimers, in which each protomer fulfils its specific task by binding to different GPCR-interacting proteins.

Several recent studies have suggested that heterodimerization could affect agonist-promoted GPCR endocytosis, a well-characterized process classically involved in signal attenuation. For many documented heterodimers, stimulation of only one of the protomers was sufficient to promote cointernalization of the two receptors (reviewed in ref 52). By contrast, receptors that do not undergo efficient agonist-promoted endocytosis were found to act as dominant negatives for endocytosis-prone receptors after heterodimerization (reviewed in ref 52). Although of significant potential interest, the physiological consequences of these observations on the regulation of GPCR desensitization/resensitization cycles remain to be determined. Collectively, dimerization may serve to affect receptor mobility at the cell surface and in intracellular trafficking.[59]

Evidence is now emerging that GPCR dimers are transient,[1095−1098] undergoing interconversions between monomers and dimers in the second time scale or lower.[1096,1098]

6.2. Insights from in Vitro Experiments into the GPCR Regions Involved in Receptor−Receptor Interaction

The extremely numerous experimental evidence for GPCR dimerization/oligomerization, however, provided very little insight into the architecture of the supramolecular receptor assemblies (reviewed in refs 45−61). As already reported in the text above, the geometrical constraints from AFM measurements led to the proposal of a semiempirical model of a multimeric rhodopsin structure.[176] According to this model, two monomers of rhodopsin interact with each other through E2, I2, H4, and H5 of both monomers (Figure 5). An elegant study based on a combination of in vitro biochemical and biophysical experiments on the glycoprotein hormone receptors provides evidence that these receptors form homo- and heterodimers via interactions involving primarily the heptahelical domains and that hormone binding occurs with a strong negative cooperativity.[700] For family A GPCRs, recurrent evidence for the involvement of H6 in the intermonomer interface came from early experiments with synthetic peptides holding the sequence of such a helix, which appeared to inhibit homodimerization of either β_2AR or D_2R.[1099,1100] For the D_2R, a peptide from the H7 sequence proved to exert an inhibitory effect as well.[1100] The involvement of H5 and H6 from D_2 in the heterodimerization with the $A_{2A}R$ was indicated by BRET experiments using a $D_{2[1-4,7]}R$ chimera, containing H5, H6, I3, and E3 from the D_1R sequence, a receptor that does not dimerize with $A_{2A}R$.[605] In fact, in contrast to the wild type D_2R, the $D_{2[1-4,7]}R$ chimera was not able to compete

for the specific BRET between $A_{2A}R$ and D_2R.[605] Recent experiments on purified leukotriene B_4 receptor provided evidence for the central role of H6 in stabilizing the receptor homodimer.[1064] Also, H4 has been suggested to mediate intermonomer contacts on the basis of the results of cysteine cross-linking experiments on the D_2R.[1101] Successive experiments highlighted potential rearrangements of the D_2R dimer architecture depending on the receptor functional state, the H4−H5 and H4−H4 contact dimers being, respectively, associated with inactive and active states.[1102] In a more recent study, the same authors provided evidence that D_2R forms higher order oligomers in living cells and that H1 and H8 form a second symmetric interface in addition to the previously identified H4 interface.[1103] Truncation mutants by successive deletions of transmembrane helices from amino- and/or carboxy-terminations of the D_2R suggested that, in addition to H4, other receptor portions mediate homodimerization.[1104] Cysteine cross-linking experiments on the δ opioid receptor highlighted as well H4 and/or H5 at the homodimer interface. Improvements in the resolution level of the homodimer architecture were attempted by CG well-tempered metadynamics simulations followed by umbrella sampling simulations, which predicted the H4 dimer as more stable than the 4/5 dimer.[1105]

The involvement of H1 and H8 in GPCR oligomerization was recently proposed for the β_2AR as well.[1106]

In vitro disulfide-trapping experiments on the $5HT_{2c}$ receptor suggest the existence of dimer architectures insensitive and sensitive to the functional states of the receptor.[1107] In this respect, state-insensitive architectures were suggested to involve H1−H1 contacts, whereas state-sensitive architectures were suggested to involve H4−H5 contacts.[1107]

In vitro experiments aimed at inducing disulfide-mediated dimerization of the α-factor pheromone receptor, Ste2p, highlighted H7−H7 dimers that decrease in the presence of the α-factor ligand and H1−H1 dimers not affected by ligand binding.[1108] A similar investigation on the same receptor highlighted the involvement of H1 and H4 in receptor oligomerization.[1109]

Interactions between H1 and H4 were suggested to mediate the homodimerization of the CCR5 receptor, on the basis of the experimental observation that the combination of two point mutations, i.e., I52(1.54)V and V150(4.47)A, impaired receptor function and prevented FRET, differently from the case of the wild type.[1110] This hypothesis has recently been challenged by Lemay et al.[1111] Furthermore, FRET experiments using either various α_{1b}AR fragments or α_{1b}/β_2 chimeras suggested that, in the whole α_{1b}AR, H1 and H7, which are adjacent in the helix bundle, act in concert in favoring receptor homo-oligomerization, with H1 being the prominent interface.[1112] Other FRET-based experiments on the same GPCR suggested the formation of H1−H1 and H4−H4 contacts in an oligomeric organization of the receptor.[1113] Curiously, in vitro experiments on the M_3-muscarinic receptor indicated that C140(3.25) and C220 in E2, homologous to the amino acids that in the rhodopsin structure are involved in an intramolecular disulfide bond, can also participate in the formation of intermolecular disulfide bonds in a dimer.[1114] This was inferred from the observation that C140(3.25)A and C220A mutations prevented the formation of disulfide-linked receptor aggregates.[1114]

X-ray determinations provide some information on the likely architecture of selected receptor dimers. In fact, as stated above in the text, rhodopsin crystals show dimeric architectures characterized by H1−H1 or H8−H8 contacts all compatible with the AFM images.[182] A similar architecture was also found for the Ops* apoprotein.[107] With respect to the β_2AR, crystal packing in the presence of cholesterol shows a significant involvement of the hydrophobic molecule in the intermonomer interface.[94] In this framework, protein−protein contacts are minimal and include a pair of salt bridges between $K60^{(1.59)}$ and E338 from H8.[94] Finally, the crystal structure of CXCR4 in complex with either IT1t or the CVX15 cyclic peptide antagonists shows a dimer interface essentially contributed by amino acids from the extracellular halves of H5 and H6, with emphasis on the former.[111] Additional contacts involving the cytosolic ends of H3, H4, and I2 are shown by the CXCR4 complex with the cyclic peptide.[111] The crystallographic dimers of the CXCR4 seem to be somewhat compatible with the homodimeric architecture inferred from the design of bivalent CXCR4 ligands with rigid linkers.[1115]

Although the involvement of the intracellular regions cannot be excluded,[1116] consensus emerges on H1 and H4 being involved in GPCR dimerization/oligomerization (reviewed also in ref 1117). However, it should be considered also the possibility that different dimeric architectures may exist in a dynamic equilibrium, as recently inferred from a study on M_3-muscarinic receptor dimerization/oligomerization.[1118] Furthermore, different receptor portions are expected to be simultaneously involved in the formation of high-order oligomers.

6.3. Computational Modeling of GPCR Dimerization/Oligomerization

Knowledge about the most likely architectures of GPCR dimers is still ill-defined. Sequence-based and docking-based approaches investigated dimerization in different GPCRs highlighting the involvement of different helices in the intermonomer interfaces (reviewed here below and in refs 1119−1123) Gouldson and co-workers have been pioneers in studying GPCR dimerization by using computational modeling and bioinformatics tools (reviewed also in refs 423,1120,1122,1124).[980,1125] They initially proposed a mechanism of receptor activation involving domain swapping, essentially supported by the results by Maggio and co-workers on chimeric M_3-muscarinic and α_2-adrenergic receptors.[1026] MD simulations were used to analyze the proposed mechanism of dimer formation.[1125] Computations were carried out on a β_2AR model constructed on the basis of the 3D electron density map of rhodopsin.[15] Three possible dimer arrangements were investigated: a H1−H2 dimer, a H1−H7 dimer, and a H5−H6 domain-swapped dimer. A single ligand was docked into half of the receptor dimer, and the complexes underwent energy minimization and a MD simulation of up to 450 ps. The potential energy of these complexes, plotted against simulation time, revealed that both the apo H1−H2 dimer and a H1−H7 dimer were significantly lower in energy, which was also the case when an antagonist was present. However, when an agonist was docked, the energy of the H5−H6 dimer was significantly lowered relative to those of the other structures. This was thought to be consistent with the idea that agonist-induced activation is caused by a shift in the equilibrium toward the H5−H6 dimer. Since simulations were done on a dimer model in the absence of loops, the H5−H6 contact dimer and the H5−H6 domain-swapped dimer were identical (reviewed also in ref 423).[980,1125]

To provide support to the inferences of their simplified molecular models, the authors integrated the results of MD with

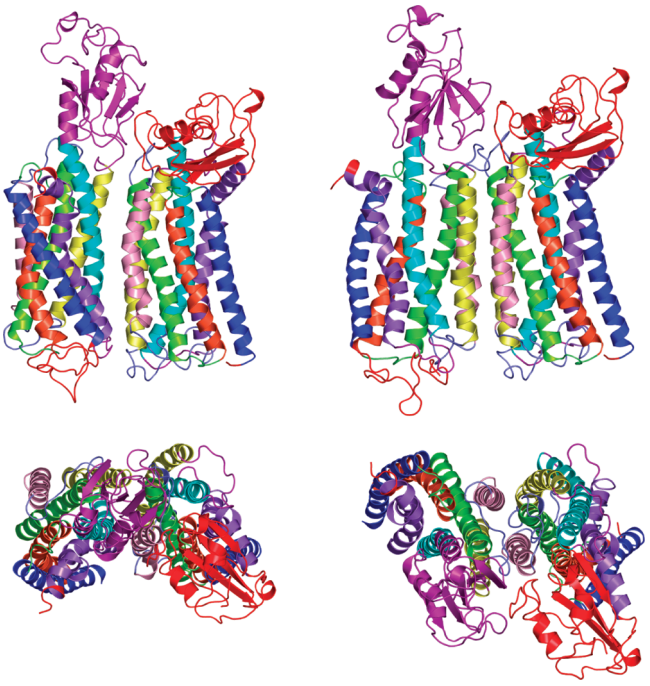

Figure 25. Examples of the $D_2R-A_{2A}R$ heterodimers belonging to CLUSTER 1 (top and bottom left) and to CLUSTER 2 (top and bottom right).[605] In the top views, the helix bundles are seen in a direction parallel to the membrane surface, with the intracellular side being at the top. In the bottom views, the helix bundles are seen from the intracellular side in a direction almost perpendicular to the membrane surface. H1, H2, H3,H4, H5, H6, and H7 are respectively colored in blue, orange, yellow−green, pink, yellow, cyan, and violet. The amino acid stretch corresponding to rhodopsin's H8 is colored in violet as well. The N- and C-termini are in red, I1 and E1 are in lime, I2 and E2 are in slate, and I3 and E3 are in purple. Drawings were done by means of the software PYMOL 0.97 (http://pymol.sourceforge.net/).

those of sequence analyses, using both the correlated mutation (CM)[1126] and evolutionary trace (ET)[1127,1128] methods.[1061,1125] In particular, they examined the occurrence of both correlated mutations and class-conserved residues. The CM method has been shown to provide information about interdomain contacts.[1126] The correlation is interpreted as a result of the tendency of positions in proteins to mutate in a coordinated manner if the interface has to be preserved for structural or functional reasons. Thus, sequence changes occurring during evolution at the interface of dimerization of a given monomer A would be compensated by changes in the interacting monomer B, to preserve the interaction interface. The ET method is another approach to determining functional sites for a protein, given its 3D structure and a multiple sequence alignment.[1127,1128] It bears some similarities to correlated mutation analysis, as the evolutionary trace residues may also be correlated, but it has the advantage that conserved residues are also included in the analysis.[1127,1128] The basic assumptions of the ET method are as follows: (a) that within a multiple sequence alignment the protein family retains its fold, on the basis of the idea that proteins that have evolved from a common ancestor will show similar backbone structure;[615] (b) that the location of the functional sites is conserved; (c) that these sites have distinctly lower mutation rates because of the evolutionary pressures of residues defining the functional sites; and (d) that this lower mutation rate is punctuated by mutation events that cause divergence.[1127]

For the adrenergic receptors, correlated mutation analysis on 50 aligned sequences showed that the correlated mutations do accumulate at the H5−H6 interface.[1125] The remaining external correlated residues on H1, H2, and H7 were thought to be involved in the formation of a H1−H7 dimer intermediate or in the formation of higher order oligomers.[1125] The ET method was applied to over 700 aligned GPCR sequences.[1061] The method predicted the occurrence of functionally important clusters of residues on the external faces of H5 and H6 for each family or subfamily of receptors; similar clusters were observed on H2 and H3. The probability that these clusters are not random was determined using MC techniques. The cluster on H5 and H6 is consistent with both H5−H6 contact- and H5−H6 domain-swapped dimer formation. The observation of functionally important clusters of residues on H2 and H3 raised some possible interpretations, including heterodimerization and oligomerization.[1061] In a more recent report, being aware of some experimental evidence against domain swapping as a general mechanism for receptor dimerization,[433,1129] and conscious that their computational approaches were unable to distinguish between contact- and domain-swapped dimers, the authors proposed that domain-swapped and contact dimers are essentially equivalent in their ability to signal, and this could underlie any failure to observe domain swapping. The role of domain swapping in GPCR dimerization still remains an open question, as it is apparently supported also by recent in vitro evidence,[1130] although it remains inconsistent with oligomerization. The same team, very recently, combined the ET method with the entropy method to improve predictions.[1131] They, indeed, recognized that the CM analysis, while being mathematically well-defined, had the limit to predict relatively few amino acids, inconsistent with the expected extensions of protein−protein interfaces.[1131] On the other hand, the ET method, although able to predict protein−protein contact areas, was, however, subjective. While earlier work tended to favor H6 as the most likely dimerization interface, the novel analyses favored H4.[1131]

A modification of the CM approach, the so-called "subtractive correlated mutation method", has been used to predict homo- and heterodimer interfaces in the opioid subfamily of GPCRs.[633,1132] Application of the method to δ and μ opioid receptors showed that most of the correlated residues of the δ opioid receptor are located on the outer (lipid-facing) surface of H4, H5, and H6, whereas, in the μ opioid receptor, H1 is the helix that is likely to be involved in the heterodimerization with δ. Since H4 and H6 cannot participate simultaneously in the intermonomer interface, these results were thought consistent with higher order oligomers. The same study applied to homodimerization of the δ, κ, and μ opioid subtypes suggested that (a) H4 and/or H5 would participate in the formation of the δ-homodimers; that (b) H5 would participate in the formation of κ-homodimers; and that (c) H1 would participate in homodimerization of the μ-subtype.[633] The consistency with the results of in vitro experiments, which implicate disulfide bonds in κ homodimerization and in $\delta-\mu$ heterodimerization[1079,1133] as well as the need of the intact C-tail for δ homodimerization,[1134] will be the challenge for further computational investigations.

The combination of CMA and automatic methods, such as the level entropy and the sequence space automatization methods, aimed at detecting amino acid positions that could have some

functional significance for the whole family and, at the same time, are specific for each subfamily (i.e., tree-determinant positions),[1135] was used to predict the interface in CCR5 homodimers.[1110] With this approach, positions 1.54 and 4.47 were predicted to participate in the interface.[1110]

A hidden-site class model of evolution, which employs different substitution matrixes to represent substitutions in different parts of the protein, was used to predict possible dimerization interfaces in aminergic GPCRs.[1136] The approach predicted the involvement of H5 and H6 in most aminergic subfamilies and H4 and H5 in the muscarinic and opsin subfamilies.[1136]

Predictions of oligomerization interfaces in a number of family A GPCRs belonging to the opsin, dopamine, adrenergic, and muscarinic acetylcholine families were also done by a multistep method made of two convergent sets of in silico experiments, one sequence-based and the other structure-based.[1137] The sequence-based set of experiments consists of multiple sequence alignment and search for conservation patterns. The structure-based set consists of reducing the 3D coordinates of the rhodopsin structure to a bidimensional plane and individuation of the residues on the molecular surface of the rhodopsin monomer, in particular, the lipid-facing ones. The integration of the two sets of experiments leads to 2D maps of conserved lipid-exposed residue clusters, which are interpreted as potentially involved in the dimerization interface. The predicted interfaces differed among subtypes. The following domains were predicted as implicated in homodimerization of selected receptor subtypes: (a) H4, H5, and I2, for rhodopsin, (b) H4, for the D_2R, (c) H6, for the β_2AR, and (d) amino acids from the cytosolic extension of H3 as well as from I2, H4, and I3, for the M_3-muscarinic receptor.[1137] The prediction method by Nemoto and Toh is now available through the G protein-coupled Receptor Interface Partners (GRIP) server (http://grip.cbrc.jp/GRIP/index.html).[621]

The CM analysis predicted that CCR5 homodimerization would involve H1−H4 contacts.[1138]

Collectively, the different sequence-based methods found consensus in predicting H4, H5, and H6 as the domains most likely involved in GPCR oligomerization (reviewed also in ref 1139). Despite this general consensus, it is clear that different sequence analysis methods identify different key positions in different receptor subfamilies; this is partly because each subfamily is different, but the differences may also arise because of insufficient sequence data.[1131,1139] Furthermore, predictions by sequence-based methods have low resolution, as interatomic interactions are not explicitly considered.[1131]

About seven years ago, we employed a computational approach based upon rigid-body docking to simulate the homodimerization of mutation- and ligand-induced active states of the α_{1b}AR.[511] Simulations were carried out on ab initio models of the receptor. The best resulting dimer structures for the D142(3.49)A active mutant and the epinephrine-bound receptor were found to involve H5, H6, and H7.[511]

Very recently, we have developed a computational procedure for predicting the supramolecular organization of TM α-helical proteins.[1140] The approach consists of rigid-body docking by means of the ZDOCK program.[1141] The best solutions selected by the docking program(s) as the best in terms of shape complementarity are then subjected to an "in-house" made filter, i.e., the "membrane topology" filter (FiPD; http://www.csbl.unimore.it/wp_csbl/?page_id=31), which discharges all the solutions that violate the membrane topology requirements. In detail, the filter discards all the solutions characterized by a deviation angle from the original z-axis, i.e., tilt angle, and a displacement of the geometrical center along the z-axis, i.e., z-offset, above-defined threshold values. For the tilt angle and the z-offset, thresholds of 0.4 rad and 6.0 Å were, respectively, employed. Discarded solutions generally constitute more than 94% of the solutions selected by the docking program, thus improving the effectiveness of the following cluster analysis. The strength of the approach stands in its independence from the size of the system, symmetry information, and extension of the water-soluble domains.[1140] Benchmarks of the approach, done on the tetrameric potassium channel (Kch, 384 amino acids),[1142] on the pentameric MscL (540 amino acids)[1143] and eptameric MscS (1771 amino acids)[1144] mechanosensitive channels, and on trimeric bacteriorhodopsin (698 amino acids),[422] in all the test cases led to nativelike quaternary structures, i.e., with C_α-RMSDs lower than 2.5 Å from the native oligomer.[1140]

The effectiveness of the prediction protocol makes it suitable for ab initio quaternary structure predictions of other integral membrane proteins, including up-and-down α-helical bundles like GPCRs,[324,924,1145−1147] or β-barrels like the OMPLA protein.[1148] An attempt in this respect has already been reported, though based on an early and different version of the computational protocol.[605] In detail, integrating the rigid-body docking approach with the results of protein engineering and FRET and BRET experiments provided insights into the putative interaction interface of D_2R−$A_{2A}R$ heterodimers.[605] The initial models of the two receptors were achieved by comparative modeling, using modified rhodopsin structures as templates. The whole sequences of both receptors were modeled, since dimerization and/or oligomerization might involve also the cytosolic and/or the extracellular domains, as recently suggested for rhodopsin.[176] Since most of the structural errors are expected to reside in the intracellular and extracellular domains, nine average minimized structures of the $A_{2A}R$, differing in the conformations of the intracellular and extracellular loops as well as in the topology of the huge C-tail, were used to probe the effect of such structural differences on the results of docking simulations. Each of these structures was docked with the selected average minimized structure of D_2R. The different $A_{2A}R$ structures share preferential docking modes at the D_2R. These docking modes were broadly grouped into two clusters, CLUSTER 1 and CLUSTER 2 (Figure 25). In particular, in the most populated cluster, CLUSTER 1, H5 and/or H6 and the N-terminal portion of I3, from D_2R, respectively, approach H4 and the C-terminal portion of the C-tail, from the $A_{2A}R$ (Figure 25, left). H7 of D_2R may also participate, together with H6, in the contacts with H4 of $A_{2A}R$. A very short but significant portion of the huge I3 of D_2R, i.e., the N-terminal 217−220 amino acid stretch that is made of four consecutive arginines ^{217}RRRR^{220}, is frequently involved in the heterodimer interface (Figure 25, left).[605] Some of the four cationic amino acids are frequently found interacting with D401 and/or D402 in the C-terminal portion of the $A_{2A}R$ C-tail. A few more amino acids from the $A_{2A}R$ C-tail are suggested to participate in the heterodimer interface. Thus, very limited and almost invariant portions of the D_2R I3 and of the $A_{2A}R$ C-tail are likely to mediate D_2R−$A_{2A}R$ contacts. The heterodimer architecture shared by the members of CLUSTER 1 found consistency with the results of BRET experiments using a D_2R/D_1R chimera, which implicated the H5−I3−H6 portion of D_2R in the interaction with $A_{2A}R$.[605] The predicted interface according to the members of CLUSTER 1 was also consistent with the results

dx.doi.org/10.1021/cr100437t |Chem. Rev. 2011, 111, PR438–PR535

of pull-down and mass spectrometry experiments, which suggested that $A_{2A}R-D_2R$ heteromerization depends on an electrostatic interaction between an arginine-rich epitope from the I3 of the D_2R ^{217}RRRRKR^{222} and two adjacent aspartates (D401 and D402) or a phosphorylated Ser (S374) residue in the C-tail of the $A_{2A}R$.[1149]

The second cluster of docking solutions, CLUSTER 2, less populated than CLUSTER 1 but characterized by high docking scores, resembled the intradimer contact model proposed for rhodopsin (Figure 25, right).[176] In this cluster, the heterodimer interface is mainly formed by I2, H4, H3, and H5, from D_2R, and I2, H5, H3, and H4, from $A_{2A}R$. In these dimers, the extracellular end of the interface is made of contacts between aromatic amino acids from E2 and H5. These features could have functional implications, as the extracellular end of H5 is involved in agonist binding. The role of agonist-induced activation on the homo- and heterodimerization of these receptors is still obscure. Recent experimental evidence suggest that it may have a role in the formation of higher order oligomers, rather than in the formation of dimers, which should be constitutive features of the receptors.[605,1150] Collectively, the results of simulations of $D_2R-A_{2A}R$ heterodimerization showed a very limited involvement of the intracellular and extracellular domains in the intermonomer interfaces, thus overemphasizing the role of the TM helices. These results support the reliability of predictions, as the models of the TM helix bundles are expected to be acceptably accurate. In a recent study on the design of dopamine−adenosine heterobivalent ligands, the predicted $D_2R-A_{2A}R$ heterodimer from CLUSTER 2 was used as a target of preliminary docking experiments aimed at assessing whether the shortest linker (26 atom-long) would be long enough to allow the two pharmacophoric moieties to dock into the putative binding sites of the two protomers.[924] The estimated maximum inter-Cα-atom distance between the two binding pockets of the receptors that participate in the dimer was in the range of 40−45 Å. Prediction found support in two alternative heterodimer models made by two variances of a new D_2R model based upon the crystal structure of β_2AR and by the crystal structure of $A_{2A}R$.[924] These two alternative models, which were achieved by using the FiPD-based filtering approach,[1140] are, respectively, characterized by contacts between H1, from D_2R, and both H4 and H5 from $A_{2A}R$, and by contacts between H1, H2, and H4 from D_2R and H4, H2, and H1 from $A_{2A}R$. Although the intermonomer interfaces vary in the three different heterodimers, the two pharmacophoric moieties of the designed heterobivalent ligand, especially the D_2R moiety, dock into the same receptor sites.[924]

We are extensively challenging the computational approach in quaternary structure predictions of a number of GPCRs, including members of the amine,[924] hormone[1145] peptide,[1146] prostanoid,[1147] and purine,[324,924] subfamilies. In this respect, for the LHR, quaternary structure predictions emphasized the role of H4, H5, and H6, with prominence to H4, in mediating intermonomer interactions.[1145] In a study on the NTS1 receptor, a protocol developed for estimating mutational effects on the binding free energy of glycophorin A (GpA) homodimers[1151] was combined with the FiPD-based protocol to help selection of the most reliable dimer architecture(s).[1146] This was made possible by the availability of in vitro-determined intermonomer binding affinities for the NTS1, which represents a unique case within the rhodopsin family.[1071] Binding affinity estimations were done following an adjustment of the correlative model between ZD-score, which is essentially a size/shape descriptor, and free energy of GpA dimerization. This adjustment consisted in dividing the ZD-score by the number of native interface residues in order to make the correlative model almost independent of the extension of the interface and, therefore, applicable to differently sized systems like GpA and GPCRs. Intermonomer interfaces compatible with in vitro binding affinity constants were found to essentially involve H1, H2, and H4, and do not include disulfide bridges. In the desirable future cases, in which in vitro intermonomer binding affinities will be available for other GPCRs, the correlative model will work as an additional criterion for helping selection of the most likely dimers. Another application of the FiPD-based protocol includes the design of mutants of the TXA_2R α and β isoforms, no more able to talk between each other.[1147] The results of this study suggest that the heterodimers between the two TXA_2R isoforms are essentially characterized by contacts between hydrophobic residues in H1 from both protomers, and, to a lower extent, by H1−H2,E1 and H8−H8 contacts.

The representation of GPCR structures as networks of interacting amino acids can be a meaningful way to decipher the impact of ligand and dimerization/oligomerization on the molecular communication intrinsic to the protein fold, which is likely to serve to protein stability and function. It may represent also a tool to highlight asymmetry in supramolecular assemblies. This has been done in a recent investigation on the crystal structure of the $A_{2A}R$, in which the MD trajectories of three alternative homodimers predicted by the FiPD-based protocol were analyzed, through the PSN analysis, in terms of information processing networks, in which privileged residues are deputed to receive and propagate information. The dynamic network of intramolecular interactions characterizing the $A_{2A}R-ZMA$ complex in its monomeric state was compared with that of the same complex in three different dimeric forms, as well as with that of the apo-protomer. The results of the study emphasized the roles of H1 in $A_{2A}R$ homodimerization and of highly conserved amino acids in H1,H2, H6, and H7 in maintaining the structure network of the $A_{2A}R$. $A_{2A}R$ dimerization resulted to affect the communication networks intrinsic to the receptor fold in a way dependent on the dimer architecture. Certain architectures retain the most recurrent communication paths with respect to the monomeric antagonist-bound form but enhancing path numbers and frequencies, whereas some others impair ligand-mediated communication networks. Ligand binding affects the network as well. Collectively, the study suggests that the communication network that pertains to the functional dynamics of a GPCR is influenced by ligand functionality, oligomeric order, and architecture of the supramolecular assembly.

The FiPD-based approach was employed also by another group to predict likely heterodimers of the δ and μ opioid receptors.[1152] The most likely heterodimer interface was formed between H1,H7 of μ and H4,H5 of δ, with emphasis on the H1−H4 interface. Another possible interface is H6,H7 of μ and H4,H5 of δ, with emphasis on the H6−H4 interface.[1152]

Rosetta docking was used as well for quaternary structure predictions of GPCRs.[1153,1154,1155] In this respect, selection of the most reliable heterodimer between a β_2AR-based model of the 5-HT_{2A} serotonin receptor and a rhodopsin-based model of the class C metabotropic glutamate receptor 2 (mGluR2) was done upon visual inspection and structural similarity (in terms of rmsd) to the semiempirical model of rhodopsin (1N3M).[176] Comparative MD simulations between the predicted heterodimer and monomeric 5-HT_{2A} receptor highlighted the effects of dimerization on the binding pocket of the latter.[1153]

dx.doi.org/10.1021/cr100437t |Chem. Rev. 2011, 111, PR438–PR535

The fit-centroids-normal method was employed to predict more likely homodimers of a rhodopsin-based model of the A_3R.[1156] In this respect, an initial dimeric model was achieved by superimposing each protomer to the semiempirical oligomeric model of rhodopsin. This initial dimer served to generate various TM contact dimers, (H1−H2, H2−H3, H2−H4, H3−H4, H4−H5, H5−H6, H6−H7, and H7−H1) by means of the fit-centroids-normal method. Following MD simulations the most energetically favorable contact models were identified, which were the H4−H5 and H1−H2 dimers, the former resulting as the most favored according to the extension of the contact surface.

Manual docking was used as well for building GPCR dimers.[1157,1158] In more detail, a tetramer of the V_2R was manually built based upon information from in vitro experiments and subjected to MD simulations in explicit membrane/water. The study was aimed at highlighting residues responsible for the oligomer stability.[1157] Manual docking was employed as well to build a putative homodimer of the δ opioid receptor, characterized by an H4−H4 interface.[1158] The structural model was coarse grained together with the phospholipid environment and subjected to umbrella sampling simulations, leading to the conclusion that such homodimers have a short lifetime in the membrane.[1158]

Computational models of GPCR dimerization are being used also to assist the design of bivalent ligands.[924,1159] In this respect, Russo and co-workers provided direct evidence for the functional interaction of both pharmacophores of bivalent ligands with the 5-HT_4 serotonin receptor.[1159]

Although sequence-analysis-based approaches can be sources of invaluable information, the potential of molecular simulation methods is significantly higher and is going to increase with improvements in the quality of the GPCR models. Given the approximations in the current protein−protein docking algorithms, an integration between sequence- and structure-based approaches and in vitro experiments is, however, expected to improve the accuracy of quaternary structure predictions.

We regret, however that, so far, only very few predictions of the architecture of GPCRs dimers/oligomers relied on docking sampling (for references, see above).

While protein−protein docking simulations are essential to gain insight, at the atomic level, into the architecture of the intermonomer interfaces, a mesoscopic MC simulation approach, such as that proposed by Woolf and Linderman, might create a more direct link with in vitro experiments on GPCR oligomerization and localization in selected membrane compartments.[1160,1161] By incorporating information from in vitro experiments, the computational approach by Woolf and Linderman has begun to address the problem of how the kinetics of protein−protein binding affects the overall organization of the membrane and how dimerization affects the global protein organization.[1160,1161] Preliminary results by this approach suggest that changes in dimerization interactions affect cellular physiology. The possibility of predicting the ligand's ability to induce homo- or heterodimerization is another intriguing potential of this approach in drug discovery. Using a combination of stochastic (MC) and deterministic modeling, Fallahi-Sichani and Linderman proposed a novel mechanism for lipid raft partitioning of GPCRs based on reversible dimerization of receptors and demonstrated that such localization can affect GPCR signaling.[1162] Briefly, the kinetic MC model served to determine the effect of a ligand-induced change in the dimerization status of receptors on localization within low diffusivity microdomains (lipid rafts) at the cell surface, and to estimate the time-scale and level of receptor clustering and declustering. On the other hand, the deterministic ordinary differential equation model based on the collision coupling model served to study the effect of receptor localization within lipid rafts on downstream signaling events. Linking the two approaches allowed the authors to study and analyze G protein activation while incorporating the effects of receptor organization. On the basis of the results of simulations, the authors proposed a mechanism by which dimerization-inducing or dimerization-inhibiting characteristics of ligands can influence GPCR signaling by controlling receptor organization on the cell membrane.[1162]

The integration between atomistic and mesoscopic simulations is expected to be a promising tool to unravel functioning mechanisms that involve intricate protein networks.

7. RECEPTOR-G PROTEIN INTERACTION

7.1. Inactive and Active States of Heterotrimeric G Proteins and Structural Features of the Receptor-G Protein Interface: Insights from Low Resolution in Vitro Experiments

G proteins consist of three subunits α, β, and γ, forming one of nature's most important miniature (nano-) machines (reviewed in refs 25,27,1163). The α-subunits are enzymes of the Ras superfamily, which hydrolyze GTP to regulate events within cells and to transduce external signals. In the inactive state, G proteins form membrane-associated $\alpha\beta\gamma$ heterotrimers, with GDP tightly bound to the α-subunit. Upon activation by extracellular signals, receptors catalyze the exchange of bound GDP for GTP. The GTP-bound form of the heterotrimer is unstable and heterolytically dissociates to form active GTP-α and $\beta\gamma$ complexes (reviewed in refs 27,1164,1165). Acting either coordinately or independently, these two species bind and modulate the activities of downstream effector molecules. G proteins are released from effectors upon the breakdown of GTP that results from the slow GTPase activity of the α-subunit. The inactive α-subunit can recombine with $\beta\gamma$, reforming the heterotrimer, which can then reassociate with its receptor and undergo a new cycle of signal transduction. Recent experimental evidence, however, indicate that G protein activation may not be concurrent with dissociation of α from $\beta\gamma$.[1166,1167] The family of heterotrimeric G proteins includes over 20 isoforms from four classes of α (Gs, Gi, Gq, and G12), five of β, and at least six of γ (reviewed in refs 25,1164,1165).

Crystallographic studies of G protein α-subunits and heterotrimers provided significant insight into our understanding of how these extraordinary nanomachines might work (reviewed in refs 1063,1164). Structural studies of α-subunits have focused on Gt_α, transducin involved in vertebrate vision (reviewed in refs 27,1164,1168), $Gi_{\alpha1}$ (reviewed in refs 27,1164,1168), and Gs_α (reviewed in ref 27),[1169] respectively, involved in hormone-regulated inhibition and activation of adenylate cyclase as well as G13 (reviewed in ref 27)[1170] and Gq, involved in phosphoinositide hydrolysis by activation of phospholipase C.[1171] The structures of the GDP-bound forms of the $Gi_{\alpha1\beta1\gamma2}$ and of the $Gt_{\alpha\beta1\gamma1}$ heterotrimers provided the first view of the β-subunit in complex with γ.[1172,1173] Recently, the structure of heterotrimeric Gq has been solved as well, complexed with the YM-254890 peptide inhibitor of the GDP/GTP exchange reaction.[1171] Structural analysis shows that the YM-254890 binds the

dx.doi.org/10.1021/cr100437t |Chem. Rev. 2011, 111, PR438–PR535

hydrophobic cleft between two interdomain linkers connecting the GTPase and helical domains of the α-subunit. The binding stabilizes an inactive GDP-bound form through direct interactions with switch I (swI) and impairs the flexibility of the linker.[1171] The α-subunit consists of two domains, the GTPase domain, which contains a six-stranded β-sheet surrounded by six α-helices, and the helical domain, constituted by a long central helix surrounded by five shorter helices. GDP is bound into a cleft between the GTPase and helical domains (Figure 26). Both domains have almost identical structures in the GTP- and GDP-bound states. Significant changes are observed within the GTPase domain contacting $Gt_{\beta\gamma}$; in fact, these regions are disordered in the inactive heterotrimeric forms, whereas they are ordered in the Mg^{2+}-GTPγS-activated structures of Gt_α and $Gi_{\alpha1}$ (reviewed in ref 1164). This finds support also in NMR analyses suggesting that the inactive heterotrimer is in an open conformation with the $G_{\beta\gamma}-G_\alpha$ interface being solvent-exposed and flexible.[1174] The study showed that the $G_{\beta\gamma}$ dimer explores a range of conformations that can be exploited during molecular recognition by diverse binding partners. Computational experiments suggested that heterotrimer formation antagonizes the electrostatic repulsion between Gt_α and the membrane surface, thus favoring the anchoring to the membrane.[510,1175] The combined constraints of electrostatics and lipid anchors substantially limit the rotational degrees of freedom of the membrane-bound transducin heterotrimer. This may contribute to a faster transducin activation rate by accelerating transducin-rhodopsin complex formation.[1175]

The N-terminal region of the α-subunit consists of a long α-helix pointing out from the rest of the subunit (Figures 26, 27, 29−31). This structural feature was revealed by the structures of heterotrimeric Gt and Gi and remarked by the recent structure of heterotrimeric Gq[1171] as the α-helical conformation of the N-term is stabilized by the $\beta\gamma$ complex, whereas such a domain is disordered in the isolated α-subunits.[1164,1176] The last 10 amino acids of the Gt_α are predicted to hold an α-helical conformation in the MII-bound forms, whereas this short segment appears to be disordered in the receptor-dissociated forms of the α-subunit.[1164,1177,1178] The β-subunit, a member of the WD family, has a long N-terminal helix followed by a repeating module of seven β-sheets, each with four antiparallel strands, forming a β-propeller structure (Figures 26, 27, 28, 29−31).[1164,1168,1172,1173] The γ-subunit contains two helices: the N-terminal helix interacts with the N-terminal helix of β, whereas the remaining polypeptide chain of γ interacts with the β-propeller structure of β.[1164,1168,1172,1173] Similarly to the C-tail of the α-subunit, the C-tail of the γ chain (i.e., the (60−71) farnesyl peptide) holds a regular α-helical structure when bound to MII, whereas its conformation is disordered in the receptor-dissociated forms of the $\beta\gamma$ complex.[1179] Mutational analysis of the C-terminal region of the Gtγ-subunit highlights the influence of this region on rhodopsin−Gt conformation.[1180] Thus, in vitro experiments suggest that activated rhodopsin controls the conformation of the C-tails of the G protein α- and γ-subunits.[1177−1179]

The gross experimental information on receptor-G protein interaction concern the rhodopsin−transducin system (reviewed in refs 1063,1180,1182).

Early experimental results on rhodopsin suggested that I2 and I3 of rhodopsin are involved in binding and/or activation of transducin, whereas the peptide corresponding to I1 of rhodopsin does not compete with MII for binding to

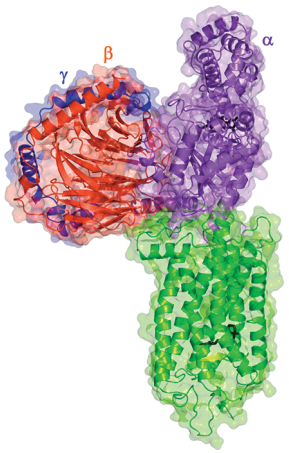

Figure 26. Computational model of the complex between monomeric dark rhodopsin, 1U19, and heterotrimeric Gt.[1181] The rhodopsin molecule is colored in yellow−green, whereas the α-, β-, and γ-subunits of the Gt are colored in violet, orange, and blue, respectively. The retinal and GDP molecules are represented by black sticks. The molecular surface is also shown colored according to the protein chains. Drawings were done by means of the software PYMOL 0.97 (http://pymol.sourceforge.net/).

Gt.[1183,1184] On the same line, the C-terminal region of rhodopsin seems not to be essential for the functional coupling to transducin.[1185] The important role of I2 and I3 in G protein recognition has also been demonstrated by several experiments on different GPCRs.[145,1185−1192] Experimental evidence suggest that the amino acids C140(3.55), K141, R147, and F148, at the end of H3 as well as at the N- and C-termini of I2, as well as residues T229, V230, S240, T242(6.25), T243(6.26), and Q244(6.27), in I3 and the cytosolic extension of H6, participate in the interaction with Gt.[1193] The loop regions proximal to the TM helices appear to be more important for the MII−Gt_α coupling than regions in the middle. The cytosolic extension of H3, including the conserved E/DRY motif, and the N-terminal end of I2 have been widely implicated in Gt_α activation.[1194−1196] The cytosolic extension of H3 and the N-terminus of I2, in concert with the C-terminus of I3 and the cytosolic extension of H6, are proposed to be involved in the recognition of the Gt_α C-terminus.[1195] In a recent study, the I3 of rhodopsin was demonstrated as one of the regions responsible for the specific coupling with the Gt. It has also been inferred that the 6-amino acid sequence adjacent to the C-terminal 5-amino acids of Gt_α interacts with I3 of MII.[1197] Recent experiments demonstrated that the role of H6 movements during MII formation is to provide a binding site on the cytoplasmic face of rhodopsin for the Gt_α C-terminus. This movement appears to open a cleft and expose a hydrophobic patch, which directly interacts with the Gt_α C-terminus and increases the affinity for transducin. These results also suggest that the Gt_α C-terminus binding is specific for the MII state and that the presence of the retinal Schiff base linkage is required to maintain the exposure of the cleft required for interaction with such domains of transducin. The amino acids L226(5.61), T229, and V230, at the boundaries of H5 and I3, which lie in the solvent-exposed cleft, are suggested to play a key role by imparting high affinity binding for the transducin Gt_α C-terminus.[245] FTIR studies indicated that, upon formation of the complex between MII and the 11-residue C-terminal peptide from transducin, both the peptide and the receptor undergo

dx.doi.org/10.1021/cr100437t |*Chem. Rev.* 2011, 111, PR438–PR535

conformational changes, thus suggesting that the conformation of the MII−peptide complex is different from that of free MII.[1198] The recent crystal structures of Ops* and MII in complex with the GtCT peptide show that the peptide binds to a cleft opened between the cytosolic extensions of H3 and H6, as well as to a H7−H8 kink (Figures 7 and 8).[108,110] Contacts along the inner surface of H5 and H6 seem to induce an α-helical conformation in GtCt with a C-terminal reverse turn. Main-chain carbonyl groups in the reverse turn constitute the center of a hydrogen-bonded network, which links the two receptor regions containing the conserved E/DRY and NPxxY(x)5,6F motifs.[108] Interestingly, the structural differences between free and GtCT-bound forms of both Ops* and MII are negligible.[107,108,110] The Ops*-GtCT crystallographic complex has been recently employed as a template to build interaction models between the thyrotropin receptor (TSHR) and heterotrimeric Gs and Gq.[1199] In this respect, the docking orientations of the two G proteins were achieved by simply superimposing their C-termini onto the GtCT in the crystallographic complex.[1199]

Experimental evidence suggest that different G protein portions participate in the receptor−G protein interface. It has been, in fact, demonstrated that, to stabilize the high affinity state of the A1 adenosine receptor, a multiple interaction between the receptor and the G_α or even the heterotrimeric G protein is required.[1200] The crucial role of the C-terminal amino acids in coupling to the receptor was widely demonstrated for different α-subunits.[1165,1177,1178,1201−1207] A C-terminal 11-amino acid peptide from transducin, Gt_α-(340−350), has been shown to both bind and stabilize the MII conformation, mimicking heterotrimeric Gt. Indeed, using a combinatorial library, analogues of Gt_α-(340−350) were identified that bound light-activated rhodopsin with high affinity.[1063,1208,1209] The same authors made peptides with key substitutions either on the background of the native Gt_α-(340−350) sequence or on the high affinity sequences and used the stabilization of MII as a tool to determine which amino acids are critical in the G protein−rhodopsin interaction.[1209] Removal of the positive charge at the N-termini by acylation, or delocalization of the charge by K to R substitution enhanced the affinity of the Gt_α-(340−350) peptides for MII, whereas a decrease in affinity was observed following C-terminal amidation.[1209] C347, a residue conserved in pertussis toxin-sensitive G proteins, was shown to interact with a hydrophobic site in MII.[1209]

The role of the $\alpha4/\beta6$ loop of the α-subunit in receptor−G protein interaction is supported by the results of proteolytic digestion experiments and alanine scanning mutagenesis on transducin as well as by biochemical studies on $Gt_\alpha/Gi_{\alpha1}$ chimerae.[1210−1213]

More resolved information came from mutational and cross-linking studies aimed at identifying residues in Gt_α and rhodopsin that are in close proximity. Acharya et al. identified Y136-(3.51)−V139(3.54) in H3 of rhodopsin as interaction sites with Gt_α.[1195] Experimental evidence from Khorana's group seem to indicate that L19−R28, R310−K313, and E342−K345 of Gt_α are cross-linked to S240C in I3 of MII.[1214,1215] Evidence for interactions between the N310−Q312 region (H8) of rhodopsin and residues 340−350 of Gt_α has also been reported.[1216,1217]

Using stabilization and photoregeneration of the receptor's signaling state and Gt activation assays, Herrmann and co-workers provided evidence for a two-site sequential fit mechanism of Gt activation. According to this model, receptor−G protein recognition is suggested to be initiated by an encounter of Gt_γ(50−71)farnesyl with MII. This would make the C-terminal tail of the Gt_α available for binding with MII, triggering the GDP release and the formation of a stable empty site complex that is ready to receive the activating cofactor, GTP.[1218] Successive studies by the same authors indicated that the native N-terminally fatty-acylated G_α is competent to interact with activated receptor even in the absence of $G_{\beta\gamma}$, whereas nonacylated G_α requires $G_{\beta\gamma}$ for interaction.[1219] Experiments with N-terminally truncated G_α subunits suggest that in the second step of the catalytic process, the receptor binds to the $\alpha N/\beta1$-loop region of G_α to reduce nucleotide affinity and to make the G_α C-term available for subsequent interaction with the receptor.[1219]

In summary, the patchwork of the most relevant information from in vitro experiments on rhodopsin−transducin recognition suggests that the $\alpha4/\beta6$ loop and the C-terminus of Gt_α recognize a solvent-accessible cleft on MII, formed by amino acids from the cytosolic extensions of H3, H5, and H6, from the N-terminus of I2, and from the N-terminus of H8.

A recent study on the M_3-muscarinic receptor (M_3R) analyzed the ability of ~250 combinations of cysteine-substituted M_3R and Gq_α proteins to undergo cross-link formation. The identification of specific M_3R-Gq_α contact sites, in both the inactive and active receptor conformations, let the authors draw conclusions on the basic architecture of the M_3R-Gq_α interface.[34] In more detail, most M_3R-Gq_α contact sites identified in the inactive state of the M_3R were also observed following receptor activation by carbachol. These results indicated that the M_3R is precoupled to Gq before receptor activation, and that carbachol-mediated M_3R activation does not result in the dissociation of the receptor−Gq complex.[34] Agonist-independent cross-links occurred between a residue located on the surface-exposed side of αN of Gq_α (R31C) and a residue located in I2 of the M_3R (L173C), suggesting that direct contacts between αN and I2 play a role in productive G protein−receptor coupling. On the other hand, agonist-induced cross-links involve the $\alpha4/\beta6$ loop of Gq_α (D321C) and the N-terminal segment of H8 of the M_3R (K546C, T549C and T552C), suggesting that receptor activation leads to a structural change at the receptor−Gq interface that increases the proximity between the N-terminal portion of H8 of the M_3R and the $\alpha4/\beta6$ loop of Gq_α. The recent crystallographic complex between β_2AR and nucleotide-free Gs seems not compatible with cysteine cross-linking between the receptor H8 and the $\alpha4/\beta6$ loop of Gs (Figure 27). The agonist carbachol also promoted significant cross-linking between a residue located at the cytoplasmic end of H6 of the M_3R (A488C) and the last three residues of Gq_α(N375C, L358C and V359C), consistent with the crystal structure of the Ops*−GtCT complex. Finally, agonist-induced cross-links include also those between the N-terminal portion of H8 of the M_3R (T549C and T552C) and the C-term of Gq_α, indicating that these regions move closer to each other following M_3R activation.[34]

Very recent in vitro experiments provide evidence for possible interactions between inactivated rhodopsin and Gt_α, thus suggesting that the cytosolic domains in the crystal structures of inactive rhodopsin can recognize transducin and that the accomplishment of the MII state would require a precoupling between dark rhodopsin and transducin (reviewed also in ref 1091).[30,1220] However, experimental evidence that dark rhodopsin and heterotrimeric transducin may exist as a preformed complex has appeared early in the literature, although it was not pursued any further.[1221] This hypothesis is also supported by the experimental evidence that proton uptake from the cytosol, which

dx.doi.org/10.1021/cr100437t |Chem. Rev. 2011, 111, PR438–PR535

accompanies MII formation, would require the presence of transducin to occur.[207] The constitutive close proximity of rhodopsin and transducin would permit rapid Gt binding and signal transmission to specific effectors. However, this binding cannot be too stable because amplification of the signal requires that a single activated receptor catalyzes the nucleotide exchange on 10−100 G protein molecules (reviewed in ref 1091). A "dynamic scaffolding" mechanism for rhodopsin−transducin interaction was recently proposed, in which prevalently dimeric rhodopsin forms transient complexes with Gt in the dark (∼25% of Gt precoupled to Rho) without slowing down the phototransduction cascade.[751] The hypothesis of receptor−G protein precoupling may be a common feature to all GPCRs, as also demonstrated by recent PWR spectroscopy observations of a binding between a ligand-free δ opioid receptor and the G protein as well as by a number of studies on other GPCRs.[29,31−34]

A debated aspect of receptor−G protein recognition is the stoichiometry of the complex, i.e., whether heterotrimeric G protein recognizes a monomeric or dimeric receptor (reviewed in also in refs 64,1091).

7.2. Insights into the Mechanism of Receptor-Catalyzed Nucleotide Release from Low-Resolution Biophysical Experiments

Different mechanisms of receptor-catalyzed GDP release have been proposed (reviewed also in ref 1091). According to the so-called "lever-arm" model, the $\beta3/\alpha2$ loop of the α-subunit acts as a potential "lip" that occludes GDP release.[1222,1223] According to this model, GPCRs would use the G_α N-term to tilt $G_{\beta\gamma}$ away from G_α, thereby opening the $\beta3/\alpha2$ lip. The recently released crystal structure of the guanine nucleotide exchange factor (GEF) peptide KB-752 bound to $Gi1_\alpha$ seems to support the "lever-arm" model.[1224] Indeed, by binding between swII and the $\alpha3$-helix, KB-752 pushes the $\alpha2$-helix away from the nucleotide. Displacement of swII results in the $\beta3/\alpha2$ loop also being pulled away from the nucleotide in a way that might allow more efficient GDP egress. Thus, according to this model, the proposed egress route for GDP lies at the $G_\alpha-G_\beta$ interface, which becomes more accessible following the displacement of the occlusive $\beta3/\alpha2$ loop. An alternative hypothesis on the mechanism of receptor-catalyzed nucleotide exchange suggests that GPCRs use the G_α N-term to move $G_{\beta\gamma}$ in an opposite fashion to that proposed by the "lever-arm" model.[1225] According to this "gear-shift" model, $G_{\beta\gamma}$ is shifted toward G_ω resulting in a closely packing $G_\alpha-G_\beta$ interface. This $G_{\beta\gamma}$ shift is proposed to alter the conformation of the $\alpha5$-helix. A different GDP exit route, as compared to the one proposed by the "lever-arm" model or inferred from the crystal structure of the KB-752−$Gi1_\alpha$ complex, is proposed by the C-term "latch" hypothesis (reviewed also in ref 1091). The latter is based on the results of site directed mutagenesis experiments implicating the C-term of the $\alpha5$-helix in receptor-catalyzed GDP exchange,[1226,1227] as well as on the results of very recent SDSL experiments on $Gi1_\alpha$.[1228−1230] The latter, indeed, identified a possible allosteric pathway propagated along swI at the $G_\alpha-G_\beta$ interface to the αF-helix, which, like the $\alpha5$-helix and the $\beta6/\alpha5$ loop, forms part of a putative GDP exit route.[1229] The authors suggested that the receptor induces a rotation-translation motion in the $\alpha5$-helix that preserves its overall helical structure.[1228,1229] Collectively, the results suggest that the receptor uses contacts with the extreme C-term to communicate structural changes through the $\alpha5$-helix, presumably to the $\beta6/\alpha5$ loop to induce the release of GDP. However, these studies also revealed changes in the EPR spectra of labeled residues in the $\beta2/\beta3$ loop and the $\beta6$-strand, suggesting that these regions are mobile during receptor activation and thus may also play a crucial role in receptor-mediated activation of G_α (reviewed also in ref 1091). SDSL experiments also indicated that swII undergoes increase in dynamics following $Gi1_\alpha$−receptor coupling, suggesting that the $\alpha2/\beta4$ loop and the $\alpha4$-helix are receptor binding regions. Recent advances in SDSL and DEER spectroscopy as well as cross-linking experiments on heterotrimeric Gi activation by photoactivated rhodopsin provided evidence for significant displacements of the α-helical domain with respect to the Ras-like domain as associated with GDP release. The largest increase in distance between the two domains, i.e., ∼20 Å, concerned positions 90 at the C-term of αA and 238 in swIII.[1231] Cross-linking the two amino acids resulted in severely impaired rates of receptor-mediated nucleotide exchange as compared to either the parent or uncross-linked protein, thus demonstrating the essential nature of the domain separation in receptor-mediated G protein activation.[1231]

The crystal structure of $Gi1_\alpha$ in complex with the N-terminal portion of I3 of D_2R (D_2N) shows that the peptide binds to the $\alpha4/\beta6$ loop of G_α. Binding of D_2N results in a displacement of the $\beta6$-strand compared to the peptide-free G protein. In line with the C-term "latch" model, these data suggest that the receptor uses the $\beta6$-strand, perhaps in combination with the $\alpha5$-helix, to communicate structural changes to the $\beta6/\alpha5$ loop, thus disrupting contacts with GDP, which is then released (reviewed also in ref 1091).[1232] A possible convergence between "lever-arm" and C-term "latch" models has been hypothesized based upon the synergistic effect of D_2N and KB-752 peptides, suggesting that modulation of the $\beta6/\alpha5$ loop alone is insufficient for maximal GEF activity.[1233] It has been hence suggested that the receptor uses direct contacts with the $\beta6$-strand and $\alpha5$-helix to release the contacts between guanine base and $\beta6/\alpha5$ loop, coincident with $G_{\beta\gamma}$-mediated levering of the $\beta3/\alpha2$ loop to remove the occlusive lip that blocks GDP release, thereby causing maximally efficient nucleotide release.[1233]

The crystal structure of a GDP-bound constitutively active mutant of $Gi1_\alpha$ (T329A) shows substantial conformational rearrangement of the swI region and additional alterations of the side chains lining the catalytic pocket that disrupt the Mg^{2+} coordination sphere and dislodge bound Mg^{2+}.[1234] On the basis of a structural analysis, the authors proposed a "sequential release" mechanism whereby a transient conformational change in the $\alpha5$-helix alters swI to induce GDP release.

NMR is proving to be a powerful tool to investigate receptor-induced changes in G_α.[1235−1238] In this context, it was shown that $G_{\beta\gamma}$ binding induces structural changes in the swII and the C-terminal regions, shifting the G_α structure toward a "preactivated" form, which displays at least two conformational states for the C-term that are in slow exchange.[1235,1238] These changes in the G_α structure may both potentiate interactions with activated receptor and preorganize the guanine nucleotide pocket for GDP/GTP exchange. These studies suggested also correlated changes in the guanine nucleotide binding pocket and the C-terminal region during the course of receptor-catalyzed nucleotide exchange.

dx.doi.org/10.1021/cr100437t |Chem. Rev. 2011, 111, PR438–PR535

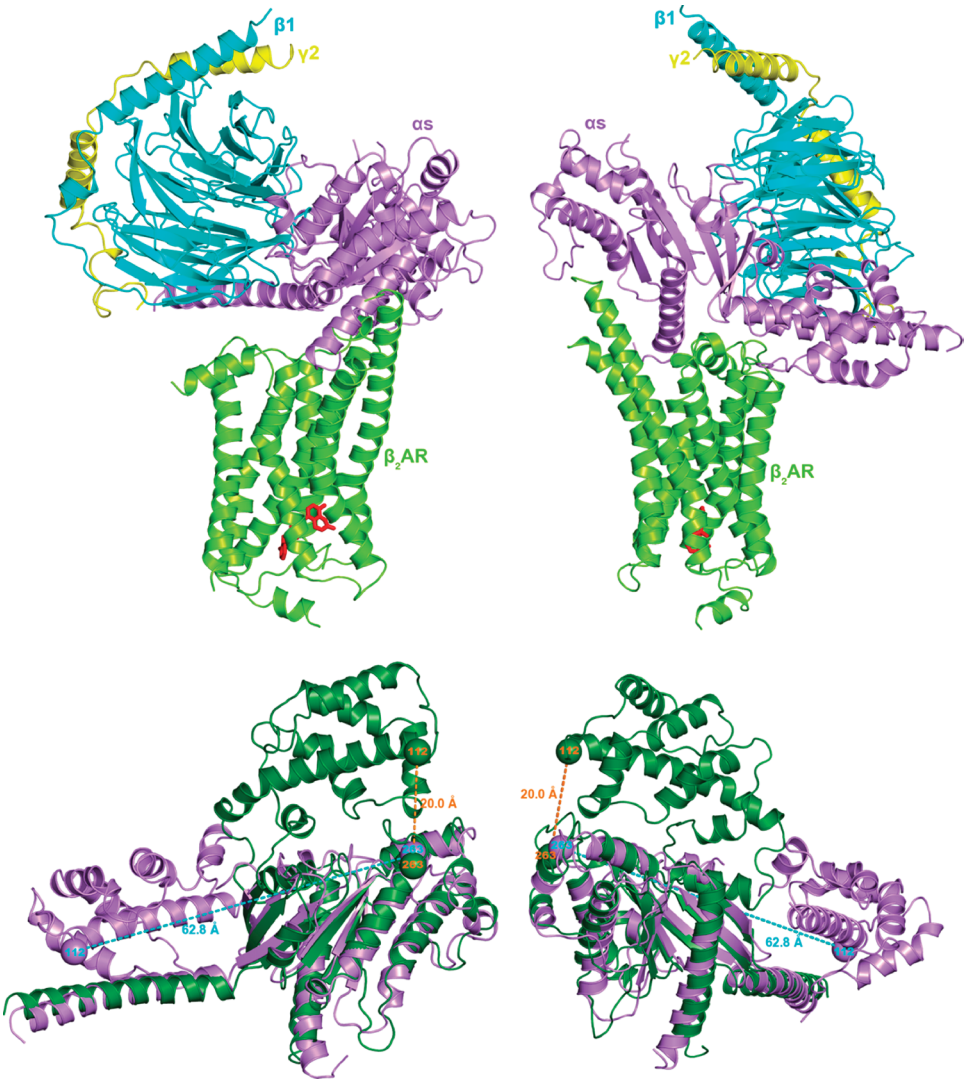

Figure 27. Crystal structure of β_2AR in complex with nucleotide-free Gs heterotrimer. (top) Two side views of the complex are shown. The Gsα-, β-, and γ-subunits are, respectively, violet, cyan, and yellow; the β_2AR is yellow−green, and the agonist BI-167107 (represented in sticks) is red. (bottom) The crystal structure of nucleotide-free Gsα (violet) is superimposed to the computational model of the GDP-bound form of the protein (dark green). The distances between the Cα-atoms of N112 (in αA) and T263 (in swIII) are shown on both proteins.

7.3. Insights into Receptor-G Protein Coupling from the Crystal Structure of the Agonist−β_2AR−Gs Ternary Complex

The first crystal structure of a G protein heterotrimer in complex with a GPCR was released on July 2011 (PDB code 3SN6, 3.20 Å; Figure 27).[100] It concerns the agonist-bound human β_2AR in complex with the nucleotide-free Gs heterotrimer. Removal of GDP was essential because both GDP and GTP can disrupt the high-affinity interaction between β_2AR and Gs. To favor crystallization, the unstructured N-term of the β_2AR was replaced with the T4L. As an additional strategy to facilitate crystallogenesis, the T4L−β_2AR−Gs complex was cocrystallized with a nanobody (Nb35) docked at the interface between the Ras-like domain and the β-subunit. The latter strategy was instrumental in overcoming the high flexibility observed for the α-helical domain in single particle electron microscopy analysis of the detergent-solubilized complex.[100] It cannot be excluded the possibility that Nb35 may influence the relative orientation of the GαRas−G$\beta\gamma$ interface in the crystal structure.[100]

The β_2AR structure from the complex is quite similar to the one in complex with Nb80 (PDB code 3P0G). The Cα-rmsd concerning all the corresponding amino acid residues in the two structures is 1.01 Å. They differ mostly at the cytoplasmic ends of H5 and H6 where they interact with the different proteins, the largest divergence being a 3 Å outward movement of the cytosolic end of H6.

In the β_2AR−Gs complex, the hydrophobic face of GsCt, i.e., made by L388, L393, and L394, docks on a hydrophobic surface of the receptor contributed by amino acids on the cytosolic ends of H3, H5, and H6 (Figure 28). The arginine of the E/DRY motif is a receptor recognition point for Gs, interacting with Y391.

Collectively, the orientation of GsCT onto the cytosolic crevice of the β_2AR is different from that of GtCT onto opsin (Figure 29A,B). This occurs in spite of the identical conformation of the two C-terminal peptides (Figure 29C). This may be due either to the fact that GsCT in the crystals is part of the whole α-subunit, whereas GtCT is an isolated peptide, and/or to the

dx.doi.org/10.1021/cr100437t |*Chem. Rev.* 2011, 111, PR438–PR535

structural differences between the active states of β_2AR and (rhod)opsin, and/or to the peculiar orientation and conformation of the α5-helix in the nucleotide-free Gs, which differs from that of GDP-bound Gt (Figure 29D,E). The latter option would be consistent with the observation that docking simulations between Ops* and the GDP-bound Gt heterotrimer incorporating the crystallographic GtGT predicts an interaction mode of GtCT very similar (i.e., Cα-rmsd of 0.34 Å) to the crystallographic complex (manuscript in preparation). In contrast, docking simulations of either the β_2AR from the 3P0G complex (i.e., in its original form or with a completed I3[607]) or the β_2AR from the 35N6 complex with GDP-bound heterotrimeric Gs could not predict an interaction mode of the heterotrimer significantly similar to the crystallographic complex (see ref 607 and unpublished results). These results would suggest that the orientation of the isolated GtCT into both Ops* and MII is close to the interaction mode that the same portion would make in the context of a GDP-bound heterotrimer, i.e., at the early stages of receptor-catalized GDP release. In contrast, the interaction mode of GsGT in the crystallographic complex would represent a late stage in the process of receptor−G protein recognition.

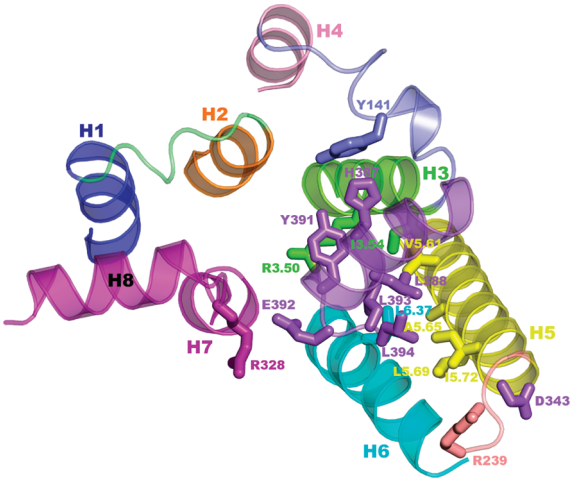

Figure 28. Details of interaction between β_2AR and Gsα. The receptor is seen from the intracellular side in a direction perpendicular to the membrane surface. Helices 1, 2, 3, 4, 5, 6, and 7 are, respectively, blue, orange, yellow−green, pink, yellow, cyan, and magenta; helix 8 is magenta as well. Gs$_\alpha$ is violet. Selected amino acid side chains on both proteins are shown in sticks.

The 6 Å displacement toward the receptor and rotation of the α5-helix found in the β_2AR−Gs complex are likely the triggers of the receptor-induced structural changes in the G protein α-subunit.[100] Consistent with the inferences from biophysical experiments (i.e., see the previous section), the movements of the α5-helix are associated with an outward displacement of the β6/α5 loop that is shifted outward from the nucleotide binding cleft. The movements of the α5-helix are associated with changes in interactions between this helix and the β6-strand, the αN-β1 loop, and the α1-helix. The β1-strand forms another link between the β_2AR and the nucleotide-binding pocket. The carboxy-terminal end of this strand changes conformation around G47, and there are further changes in the β1-α1 loop (P-loop) that coordinates the β-phosphate in the GTP-bound form. The α5-helix and the β1-strand appear to be the mediators of receptor-induced signal propagation from the Ras-like domain to the α-helical domain.

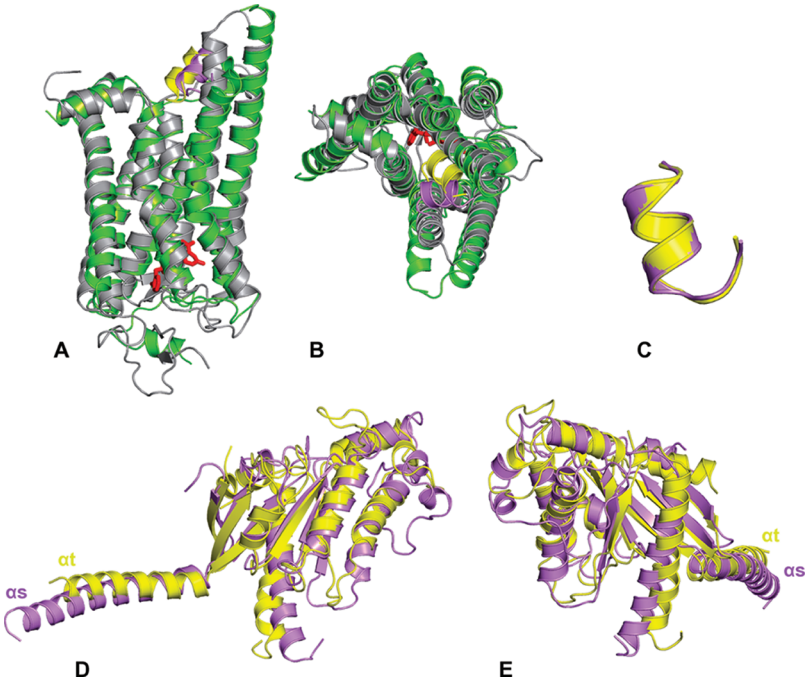

Figure 29. Comparisons between the crystallographic complexes the β_2AR−GsCT and opsin−GtCT as well as the crystal structures of GsαRas and GtαRas. (A,B) The superimpositions of the β_2AR−GsCt and opsin−GtCt are seen, respectively, in a direction parallel (the cytosolic end being on top) and perpendicular to the membrane surface. The β_2AR is yellow−green, opsin is gray, GsCt is violet, and GtCt is yellow. The β_2AR agonist is represented in red sticks. (C) The superimposed structures of GsCt (violet) and GtCt (yellow) are shown. In (D,E), the superimposed structures of the αN and the Ras-like domains of nucleotide-free Gs (violet) and GDP-bound Gt (yellow) are shown.

dx.doi.org/10.1021/cr100437t |*Chem. Rev.* 2011, 111, PR438–PR535

The $\beta\gamma$ dimer does not make contacts with monomeric β_2AR. It cannot be, however, excluded that it would be involved in contacts with a second receptor protomer in a dimer.[100]

The most surprising feature of the β_2AR−Gs complex is the dramatic displacement of the α-helical domain with respect to the Ras-like domain (Figure 27). Indeed, the distance between the C-term of αA (i.e., the Cα-atom of N112) and swIII (i.e., the Cα-atom of T263) increases by 43 Å on going from the receptor-free GDP-bound state to the receptor-bound nucleotide-free state of Gs (Figure 27). Such a tremendous displacement is ∼40 Å longer than the maximal displacement estimated on the Gi−rhodopsin complex,[1231] raising the question whether it may represent a physiological condition or an artifact of crystallization. In this respect, it has been argued that the position of the α-helical domain in the crystallographic β_2AR−Gs complex may reflect only one of an ensemble of conformations that it can adopt under physiological conditions, which has been stabilized by crystal packing interactions.

Irrespective of whether the extent of the structural uncoupling of the α-helical domain from the Ras-like domain in the β_2AR−Gs complex is reliable or not, it is now unquestionable the evidence that the receptor-catalyzed nucleotide-exchange on heterotrimeric G proteins requires a significant displacement of the α-helical domain away from the Ras-like domain. The triggers of such displacement would include motions of the α5-helix that represent a fundamental recognition point for the receptor.

By combining the information from the crystallographic structures of the receptor−G protein complexes available so far, a possible mechanism of receptor-catalyzed GDP release has been proposed.[100] Consistent with the results of our docking simulations discussed above, it has been argued that the docking mode of GtCt onto Ops* or MII represents the early step in receptor recognition by the GDP-bound heterotrimeric G protein.[100] In this framework, it has been hypothesized that the first interaction of the β_2AR with the Gs heterotrimer would require a movement of the carboxy terminus of the α5-helix away from the β6-strand to permit interactions with the β_2AR similar to those observed in MII or Ops*. The subsequent formation of more extensive interactions between the β_2AR I2 and the amino terminus of Gαs would require a rotation of GαsRas relative to the receptor associated with further conformational changes in both β_2AR and GαsRas. Uncoupling of the α-helical domain from the Ras-like domain would be a consequence of nucleotide release or at least a coincident event.[100] The details of the early events in receptor-induced nucleotide exchange and the role of the $\beta\gamma$ dimer in such process, however, await elucidation.

7.4. Bioinformatics and Computational Modeling Approaches to Predictions of the Receptor−G Protein Interface

Most of the computational approaches aimed at predicting the receptor−G protein interface in the years that preceded the release of the first crystal structure of rhodopsin were essentially based on sequence analyses approaches such as the ET method.[1127,1239] Mapping the results of the ET method into the van der Waals surface of the G_α led to identifying residues in β4, the α4/β6 loop, β6, α5, and the C-terminus as potential recognition points for the receptor. Many of the residues identified have also been implicated by in vitro experiments.[1127,1212,1239]

A successive reinvestigation, through the ET method, of the potential receptor contact sites on the G protein, in light of emerging evidence for GPCR dimerization, predicted an ET functional site approximately twice as big as was originally reported by Lichtarge et al.[1061,1239] The ET functional sites predicted by Dean et al. involved both the RAS and the α-helical domain of the α-subunit and were estimated to be large enough to interact with a GPCR dimer.[1061] The simultaneous interactions between the N-terminus of the α-subunit and phospholipids and between the α-helical domain of the α-subunit and the receptor were thought possible only if the reciprocal orientation of these two portions of the α-subunit is similar to that in the crystal structure of the RGS-bound form of AlF4-activated $Gi_{\alpha1}$.[1240]

Other sequence analyses on the G_α chains identified 12 residues, which are fully conserved.[1241] However, the majority of these were found to be involved in the GDP/GTP binding site. A correlated mutational analysis of these sequences identified residue groups that had remained conserved or mutated as a group. These groups included residues in the β2/β3 loop as well as in the N-terminal and α5 helices. Mapping these residues in the crystal structure showed that they clustered around a conserved negatively charged aspartate at position 337 and suitable for interacting with the receptor. It was, therefore, suggested that this conserved aspartate and the surrounding residues form the binding site for R3.50 of the E/DRY motif in the receptor, consistent with a number of in vitro deletion experiments.[1241] The authors also assumed that the C-tail of the receptor interacts with the N-terminal helix and possibly with the last 10 amino acids of the α-subunit.[1241]

Early computational modeling of receptor−G protein interaction was done by Mahmoudian.[1242] The target of the study was the complex of the human Gs_α with the β_3AR.[1242] The crystal structure of the *E. coli* EF-tu nucleotide binding domain was used as the backbone for the Gs_α model, with its amino acid sequence being mutated to the Gs_α sequence. This procedure produced the core of the Gs_α protein, to which a number of loops were added using the COMPOSER program.[1243,1244] The β_3AR model was achieved by comparative modeling using the BRD structure as a template.[1242] The receptor−G protein complex was built using interactive molecular graphics based on low resolution experimental constraints. Interface domains from the receptor involved I3 and the C-terminus, whereas the Gs_α side of the interface was made by the N-terminus and the C-terminus.[1242]

We employed computational modeling to investigate the early steps of receptor−G protein recognition.[510,511] On the basis of the inference that the mutation-induced active states of the α_{1b}AR share the opening of a solvent accessible cleft between I2 and I3, electrostatic analysis and rigid body docking simulations were carried out to identify whether the solvent exposure of peculiar receptor portions is important in receptor−G protein recognition.[510,511] The ab initio models of the free and agonist-bound forms of wild type α_{1b}AR and of the free forms of the D142(3.49)A and A293(6.34)E constitutively active mutants of the receptor were docked with their cognate heterotrimeric $Gq_{\alpha\beta1\gamma2}$ heterotrimer using the ESCHER program.[1245] Attempts to address the issue of G protein coupling selectivity were also made by docking the same inactive and active receptor forms with heterotrimeric Gs and Gi and Gt.[510] The models of

dx.doi.org/10.1021/cr100437t |*Chem. Rev.* 2011, 111, PR438–PR535

Figure 30. Two side views of the computational model of the complex between a rhodopsin tetramer and heterotrimeric Gt.[1062] The four rhodopsin monomers are colored in yellow−green, gray, purple, and cyan, whereas the α-, β-, and γ-subunits of the Gt are colored in violet, orange, and blue, respectively. Drawings were done by means of the software PYMOL 0.97 (http://pymol.sourceforge.net/).

the Gq_α and Gs_α were achieved by comparative modeling using the structures of heterotrimeric Gi_α (PDB entry 1GP2)[1172] as a template.[510] All the incomplete termini of the $\alpha\beta\gamma$-subunits were modeled. Consistent with the experimental findings, it was found that the cytosolic crevice formed by I2, I3, and the cytosolic extensions of H5 and H6 and characterized by a large solvent accessible surface and a positive electrostatic potential participates in the receptor−G protein interface. A suggestion from this computational study was that while the cationic nature of the cytosolic portions of the receptor seems to complement an anionic surface of the Gq_α protein, only a selected number of cationic residues could be contact sites on the receptor for the G protein.[510] Thus, although the majority of cationic residues on the cytosolic surface of the α_{1b}AR contribute to reciprocal electrostatic properties between the receptor and the Gq_α, they appear to not be directly involved in receptor−G protein interaction and/or receptor-induced G protein activation.[510] These results are in agreement with the experimental findings that mutating the majority of basic residues in the cytosolic loops and extensions of H4, H5, and H6 of the α_{1b}AR did not impair the receptor-mediated IP response, thus demonstrating that most basic amino acids play no direct role in receptor−G protein coupling.[132] The results of computational modeling overemphasized the role of R254 and K258, in I3, as potential contact sites on the receptor for the Gq_α.[510] These predictions found validation in in vitro findings that, among all the basic residues of the cytosolic surface of the receptor, only the combined mutations of R254 and K258 totally impaired the IP response of the agonist-stimulated receptor as well as of the constitutively active mutants D142(3.49)A and A293(6.34)E.[132]

Consistent with the results of many in vitro experiments, computations suggested that the G protein solvent-exposed portions that recognize the intracellular loops of activated receptors are the N-terminal portion of α3, αG, the αG/α4 loop, α4, the α4/β6 loop, α5, and the C-terminus.[510] Docking simulations suggested also that the two constitutively active mutants D142(3.49)A and A293(6.34)E recognize different G proteins with similar selectivity orders, i.e., $Gq_\alpha \sim Gs_\alpha > Gi_\alpha \gg Gt_\alpha$.[510]

Yeagle and co-workers proposed an interaction model between their computational model of MII and heterotrimeric Gt.[250] The construction of the complex was driven by the experimental information on rhodopsin−transducin interaction, taking also into account the electrostatic complementarity between interacting domains. In the model, the N-terminal helix of the Gt_α binds to the groove that becomes more exposed on the cytosol when MII is formed. Furthermore, the C-terminus of Gt_α binds to the crevice at the bottom of the groove in the cytoplasmic surface of MII, between I2 and I3. This mode of binding places residues K340 and D341 of Gt_α close to E134(3.49) and R135(3.50) of MII, which are hypothesized to be separated from E247(6.30) upon MII formation. The authors hypothesized that the C-terminus of Gt_α may substitute, in part, for the interactions of E134(3.49) and R135(3.50) with E247(6.30).[250]

An invaluable framework to interpret the results of biophysical and biochemical experiments on rhodopsin−transducin interaction is represented by the crystal structures of rhodopsin[16,89−92] and the rhodopsin semiempirical oligomeric model recently built, based upon geometrical constraints from AFM experiments.[63,176] An interaction model between the $Gt_{\alpha\beta1\gamma1}$ heterotrimer and a tetrameric model of rhodopsin has very recently been produced by computational modeling (Figure 30).[1062] In detail, after modeling of all the missing termini in heterotrimeric Gt,[1173] transducin was docked to the rhodopsin dimer, where one molecule was activated by movement and rotation of H6, followed by slight movements of neighboring helices to accommodate changes in the structure.[1062] The least amount of tension

dx.doi.org/10.1021/cr100437t |*Chem. Rev.* 2011, 111, PR438–PR535

was achieved during docking of the C-terminal region of Gt_α along the longest primary axis of activated rhodopsin. Docking was continued until the N-terminal helix of Gt_α (parallel to the cytoplasmic surface of the rhodopsin dimer) interacted firmly with the cytoplasmic cavities of adjacent inactive rhodopsin in the dimer. Next, β- and γ-subunits were added, obtained from the crystal structure of Gt,[1173] and the whole complex was optimized by energy minimization. Short molecular dynamics runs of 5−10 ps were applied to different parts of the model to ensure proper interactions between molecules in the complex. A longer molecular dynamics run (100 ps) validated that the complex is stable.[1062] Despite the probable artifacts in the MII model and the extremely short time length of MD simulations, such a computational experiment resulted in an intriguing supramolecular model comprising tetrameric rhodopsin and heterotrimeric Gt (Figure 30).[1062] According to this model, the activated rhodopsin mainly interacts with the RAS-like domain of the Gt_α, with all the cytosolic domains plus the cytosolic ends of H3 and H6 being involved in this interaction. Interactions of the N-terminal region of Gt_α with the second rhodopsin molecule in the dimer mainly involve I1, I2, H6, and the C-tail of the photoreceptor (Figure 30). Gt_β interacts with all four rhodopsin monomers in the tetramer, whereas Gt_γ forms hydrogen bonds with two rhodopsin monomers (Figure 30).[1062] These interactions are suggested to provide a temporary anchor and can be replaced with water when $Gt_{\beta\gamma}$ dissociates.[1062] The oligomeric model of rhodopsin−transducin interaction by Filipek and co-workers, thus, suggests that the Gt heterotrimer covers two rhodopsin dimers, and when $\beta\gamma$-subunits dissociate away, another Gt heterotrimer can bind to an adjacent tetramer. After dissociation of $\beta\gamma$-subunits from the second Gt, the next Gt can bind to a neighboring rhodopsin tetramer, and so forth. Both α-subunits not only bind to adjacent rhodopsin dimers but also interact with each other when located on adjacent rhodopsin dimers, suggesting that one Gt_α can facilitate binding of a second G protein on an adjacent rhodopsin tetramer.[1062] In a successive study by the same authors, the supramolecular model made of two rhodopsin dimers and one Gt heterotrimer was successively subjected to a putative stability check by short (2 ns) MD simulations in explicit membrane/water.[1246] Computations were also aimed at investigating the interaction modes of the post-translational hydrophobic modifications which work as membrane anchors of Gt.[1246]

An alternative oligomeric model of activated rhodopsin (i.e., with H6/I3 moved 8 Å away from the helix bundle)[1247] in complex with heterotrimeric Gt has been proposed.[181] In this model, E134(3.49) and R135(3.50) of the rhodopsin's E/DRY motif interact respectively with K345 and D346 from the C-tail of Gt_α.[181] In successive studies by the same authors, the complex between "activated rhodopsin" and the C-terminal peptide from Gt_α was used as a template for modeling the agonist-induced active states of the oxytocin and vasopressin receptors.[1248,1249] In these complexes, the cytosolic cavity opened as a consequence of the outward movements of H6 was stabilized by the docking of the C-terminal peptide of the cognate G protein. These models were employed to analyze the agonist binding modes.[1248,1249]

Nikiforovich and co-workers proposed a complex between a computational model of a putative active form of rhodopsin and heterotrimeric Gt built based upon predictions of a putative interaction model between the receptor and GtCT.[1250] A number of reports by the same authors describe the prediction protocol and the analysis of the predicted rhodopsin−GtCT complex.[1250−1253] Briefly, starting configurations of GtCT in the cavity formed by the three intracellular loops and H8 of rhodopsin were adjusted by energy minimization in the multidimensional space of "global" and "local" coordinates.[1250] The packing protocol was the same as the one previously used to assemble the TM regions of rhodopsin.[252] A tentative complex between heterotrimeric Gt and the model of rhodopsin was thus built on the bases of the most reliable fit between whole Gt and GtCT in the context of the receptor, as well as of the ability to interact with two rhodopsin monomers in the semiempirical tetramer assembly.[176] Comparisons of the different existing complexes between heterotrimeric transducin and tetrameric rhodopsin highlighted divergences in $Gt_{\alpha\beta\gamma}$ rotation around the axis normal to the membrane surface, implying divergences in the interactions with the different protomers in the tetramer.[1250]

In a very recent study, we have challenged the excellent protein−protein docking program ZDOCK[1141] in predicting the architecture of possible complexes between dark rhodopsin, in its monomeric, dimeric, and tetrameric forms, and heterotrimeric Gt.[1181,1254] In this respect, a number of structural models of dark rhodopsin, differing in the cytosolic domains,[90−92,176] and a number of Gt heterotrimers, essentially differing in the conformation of the C-tails of the α- and γ-subunits, have been probed.[1181,1254] The most convincing results have been achieved by using the most highly resolved rhodopsin structure, 1U19.[92] The results of these computational experiments, based upon the accomplishment of shape and electrostatic complementarities, desolvation effects, and consistency with in vitro experiments, suggest that dark rhodopsin has the potential to recognize GDP-bound heterotrimeric Gt and that the conformation of the C-tail of Gt_α affects the orientation of the Gt, used as a probe versus the target rhodopsin.[1181] One of the most reliable rhodopsin−Gt complexes, obtained using monomeric rhodopsin as a target, is shown in Figure 26. Since the arrangements of the cytosolic domains of dark rhodopsin and of MI seem to be almost identical, on the basis of recent evidence from electron microscopy experiments,[204] simulations of rhodopsin−transducin recognition using dark rhodopsin or MI would be equivalent. The predicted complex between dark rhodopsin and heterotrimeric Gt[1181] served as an input of submicrosecond MD simulations in explicit membrane, which suggested that the dark-state fluctuations sample conformations consistent with the activated state.[1255]

Using the same computational strategies, in a successive study, we compared the structure of the photoactivated deprotonated rhodopsin intermediate (i.e., 2I37)[116] with two different structures of dark rhodopsin (i.e., 1U19[92] and 2I36[116]).[1256] Both the intrinsic and intermolecular-interaction features of dark and photoactivated deprotonated rhodopsin suggest that the two receptor forms recognize Gt in a similar way, characterized by the docking of the Gt_α C-tail in the proximity to the E/DRY motif of rhodopsin.[1256] Indeed, all the predicted complexes share a common Coulombic interaction between the arginine of the E/DRY motif and the C-terminal carboxylate of Gt_α. The differences in the G protein recognition modes by dark and photoactivated deprotonated rhodopsin intermediate correlate, at least in part, with the differences in the solvent accessibility of the cytosolic extensions of H3, H5, and H6, which are slightly more exposed in the latter. In contrast, the extension of the cytosolic crevice in the Ops* or MII states is significantly higher than in all the preceding rhodopsin states. This implies significant changes in the modes these signaling productive states recognize

dx.doi.org/10.1021/cr100437t |Chem. Rev. 2011, 111, PR438–PR535

transducin, compared to the dark state (manuscript in preparation). Indeed, docking simulations between heterotrimeric Gt and Ops* predicted an orientation of GtCT very similar to that in the 3DQB crystallographic complex (i.e., Cα-rmsd of 0.34 Å; manuscript in preparation). In the predicted complex, the GtCT portion penetrates the cytosolic crevice of Ops* much more than it does in the structure of the dark or the photoactivated deptotonated states. The overall architecture of the complexes made by dark rhodopsin and Ops* is different. Taken together, the results of docking simulations between (rhod)opsins and heterotrimeric Gt suggest that the interaction between the E/DRY arginine and the C-term of transducin would remain a common motif in the interface between transducin and any rhodopsin state. However, the interaction mode of transducin with the signaling productive states differs and is tighter compared to the dark state. This would relate, at least in part, to the slower dissociation rate of Gt from MII or Ops* compared to the dark state.[751]

Collectively, the results of our experiments suggest that MII formation follows the precoupling between dark rhodopsin and heterotrimeric transducin.[1181] Our conclusions find support in recent evidence from PWR spectroscopy[30] (see also ref 1091) and in previous evidence that proton uptake from the cytoplasm, which accompanies the transition from MI to MII, would require the presence of transducin to occur.[207] Furthermore, very recent determinations by surface plasmon resonance spectroscopy provide support to our results, by showing that ∼25% of the Gt molecules form transient complexes with rhodopsin in the dark.[751]

A worthy result is that the most reliable complex between monomeric rhodopsin and Gt is found also when dimeric or tetrameric rhodopsin is used as a target. This suggests that the receptor monomer holds the structural determinants for G protein activation, consistent with the results of in vitro experiments.[175,1254] In this respect, consistent with a number of experimental evidence,[184,1068] the complex between one rhodopsin molecule and one heterotrimeric Gt should be considered as the functional unit.[1254] Thus, assuming the reliability of the paracrystalline organization of rhodopsin in disk membranes, the role of such an ordered supramolecular assembly is still unclear (reviewed also in ref 1091). A hypothesis in this respect was inferred from mesoscopic MC simulations of stochastic encounters between activated rhodopsin and Gt in disk membranes. The study suggested that the high density of dark rhodopsin molecules and its highly ordered packing would provide a kinetic advantage for rapid photoresponses as compared with freely diffusing randomly distributed monomers.[1257] An alternative hypothesis would reconcile reliability of rhodopsin oligomerization with evidence that monomeric rhodopsin holds the molecular determinants to recognize and activate transducin.[1093] It was, indeed, shown that rhodopsin oligomerization produces fractions of immobile receptor, which would be virtually excluded from phototransduction.[1093] In this respect, oligomerization, if physiologically controlled, could be a mechanism of adaptation that would adjust photoreceptor sensitivity according to its operating conditions.[1093]

A putative activating helix switch in the rhodopsin−transducin interface was inferred from docking experiments between the GtCT from the crystallographic 3DQB complex and Ops*.[1258] Docking analysis highlighted two alternative docking poses of GtCT: a stable or S-interaction, similar to the one in the crystallographic complex, and an intermediary or I-interaction, distinguished by a tilt (42°) and rotation (90°) of the α5-helix relative to the S-interaction. When interpreted in the context of the whole Gt_α, these poses were postulated to represent putative states in receptor-catalyzed nucleotide switch. In this respect, the authors proposed a "helix switch" mechanism where the α5-helix undergoes a rotational and translational motion that destabilizes the GDP binding site ultimately leading to GDP exit.[1258]

Computational models of $G13_\alpha$ and of the TXA_2R, the latter based on the crystal structure of dark rhodopsin, served to predict a putative complex characterized by contacts between the C-term of the G protein, modeled in random conformation, and I3 of the receptor.[1259] In this complex, the G protein does not penetrate the cavity between H3 and H6 and the orientation of αN seems not compatible with the expected membrane topology, being far from the putative membrane surface.

Putative interaction modes between a computational model of heterotrimeric Gs and an inactive (i.e., the crystal structure) or active (i.e., a comparative model based upon Ops* structure) forms of the β_2AR were inferred from a systematic scan of the potential energy surfaces of the two interaction partners.[1260] The two predicted interaction models involving the "active" form of the receptor share the docking of the C-term of the α-subunit in between H3 and H6, whereas the N-term of the α-subunit docks either between H2 and H4 or between H6 and H7.[1260]

7.5. Atomistic Simulations of Receptor's Impact on the Intrinsic Dynamics of the G protein

Our computational experiments on mutation- and ligand-induced active and inactive states of a number of GPCRs converged on the finding that the opening of a solvent accessible crevice in between H3 and H6, i.e., in the neighborhoods of the E/DRY arginine, is the major structural marker of the active states (reviewed also in refs 232,233). Docking simulations (by means of ZDOCK)[1141] with heterotrimeric G proteins, consistent with the crystal structures of free and GtCT-bound Ops* and MII, suggest that such crevice recognizes the C-term of the α-subunit.[145,147,607,1261] In this context, we reported the first attempt in the literature to investigate, by molecular simulations, the impact of a GPCR, the TXA_2R, on the dynamics of the cognate G protein, $Gq_{\alpha\beta1\gamma2}$.[147] The study was essentially based on the comparative analysis of the MD trajectories of free and receptor-bound G protein.[147] Collectively, the results of this study suggest that the increase in solvent accessibility in the neighborhoods of the highly conserved E/DRY receptor motif, in response to agonist binding, is instrumental in favoring the penetration of the C-term of Gq_α in between the cytosolic ends of H3, H5, and H6. The arginine of the E/DRY motif is, thus, predicted to be an important mediator of the intramolecular and intermolecular communication involving the TXA_2R. Additional portions of Gq_α contributing to the interface were predicted to include the α4/β6 loop that recognizes the cytosolic extension of H6, as well as the α2/β4 and α3/β5 loops that recognize H8 and the C-tail of the receptor. The formation of such a composite receptor−G protein interface was suggested to be instrumental for activated receptor to induce concerted motions in selected G protein loops (i.e., the α1/β1 and β6/α5 loops), helices (i.e., α1, αF, α2, αG, and α5) as well as linkers and switches (i.e., linker 1, swI, and swII). The α5-helix of Gq_α was relevant in mediating receptor effects on the dynamics of the G protein. In fact, its motion was found to influence directly the motion of

dx.doi.org/10.1021/cr100437t |Chem. Rev. 2011, 111, PR438–PR535

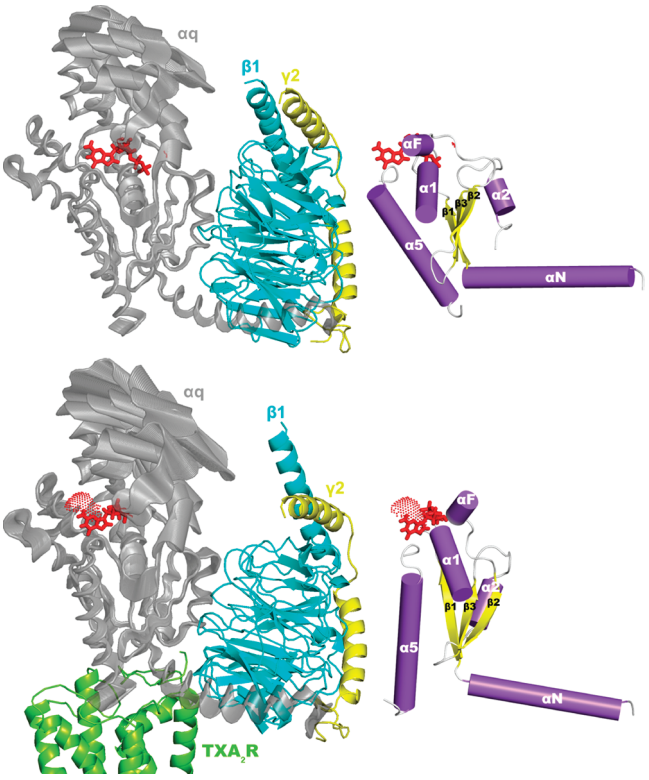

Figure 31. Effects of receptor binding on the dynamics of Gq_α. Left panel: Cα-atom displacements of Gq_α in its free (top) and receptor-bound (bottom) states along the second eigenvector from a PCA run on a concatenated trajectory made of 12000 frames.[147] A number of conformations were generated between the minimum and maximum projection on the selected eigenvector. The conformations were then displayed simultaneously. The entire heterotrimer is shown, the α-, β- and γ-subunits being, respectively gray, cyan, and yellow. The TXA_2R in the bottom-left image is yellow−green. The GDP molecule is shown as red sticks. The SAS computed on the nucleotide is shown as well as red dots. Right panel: Details of Gq_α from the structures averaged over the third and fourth ns of a 6 ns MD trajectory, concerning the receptor-free (top) and receptor-bound forms (bottom).[147] Only the β1-strand, the $\beta1/\alpha1$ loop, the α1-helix, the αF-helix, switch I, the $\beta2/\beta3$ hairpin, swII, the α2 helix, the $\beta6/\alpha5$ loop, and the α5-helix are shown. The G protein domains are colored according to secondary structure, i.e., violet and yellow, indicate, respectively, α-helices and β-strands. GDP is red. These domains have been selected as they undergo motions that correlate with the formation of a GDP exit route in response to receptor binding.

the $\beta6/\alpha5$ loop and, indirectly, i.e., via the $\beta2/\beta3$ hairpin (inter-switch), the motion of both swI and swII. The motion of the inter-switch resulted in conformational changes of the αF helix, associated with an increase in solvent accessibility of GDP (Figure 31). Other elements that were suggested to favor the solvent exposure of GDP include a concerted motion of the α-helical domain with respect to the Ras-like domain, feature intrinsic to the G protein fold, but amplified by receptor binding (Figure 31). Consistent with the C-term "latch" model of receptor-catalyzed nucleotide exchange, that model predicted a nucleotide exit route as located in between the αF-helix and $\beta6/\alpha5$ loop of Gq_α (Figure 31).[147] In spite of the extremely short length of simulations, the study suggested for the first time the displacement of the α-helical domain with respect to the Ras-like domain as one of the early events in receptor-catalyzed GDP release. We have observed a receptor-induced uncoupling of the α-helical domain from the Ras-like domain also in longer MD simulations of a predicted complex between Ops* and GDP-bound heterotrimeric Gt. These inferences from computational experiments find now support in the crystallographic complex between the β_2AR and nucleotide-free Gs heterotrimer[100] as well s in the spectroscopic measurements on the Gi activation by rhodopsin.[1231]

8. CONCLUSIONS AND PERSPECTIVES

GPCRs constitute the largest superfamily of membrane proteins known to date and regulate any aspect of cell activity by transmitting extracellular signals inside the cell (reviewed in refs 1,4−7). They have an enormous physiological and biomedical relevance, being the primary site of action of many of today's life-saving drugs and the most promising targets for those to be developed in the future (reviewed in refs 1,4−7). Therefore, it is not surprising that there are a tremendous number of reports published so far concerning in vitro, in vivo, and computational experiments on these systems, which make it very difficult to produce a comprehensive review.

The main drawbacks of computational modeling of GPCRs are the few high resolution structural data available on these proteins. The last 11 years were, however, groundbreaking in that respect as the first crystal structure of a GPCR, dark rhodopsin (released in 2000)[16] was followed by the release of six nonopsin GPCR structures in complex with functionally different ligands (starting from 2007),[93−97,99−105,111−113] of the constitutively active Ops* in 2008,[107,108] and of MII in 2011.[110] Before the release of rhodopsin structure, extremely variable computational approaches, more or less integrated with the available information from in vitro experiments, have been challenged in building 3D models of these receptors. These models proved to have high interpretative and predictive potential toward low resolution in vitro experiments. A significant example of this is a constitutively active receptor mutant designed on the basis of predictions of a computational model.[81,82,127] Along the same line, computational models of GPCRs have been successful in interpreting the results of SAR (QSAR) analyses and eventually in aiding lead optimization in those cases in which highly informative and robust ligand-based SAR could be available. Such models indeed had low potential in de novo drug design, which would require a highly resolved knowledge of the target binding site.

The need for GPCR structure prediction spurred the development of different, more or less complicated ab initio approaches, which proved successful in predicting the architecture of α-helical membrane proteins in those cases in which only low resolution 2D electron density maps are available.[13,500]

The significant advances in GPCR crystallography over the last five years and the good future perspectives in that respect (http://cmpd.scripps.edu/) offer the opportunity to improve significantly the reliability and quality of the computational models achieved by comparative modeling. Indeed, we believe that the ad hoc transfer of the stereochemical restraints from a homologous template to the target receptor is currently the most successful approach. This requires selection of the proper template by careful sequence comparisons, which is a crucial step in comparative modeling. Selection of the proper template is

trivial if the target is a close homologue of one of the available templates, which at the moment is the case of selected members of only four GPCR subfamilies. Thus, since sequence identity between the available targets and the homologous GPCRs is collectively low and, in most cases, extra restraints need to be introduced and/or ab initio modeling has to be integrated with comparative modeling. This situation urges the need to develop effective strategies that mix comparative modeling of the portions that align well with the template with ab initio modeling of sequence-divergent portions. For sure, a significant aid to structure prediction protocols will derive from an amplification of the spectrum of crystal structures, possibly covering the principal subfamilies.

The best structure achieved by comparative modeling cannot be used as it is, but rather it must be considered as the starting point of further calculations aimed at improving the reliability of the computational model. These conclusions, which are based upon critical comparisons between rhodopsin and each member of family A, discourage automatic high throughput modeling of GPCRs based upon the rhodopsin structure and discourage the use of high throughput modeled GPCRs as targets of high throughput screening of libraries of compounds. In fact, in the majority of the virtual screening experiments based on GPCR models, the receptor model was first primed with a representative ligand[251,556,646,1005] or built by adding external restraints concerning information on ligand binding.[672,824] Along this line, the latest "GPCR Dock 2010" assessment indicated that fully automatic solutions for docking to modeled GPCRs remain out of reach.[566] In summary, improving the effectiveness of comparative modeling is imperative for structure-based drug design (see also refs 554,628,705).

GPCRs are allosteric proteins which exist as complex statistical conformation ensembles.[719,739,1262] They hold regions at high stability (i.e., low flexibility) and regions at low stability (i.e., high flexibility) that communicate with each other, even if distal. The functional properties of a GPCR are related to the distribution of states within the native ensemble.[719,739] Such a distribution is differently affected by ligands and/or interacting proteins and/or amino acid mutations.[719,739] Of course, the different oligomeric states of a GPCR contribute to differentiating the distribution of the receptor states.

The challenge of future computational modeling approaches is to provide a stochastic description of the GPCR systems and to predict, with atomic detail, the mechanisms by which structural information is transferred from the extracellular site to the intracellular site of the same receptor molecule or within a molecular network of receptors or within a multicomponent signaling unit. This would require an extensive integration between different molecular simulation methods and a careful weighing of approximations. In this respect, we think that continuous electrostatic models of the protein environment should be supported over explicit representation of lipids and water, to allow effective simulations of multiprotein assemblies. Explicit membrane/water representation does not necessarily improve the reliability of the system, as the lipid composition of a biological membrane is quite variable and the lipid-receptor stoichiometry is ill-defined, due also to indeterminations in the oligomeric states of the receptor. Promising approaches in the desired direction to reducing the system's degrees of freedom and gaining insights into long time scale processes include the employment of CG molecular mechanics force fields.[292−294]

GPCRs are very complex integrated chemical information systems that can be described and represented by chemical−structural formalisms. Quantitative molecular descriptors can be computed on average structural representatives of relevant conformational ensembles rather than on a single structure. This approach is expected to increase the information content of the selected molecular descriptors and overcome, at least in part, the inadequacy of the static single structure description.

The huge complexity of the GPCR-mediated signaling would benefit from system biology-based modeling[748−751] better if integrated with molecular structure/dynamics information. A possible way to bridge the gap between molecular and systems biology and adequately describe the relevant macromolecular signaling machineries involving GPCRs would be to combine high-content miniaturized experimental platforms with computational approaches.[1263] In this respect, a bottom-up approach using multicolor single-molecule detection fluorescence experiments in biochemically defined systems complemented by MD models of macromolecular complexes would be an attractive perspective.

The future of computational modeling of GPCRs relies in protein−protein and ligand−protein docking as well as in effective and exhaustive molecular simulation approaches aimed at predicting the probability distribution of the conformational ensembles of supramolecular assemblies. Moreover, the collective organizing principles of GPCRs appropriate to the mesoscopic scale domain will probably be the next formidable challenge for theoretical and computational modeling approaches aimed at describing the mesoscopic principles of GPCR-mediated signal transduction. These mesoscopic principles formally derive from atomistic/molecular rules but are, at the same time, independent of them.[1264]

AUTHOR INFORMATION

Corresponding Author

*Phone: 059 205 5114. Fax: 059 373 543. E-mail: fanelli@unimo.it.

BIOGRAPHIES

Francesca Fanelli graduated in Medicinal Chemistry (1989) and received her Ph.D. education in Computational Biophysical Chemistry (1994). She is now an Associate Scientist of the Dulbecco Telethon Institute and an Associate Professor of Molecular Modeling & Engineering at the University of Modena and Reggio Emilia. Her research since 1991 has been almost entirely devoted to developing computational protocols and molecular models to unravel the chemical communication mechanisms involving G protein-coupled receptors.

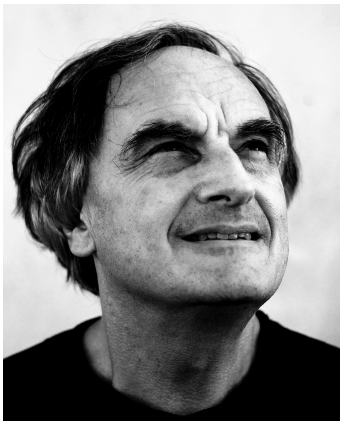

Pier G. De Benedetti is Professor of Biophysical Chemistry at Modena and Reggio Emilia University, where he received his education in Chemistry. His research is mainly devoted to modeling the structure−property and structure−function relationships in complex molecular (bio)systems. He loves the wind and the sea.

9. ACKNOWLEDGMENT

We thank Susanna Cotecchia and Tommaso Costa for valuable discussion. We are very grateful to Ongun Onaran for the valuable hints about the thermodynamic models and for providing us with effective schematizations of such models (i.e., shown in Figure 20). We thank Chris Reynolds for giving us the coordinates of their computational models of inactive and active rhodopsin, shown in Figure 10. We are also grateful to Slawomir Filipek for sending us the coordinates of the complex between tetrameric rhodopsin and heterotrimeric transducin, shown in Figure 26. We apologize to the investigators whose contributions have been unintentionally neglected in this review. This study was supported by Telethon-Italy grant no. TCP00068 (to F.F.). Drawings were done by means of the software PYMOL 1.1r1 (http://pymol.sourceforge.net/).

REFERENCES

(1) Pierce, K. L.; Premont, R. T.; Lefkowitz, R. J. *Nature Rev. Mol. Cell Biol.* **2002**, *3*, 639.
(2) Brady, A. E.; Limbird, L. E. *Cell Signalling* **2002**, *14*, 297.
(3) Zhang, M.; Wang, W. *Acc. Chem. Res.* **2003**, *36*, 530.
(4) Bockaert, J.; Pin, J. P. *EMBO J.* **1999**, *18*, 1723.
(5) Gether, U. *Endocr. Rev.* **2000**, *21*, 90.
(6) Lefkowitz, R. J. *Nature Cell Biol.* **2000**, *2*, E133.
(7) Kristiansen, K. *Pharmacol. Ther.* **2004**, *103*, 21.
(8) Dorsam, R. T.; Gutkind, J. S. *Nature Rev. Cancer* **2007**, *7*, 79.
(9) Lappano, R.; Maggiolini, M. *Nature Rev. Drug Discovery* **2011**, *10*, 47.
(10) Thathiah, A.; De Strooper, B. *Nature Rev. Neurosci.* **2011**, *12*, 73.
(11) Tyndall, J. D.; Pfeiffer, B.; Abbenante, G.; Fairlie, D. P. *Chem. Rev.* **2005**, *105*, 793.
(12) Schertler, G. F.; Villa, C.; Henderson, R. *Nature* **1993**, *362*, 770.
(13) Baldwin, J. M. *EMBO J.* **1993**, *12*, 1693.
(14) Baldwin, J. M.; Schertler, G. F.; Unger, V. M. *J. Mol. Biol.* **1997**, *272*, 144.
(15) Unger, V. M.; Hargrave, P. A.; Baldwin, J. M.; Schertler, G. F. *Nature* **1997**, *389*, 203.
(16) Palczewski, K.; Kumasaka, T.; Hori, T.; Behnke, C. A.; Motoshima, H.; Fox, B. A.; Le Trong, I.; Teller, D. C.; Okada, T.; Stenkamp, R. E.; Yamamoto, M.; Miyano, M. *Science* **2000**, *289*, 739.
(17) Kunishima, N.; Shimada, Y.; Tsuji, Y.; Sato, T.; Yamamoto, M.; Kumasaka, T.; Nakanishi, S.; Jingami, H.; Morikawa, K. *Nature* **2000**, *407*, 971.
(18) Fan, Q. R.; Hendrickson, W. A. *Nature* **2005**, *433*, 269.
(19) Parthier, C.; Reedtz-Runge, S.; Rudolph, R.; Stubbs, M. T. *Trends Biochem. Sci.* **2009**, *34*, 303.
(20) Foord, S. M. *Curr. Opin. Pharmacol.* **2002**, *2*, 561.
(21) Fredriksson, R.; Lagerstrom, M. C.; Lundin, L. G.; Schioth, H. B. *Mol. Pharmacol.* **2003**, *63*, 1256.
(22) Fredriksson, R.; Schioth, H. B. *Mol. Pharmacol.* **2005**, *67*, 1414.
(23) Kolakowski, L. F., Jr. *Receptors Channels* **1994**, *2*, 1.
(24) Eilers, M.; Hornak, V.; Smith, S. O.; Konopka, J. B. *Biochemistry* **2005**, *44*, 8959.
(25) Gilman, A. G. *Annu. Rev. Biochem.* **1987**, *56*, 615.
(26) Bourne, H. R.; Sanders, D. A.; McCormick, F. *Nature* **1991**, *349*, 117.
(27) Oldham, W. M.; Hamm, H. E. *Q. Rev. Biophys.* **2006**, *39*, 117.
(28) Bosier, B.; Hermans, E. *Trends Pharmacol. Sci.* **2007**, *28*, 438.
(29) Alves, I. D.; Salamon, Z.; Varga, E.; Yamamura, H. I.; Tollin, G.; Hruby, V. J. *J. Biol. Chem.* **2003**, *278*, 48890.
(30) Alves, I. D.; Salgado, G. F.; Salamon, Z.; Brown, M. F.; Tollin, G.; Hruby, V. J. *Biophys. J.* **2005**, *88*, 198.
(31) Nobles, M.; Benians, A.; Tinker, A. *Proc. Natl. Acad. Sci. U.S.A.* **2005**, *102*, 18706.
(32) Gales, C.; Van Durm, J. J.; Schaak, S.; Pontier, S.; Percherancier, Y.; Audet, M.; Paris, H.; Bouvier, M. *Nature Struct. Mol. Biol.* **2006**, *13*, 778.
(33) Philip, F.; Sengupta, P.; Scarlata, S. *J. Biol. Chem* . **2007**, *282*, 19203.
(34) Hu, J.; Wang, Y.; Zhang, X.; Lloyd, J. R.; Li, J. H.; Karpiak, J.; Costanzi, S.; Wess, J. *Nature Chem. Biol.* **2010**, *6*, 541.
(35) Marinissen, M. J.; Gutkind, J. S. *Trends Pharmacol. Sci.* **2001**, *22*, 368.
(36) Brzostowski, J. A.; Kimmel, A. R. *Trends Biochem. Sci.* **2001**, *26*, 291.
(37) Luttrell, L. M.; Roudabush, F. L.; Choy, E. W.; Miller, W. E.; Field, M. E.; Pierce, K. L.; Lefkowitz, R. J. *Proc. Natl. Acad. Sci. U.S.A.* **2001**, *98*, 2449.
(38) Hall, R. A.; Lefkowitz, R. J. *Circ. Res.* **2002**, *91*, 672.
(39) Bockaert, J.; Perroy, J.; Becamel, C.; Marin, P.; Fagni, L. *Annu. Rev. Pharmacol. Toxicol.* **2010**, *50*, 89.
(40) Ritter, S. L.; Hall, R. A. *Nature Rev. Mol. Cell Biol.* **2009**, *10*, 819.
(41) Arvanitakis, L.; Geras-Raaka, E.; Gershengorn, M. C. *Trends Endocrinol. Metab.* **1998**, *9*, 27.
(42) Krupnick, J. G.; Benovic, J. L. *Annu. Rev. Pharmacol. Toxicol.* **1998**, *38*, 289.
(43) Breton, B.; Lagace, M.; Bouvier, M. *FASEB J.* **2010**, *24*, 4733.
(44) Calebiro, D.; Nikolaev, V. O.; Persani, L.; Lohse, M. J. *Trends Pharmacol. Sci* . **2010**, *31*, 221.
(45) Bouvier, M. *Nature Rev. Neurosci.* **2001**, *2*, 274.
(46) Milligan, G. *J. Cell. Sci.* **2001**, *114*, 1265.
(47) Rios, C. D.; Jordan, B. A.; Gomes, I.; Devi, L. A. *Pharmacol. Ther.* **2001**, *92*, 71.
(48) George, S. R.; O'Dowd, B. F.; Lee, S. P. *Nature Rev. Drug Discovery* **2002**, *1*, 808.
(49) Agnati, L. F.; Ferre, S.; Lluis, C.; Franco, R.; Fuxe, K. *Pharmacol. Rev.* **2003**, *55*, 509.
(50) Franco, R.; Canals, M.; Marcellino, D.; Ferre, S.; Agnati, L.; Mallol, J.; Casado, V.; Ciruela, F.; Fuxe, K.; Lluis, C.; Canela, E. I. *Trends Biochem. Sci.* **2003**, *28*, 238.
(51) Kroeger, K. M.; Pfleger, K. D.; Eidne, K. A. *Front. Neuroendocrinol.* **2003**, *24*, 254.
(52) Terrillon, S.; Bouvier, M. *EMBO Rep.* **2004**, *5*, 30.
(53) Park, P. S.; Filipek, S.; Wells, J. W.; Palczewski, K. *Biochemistry* **2004**, *43*, 15643.

(54) Maggio, R.; Novi, F.; Scarselli, M.; Corsini, G. U. *FEBS J.* **2005**, *272*, 2939.
(55) Bulenger, S.; Marullo, S.; Bouvier, M. *Trends Pharmacol. Sci.* **2005**, *26*, 131.
(56) Milligan, G. *Br. J. Pharmacol.* **2009**, *158*, 5.
(57) Albizu, L.; Cottet, M.; Kralikova, M.; Stoev, S.; Seyer, R.; Brabet, I.; Roux, T.; Bazin, H.; Bourrier, E.; Lamarque, L.; Breton, C.; Rives, M. L.; Newman, A.; Javitch, J.; Trinquet, E.; Manning, M.; Pin, J. P.; Mouillac, B.; Durroux, T. *Nature Chem. Biol.* **2010**, *6*, 587.
(58) Ferre, S.; Franco, R. *Curr. Opin. Pharmacol.* **2010**, *10*, 1.
(59) Lohse, M. J. *Curr. Opin. Pharmacol.* **2010**, *10*, 53.
(60) Milligan, G. *Curr. Opin. Pharmacol.* **2010**, *10*, 23.
(61) Palczewski, K. *Trends Biochem. Sci.* **2010**, *35*, 595.
(62) Reddy, P. S.; Corley, R. B. *Bioessays* **1998**, *20*, 546.
(63) Fotiadis, D.; Liang, Y.; Filipek, S.; Saperstein, D. A.; Engel, A.; Palczewski, K. *Nature* **2003**, *421*, 127.
(64) Gurevich, V. V.; Gurevich, E. V. *Trends Pharmacol. Sci.* **2008**, *29*, 234.
(65) Han, Y.; Moreira, I. S.; Urizar, E.; Weinstein, H.; Javitch, J. A. *Nature Chem. Biol.* **2009**, *5*, 688.
(66) Rovira, X.; Pin, J. P.; Giraldo, J. *Trends Pharmacol. Sci.* **2010**, *31*, 15.
(67) Milligan, G. *Drug Discovery Today* **2006**, *11*, 541.
(68) Dalrymple, M. B.; Pfleger, K. D.; Eidne, K. A. *Pharmacol. Ther.* **2008**, *118*, 359.
(69) Panetta, R.; Greenwood, M. T. *Drug Discovery Today.* **2008**, *13*, 1059.
(70) Wang, J.; Norcross, M. *Drug Discovery Today* **2008**, *13*, 625.
(71) Casado, V.; Cortes, A.; Mallol, J.; Perez-Capote, K.; Ferre, S.; Lluis, C.; Franco, R.; Canela, E. I. *Pharmacol. Ther.* **2009**, *124*, 248.
(72) Albizu, L.; Moreno, J. L.; Gonzalez-Maeso, J.; Sealfon, S. C. *CNS Neurol. Disord. Drug Targets* **2010**, *9*, 636.
(73) Maggio, R.; Millan, M. J. *Curr. Opin. Pharmacol.* **2010**, *10*, 100.
(74) Marshall, F. H.; Foord, S. M. *Adv. Pharmacol.* **2010**, *58*, 63.
(75) Rozenfeld, R.; Devi, L. A. *Trends Pharmacol. Sci.* **2010**, *31*, 124.
(76) Rozenfeld, R.; Gupta, A.; Gagnidze, K.; Lim, M. P.; Gomes, I.; Lee-Ramos, D.; Nieto, N.; Devi, L. A. *EMBO J.* **2011**, *30*, 2350.
(77) Gonzalez-Maeso, J.; Ang, R. L.; Yuen, T.; Chan, P.; Weisstaub, N. V.; Lopez-Gimenez, J. F.; Zhou, M.; Okawa, Y.; Callado, L. F.; Milligan, G.; Gingrich, J. A.; Filizola, M.; Meana, J. J.; Sealfon, S. C. *Nature* **2008**, *452*, 93.
(78) Joiner, M. L.; Lise, M. F.; Yuen, E. Y.; Kam, A. Y.; Zhang, M.; Hall, D. D.; Malik, Z. A.; Qian, H.; Chen, Y.; Ulrich, J. D.; Burette, A. C.; Weinberg, R. J.; Law, P. Y.; El-Husseini, A.; Yan, Z.; Hell, J. W. *EMBO J.* **2010**, *29*, 482.
(79) Lefkowitz, R. J.; Cotecchia, S.; Samama, P.; Costa, T. *Trends Pharmacol. Sci.* **1993**, *14*, 303.
(80) Costa, T.; Cotecchia, S. *Trends Pharmacol. Sci.* **2005**, *26*, 618.
(81) Cotecchia, S.; Fanelli, F.; Scheer, A.; De Benedetti, P. G. In *Structure/Function Analysis of GPCRs*; Wess, J., Ed.; Wiley-Liss: New York, 1999; pp 167−183.
(82) Cotecchia, S.; Fanelli, F.; Scheer, A.; Costa, T. In *G Protein-Coupled Receptors as Drug Targets. Analysis of Activation and Constitutive Activity*; Seifert, R., Wieland, T., Eds., WILEY-VCH: Weinheim, 2005; pp 159−176.
(83) Chalmers, D. T.; Behan, D. P. *Nature Rev. Drug Discovery* **2002**, *1*, 599.
(84) Shenker, A. *Baillieres Clin. Endocrinol. Metab.* **1995**, *9*, 427.
(85) Themmen, A. P.; Martens, J. W.; Brunner, H. G. *Mol. Cell. Endocrinol.* **1998**, *145*, 137.
(86) Tao, Y. X. *Pharmacol. Ther.* **2008**, *120*, 129.
(87) Mendes, H. F.; van der Spuy, J.; Chapple, J. P.; Cheetham, M. E. *Trends. Mol. Med.* **2005**, *11*, 177.
(88) Vassart, G.; Costagliola, S. *Nature Rev. Endocrinol.* **2011**, *7*, 362.
(89) Teller, D. C.; Okada, T.; Behnke, C. A.; Palczewski, K.; Stenkamp, R. E. *Biochemistry* **2001**, *40*, 7761.
(90) Okada, T.; Fujiyoshi, Y.; Silow, M.; Navarro, J.; Landau, E. M.; Shichida, Y. *Proc. Natl. Acad. Sci. U.S.A.* **2002**, *99*, 5982.
(91) Li, J.; Edwards, P. C.; Burghammer, M.; Villa, C.; Schertler, G. F. *J. Mol. Biol.* **2004**, *343*, 1409.
(92) Okada, T.; Sugihara, M.; Bondar, A. N.; Elstner, M.; Entel, P.; Buss, V. *J. Mol. Biol.* **2004**, *342*, 571.
(93) Rasmussen, S. G.; Choi, H. J.; Rosenbaum, D. M.; Kobilka, T. S.; Thian, F. S.; Edwards, P. C.; Burghammer, M.; Ratnala, V. R.; Sanishvili, R.; Fischetti, R. F.; Schertler, G. F.; Weis, W. I.; Kobilka, B. K. *Nature* **2007**, *450*, 383.
(94) Cherezov, V.; Rosenbaum, D. M.; Hanson, M. A.; Rasmussen, S. G.; Thian, F. S.; Kobilka, T. S.; Choi, H. J.; Kuhn, P.; Weis, W. I.; Kobilka, B. K.; Stevens, R. C. *Science* **2007**, *318*, 1258.
(95) Warne, T.; Serrano-Vega, M. J.; Baker, J. G.; Moukhametzianov, R.; Edwards, P. C.; Henderson, R.; Leslie, A. G.; Tate, C. G.; Schertler, G. F. *Nature* **2008**, *454*, 486.
(96) Hanson, M. A.; Cherezov, V.; Griffith, M. T.; Roth, C. B.; Jaakola, V. P.; Chien, E. Y.; Velasquez, J.; Kuhn, P.; Stevens, R. C. *Structure* **2008**, *16*, 897.
(97) Wacker, D.; Fenalti, G.; Brown, M. A.; Katritch, V.; Abagyan, R.; Cherezov, V.; Stevens, R. C. *J. Am. Chem. Soc.* **2010**, *132*, 11443.
(98) Moukhametzianov, R.; Warne, T.; Edwards, P. C.; Serrano-Vega, M. J.; Leslie, A. G.; Tate, C. G.; Schertler, G. F. *Proc. Natl. Acad. Sci. U.S.A.* **2011**, *108*, 8228.
(99) Rasmussen, S. G.; Choi, H. J.; Fung, J. J.; Pardon, E.; Casarosa, P.; Chae, P. S.; Devree, B. T.; Rosenbaum, D. M.; Thian, F. S.; Kobilka, T. S.; Schnapp, A.; Konetzki, I.; Sunahara, R. K.; Gellman, S. H.; Pautsch, A.; Steyaert, J.; Weis, W. I.; Kobilka, B. K. *Nature* **2011**, *469*, 175.
(100) Rasmussen, S. G.; Devree, B. T.; Zou, Y.; Kruse, A. C.; Chung, K. Y.; Kobilka, T. S.; Thian, F. S.; Chae, P. S.; Pardon, E.; Calinski, D.; Mathiesen, J. M.; Shah, S. T.; Lyons, J. A.; Caffrey, M.; Gellman, S. H.; Steyaert, J.; Skiniotis, G.; Weis, W. I.; Sunahara, R. K.; Kobilka, B. K. *Nature* **2011**, *477*, 549.
(101) Rosenbaum, D. M.; Zhang, C.; Lyons, J. A.; Holl, R.; Aragao, D.; Arlow, D. H.; Rasmussen, S. G.; Choi, H. J.; Devree, B. T.; Sunahara, R. K.; Chae, P. S.; Gellman, S. H.; Dror, R. O.; Shaw, D. E.; Weis, W. I.; Caffrey, M.; Gmeiner, P.; Kobilka, B. K. *Nature* **2011**, *469*, 236.
(102) Warne, T.; Moukhametzianov, R.; Baker, J. G.; Nehme, R.; Edwards, P. C.; Leslie, A. G.; Schertler, G. F.; Tate, C. G. *Nature* **2011**, *469*, 241.
(103) Jaakola, V. P.; Griffith, M. T.; Hanson, M. A.; Cherezov, V.; Chien, E. Y.; Lane, J. R.; Ijzerman, A. P.; Stevens, R. C. *Science* **2008**, *322*, 1211.
(104) Lebon, G.; Warne, T.; Edwards, P. C.; Bennett, K.; Langmead, C. J.; Leslie, A. G.; Tate, C. G. *Nature* **2011**, *474*, 521.
(105) Xu, F.; Wu, H.; Katritch, V.; Han, G. W.; Jacobson, K. A.; Gao, Z. G.; Cherezov, V.; Stevens, R. C. *Science* **2011**, *332*, 322.
(106) Murakami, M.; Kouyama, T. *Nature* **2008**, *453*, 363.
(107) Park, J. H.; Scheerer, P.; Hofmann, K. P.; Choe, H. W.; Ernst, O. P. *Nature* **2008**, *454*, 183.
(108) Scheerer, P.; Park, J. H.; Hildebrand, P. W.; Kim, Y. J.; Krauss, N.; Choe, H. W.; Hofmann, K. P.; Ernst, O. P. *Nature* **2008**, *455*, 497.
(109) Standfuss, J.; Edwards, P. C.; D'Antona, A.; Fransen, M.; Xie, G.; Oprian, D. D.; Schertler, G. F. *Nature* **2011**, *471*, 656.
(110) Choe, H. W.; Kim, Y. J.; Park, J. H.; Morizumi, T.; Pai, E. F.; Krauss, N.; Hofmann, K. P.; Scheerer, P.; Ernst, O. P. *Nature* **2011**, *471*, 651.
(111) Wu, B.; Chien, E. Y.; Mol, C. D.; Fenalti, G.; Liu, W.; Katritch, V.; Abagyan, R.; Brooun, A.; Wells, P.; Bi, F. C.; Hamel, D. J.; Kuhn, P.; Handel, T. M.; Cherezov, V.; Stevens, R. C. *Science* **2010**, *330*, 1066.
(112) Chien, E. Y.; Liu, W.; Zhao, Q.; Katritch, V.; Han, G. W.; Hanson, M. A.; Shi, L.; Newman, A. H.; Javitch, J. A.; Cherezov, V.; Stevens, R. C. *Science* **2010**, *330*, 1091.
(113) Shimamura, T.; Shiroishi, M.; Weyand, S.; Tsujimoto, H.; Winter, G.; Katritch, V.; Abagyan, R.; Cherezov, V.; Liu, W.; Han, G. W.; Kobayashi, T.; Stevens, R. C.; Iwata, S. *Nature* **2011**, *475*, 65.
(114) Nakamichi, H.; Okada, T. *Proc. Natl. Acad. Sci. U.S.A.* **2006**, *103*, 12729.
(115) Nakamichi, H.; Okada, T. *Angew. Chem., Int. Ed. Engl.* **2006**, *45*, 4270.
(116) Salom, D.; Lodowski, D. T.; Stenkamp, R. E.; Le Trong, I.; Golczak, M.; Jastrzebska, B.; Harris, T.; Ballesteros, J. A.; Palczewski, K. *Proc. Natl. Acad. Sci. U.S.A.* **2006**, *103*, 16123.

(117) Standfuss, J.; Xie, G.; Edwards, P. C.; Burghammer, M.; Oprian, D. D.; Schertler, G. F. *J. Mol. Biol.* **2007**, *372*, 1179.
(118) Nakamichi, H.; Okada, T. *Photochem. Photobiol.* **2007**, *83*, 232.
(119) Shimamura, T.; Hiraki, K.; Takahashi, N.; Hori, T.; Ago, H.; Masuda, K.; Takio, K.; Ishiguro, M.; Miyano, M. *J. Biol. Chem.* **2008**, *283*, 17753.
(120) Stenkamp, R. E. *Acta Crystallogr., Sect. D: Biol. Crystallogr.* **2008**, *D64*, 902.
(121) Wensel, T. G. *Vision Res.* **2008**, *48*, 2052.
(122) Palczewski, K. *Annu. Rev. Biochem.* **2006**, *75*, 743.
(123) Matsuyama, T.; Yamashita, T.; Imai, H.; Shichida, Y. *J. Biol. Chem.* **2010**, *285*, 8114.
(124) Nakamichi, H.; Buss, V.; Okada, T. *Biophys. J.* **2007**, *92*, L106.
(125) Ballesteros, J. A.; Weinstein, H. *Methods. Neurosci.* **1995**, *25*, 366.
(126) Cohen, G. B.; Yang, T.; Robinson, P. R.; Oprian, D. D. *Biochemistry* **1993**, *32*, 6111.
(127) Scheer, A.; Fanelli, F.; Costa, T.; De Benedetti, P. G.; Cotecchia, S. *EMBO J.* **1996**, *15*, 3566.
(128) Scheer, A.; Fanelli, F.; Costa, T.; De Benedetti, P. G.; Cotecchia, S. *Proc. Natl. Acad. Sci. U.S.A.* **1997**, *94*, 808.
(129) Ballesteros, J.; Kitanovic, S.; Guarnieri, F.; Davies, P.; Fromme, B. J.; Konvicka, K.; Chi, L.; Millar, R. P.; Davidson, J. S.; Weinstein, H.; Sealfon, S. C. *J. Biol. Chem.* **1998**, *273*, 10445.
(130) Fanelli, F.; Barbier, P.; Zanchetta, D.; De Benedetti, P. G.; Chini, B. *Mol. Pharmacol.* **1999**, *56*, 214.
(131) Ballesteros, J. A.; Jensen, A. D.; Liapakis, G.; Rasmussen, S. G.; Shi, L.; Gether, U.; Javitch, J. A. *J. Biol. Chem.* **2001**, *276*, 29171.
(132) Greasley, P. J.; Fanelli, F.; Scheer, A.; Abuin, L.; Nenniger-Tosato, M.; DeBenedetti, P. G.; Cotecchia, S. *J. Biol. Chem.* **2001**, *276*, 46485.
(133) Li, J.; Huang, P.; Chen, C.; de Riel, J. K.; Weinstein, H.; Liu-Chen, L. Y. *Biochemistry* **2001**, *40*, 12039.
(134) Greasley, P. J.; Fanelli, F.; Rossier, O.; Abuin, L.; Cotecchia, S. *Mol. Pharmacol.* **2002**, *61*, 1025.
(135) Angelova, K.; Fanelli, F.; Puett, D. *J. Biol. Chem.* **2002**, *277*, 32202.
(136) Visiers, I.; Ebersole, B.; Dracheva, S.; Ballesteros, J.; Sealfon, S. C.; Weinstein, H. *Int. J. Quantum Chem.* **2002**, *88*, 65.
(137) Shapiro, D. A.; Kristiansen, K.; Weiner, D. M.; Kroeze, W. K.; Roth, B. L. *J. Biol. Chem.* **2002**, *277*, 11441.
(138) Seeber, M.; De Benedetti, P. G.; Fanelli, F. *J. Chem. Inf. Comput. Sci.* **2003**, *43*, 1520.
(139) Fanelli, F.; Verhoef-Post, M.; Timmerman, M.; Zeilemaker, A.; Martens, J. W.; Themmen, A. P. *Mol. Endocrinol.* **2004**, *18*, 1499.
(140) Vassart, G.; Pardo, L.; Costagliola, S. *Trends Biochem. Sci.* **2004**, *29*, 119.
(141) Favre, N.; Fanelli, F.; Missotten, M.; Nichols, A.; Wilson, J.; Di Tiani, M.; Rommel, C.; Scheer, A. *Biochemistry* **2005**, *44*, 9990.
(142) Zhang, M.; Mizrachi, D.; Fanelli, F.; Segaloff, D. L. *J. Biol. Chem.* **2005**, *280*, 26169.
(143) Flanagan, C. A. *Mol. Pharmacol.* **2005**, *68*, 1.
(144) Rosenkilde, M. M.; Kledal, T. N.; Schwartz, T. W. *Mol. Pharmacol.* **2005**, *68*, 11.
(145) Angelova, K.; Fanelli, F.; Puett, D. *Mol. Endocrinol.* **2008**, *22*, 126.
(146) Feng, X.; Muller, T.; Mizrachi, D.; Fanelli, F.; Segaloff, D. L. *Endocrinology* **2008**, *149*, 1705.
(147) Raimondi, F.; Seeber, M.; De Benedetti, P. G.; Fanelli, F. *J. Am. Chem. Soc.* **2008**, *130*, 4310.
(148) Zhang, M.; Tao, Y. X.; Ryan, G. L.; Feng, X.; Fanelli, F.; Segaloff, D. L. *J. Biol. Chem.* **2007**, *282*, 25527.
(149) Yao, X.; Parnot, C.; Deupi, X.; Ratnala, V. R.; Swaminath, G.; Farrens, D.; Kobilka, B. *Nature Chem. Biol.* **2006**, *2*, 417.
(150) Mirzadegan, T.; Benko, G.; Filipek, S.; Palczewski, K. *Biochemistry* **2003**, *42*, 2759.
(151) Fritze, O.; Filipek, S.; Kuksa, V.; Palczewski, K.; Hofmann, K. P.; Ernst, O. P. *Proc. Natl. Acad. Sci. U.S.A.* **2003**, *100*, 2290.
(152) Jacobs, D. J.; Rader, A. J.; Kuhn, L. A.; Thorpe, M. F. *Proteins* **2001**, *44*, 150.
(153) Bahar, I.; Atilgan, A. R.; Erman, B. *Fold. Des.* **1997**, *2*, 173.
(154) Rader, A. J.; Anderson, G.; Isin, B.; Khorana, H. G.; Bahar, I.; Klein-Seetharaman, J. *Proc. Natl. Acad. Sci. U.S.A.* **2004**, *101*, 7246.
(155) Klco, J. M.; Wiegand, C. B.; Narzinski, K.; Baranski, T. J. *Nature Struct. Mol. Biol.* **2005**, *12*, 320.
(156) Massotte, D.; Kieffer, B. L. *Nature. Struct. Mol. Biol.* **2005**, *12*, 287.
(157) Findlay, J. B.; Pappin, D. J. *Biochem. J.* **1986**, *238*, 625.
(158) Gouldson, P. R.; Snell, C. R.; Reynolds, C. A. *J. Med. Chem.* **1997**, *40*, 3871.
(159) Konvicka, K.; Guarnieri, F.; Ballesteros, J. A.; Weinstein, H. *Biophys. J.* **1998**, *75*, 601.
(160) Angel, T. E.; Gupta, S.; Jastrzebska, B.; Palczewski, K.; Chance, M. R. *Proc. Natl. Acad. Sci. U.S.A.* **2009**, *106*, 14367.
(161) Grossfield, A.; Pitman, M. C.; Feller, S. E.; Soubias, O.; Gawrisch, K. *J. Mol. Biol.* **2008**, *381*, 478.
(162) Pardo, L.; Deupi, X.; Dolker, N.; Lopez-Rodriguez, M. L.; Campillo, M. *ChemBioChem* **2007**, *8*, 19.
(163) Angel, T. E.; Chance, M. R.; Palczewski, K. *Proc. Natl. Acad. Sci. U.S.A.* **2009**, *106*, 8555.
(164) Nygaard, R.; Valentin-Hansen, L.; Mokrosinski, J.; Frimurer, T. M.; Schwartz, T. W. *J. Biol. Chem.* **2010**, *285*, 19625.
(165) Sekharan, S.; Altun, A.; Morokuma, K. *Chemistry* **2010**, *16*, 1744.
(166) Sekharan, S.; Morokuma, K. *J. Am. Chem. Soc.* **2011**, *133*, 4734.
(167) Sugihara, M.; Fujibuchi, W.; Suwa, M. *J. Phys. Chem. B* **2011**, *115*, 6172.
(168) Fotiadis, D.; Jastrzebska, B.; Philippsen, A.; Muller, D. J.; Palczewski, K.; Engel, A. *Curr. Opin. Struct. Biol.* **2006**, *16*, 252.
(169) Chabre, M.; Cone, R.; Saibil, H. *Nature* **2003**, *426*, 30.
(170) Fotiadis, D.; Liang, Y.; Filipek, S.; Saperstein, D. A.; Engel, A.; Palczewski, K. *FEBS Lett.* **2004**, *564*, 281.
(171) Jastrzebska, B.; Maeda, T.; Zhu, L.; Fotiadis, D.; Filipek, S.; Engel, A.; Stenkamp, R. E.; Palczewski, K. *J. Biol. Chem.* **2004**, *279*, 54663.
(172) Suda, K.; Filipek, S.; Palczewski, K.; Engel, A.; Fotiadis, D. *Mol. Membr. Biol.* **2004**, *21*, 435.
(173) Jastrzebska, B.; Fotiadis, D.; Jang, G. F.; Stenkamp, R. E.; Engel, A.; Palczewski, K. *J. Biol. Chem.* **2006**, *281*, 11917.
(174) Chabre, M.; Deterre, P.; Antonny, B. *Trends Pharmacol. Sci.* **2009**, *30*, 182.
(175) Chabre, M.; le Maire, M. *Biochemistry* **2005**, *44*, 9395.
(176) Liang, Y.; Fotiadis, D.; Filipek, S.; Saperstein, D. A.; Palczewski, K.; Engel, A. *J. Biol. Chem.* **2003**, *278*, 21655.
(177) Sali, A.; Blundell, T. L. *J. Mol. Biol.* **1993**, *234*, 779.
(178) Okada, T. *Biochem. Soc. Trans.* **2004**, *32*, 738.
(179) Filipek, S. *J. Mol. Model.* **2005**, *11*, 385.
(180) Kota, P.; Reeves, P. J.; Rajbhandary, U. L.; Khorana, H. G. *Proc. Natl. Acad. Sci. U.S.A.* **2006**, *103*, 3054.
(181) Ciarkowski, J.; Witt, M.; Slusarz, R. *J. Mol. Model.* **2005**, *11*, 407.
(182) Lodowski, D. T.; Salom, D.; Le Trong, I.; Teller, D. C.; Ballesteros, J. A.; Palczewski, K.; Stenkamp, R. E. *J. Struct. Biol.* **2007**, *158*, 455.
(183) Davies, A.; Gowen, B. E.; Krebs, A. M.; Schertler, G. F.; Saibil, H. R. *J. Mol. Biol.* **2001**, *314*, 455.
(184) Bayburt, T. H.; Leitz, A. J.; Xie, G.; Oprian, D. D.; Sligar, S. G. *J. Biol. Chem.* **2007**, *282*, 14875.
(185) Ernst, O. P.; Gramse, V.; Kolbe, M.; Hofmann, K. P.; Heck, M. *Proc. Natl. Acad. of Sci.U.S.A.* **2007**, *104*, 10859.
(186) Meng, E. C.; Bourne, H. R. *Trends Pharmacol. Sci.* **2001**, *22*, 587.
(187) Brown, M. F.; Heyn, M. P.; Job, C.; Kim, S.; Moltke, S.; Nakanishi, K.; Nevzorov, A. A.; Struts, A. V.; Salgado, G. F.; Wallat, I. *Biochim. Biophys. Acta* **2007**, *1768*, 2979.
(188) Brown, M. F.; Martinez-Mayorga, K.; Nakanishi, K.; Salgado, G. F.; Struts, A. V. *Photochem. Photobiol.* **2009**, *85*, 442.
(189) Hofmann, K. P.; Scheerer, P.; Hildebrand, P. W.; Choe, H. W.; Park, J. H.; Heck, M.; Ernst, O. P. *Trends Biochem. Sci.* **2009**, *34*, 540.
(190) Goncalves, J. A.; Ahuja, S.; Erfani, S.; Eilers, M.; Smith, S. O. *Prog. Nucl. Magn. Reson. Spectrosc.* **2010**, *57*, 159.

(191) Choe, H. W.; Park, J. H.; Kim, Y. J.; Ernst, O. P. *Neuropharmacology* **2011**, *60*, 52.
(192) McBee, J. K.; Palczewski, K.; Baehr, W.; Pepperberg, D. R. *Prog. Retin. Eye Res.* **2001**, *20*, 469.
(193) Okada, T.; Ernst, O. P.; Palczewski, K.; Hofmann, K. P. *Trends Biochem. Sci.* **2001**, *26*, 318.
(194) Kliger, D. S.; Lewis, J. W. *Israel J. Chem.* **1995**, *35*, 289.
(195) Yan, E. C.; Kazmi, M. A.; Ganim, Z.; Hou, J. M.; Pan, D.; Chang, B. S.; Sakmar, T. P.; Mathies, R. A. *Proc. Natl. Acad. Sci. U.S.A.* **2003**, *100*, 9262.
(196) Bartl, F. J.; Ritter, E.; Hofmann, K. P. *J. Biol. Chem.* **2001**, *276*, 30161.
(197) Heck, M.; Schadel, S. A.; Maretzki, D.; Bartl, F. J.; Ritter, E.; Palczewski, K.; Hofmann, K. P. *J. Biol. Chem.* **2003**, *278*, 3162.
(198) Fahmy, K.; Jager, F.; Beck, M.; Zvyaga, T. A.; Sakmar, T. P.; Siebert, F. *Proc. Natl. Acad. Sci. U.S.A.* **1993**, *90*, 10206.
(199) Khrenova, M. G.; Bochenkova, A. V.; Nemukhin, A. V. *Proteins* **2010**, *78*, 614.
(200) Kukura, P.; McCamant, D. W.; Yoon, S.; Wandschneider, D. B.; Mathies, R. A. *Science* **2005**, *310*, 1006.
(201) Polli, D.; Altoe, P.; Weingart, O.; Spillane, K. M.; Manzoni, C.; Brida, D.; Tomasello, G.; Orlandi, G.; Kukura, P.; Mathies, R. A.; Garavelli, M.; Cerullo, G. *Nature* **2010**, *467*, 440.
(202) Sandberg, M. N.; Amora, T. L.; Ramos, L. S.; Chen, M. H.; Knox, B. E.; Birge, R. R. *J. Am. Chem. Soc.* **2011**, *133*, 2808.
(203) Ludeke, S.; Beck, M.; Yan, E. C.; Sakmar, T. P.; Siebert, F.; Vogel, R. *J. Mol. Biol.* **2005**, *353*, 345.
(204) Ruprecht, J. J.; Mielke, T.; Vogel, R.; Villa, C.; Schertler, G. F. *EMBO J.* **2004**, *23*, 3609.
(205) Ye, S.; Zaitseva, E.; Caltabiano, G.; Schertler, G. F.; Sakmar, T. P.; Deupi, X.; Vogel, R. *Nature* **2010**, *464*, 1386.
(206) Arnis, S.; Hofmann, K. P. *Proc. Natl. Acad. Sci. U.S.A.* **1993**, *90*, 7849.
(207) Fahmy, K.; Sakmar, T. P.; Siebert, F. *Biochemistry* **2000**, *39*, 10607.
(208) Kim, J. M.; Altenbach, C.; Thurmond, R. L.; Khorana, H. G.; Hubbell, W. L. *Proc. Natl. Acad. Sci. U.S.A.* **1997**, *94*, 14273.
(209) Arnis, S.; Fahmy, K.; Hofmann, K. P.; Sakmar, T. P. *J. Biol. Chem.* **1994**, *269*, 23879.
(210) Meyer, C. K.; Bohme, M.; Ockenfels, A.; Gartner, W.; Hofmann, K. P.; Ernst, O. P. *J. Biol. Chem.* **2000**, *275*, 19713.
(211) Zaitseva, E.; Brown, M. F.; Vogel, R. *J. Am. Chem. Soc.* **2010**, *132*, 4815.
(212) Lehmann, N.; Alexiev, U.; Fahmy, K. *J. Mol. Biol.* **2007**, *366*, 1129.
(213) Knierim, B.; Hofmann, K. P.; Ernst, O. P.; Hubbell, W. L. *Proc. Natl. Acad. Sci. U.S.A.* **2007**, *104*, 20290.
(214) Mahalingam, M.; Martinez-Mayorga, K.; Brown, M. F.; Vogel, R. *Proc. Natl. Acad. Sci. U.S.A.* **2008**, *105*, 17795.
(215) Madathil, S.; Fahmy, K. *J. Biol. Chem.* **2009**, *284*, 28801.
(216) Sato, K.; Morizumi, T.; Yamashita, T.; Shichida, Y. *Biochemistry* **2010**, *49*, 736.
(217) Hoersch, D.; Otto, H.; Wallat, I.; Heyn, M. P. *Biochemistry* **2008**, *47*, 11518.
(218) Struts, A. V.; Salgado, G. F.; Martinez-Mayorga, K.; Brown, M. F. *Nature Struct. Mol. Biol.* **2011**, *18*, 392.
(219) Struts, A. V.; Salgado, G. F.; Brown, M. F. *Proc. Natl. Acad. Sci. U.S.A.* **2011**, *108*, 8263.
(220) Palczewski, K. *Eur. J. Biochem.* **1997**, *248*, 261.
(221) Pulvermuller, A.; Palczewski, K.; Hofmann, K. P. *Biochemistry* **1993**, *32*, 14082.
(222) Farrens, D. L.; Khorana, H. G. *J. Biol. Chem.* **1995**, *270*, 5073.
(223) Heck, M.; Schadel, S. A.; Maretzki, D.; Hofmann, K. P. *Vision Res.* **2003**, *43*, 3003.
(224) Ritter, E.; Zimmermann, K.; Heck, M.; Hofmann, K. P.; Bartl, F. J. *J. Biol. Chem.* **2004**, *279*, 48102.
(225) Schadel, S. A.; Heck, M.; Maretzki, D.; Filipek, S.; Teller, D. C.; Palczewski, K.; Hofmann, K. P. *J. Biol. Chem.* **2003**, *278*, 24896.
(226) Melia, T. J., Jr.; Cowan, C. W.; Angleson, J. K.; Wensel, T. G. *Biophys. J.* **1997**, *73*, 3182.
(227) Hildebrand, P. W.; Scheerer, P.; Park, J. H.; Choe, H. W.; Piechnick, R.; Ernst, O. P.; Hofmann, K. P.; Heck, M. *PLoS One* **2009**, *4*, e4382.
(228) Wang, T.; Duan, Y. *J. Mol. Recognit.* **2011**, *24*, 350.
(229) Altenbach, C.; Kusnetzow, A. K.; Ernst, O. P.; Hofmann, K. P.; Hubbell, W. L. *Proc. Natl. Acad. Sci. U.S.A.* **2008**, *105*, 7439.
(230) Elgeti, M.; Kazmin, R.; Heck, M.; Morizumi, T.; Ritter, E.; Scheerer, P.; Ernst, O. P.; Siebert, F.; Hofmann, K. P.; Bartl, F. J. *J. Am. Chem. Soc.* **2011**, *133*, 7159.
(231) Ascoli, M.; Fanelli, F.; Segaloff, D. L. *Endocr. Rev.* **2002**, *23*, 141.
(232) Fanelli, F.; De Benedetti, P. G. *J. Comput.-Aided. Mol. Des.* **2006**, *20*, 449.
(233) Fanelli, F.; De Benedetti, P. G.; Raimondi, F.; Seeber, M. *Curr. Protein Pept. Sci.* **2009**, *10*, 173.
(234) Goncalves, J. A.; South, K.; Ahuja, S.; Zaitseva, E.; Opefi, C. A.; Eilers, M.; Vogel, R.; Reeves, P. J.; Smith, S. O. *Proc. Natl. Acad. Sci. U.S.A.* **2010**, *107*, 19861.
(235) Borhan, B.; Souto, M. L.; Imai, H.; Shichida, Y.; Nakanishi, K. *Science* **2000**, *288*, 2209.
(236) Patel, A. B.; Crocker, E.; Eilers, M.; Hirshfeld, A.; Sheves, M.; Smith, S. O. *Proc. Natl. Acad. Sci. U.S.A.* **2004**, *101*, 10048.
(237) Patel, A. B.; Crocker, E.; Reeves, P. J.; Getmanova, E. V.; Eilers, M.; Khorana, H. G.; Smith, S. O. *J. Mol. Biol.* **2005**, *347*, 803.
(238) Spooner, P. J.; Sharples, J. M.; Goodall, S. C.; Bovee-Geurts, P. H.; Verhoeven, M. A.; Lugtenburg, J.; Pistorius, A. M.; Degrip, W. J.; Watts, A. *J. Mol. Biol.* **2004**, *343*, 719.
(239) Klein-Seetharaman, J.; Yanamala, N. V.; Javeed, F.; Reeves, P. J.; Getmanova, E. V.; Loewen, M. C.; Schwalbe, H.; Khorana, H. G. *Proc. Natl. Acad. Sci. U.S.A.* **2004**, *101*, 3409.
(240) Getmanova, E.; Patel, A. B.; Klein-Seetharaman, J.; Loewen, M. C.; Reeves, P. J.; Friedman, N.; Sheves, M.; Smith, S. O.; Khorana, H. G. *Biochemistry* **2004**, *43*, 1126.
(241) Yu, H.; Kono, M.; Oprian, D. D. *Biochemistry* **1999**, *38*, 12028.
(242) Farahbakhsh, Z. T.; Ridge, K. D.; Khorana, H. G.; Hubbell, W. L. *Biochemistry* **1995**, *34*, 8812.
(243) Altenbach, C.; Yang, K.; Farrens, D. L.; Farahbakhsh, Z. T.; Khorana, H. G.; Hubbell, W. L. *Biochemistry* **1996**, *35*, 12470.
(244) Altenbach, C.; Cai, K.; Khorana, H. G.; Hubbell, W. L. *Biochemistry* **1999**, *38*, 7931.
(245) Janz, J. M.; Farrens, D. L. *J. Biol. Chem.* **2004**, *279*, 29767.
(246) Altenbach, C.; Klein-Seetharaman, J.; Hwa, J.; Khorana, H. G.; Hubbell, W. L. *Biochemistry* **1999**, *38*, 7945.
(247) Kusnetzow, A. K.; Altenbach, C.; Hubbell, W. L. *Biochemistry* **2006**, *45*, 5538.
(248) Kim, J. M.; Altenbach, C.; Kono, M.; Oprian, D. D.; Hubbell, W. L.; Khorana, H. G. *Proc. Natl. Acad. Sci. U.S.A.* **2004**, *101*, 12508.
(249) Choi, G.; Landin, J.; Galan, J. F.; Birge, R. R.; Albert, A. D.; Yeagle, P. L. *Biochemistry* **2002**, *41*, 7318.
(250) Yeagle, P. L.; Albert, A. D. *Biochemistry* **2003**, *42*, 1365.
(251) Gouldson, P. R.; Kidley, N. J.; Bywater, R. P.; Psaroudakis, G.; Brooks, H. D.; Diaz, C.; Shire, D.; Reynolds, C. A. *Proteins* **2004**, *56*, 67.
(252) Nikiforovich, G. V.; Marshall, G. R. *Biochemistry* **2003**, *42*, 9110.
(253) Pogozheva, I. D.; Lomize, A. L.; Mosberg, H. I. *Biophys. J.* **1997**, *72*, 1963.
(254) Ahuja, S.; Hornak, V.; Yan, E. C.; Syrett, N.; Goncalves, J. A.; Hirshfeld, A.; Ziliox, M.; Sakmar, T. P.; Sheves, M.; Reeves, P. J.; Smith, S. O.; Eilers, M. *Nature Struct. Mol. Biol.* **2009**, *16*, 168.
(255) Sakai, K.; Imamoto, Y.; Yamashita, T.; Shichida, Y. *Photochem. Photobiol. Sci.* **2010**, *9*, 1490.
(256) Smith, S. O. *Annu. Rev. Biophys.* **2010**, *39*, 309.
(257) Ahuja, S.; Smith, S. O. *Trends Pharmacol. Sci.* **2009**, *30*, 494.
(258) Frutos, L. M.; Andruniow, T.; Santoro, F.; Ferre, N.; Olivucci, M. *Proc. Natl. Acad. Sci. U.S.A.* **2007**, *104*, 7764.
(259) Schapiro, I.; Ryazantsev, M. N.; Frutos, L. M.; Ferre, N.; Lindh, R.; Olivucci, M. *J. Am. Chem. Soc.* **2011**, *133*, 3354.
(260) Lau, P. W.; Grossfield, A.; Feller, S. E.; Pitman, M. C.; Brown, M. F. *J. Mol. Biol.* **2007**, *372*, 906.

(261) Struts, A. V.; Salgado, G. F.; Tanaka, K.; Krane, S.; Nakanishi, K.; Brown, M. F. *J. Mol. Biol.* **2007**, *372*, 50.
(262) Huber, T.; Botelho, A. V.; Beyer, K.; Brown, M. F. *Biophys. J.* **2004**, *86*, 2078.
(263) Crozier, P. S.; Stevens, M. J.; Forrest, L. R.; Woolf, T. B. *J. Mol. Biol* . **2003**, *333*, 493.
(264) Pitman, M. C.; Grossfield, A.; Suits, F.; Feller, S. E. *J. Am. Chem. Soc.* **2005**, *127*, 4576.
(265) Cordomi, A.; Perez, J. J. *J. Phys. Chem. B* **2007**, *111*, 7052.
(266) Cordomi, A.; Ramon, E.; Garriga, P.; Perez, J. J. *J. Biomol. Struct. Dyn.* **2008**, *25*, 573.
(267) Khelashvili, G.; Grossfield, A.; Feller, S. E.; Pitman, M. C.; Weinstein, H. *Proteins* **2009**, *76*, 403.
(268) Rohrig, U. F.; Guidoni, L.; Rothlisberger, U. *Biochemistry* **2002**, *41*, 10799.
(269) Saam, J.; Tajkhorshid, E.; Hayashi, S.; Schulten, K. *Biophys. J.* **2002**, *83*, 3097.
(270) Yeagle, P. L.; Choi, G.; Albert, A. D. *Biochemistry* **2001**, *40*, 11932.
(271) Niv, M. Y.; Skrabanek, L.; Filizola, M.; Weinstein, H. *J. Comput.-Aided Mol. Des.* **2006**, *20*, 437.
(272) Tikhonova, I. G.; Best, R. B.; Engel, S.; Gershengorn, M. C.; Hummer, G.; Costanzi, S. *J. Am. Chem. Soc.* **2008**, *130*, 10141.
(273) Hornak, V.; Ahuja, S.; Eilers, M.; Goncalves, J. A.; Sheves, M.; Reeves, P. J.; Smith, S. O. *J. Mol. Biol.* **2010**, *396*, 510.
(274) Isin, B.; Schulten, K.; Tajkhorshid, E.; Bahar, I. *Biophys. J.* **2008**, *95*, 789.
(275) Bahar, I.; Lezon, T. R.; Bakan, A.; Shrivastava, I. H. *Chem. Rev.* **2010**, *110*, 1463.
(276) Isin, B.; Rader, A. J.; Dhiman, H. K.; Klein-Seetharaman, J.; Bahar, I. *Proteins* **2006**, *65*, 970.
(277) Kong, Y.; Karplus, M. *Structure* **2007**, *15*, 611.
(278) Nikiforovich, G. V.; Marshall, G. R. *Biochem. Biophys. Res. Commun.* **2006**, *345*, 430.
(279) Chambers, J. J.; Nichols, D. E. *J. Comput.-Aided Mol. Des.* **2002**, *16*, 511.
(280) Ishiguro, M.; Hirano, T.; Oyama, Y. *ChemBioChem* **2003**, *4*, 228.
(281) Ishiguro, M.; Oyama, Y.; Hirano, T. *ChemBioChem* **2004**, *5*, 298.
(282) Ishiguro, M. *ChemBioChem* **2004**, *5*, 1210.
(283) Akuzawa, N.; Takeda, S.; Ishiguro, M. *J. Biochem.* **2007**, *141*, 907.
(284) Bhattacharya, S.; Hall, S. E.; Vaidehi, N. *J. Mol. Biol.* **2008**, *382*, 539.
(285) Vaidehi, N. *Drug Discovery Today* **2010**, *15*, 951.
(286) Provasi, D.; Filizola, M. *Biophys. J.* **2010**, *98*, 2347.
(287) Cordomi, A.; Perez, J. J. *J. Biomol. Struct. Dyn.* **2009**, *27*, 127.
(288) Filizola, M.; Wang, S. X.; Weinstein, H. *J. Comput.-Aided Mol. Des.* **2006**, *20*, 405.
(289) Neri, M.; Vanni, S.; Tavernelli, I.; Rothlisberger, U. *Biochemistry* **2010**, *49*, 4827.
(290) Niv, M. Y.; Filizola, M. *Proteins* **2008**, *71*, 575.
(291) Taylor, M. S.; Fung, H. K.; Rajgaria, R.; Filizola, M.; Weinstein, H.; Floudas, C. A. *Biophys. J.* **2008**, *94*, 2470.
(292) Marrink, S. J.; Risselada, H. J.; Yefimov, S.; Tieleman, D. P.; de Vries, A. H. *J. Phys. Chem. B* **2007**, *111*, 7812.
(293) Periole, X.; Huber, T.; Marrink, S. J.; Sakmar, T. P. *J. Am. Chem. Soc.* **2007**, *129*, 10126.
(294) Periole, X.; Cavalli, M.; Marrink, S. J.; Ceruso, M. A. *J. Chem. Theory Comput.* **2009**, *5*, 2531.
(295) Spijker, P.; van Hoof, B.; Debertrand, M.; Markvoort, A. J.; Vaidehi, N.; Hilbers, P. A. *Int. J. Mol. Sci.* **2010**, *11*, 2393.
(296) Sanders, C. R.; Myers, J. K. *Annu. Rev. Biophys. Biomol. Struct.* **2004**, *33*, 25.
(297) Kennan, A.; Aherne, A.; Humphries, P. *Trends Genet.* **2005**, *21*, 103.
(298) Rakoczy, E. P.; Kiel, C.; McKeone, R.; Stricher, F.; Serrano, L. *J. Mol. Biol.* **2010**, *405*, 584.
(299) Felline, A.; Seeber, M.; Rao, F.; Fanelli, F. *J. Chem. Theory Comput.* **2009**, *5*, 2472.
(300) Fanelli, F.; Seeber, M. *FASEB J.* **2010**, *24*, 3196.
(301) Seeber, M.; Felline, A.; Raimondi, F.; Muff, S.; Friedman, R.; Rao, F.; Caflisch, A.; Fanelli, F. *J. Comput. Chem.* **2011**, *32*, 1183.
(302) Sapra, K. T.; Park, P. S.; Palczewski, K.; Muller, D. J. *Langmuir* **2008**, *24*, 1330.
(303) Tanuj Sapra, K.; Park, P. S.; Filipek, S.; Engel, A.; Muller, D. J.; Palczewski, K. *J Mol. Biol* . **2006**, *358*, 255.
(304) Tastan, O.; Yu, E.; Ganapathiraju, M.; Aref, A.; Rader, A. J.; Klein-Seetharaman, J. *Photochem. Photobiol.* **2007**, *83*, 351.
(305) Rosenbaum, D. M.; Cherezov, V.; Hanson, M. A.; Rasmussen, S. G.; Thian, F. S.; Kobilka, T. S.; Choi, H. J.; Yao, X. J.; Weis, W. I.; Stevens, R. C.; Kobilka, B. K. *Science* **2007**, *318*, 1266.
(306) Rosenbaum, D. M.; Rasmussen, S. G.; Kobilka, B. K. *Nature* **2009**, *459*, 356.
(307) Alkhalfioui, F.; Magnin, T.; Wagner, R. *Curr. Opin. Pharmacol.* **2009**, *9*, 629.
(308) Roth, C. B.; Hanson, M. A.; Stevens, R. C. *J. Mol. Biol.* **2008**, *376*, 1305.
(309) Hanson, M. A.; Stevens, R. C. *Structure* **2009**, *17*, 8.
(310) Topiol, S.; Sabio, M. *Biochem. Pharmacol.* **2009**, *78*, 11.
(311) Mustafi, D.; Palczewski, K. *Mol. Pharmacol.* **2009**, *75*, 1.
(312) Lodowski, D. T.; Angel, T. E.; Palczewski, K. *Photochem. Photobiol.* **2009**, *85*, 425.
(313) Peeters, M. C.; van Westen, G. J.; Li, Q.; Ijzerman, A. P. *Trends. Pharmacol. Sci.* **2010**, *32*, 35.
(314) Jaakola, V. P.; Lane, J. R.; Lin, J. Y.; Katritch, V.; Ijzerman, A. P.; Stevens, R. C. *J. Biol. Chem.* **2010**, *285*, 13032.
(315) Huber, T.; Menon, S.; Sakmar, T. P. *Biochemistry* **2008**, *47*, 11013.
(316) Lefkowitz, R. J.; Sun, J. P.; Shukla, A. K. *Nature Biotechnol.* **2008**, *26*, 189.
(317) Shukla, A. K.; Sun, J. P.; Lefkowitz, R. J. *Mol. Pharmacol.* **2008**, *73*, 1333.
(318) Dror, R. O.; Arlow, D. H.; Borhani, D. W.; Jensen, M. O.; Piana, S.; Shaw, D. E. *Proc. Natl. Acad. Sci. U.S.A.* **2009**, *106*, 4689.
(319) Vanni, S.; Neri, M.; Tavernelli, I.; Rothlisberger, U. *Biochemistry* **2009**, *48*, 4789.
(320) Romo, T. D.; Grossfield, A.; Pitman, M. C. *Biophys. J.* **2010**, *98*, 76.
(321) Vanni, S.; Neri, M.; Tavernelli, I.; Rothlisberger, U. *J. Mol. Biol.* **2010**, *397*, 1339.
(322) Jojart, B.; Kiss, R.; Viskolcz, B.; Kolossvary, I.; Keseru, G. M. *J. Phys. Chem. Lett.* **2010**, *1*, 1008.
(323) Rodriguez, D.; Pineiro, A.; Gutierrez-de-Teran, H. *Biochemistry* **2011**, *50*, 4194.
(324) Fanelli, F.; Felline, A. *Biochim. Biophys. Acta* **2011**, *1808*, 1256.
(325) Bhattacharya, S.; Vaidehi, N. *J. Am. Chem. Soc.* **2010**, *132*, 5205.
(326) Horn, F.; Weare, J.; Beukers, M. W.; Horsch, S.; Bairoch, A.; Chen, W.; Edvardsen, O.; Campagne, F.; Vriend, G. *Nucleic Acids Res.* **1998**, *26*, 275.
(327) Horn, F.; Vriend, G.; Cohen, F. E. *Nucleic Acids Res.* **2001**, *29*, 346.
(328) Horn, F.; Bettler, E.; Oliveira, L.; Campagne, F.; Cohen, F. E.; Vriend, G. *Nucleic Acids Res.* **2003**, *31*, 294.
(329) Vroling, B.; Sanders, M.; Baakman, C.; Borrmann, A.; Verhoeven, S.; Klomp, J.; Oliveira, L.; de Vlieg, J.; Vriend, G. *Nucleic Acids Res.* **2011**, *39*, D309.
(330) Horn, F.; Lau, A. L.; Cohen, F. E. *Bioinformatics* **2004**, *20*, 557.
(331) Crasto, C.; Marenco, L.; Miller, P.; Shepherd, G. *Nucleic Acids Res.* **2002**, *30*, 354.
(332) Kristiansen, K.; Dahl, S. G.; Edvardsen, O. *Proteins* **1996**, *26*, 81.
(333) Edvardsen, O.; Kristiansen, K. *Trends Biochem. Sci* . **1997**, *22*, 226.
(334) Beukers, M. W.; Kristiansen, I.; AP, I. J.; Edvardsen, I. *Trends Pharmacol. Sci.* **1999**, *20*, 475.

(335) Edvardsen, O.; Reiersen, A. L.; Beukers, M. W.; Kristiansen, K. *Nucleic Acids Res.* **2002**, *30*, 361.
(336) Campagne, F.; Jestin, R.; Reversat, J. L.; Bernassau, J. M.; Maigret, B. *J. Comput.-Aided Mol. Des.* **1999**, *13*, 625.
(337) Peitsch, M. C. *Biochem. Soc. Trans.* **1996**, *24*, 274.
(338) Khelashvili, G.; Dorff, K.; Shan, J.; Camacho-Artacho, M.; Skrabanek, L.; Vroling, B.; Bouvier, M.; Devi, L. A.; George, S. R.; Javitch, J. A.; Lohse, M. J.; Milligan, G.; Neubig, R. R.; Palczewski, K.; Parmentier, M.; Pin, J. P.; Vriend, G.; Campagne, F.; Filizola, M. *Bioinformatics* **2010**, *26*, 1804.
(339) Skrabanek, L.; Murcia, M.; Bouvier, M.; Devi, L.; George, S. R.; Lohse, M. J.; Milligan, G.; Neubig, R.; Palczewski, K.; Parmentier, M.; Pin, J. P.; Vriend, G.; Javitch, J. A.; Campagne, F.; Filizola, M. *BMC Bioinf.* **2007**, *8*, 177.
(340) Kazius, J.; Wurdinger, K.; van Iterson, M.; Kok, J.; Back, T.; Ijzerman, A. P. *Hum. Mutat.* **2008**, *29*, 39.
(341) Kreuchwig, A.; Kleinau, G.; Kreuchwig, F.; Worth, C. L.; Krause, G. *Mol. Endocrinol.* **2011**, *25*, 707.
(342) Bhasin, M.; Raghava, G. P. *Nucleic Acids Res.* **2004**, *32*, W383.
(343) Wen, Z.; Li, M.; Li, Y.; Guo, Y.; Wang, K. *Amino Acids* **2007**, *32*, 277.
(344) Xiao, X.; Wang, P.; Chou, K. C. *J. Comput. Chem.* **2009**, *30*, 1414.
(345) Li, Z.; Zhou, X.; Dai, Z.; Zou, X. *BMC Bioinf.* **2010**, *11*, 325.
(346) Peng, Z. L.; Yang, J. Y.; Chen, X. *BMC Bioinf.* **2010**, *11*, 420.
(347) Wistrand, M.; Kall, L.; Sonnhammer, E. L. *Protein Sci.* **2006**, *15*, 509.
(348) Naveed, M.; Khan, A. U. *Amino Acids*, **2011**, DOI: 10.1007/s00726-011-0902-6.
(349) Gaulton, A.; Attwood, T. K. *Curr. Opin. Pharmacol*. **2003**, 3, 114.
(350) Kleinau, G.; Kreuchwig, A.; Worth, C. L.; Krause, G. *Hum. Mutat.* **2010**, *31*, E1519.
(351) Elefsinioti, A. L.; Bagos, P. G.; Spyropoulos, I. C.; Hamodrakas, S. J. *BMC Bioinf.* **2004**, *5*, 208.
(352) Satagopam, V. P.; Theodoropoulou, M. C.; Stampolakis, C. K.; Pavlopoulos, G. A.; Papandreou, N. C.; Bagos, P. G.; Schneider, R.; Hamodrakas, S. J. *Database (Oxford)* **2010**, *2010*, baq019.
(353) Nemoto, W.; Fukui, K.; Toh, H. *J. Recept. Signal Transduct. Res.* **2011**, *31*, 199.
(354) Jassal, B.; Jupe, S.; Caudy, M.; Birney, E.; Stein, L.; Hermjakob, H.; D'Eustachio, P. *Database (Oxford)* **2010**, *2010*, baq018.
(355) Fang, Y. C.; Sun, W. H.; Wu, L. C.; Huang, H. D.; Juan, H. F.; Horng, J. T. *BMC Genomics* **2006**, *7*, 317.
(356) Okuno, Y.; Yang, J.; Taneishi, K.; Yabuuchi, H.; Tsujimoto, G. *Nucleic Acids Res.* **2006**, *34*, D673.
(357) van der Horst, E.; Peironcely, J. E.; Ijzerman, A. P.; Beukers, M. W.; Lane, J. R.; van Vlijmen, H. W.; Emmerich, M. T.; Okuno, Y.; Bender, A. *BMC Bioinf.* **2010**, *11*, 316.
(358) Surgand, J. S.; Rodrigo, J.; Kellenberger, E.; Rognan, D. *Proteins* **2006**, *62*, 509.
(359) Sanders, M. P.; Fleuren, W. W.; Verhoeven, S.; van den Beld, S.; Alkema, W.; de Vlieg, J.; Klomp, J. P. *BMC Bioinf.* **2011**, *12*, 332.
(360) Bromberg, Y.; Rost, B. *Nucleic Acids Res.* **2007**, *35*, 3823.
(361) Bromberg, Y.; Overton, J.; Vaisse, C.; Leibel, R. L.; Rost, B. *FASEB J.* **2009**, *23*, 3059.
(362) Zhang, J.; Zhang, Y. *Bioinformatics* **2010**, *26*, 3004.
(363) Worth, C. L.; Kreuchwig, A.; Kleinau, G.; Krause, G. *BMC Bioinf.* **2011**, *12*, 185.
(364) Henderson, R.; Schertler, G. F. *Philos. Trans. R. Soc. London* **1990**, *326*, 379.
(365) Hibert, M. F.; Trumpp-Kallmeyer, S.; Bruinvels, A.; Hoflack, J. *Mol. Pharmacol.* **1991**, *40*, 8.
(366) Ijzerman, A. P.; Van Galen, P. J.; Jacobson, K. A. *Drug Des. Discovery* **1992**, *9*, 49.
(367) Livingstone, C. D.; Strange, P. G.; Naylor, L. H. *Biochem. J.* **1992**, *287* (Pt 1), 277.
(368) Trumpp-Kallmeyer, S.; Hoflack, J.; Bruinvels, A.; Hibert, M. *J. Med. Chem.* **1992**, *35*, 3448.
(369) Cronet, P.; Sander, C.; Vriend, G. *Protein Eng.* **1993**, *6*, 59.
(370) De Benedetti, P. G.; Menziani, M. C.; Fanelli, F.; Cocchi, M. *J. Mol. Struct. (THEOCHEM)* **1993**, *285*, 147.
(371) Hoflack, J.; Hibert, M. F.; Trumpp-Kallmeyer, S.; Bidart, J. M. *Drug Des. Discovery* **1993**, *10*, 157.
(372) Huggins, J. P.; Trumpp-Kallmeyer, S.; Hibert, M. F.; Hoflack, J. M.; Fanger, B. O.; Jones, C. R. *Eur. J. Pharmacol.* **1993**, *245*, 203.
(373) Nordvall, G.; Hacksell, U. *J. Med. Chem.* **1993**, *36*, 967.
(374) Oliveira, L.; Paiva, A. C. M.; Vriend, G. *J. Comput.-Aided Mol. Des.* **1993**, *7*, 649.
(375) Yamamoto, Y.; Kamiya, K.; Terao, S. *J. Med. Chem.* **1993**, *36*, 820.
(376) Ijzerman, A. P.; van der Wenden, E. M.; van Galen, P. J.; Jacobson, K. A. *Eur. J. Pharmacol.* **1994**, *268*, 95.
(377) Fanelli, F.; Menziani, M. C.; Carotti, A.; De Benedetti, P. G. *Bioorg. Med. Chem.* **1994**, *2*, 195.
(378) Fanelli, F.; Menziani, M. C.; Cocchi, M.; Leonardi, A.; De Benedetti, P. G. *J. Mol. Struct. (THEOCHEM)* **1994**, *314*, 265.
(379) Kuipers, W.; Van Wijngaarden, I.; Ijzerman, A. P. *Drug Des. Discovery* **1994**, *11*, 231.
(380) Kyle, D. J.; Chakravarty, S.; Sinsko, J. A.; Stormann, T. M. *J. Med. Chem.* **1994**, *37*, 1347.
(381) Malmberg, A.; Nordvall, G.; Johansson, A. M.; Mohell, N.; Hacksell, U. *Mol. Pharmacol.* **1994**, *46*, 299.
(382) Teeter, M. M.; Froimowitz, M.; Stec, B.; DuRand, C. J. *J. Med. Chem.* **1994**, *37*, 2874.
(383) van Galen, P. J.; van Bergen, A. H.; Gallo-Rodriguez, C.; Melman, N.; Olah, M. E.; AP, I. J.; Stiles, G. L.; Jacobson, K. A. *Mol. Pharmacol.* **1994**, *45*, 1101.
(384) Groblewski, T.; Maigret, B.; Nouet, S.; Larguier, R.; Lombard, C.; Bonnafous, J. C.; Marie, J. *Biochem. Biophys. Res. Commun.* **1995**, *209*, 153.
(385) Hedberg, M. H.; Johansson, A. M.; Nordvall, G.; Yliniemela, A.; Li, H. B.; Martin, A. R.; Hjorth, S.; Unelius, L.; Sundell, S.; Hacksell, U. *J. Med. Chem.* **1995**, *38*, 647.
(386) Jagerschmidt, A.; Guillaume, N.; Goudreau, N.; Maigret, B.; Roques, B. P. *Mol. Pharmacol.* **1995**, *48*, 783.
(387) Joseph, M. P.; Maigret, B.; Scheraga, H. A. *Int. J. Pept. Protein* **1995**, *46*, 514.
(388) Joseph, M. P.; Maigret, B.; Bonnafous, J. C.; Marie, J.; Scheraga, H. A. *J. Protein Chem.* **1995**, *14*, 381.
(389) Kaupmann, K.; Bruns, C.; Raulf, F.; Weber, H. P.; Mattes, H.; Lubbert, H. *EMBO J.* **1995**, *14*, 727.
(390) ter Laak, A. M.; Timmerman, H.; Leurs, R.; Nederkoorn, P. H.; Smit, M. J.; Donne-Op den Kelder, G. M. *J. Comput.-Aided Mol. Des.* **1995**, *9*, 319.
(391) Yamano, Y.; Ohyama, K.; Kikyo, M.; Sano, T.; Nakagomi, Y.; Inoue, Y.; Nakamura, N.; Morishima, I.; Guo, D. F.; Hamakubo, T.; Inagami, T. *J. Biol. Chem.* **1995**, *270*, 14024.
(392) Befort, K.; Tabbara, L.; Kling, D.; Maigret, B.; Kieffer, B. L. *J. Biol. Chem.* **1996**, *271*, 10161.
(393) Forbes, I. T.; Dabbs, S.; Duckworth, D. M.; Ham, P.; Jones, G. E.; King, F. D.; Saunders, D. V.; Blaney, F. E.; Naylor, C. B.; Baxter, G. S.; Blackburn, T. P.; Kennett, G. A.; Wood, M. D. *J. Med. Chem.* **1996**, *39*, 4966.
(394) Jagerschmidt, A.; Guillaume-Rousselet, N.; Vikland, M. L.; Goudreau, N.; Maigret, B.; Roques, B. P. *Eur. J. Pharmacol.* **1996**, *296*, 97.
(395) Wieland, K.; Zuurmond, H. M.; Krasel, C.; Ijzerman, A. P.; Lohse, M. J. *Proc. Natl. Acad. Sci. U.S.A.* **1996**, *93*, 9276.
(396) Bromidge, S. M.; Duckworth, M.; Forbes, I. T.; Ham, P.; King, F. D.; Thewlis, K. M.; Blaney, F. E.; Naylor, C. B.; Blackburn, T. P.; Kennett, G. A.; Wood, M. D.; Clarke, S. E. *J. Med. Chem.* **1997**, *40*, 3494.
(397) Mahmoudian, M. *J. Mol. Graphics Modell.* **1997**, *15*, 149.
(398) Kuipers, W.; Link, R.; Standaar, P. J.; Stoit, A. R.; Van Wijngaarden, I.; Leurs, R.; Ijzerman, A. P. *Mol. Pharmacol.* **1997**, *51*, 889.
(399) Bromidge, S. M.; Dabbs, S.; Davies, D. T.; Duckworth, D. M.; Forbes, I. T.; Ham, P.; Jones, G. E.; King, F. D.; Saunders, D. V.; Starr, S.; Thewlis, K. M.; Wyman, P. A.; Blaney, F. E.; Naylor, C. B.; Bailey, F.;

Blackburn, T. P.; Holland, V.; Kennett, G. A.; Riley, G. J.; Wood, M. D. *J. Med. Chem.* **1998**, *41*, 1598.
(400) Spedding, M.; Newman-Tancredi, A.; Millan, M. J.; Dacquet, C.; Michel, A. N.; Jacoby, E.; Vickery, B.; Tallentire, D. *Neuropharmacology* **1998**, *37*, 769.
(401) Jacoby, E.; Fauchere, J.-L.; Raimbaud, E.; Ollivier, S.; Michel, A.; Spedding, M. *Quantum Struct.-Act. Relat.* **1999**, *18*, 561.
(402) Zuurmond, H. M.; Hessling, J.; Bluml, K.; Lohse, M.; Ijzerman, A. P. *Mol. Pharmacol.* **1999**, *56*, 909.
(403) Bromidge, S. M.; Dabbs, S.; Davies, D. T.; Davies, S.; Duckworth, D. M.; Forbes, I. T.; Gaster, L. M.; Ham, P.; Jones, G. E.; King, F. D.; Mulholland, K. R.; Saunders, D. V.; Wyman, P. A.; Blaney, F. E.; Clarke, S. E.; Blackburn, T. P.; Holland, V.; Kennett, G. A.; Lightowler, S.; Middlemiss, D. N.; Trail, B.; Riley, G. J.; Wood, M. D. *J. Med. Chem.* **2000**, *43*, 1123.
(404) Lavecchia, A.; Greco, G.; Novellino, E.; Vittorio, F.; Ronsisvalle, G. *J. Med. Chem.* **2000**, *43*, 2124.
(405) Macdonald, D.; Murgolo, N.; Zhang, R.; Durkin, J. P.; Yao, X.; Strader, C. D.; Graziano, M. P. *Mol. Pharmacol.* **2000**, *58*, 217.
(406) Zhou, N.; Luo, Z.; Hall, J. W.; Luo, J.; Han, X.; Huang, Z. *Eur. J. Immunol.* **2000**, *30*, 164.
(407) Zhou, N.; Luo, Z.; Luo, J.; Liu, D.; Hall, J. W.; Pomerantz, R. J.; Huang, Z. *J. Biol. Chem.* **2001**, *276*, 42826.
(408) Iadanza, M.; Holtje, M.; Ronsisvalle, G.; Holtje, H. D. *J. Med. Chem.* **2002**, *45*, 4838.
(409) Manivet, P.; Schneider, B.; Smith, J. C.; Choi, D. S.; Maroteaux, L.; Kellermann, O.; Launay, J. M. *J. Biol. Chem.* **2002**, *277*, 17170.
(410) Marie, J.; Richard, E.; Pruneau, D.; Paquet, J. L.; Siatka, C.; Larguier, R.; Ponce, C.; Vassault, P.; Groblewski, T.; Maigret, B.; Bonnafous, J. C. *J. Biol. Chem.* **2001**, *276*, 41100.
(411) Pardo, L.; Ballesteros, J. A.; Osman, R.; Weinstein, H. *Proc. Natl. Acad. Sci. U.S.A.* **1992**, *89*, 4009.
(412) Taylor, E. W.; Agarwal, A. *FEBS Lett.* **1993**, *325*, 161.
(413) Metzger, T. G.; Paterlini, M. G.; Portoghese, P. S.; Ferguson, D. M. *J. Chem. Inf. Comput. Sci.* **1996**, *36*, 857.
(414) Metzger, T. G.; Paterlini, M. G.; Portoghese, P. S.; Ferguson, D. M. *Neurochem. Res.* **1996**, *21*, 1287.
(415) Paterlini, G.; Portoghese, P. S.; Ferguson, D. M. *J. Med. Chem.* **1997**, *40*, 3254.
(416) Soppa, J. *FEBS Lett.* **1994**, *342*, 7.
(417) Jones, D.; Thornton, J. *J. Comput.-Aided Mol. Des.* **1993**, *7*, 439.
(418) Wodak, S.; Rooman, M. *Curr. Opin. Struct. Biol.* **1993**, *3*, 247.
(419) Escrieut, C.; Gigoux, V.; Archer, E.; Verrier, S.; Maigret, B.; Behrendt, R.; Moroder, L.; Bignon, E.; Silvente-Poirot, S.; Pradayrol, L.; Fourmy, D. *J. Biol. Chem.* **2002**, *277*, 7546.
(420) Fourmy, D.; Escrieut, C.; Archer, E.; Gales, C.; Gigoux, V.; Maigret, B.; Moroder, L.; Silvente-Poirot, S.; Martinez, J.; Fehrentz, J. A.; Pradayrol, L. *Pharmacol. Toxicol.* **2002**, *91*, 313.
(421) Gales, C.; Poirot, M.; Taillefer, J.; Maigret, B.; Martinez, J.; Moroder, L.; Escrieut, C.; Pradayrol, L.; Fourmy, D.; Silvente-Poirot, S. *Mol. Pharmacol.* **2003**, *63*, 973.
(422) Essen, L.; Siegert, R.; Lehmann, W. D.; Oesterhelt, D. *Proc. Natl. Acad. Sci. U.S.A.* **1998**, *95*, 11673.
(423) Higgs, C.; Reynolds, C. A. In *Theoretical and Computational Chemistry*; Eriksson, L. A. , Ed.; Elsevier: Amsterdam, 2001; Vol. 9.
(424) Dahl, S. G.; Edvardsen, O.; Sylte, I. *Proc. Natl. Acad. Sci. U.S.A.* **1991**, *88*, 8111.
(425) MaloneyHuss, K.; Lybrand, T. P. *J. Mol. Biol.* **1992**, *225*, 859.
(426) Zhang, D.; Weinstein, H. *J. Med. Chem.* **1993**, *36*, 934.
(427) Zhang, D.; Weinstein, H. *FEBS Lett.* **1994**, *337*, 207.
(428) Almaula, N.; Ebersole, B. J.; Zhang, D.; Weinstein, H.; Sealfon, S. C. *J. Biol. Chem.* **1996**, *271*, 14672.
(429) Kontoyianni, M.; DeWeese, C.; Penzotti, J. E.; Lybrand, T. P. *J. Med. Chem.* **1996**, *39*, 4406.
(430) Ji, Z.; Hadac, E. M.; Henne, R. M.; Patel, S. A.; Lybrand, T. P.; Miller, L. J. *J. Biol. Chem.* **1997**, *272*, 24393.
(431) Hadac, E. M.; Pinon, D. I.; Ji, Z.; Holicky, E. L.; Henne, R. M.; Lybrand, T. P.; Miller, L. J. *J. Biol. Chem.* **1998**, *273*, 12988.
(432) Hamaguchi, N.; True, T. A.; Goetz, A. S.; Stouffer, M. J.; Lybrand, T. P.; Jeffs, P. W. *Biochemistry* **1998**, *37*, 5730.
(433) Hadac, E. M.; Ji, Z.; Pinon, D. I.; Henne, R. M.; Lybrand, T. P.; Miller, L. J. *J. Med. Chem.* **1999**, *42*, 2105.
(434) Ding, X. Q.; Dolu, V.; Hadac, E. M.; Holicky, E. L.; Pinon, D. I.; Lybrand, T. P.; Miller, L. J. *J. Biol. Chem.* **2001**, *276*, 4236.
(435) Elling, C. E.; Nielsen, S. M.; Schwartz, T. W. *Nature* **1995**, *374*, 74.
(436) Liu, J.; Schoneberg, T.; van Rhee, M.; Wess, J. *J. Biol. Chem.* **1995**, *270*, 19532.
(437) Mizobe, T.; Maze, M.; Lam, V.; Suryanarayana, S.; Kobilka, B. K. *J. Biol. Chem.* **1996**, *271*, 2387.
(438) Elling, C. E.; Schwartz, T. W. *EMBO J.* **1996**, *15*, 6213.
(439) Ding, X. Q.; Pinon, D. I.; Furse, K. E.; Lybrand, T. P.; Miller, L. J. *Mol. Pharmacol.* **2002**, *61*, 1041.
(440) Miller, L. J.; Lybrand, T. P. *Pharmacol. Toxicol.* **2002**, *91*, 282.
(441) Furse, K. E.; Lybrand, T. P. *J. Med. Chem.* **2003**, *46*, 4450.
(442) Harikumar, K. G.; Pinon, D. I.; Wessels, W. S.; Dawson, E. S.; Lybrand, T. P.; Prendergast, F. G.; Miller, L. J. *Mol. Pharmacol.* **2004**, *65*, 28.
(443) Perlman, J. H.; Laakkonen, L.; Osman, R.; Gershengorn, M. C. *J. Biol. Chem.* **1994**, *269*, 23383.
(444) Chini, B.; Mouillac, B.; Ala, Y.; Balestre, M. N.; Trumpp-Kallmeyer, S.; Hoflack, J.; Elands, J.; Hibert, M.; Manning, M.; Jard, S. *EMBO J.* **1995**, *14*, 2176.
(445) Kim, J.; Wess, J.; van Rhee, A. M.; Schoneberg, T.; Jacobson, K. A. *J. Biol. Chem.* **1995**, *270*, 13987.
(446) Mouillac, B.; Chini, B.; Balestre, M. N.; Elands, J.; Trumpp-Kallmeyer, S.; Hoflack, J.; Hibert, M.; Jard, S.; Barberis, C. *J. Biol. Chem.* **1995**, *270*, 25771.
(447) Van Rhee, A. M.; Fischer, B.; Van Galen, P. J.; Jacobson, K. A. *Drug Des. Discovery* **1995**, *13*, 133.
(448) Cappelli, A.; Anzini, M.; Vomero, S.; Menziani, M. C.; De Benedetti, P. G.; Sbacchi, M.; Clarke, G. D.; Mennuni, L. *J. Med. Chem.* **1996**, *39*, 860.
(449) Kristiansen, K.; Dahl, S. G. *Eur. J. Pharmacol.* **1996**, *306*, 195.
(450) Laakkonen, L. J.; Guarnieri, F.; Perlman, J. H.; Gershengorn, M. C.; Osman, R. *Biochemistry* **1996**, *35*, 7651.
(451) Perlman, J. H.; Laakkonen, L.; Guarnieri, F.; Osman, R.; Gershengorn, M. C. *Biochemistry* **1996**, *35*, 7643.
(452) Sylte, I.; Edvardsen, O.; Dahl, S. G. *Protein Eng.* **1996**, *9*, 149.
(453) Wetzel, J. M.; Salon, J. A.; Tamm, J. A.; Forray, C.; Craig, D.; Nakanishi, H.; Cui, W.; Vaysse, P. J.; Chiu, G.; Weinshank, R. L.; Hartig, P. R.; Branchek, T. A.; Gluchowski, C. *Recept. Channels* **1996**, *4*, 165.
(454) Bourdon, H.; Trumpp-Kallmeyer, S.; Schreuder, H.; Hoflack, J.; Hibert, M.; Wermuth, C. G. *J. Comput.-Aided Mol. Des.* **1997**, *11*, 317.
(455) Gouldson, P. R.; Reynolds, C. A. *Biochem. Soc. Trans.* **1997**, *25*, 1066.
(456) Jiang, Q.; Guo, D.; Lee, B. X.; Van Rhee, A. M.; Kim, Y. C.; Nicholas, R. A.; Schachter, J. B.; Harden, T. K.; Jacobson, K. A. *Mol. Pharmacol.* **1997**, *52*, 499.
(457) Lin, Z.; Shenker, A.; Pearlstein, R. *Protein Eng.* **1997**, *10*, 501.
(458) Perlman, J. H.; Colson, A. O.; Jain, R.; Czyzewski, B.; Cohen, L. A.; Osman, R.; Gershengorn, M. C. *Biochemistry* **1997**, *36*, 15670.
(459) Perlman, J. H.; Colson, A. O.; Wang, W.; Bence, K.; Osman, R.; Gershengorn, M. C. *J. Biol. Chem.* **1997**, *272*, 11937.
(460) Strahs, D.; Weinstein, H. *Protein Eng.* **1997**, *10*, 1019.
(461) Sylte, I.; Chilmonczyk, Z.; Dahl, S. G.; Cybulski, J.; Edvardsen, O. *J. Pharm. Pharmacol .* **1997**, *49*, 698.
(462) Colson, A. O.; Perlman, J. H.; Smolyar, A.; Gershengorn, M. C.; Osman, R. *Biophys. J.* **1998**, *74*, 1087.
(463) Colson, A. O.; Perlman, J. H.; Jinsi-Parimoo, A.; Nussenzveig, D. R.; Osman, R.; Gershengorn, M. C. *Mol. Pharmacol.* **1998**, *54*, 968.
(464) Cotte, N.; Balestre, M. N.; Phalipou, S.; Hibert, M.; Manning, M.; Barberis, C.; Mouillac, B. *J. Biol. Chem.* **1998**, *273*, 29462.
(465) Kim, Y. C.; de Zwart, M.; Chang, L.; Moro, S.; von Frijtag Drabbe Kunzel, J. K.; Melman, N.; AP, I. J.; Jacobson, K. A. *J. Med. Chem.* **1998**, *41*, 2835.

(466) Labbe-Jullie, C.; Barroso, S.; Nicolas-Eteve, D.; Reversat, J. L.; Botto, J. M.; Mazella, J.; Bernassau, J. M.; Kitabgi, P. *J. Biol. Chem.* **1998**, *273*, 16351.
(467) Moro, S.; Li, A. H.; Jacobson, K. A. *J. Chem. Inf. Comput. Sci.* **1998**, *38*, 1239.
(468) Moro, S.; Guo, D.; Camaioni, E.; Boyer, J. L.; Harden, T. K.; Jacobson, K. A. *J. Med. Chem.* **1998**, *41*, 1456.
(469) Prado, G. N.; Mierke, D. F.; Pellegrini, M.; Taylor, L.; Polgar, P. *J. Biol. Chem.* **1998**, *273*, 33548.
(470) Robin-Jagerschmidt, C.; Sylte, I.; Bihoreau, C.; Hendricksen, L.; Calvet, A.; Dahl, S. G.; Benicourt, C. *Mol. Cell. Endocrinol.* **1998**, *139*, 187.
(471) Sylte, I.; Robin-Jagerschmidt, C.; Bihoreau, C.; Hendricksen, L.; Calvet, A.; Benicourt, C.; Dahl, S. G. *J. Mol. Model.* **1998**, *4*, 221.
(472) Donnelly, D.; Maudsley, S.; Gent, J. P.; Moser, R. N.; Hurrell, C. R.; Findlay, J. B. *Biochem. J.* **1999**, *339*, 55.
(473) Filizola, M.; Laakkonen, L.; Loew, G. H. *Protein Eng.* **1999**, *12*, 927.
(474) Li, A. H.; Moro, S.; Forsyth, N.; Melman, N.; Ji, X. D.; Jacobson, K. A. *J. Med. Chem.* **1999**, *42*, 706.
(475) Phalipou, S.; Seyer, R.; Cotte, N.; Breton, C.; Barberis, C.; Hibert, M.; Mouillac, B. *J. Biol. Chem.* **1999**, *274*, 23316.
(476) Rivkees, S. A.; Barbhaiya, H.; AP, I. J. *J. Biol. Chem.* **1999**, *274*, 3617.
(477) Song, Z. H.; Slowey, C. A.; Hurst, D. P.; Reggio, P. H. *Mol. Pharmacol.* **1999**, *56*, 834.
(478) Sylte, I.; Andrianjara, C. R.; Calvet, A.; Pascal, Y.; Dahl, S. G. *Bioorg. Med. Chem.* **1999**, *7*, 2737.
(479) Tao, Q.; McAllister, S. D.; Andreassi, J.; Nowell, K. W.; Cabral, G. A.; Hurst, D. P.; Bachtel, K.; Ekman, M. C.; Reggio, P. H.; Abood, M. E. *Mol. Pharmacol.* **1999**, *55*, 605.
(480) Moro, S.; Hoffmann, C.; Jacobson, K. A. *Biochemistry* **1999**, *38*, 3498.
(481) Salminen, T.; Varis, M.; Nyronen, T.; Pihlavisto, M.; Hoffren, A. M.; Lonnberg, T.; Marjamaki, A.; Frang, H.; Savola, J. M.; Scheinin, M.; Johnson, M. S. *J. Biol. Chem* . **1999**, *274*, 23405.
(482) Kristiansen, K.; Kroeze, W. K.; Willins, D. L.; Gelber, E. I.; Savage, J. E.; Glennon, R. A.; Roth, B. L. *J. Pharmacol. Exp. Ther.* **2000**, *293*, 735.
(483) Nandanan, E.; Jang, S. Y.; Moro, S.; Kim, H. O.; Siddiqui, M. A.; Russ, P.; Marquez, V. E.; Busson, R.; Herdewijn, P.; Harden, T. K.; Boyer, J. L.; Jacobson, K. A. *J. Med. Chem.* **2000**, *43*, 829.
(484) Shapiro, D. A.; Kristiansen, K.; Kroeze, W. K.; Roth, B. L. *Mol. Pharmacol.* **2000**, *58*, 877.
(485) Nyronen, T.; Pihlavisto, M.; Peltonen, J. M.; Hoffren, A. M.; Varis, M.; Salminen, T.; Wurster, S.; Marjamaki, A.; Kanerva, L.; Katainen, E.; Laaksonen, L.; Savola, J. M.; Scheinin, M.; Johnson, M. S. *Mol. Pharmacol.* **2001**, *59*, 1343.
(486) Blaney, F. E.; Raveglia, L. F.; Artico, M.; Cavagnera, S.; Dartois, C.; Farina, C.; Grugni, M.; Gagliardi, S.; Luttmann, M. A.; Martinelli, M.; Nadler, G. M.; Parini, C.; Petrillo, P.; Sarau, H. M.; Scheideler, M. A.; Hay, D. W.; Giardina, G. A. *J. Med. Chem.* **2001**, *44*, 1675.
(487) Bronowska, A.; Chilmonczyk, Z.; Les, A.; Edvardsen, O.; Ostensen, R.; Sylte, I. *J. Comput.-Aided Mol. Des.* **2001**, *15*, 1005.
(488) Bronowska, A.; Les, A.; Chilmonczyk, Z.; Filipek, S.; Edvardsen, O.; Ostensen, R.; Sylte, I. *Bioorg. Med. Chem.* **2001**, *9*, 881.
(489) Carrieri, A.; Centeno, N. B.; Rodrigo, J.; Sanz, F.; Carotti, A. *Proteins* **2001**, *43*, 382.
(490) Da Settimo, F.; Primofiore, G.; Taliani, S.; Marini, A. M.; La Motta, C.; Novellino, E.; Greco, G.; Lavecchia, A.; Trincavelli, L.; Martini, C. *J. Med. Chem.* **2001**, *44*, 316.
(491) Labrou, N. E.; Bhogal, N.; Hurrell, C. R.; Findlay, J. B. *J. Biol. Chem.* **2001**, *276*, 37944.
(492) Sylte, I.; Bronowska, A.; Dahl, S. G. *Eur. J. Pharmacol.* **2001**, *416*, 33.
(493) Brea, J.; Rodrigo, J.; Carrieri, A.; Sanz, F.; Cadavid, M. I.; Enguix, M. J.; Villazon, M.; Mengod, G.; Caro, Y.; Masaguer, C. F.; Ravina, E.; Centeno, N. B.; Carotti, A.; Loza, M. I. *J. Med. Chem.* **2002**, *45*, 54.
(494) Novellino, E.; Abignente, E.; Cosimelli, B.; Greco, G.; Iadanza, M.; Laneri, S.; Lavecchia, A.; Rimoli, M. G.; Settimo, F. D.; Primofiore, G.; Tuscano, D.; Trincavelli, L.; Martini, C. *J. Med. Chem.* **2002**, *45*, 5030.
(495) Wilkes, B. C.; Masaro, L.; Schiller, P. W.; Carpenter, K. A. *J. Med. Chem.* **2002**, *45*, 4410.
(496) Lu, X.; Huang, W.; Worthington, S.; Drabik, P.; Osman, R.; Gershengorn, M. C. *Mol. Pharmacol.* **2004**, *66*, 1192.
(497) Vermeulen, E. S.; Schmidt, A. W.; Sprouse, J. S.; Wikstrom, H. V.; Grol, C. J. *J. Med. Chem.* **2003**, *46*, 5365.
(498) Vermeulen, E. S.; van Smeden, M.; Schmidt, A. W.; Sprouse, J. S.; Wikstrom, H. V.; Grol, C. J. *J. Med. Chem.* **2004**, *47*, 5451.
(499) Dastmalchi, S.; Church, W. B.; Morris, M. B. *BMC Bioinf.* **2008**, *9* (Suppl 1), S14.
(500) Herzyk, P.; Hubbard, R. E. *Biophys. J.* **1995**, *69*, 2419.
(501) Fanelli, F.; Menziani, M. C.; Cocchi, M.; De Benedetti, P. G. *J. Mol. Struct. (THEOCHEM)* **1995**, *333*, 49.
(502) Fanelli, F.; Menziani, M. C.; Scheer, A.; Cotecchia, S.; De Benedetti, P. G. *Methods* **1998**, *14*, 302.
(503) Fanelli, F.; Menziani, M. C.; De Benedetti, P. G. *Bioorg. Med. Chem.* **1995**, *3*, 1465.
(504) Fanelli, F.; Menziani, M. C.; De Benedetti, P. G. *Protein Eng.* **1995**, *8*, 557.
(505) Barlocco, D.; Fanelli, F.; Cignarella, G.; Villa, S.; Cattabeni, F.; Balduini, W.; Cimino, M.; De Benedetti, P. G. *Drug Des. Discovery* **1996**, *14*, 129.
(506) Cavalli, A.; Fanelli, F.; Taddei, C.; De Benedetti, P. G.; Cotecchia, S. *FEBS Lett.* **1996**, *399*, 9.
(507) Barlocco, D.; Cignarella, G.; Fanelli, F.; Vitalis, B.; Matyus, P.; De Benedetti, P. G. *Drug Des. Discovery* **1997**, *14*, 273.
(508) De Benedetti, P. G.; Fanelli, F.; Menziani, M. C.; Cocchi, M.; Testa, R.; Leonardi, A. *Bioorg. Med. Chem.* **1997**, *5*, 809.
(509) Reaper, C. M.; Fanelli, F.; Buckingham, S. D.; Millar, N. S.; Sattelle, D. B. *Recept. Channels* **1998**, *5*, 331.
(510) Fanelli, F.; Menziani, C.; Scheer, A.; Cotecchia, S.; De Benedetti, P. G. *Proteins* **1999**, *37*, 145.
(511) Fanelli, F.; Menziani, M. C.; Scheer, A.; Cotecchia, S.; De Benedetti, P. *Int. J. Quantum Chem.* **1999**, *73*, 71.
(512) Fanelli, F. *J. Mol. Biol.* **2000**, *296*, 1333.
(513) Scheer, A.; Costa, T.; Fanelli, F.; De Benedetti, P. G.; Mhaouty-Kodja, S.; Abuin, L.; Nenniger-Tosato, M.; Cotecchia, S. *Mol. Pharmacol.* **2000**, *57*, 219.
(514) Alkorta, I.; Du, P. *Protein Eng.* **1994**, *7*, 1231.
(515) Alkorta, I.; Loew, G. H. *Protein Eng.* **1996**, *9*, 573.
(516) Donnelly, D.; Findlay, J. B. *Curr. Opin. Struct. Biol.* **1994**, *4*, 582.
(517) Donnelly, D.; Findlay, J. B.; Blundell, T. L. *Recept. Channels* **1994**, *2*, 61.
(518) Du, P.; Salon, J. A.; Tamm, J. A.; Hou, C.; Cui, W.; Walker, M. W.; Adham, N.; Dhanoa, D. S.; Islam, I.; Vaysse, P. J.; Dowling, B.; Shifman, Y.; Boyle, N.; Rueger, H.; Schmidlin, T.; Yamaguchi, Y.; Branchek, T. A.; Weinshank, R. L.; Gluchowski, C. *Protein Eng.* **1997**, *10*, 109.
(519) Prusis, P.; Schioth, H. B.; Muceniece, R.; Herzyk, P.; Afshar, M.; Hubbard, R. E.; Wikberg, J. E. *J. Mol. Graphics Modell.* **1997**, *15*, 307.
(520) Homan, E. J.; Wikstrom, H. V.; Grol, C. J. *Bioorg. Med. Chem.* **1999**, *7*, 1805.
(521) Peitsch, M. C.; Herzyk, P.; Wells, T. N.; Hubbard, R. E. *Recept. Channels* **1996**, *4*, 161.
(522) Czaplewski, C.; Kazmierkiewicz, R.; Ciarkowski, J. *J. Comput.-Aided Mol. Des.* **1998**, *12*, 275.
(523) Czaplewski, C.; Pasenkiewicz-Gierula, M.; Ciarkowski, J. *J. Recept. Signal Transduction Res.* **1999**, *19*, 355.
(524) Politowska, E.; Czaplewski, C.; Ciarkowski, J. *Acta Biochim. Pol.* **1999**, *46*, 581.
(525) Rehwald, M.; Neuschafer-Rube, F.; de Vries, C.; Puschel, G. P. *FEBS Lett.* **1999**, *443*, 357.
(526) Ciarkowski, J.; Drabik, P.; Gieldon, A.; Kazmierkiewicz, R.; Slusarz, R. *Acta Biochim. Pol.* **2001**, *48*, 1203.

(527) Pogozheva, I. D.; Lomize, A. L.; Mosberg, H. I. *Biophys. J.* **1998**, *75*, 612.
(528) Lomize, A. L.; Pogozheva, I. D.; Mosberg, H. I. *J. Comput.-Aided Mol. Des.* **1999**, *13*, 325.
(529) Gieldon, A.; Kazmierkiewicz, R.; Slusarz, R.; Ciarkowski, J. *J. Comput.-Aided Mol. Des.* **2001**, *15*, 1085.
(530) Zhang, L.; DeHaven, R. N.; Goodman, M. *Biochemistry* **2002**, *41*, 61.
(531) Orry, A. J.; Wallace, B. A. *Biophys. J.* **2000**, *79*, 3083.
(532) Filizola, M.; Perez, J. J.; Carteni-Farina, M. *J. Comput.-Aided Mol. Des.* **1998**, *12*, 111.
(533) Filizola, M.; Carteni-Farina, M.; Perez, J. J. *J. Phys. Chem. B* **1999**, *103*, 2520.
(534) Fleishman, S. J.; Harrington, S.; Friesner, R. A.; Honig, B.; Ben-Tal, N. *Biophys. J.* **2004**, *87*, 3448.
(535) Fleishman, S. J.; Ben-Tal, N. *Curr. Opin. Struct. Biol.* **2006**, *16*, 496.
(536) Fleishman, S. J.; Unger, V. M.; Ben-Tal, N. *Trends Biochem. Sci.* **2006**, *31*, 106.
(537) Kovacs, J. A.; Yeager, M.; Abagyan, R. *Biophys. J.* **2007**, *93*, 1950.
(538) Lindert, S.; Staritzbichler, R.; Wotzel, N.; Karakas, M.; Stewart, P. L.; Meiler, J. *Structure* **2009**, *17*, 990.
(539) Floriano, W. B.; Vaidehi, N.; Goddard, W. A., 3rd; Singer, M. S.; Shepherd, G. M. *Proc. Natl. Acad. Sci. U.S.A.* **2000**, *97*, 10712.
(540) Vaidehi, N.; Floriano, W. B.; Trabanino, R.; Hall, S. E.; Freddolino, P.; Choi, E. J.; Zamanakos, G.; Goddard, W. A., III *Proc. Natl. Acad. Sci. U.S.A.* **2002**, *99*, 12622.
(541) Trabanino, R. J.; Hall, S. E.; Vaidehi, N.; Floriano, W. B.; Kam, V. W.; Goddard, W. A., III *Biophys. J.* **2004**, *86*, 1904.
(542) Hummel, P.; Vaidehi, N.; Floriano, W. B.; Hall, S. E.; Goddard, W. A., III *Protein Sci.* **2005**, *14*, 703.
(543) Vaidehi, N.; Schlyer, S.; Trabanino, R. J.; Floriano, W. B.; Abrol, R.; Sharma, S.; Kochanny, M.; Koovakat, S.; Dunning, L.; Liang, M.; Fox, J. M.; de Mendonca, F. L.; Pease, J. E.; Goddard, W. A., III; Horuk, R. *J. Biol. Chem.* **2006**, *281*, 27613.
(544) Heo, J.; Han, S. K.; Vaidehi, N.; Wendel, J.; Kekenes-Huskey, P.; Goddard, W. A., III *ChemBioChem* **2007**, *8*, 1527.
(545) Heo, J.; Vaidehi, N.; Wendel, J.; Goddard, W. A., III *J. Mol. Graphics Modell.* **2007**, *26*, 800.
(546) Ryman-Rasmussen, J. P.; Griffith, A.; Oloff, S.; Vaidehi, N.; Brown, J. T.; Goddard, W. A., III; Mailman, R. B. *Neuropharmacology* **2007**, *52*, 562.
(547) Hall, S. E.; Mao, A.; Nicolaidou, V.; Finelli, M.; Wise, E. L.; Nedjai, B.; Kanjanapangka, J.; Harirchian, P.; Chen, D.; Selchau, V.; Ribeiro, S.; Schyler, S.; Pease, J. E.; Horuk, R.; Vaidehi, N. *Mol. Pharmacol.* **2009**, *75*, 1325.
(548) Schertler, G. F. *Eye* **1998**, *12* (Pt 3b), 504.
(549) Vriend, G. *J. Mol. Graphics* **1990**, *8*, 52.
(550) Kim, S. K.; Li, Y.; Abrol, R.; Heo, J.; Goddard, W. A., III *J. Chem. Inf. Model.* **2011**, *51*, 420.
(551) Bhattacharya, S.; Hall, S. E.; Li, H.; Vaidehi, N. *Biophys. J.* **2008**, *94*, 2027.
(552) Lam, A. R.; Bhattacharya, S.; Patel, K.; Hall, S. E.; Mao, A.; Vaidehi, N. *J. Chem. Inf. Model.* **2011**, *51*, 139.
(553) Goddard, W. A., III; Kim, S. K.; Li, Y.; Trzaskowski, B.; Griffith, A. R.; Abrol, R. *J. Struct. Biol.* **2010**, *170*, 10.
(554) Michino, M.; Abola, E.; Brooks, C. L., III; Dixon, J. S.; Moult, J.; Stevens, R. C. *Nature Rev. Drug Discovery* **2009**, *8*, 455.
(555) Kim, S. K.; Riley, L.; Abrol, R.; Jacobson, K. A.; Goddard, W. A., III *Proteins* **2011**, *79*, 1878.
(556) Shacham, S.; Marantz, Y.; Bar-Haim, S.; Kalid, O.; Warshaviak, D.; Avisar, N.; Inbal, B.; Heifetz, A.; Fichman, M.; Topf, M.; Naor, Z.; Noiman, S.; Becker, O. M. *Proteins* **2004**, *57*, 51.
(557) Becker, O. M.; Shacham, S.; Marantz, Y.; Noiman, S. *Curr. Opin. Drug Discovery Dev.* **2003**, *6*, 353.
(558) Sale, K.; Faulon, J. L.; Gray, G. A.; Schoeniger, J. S.; Young, M. M. *Protein Sci.* **2004**, *13*, 2613.
(559) Nikiforovich, G. V.; Galaktionov, S.; Balodis, J.; Marshall, G. R. *Acta Biochim. Pol.* **2001**, *48*, 53.
(560) Nikiforovich, G. V.; Mihalik, B.; Catt, K. J.; Marshall, G. R. *J. Pept. Res.* **2005**, *66*, 236.
(561) Nikiforovich, G. V.; Zhang, M.; Yang, Q.; Jagadeesh, G.; Chen, H. C.; Hunyady, L.; Marshall, G. R.; Catt, K. J. *Chem. Biol. Drug Des.* **2006**, *68*, 239.
(562) Chen, C. C.; Chen, C. M. *J. Struct. Biol.* **2009**, *165*, 37.
(563) Nikiforovich, G. V.; Marshall, G. R.; Baranski, T. J. *Proteins* **2011**, *79*, 787.
(564) Park, Y.; Helms, V. *Proteins* **2006**, *64*, 895.
(565) Zhang, Y.; Devries, M. E.; Skolnick, J. *PLoS Comput. Biol.* **2006**, *2*, e13.
(566) Kufareva, I.; Rueda, M.; Katritch, V.; Stevens, R. C.; Abagyan, R. *Structure* **2011**, *19*, 1108.
(567) Gether, U.; Ballesteros, J. A.; Seifert, R.; Sanders-Bush, E.; Weinstein, H.; Kobilka, B. K. *J. Biol. Chem.* **1997**, *272*, 2587.
(568) Gether, U.; Lin, S.; Ghanouni, P.; Ballesteros, J. A.; Weinstein, H.; Kobilka, B. K. *EMBO J.* **1997**, *16*, 6737.
(569) Javitch, J. A.; Ballesteros, J. A.; Weinstein, H.; Chen, J. *Biochemistry* **1998**, *37*, 998.
(570) Javitch, J. A.; Shi, L.; Simpson, M. M.; Chen, J.; Chiappa, V.; Visiers, I.; Weinstein, H.; Ballesteros, J. A. *Biochemistry* **2000**, *39*, 12190.
(571) Sansom, M. S.; Weinstein, H. *Trends Pharmacol. Sci.* **2000**, *21*, 445.
(572) Ballesteros, J. A.; Shi, L.; Javitch, J. A. *Mol. Pharmacol.* **2001**, *60*, 1.
(573) Govaerts, C.; Blanpain, C.; Deupi, X.; Ballet, S.; Ballesteros, J. A.; Wodak, S. J.; Vassart, G.; Pardo, L.; Parmentier, M. *J. Biol. Chem.* **2001**, *276*, 13217.
(574) Shi, L.; Simpson, M. M.; Ballesteros, J. A.; Javitch, J. A. *Biochemistry* **2001**, *40*, 12339.
(575) Shi, L.; Liapakis, G.; Xu, R.; Guarnieri, F.; Ballesteros, J. A.; Javitch, J. A. *J. Biol. Chem.* **2002**, *277*, 40989.
(576) Visiers, I.; Hassan, S. A.; Weinstein, H. *Protein Eng.* **2001**, *14*, 409.
(577) Barnett-Norris, J.; Hurst, D. P.; Lynch, D. L.; Guarnieri, F.; Makriyannis, A.; Reggio, P. H. *J. Med. Chem.* **2002**, *45*, 3649.
(578) Lopez-Rodriguez, M. L.; Vicente, B.; Deupi, X.; Barrondo, S.; Olivella, M.; Morcillo, M. J.; Behamu, B.; Ballesteros, J. A.; Salles, J.; Pardo, L. *Mol. Pharmacol.* **2002**, *62*, 15.
(579) Singh, R.; Hurst, D. P.; Barnett-Norris, J.; Lynch, D. L.; Reggio, P. H.; Guarnieri, F. *J. Pept. Res.* **2002**, *60*, 357.
(580) Lin, S. W.; Sakmar, T. P. *Biochemistry* **1996**, *35*, 11149.
(581) Zhang, R.; Hurst, D. P.; Barnett-Norris, J.; Reggio, P. H.; Song, Z. H. *Mol. Pharmacol.* **2005**, *68*, 69.
(582) Lynch, D. L.; Reggio, P. H. *J. Comput.-Aided Mol. Des.* **2006**, *20*, 495.
(583) Ballesteros, J.; Palczewski, K. *Curr. Opin. Drug Discovery Dev.* **2001**, *4*, 561.
(584) Sakmar, T. P. *Curr. Opin. Cell. Biol.* **2002**, *14*, 189.
(585) Archer, E.; Maigret, B.; Escrieut, C.; Pradayrol, L.; Fourmy, D. *Trends Pharmacol. Sci.* **2003**, *24*, 36.
(586) Oliveira, L.; Hulsen, T.; Lutje Hulsik, D.; Paiva, A. C.; Vriend, G. *FEBS Lett.* **2004**, *564*, 269.
(587) Parker, M. S.; Parker, S. L. *Amino Acids* **2010**, *38*, 1.
(588) Bissantz, C.; Logean, A.; Rognan, D. *J. Chem. Inf. Comput. Sci.* **2004**, *44*, 1162.
(589) Moyle, W. R.; Campbell, R. K.; Rao, S. N.; Ayad, N. G.; Bernard, M. P.; Han, Y.; Wang, Y. *J. Biol. Chem.* **1995**, *270*, 20020.
(590) Bhowmick, N.; Huang, J.; Puett, D.; Isaacs, N. W.; Lapthorn, A. J. *Mol. Endocrinol.* **1996**, *10*, 1147.
(591) Smits, G.; Campillo, M.; Govaerts, C.; Janssens, V.; Richter, C.; Vassart, G.; Pardo, L.; Costagliola, S. *EMBO J.* **2003**, *22*, 2692.
(592) Moyle, W. R.; Xing, Y.; Lin, W.; Cao, D.; Myers, R. V.; Kerrigan, J. E.; Bernard, M. P. *J. Biol. Chem.* **2004**, *279*, 44442.
(593) Nunez Miguel, R.; Sanders, J.; Jeffreys, J.; Depraetere, H.; Evans, M.; Richards, T.; Blundell, T. L.; Rees Smith, B.; Furmaniak, J. *Thyroid* **2004**, *14*, 991.

(594) Sanders, J.; Chirgadze, D. Y.; Sanders, P.; Baker, S.; Sullivan, A.; Bhardwaja, A.; Bolton, J.; Reeve, M.; Nakatake, N.; Evans, M.; Richards, T.; Powell, M.; Miguel, R. N.; Blundell, T. L.; Furmaniak, J.; Smith, B. R. *Thyroid* **2007**, *17*, 395.
(595) Fiser, A.; Do, R. K.; Sali, A. *Protein Sci.* **2000**, *9*, 1753.
(596) Mehler, E. L.; Periole, X.; Hassan, S. A.; Weinstein, H. *J. Comput.-Aided Mol. Des.* **2002**, *16*, 841.
(597) Kortagere, S.; Roy, A.; Mehler, E. L. *J. Comput.-Aided Mol. Des.* **2006**, *20*, 427.
(598) Mehler, E. L.; Hassan, S. A.; Kortagere, S.; Weinstein, H. *Proteins* **2006**, *64*, 673.
(599) Nikiforovich, G. V.; Taylor, C. M.; Marshall, G. R.; Baranski, T. J. *Proteins* **2010**, *78*, 271.
(600) Shan, J.; Weinstein, H.; Mehler, E. L. *Biochemistry* **2010**, *49*, 10691.
(601) Nikiforovich, G. V.; Taylor, C. M.; Marshall, G. R.; Baranski, T. J. *Proc. Natl. Acad. Sci. U.S.A.* **2011**, *108*, E341.
(602) Goldfeld, D. A.; Zhu, K.; Beuming, T.; Friesner, R. A. *Proc. Natl. Acad. Sci. U.S.A.* **2011**, *108*, 8275.
(603) Carrieri, A.; Piergentili, A.; Del Bello, F.; Giannella, M.; Pigini, M.; Leonardi, A.; Fanelli, F.; Quaglia, W. *Bioorg. Med. Chem.* **2010**, *18*, 7065.
(604) Shim, J. Y.; Rudd, J.; Ding, T. T. *Proteins* **2011**, *79*, 581.
(605) Canals, M.; Marcellino, D.; Fanelli, F.; Ciruela, F.; De Benedetti, P.; Goldberg, S. R.; Neve, K.; Fuxe, K.; Agnati, L. F.; Woods, A. S.; Ferre, S.; Lluis, C.; Bouvier, M.; Franco, R. *J. Biol. Chem.* **2003**, *278*, 46741.
(606) Bellot, G.; Granier, S.; Bourguet, W.; Seyer, R.; Rahmeh, R.; Mouillac, B.; Pascal, R.; Mendre, C.; Demene, H. *J. Mol. Biol.* **2009**, *388*, 491.
(607) Demars, G.; Fanelli, F.; Puett, D. *Mol. Endocrinol.* **2011**, *25*, 1416.
(608) Vitale, R. M.; Pedone, C.; De Benedetti, P. G.; Fanelli, F. *Proteins* **2004**, *56*, 430.
(609) Rohl, C. A.; Strauss, C. E.; Chivian, D.; Baker, D. *Proteins* **2004**, *55*, 656.
(610) Fernandez-Fuentes, N.; Oliva, B.; Fiser, A. *Nucleic Acids Res.* **2006**, *34*, 2085.
(611) Rossi, K. A.; Weigelt, C. A.; Nayeem, A.; Krystek, S. R., Jr. *Protein Sci.* **2007**, *16*, 1999.
(612) Olson, M. A.; Feig, M.; Brooks, C. L., III *J. Comput. Chem.* **2008**, *29*, 820.
(613) Soto, C. S.; Fasnacht, M.; Zhu, J.; Forrest, L.; Honig, B. *Proteins* **2008**, *70*, 834.
(614) Fanelli, F.; Puett, D. *Endocrine* **2002**, *18*, 285.
(615) Chothia, C.; Lesk, A. M. *EMBO J.* **1986**, *5*, 823.
(616) Pedretti, A.; Villa, M.; Pallavicini, M.; Valoti, E.; Vistoli, G. *J. Med. Chem.* **2006**, *49*, 3077.
(617) Mobarec, J. C.; Sanchez, R.; Filizola, M. *J. Med. Chem.* **2009**, *52*, 5207.
(618) Yarnitzky, T.; Levit, A.; Niv, M. Y. *Curr. Opin. Drug Discovery Dev.* **2010**, *13*, 317.
(619) Forrest, L. R.; Tang, C. L.; Honig, B. *Biophys. J.* **2006**, *91*, 508.
(620) Sherbiny, F. F.; Schiedel, A. C.; Maass, A.; Muller, C. E. *J. Comput.-Aided Mol. Des.* **2009**, *23*, 807.
(621) Nemoto, W.; Fukui, K.; Toh, H. *J. Recept. Signal Transduction Res.* **2009**, *29*, 312.
(622) Qian, B.; Raman, S.; Das, R.; Bradley, P.; McCoy, A. J.; Read, R. J.; Baker, D. *Nature* **2007**, *450*, 259.
(623) Kimura, S. R.; Tebben, A. J.; Langley, D. R. *Proteins* **2008**, *71*, 1919.
(624) Michino, M.; Chen, J.; Stevens, R. C.; Brooks, C. L., III *Proteins* **2010**, *78*, 2189.
(625) Rai, B. K.; Tawa, G. J.; Katz, A. H.; Humblet, C. *Proteins* **2010**, *78*, 457.
(626) Nemoto, W.; Imai, T.; Takahashi, T.; Kikuchi, T.; Fujita, N. *Protein J.* **2004**, *23*, 427.
(627) Katritch, V.; Kufareva, I.; Abagyan, R. *Neuropharmacology* **2011**, *60*, 108.
(628) Katritch, V.; Rueda, M.; Lam, P. C.; Yeager, M.; Abagyan, R. *Proteins* **2010**, *78*, 197.
(629) Jacobson, K. A.; Gao, Z. G.; Chen, A.; Barak, D.; Kim, S. A.; Lee, K.; Link, A.; Rompaey, P. V.; van Calenbergh, S.; Liang, B. T. *J. Med. Chem.* **2001**, *44*, 4125.
(630) Lopez-Rodriguez, M. L.; Morcillo, M. J.; Fernandez, E.; Rosado, M. L.; Pardo, L.; Schaper, K. *J. Med. Chem.* **2001**, *44*, 198.
(631) Lopez-Rodriguez, M. L.; Murcia, M.; Benhamu, B.; Olivella, M.; Campillo, M.; Pardo, L. *J. Comput.-Aided Mol. Des.* **2001**, *15*, 1025.
(632) Baraldi, P. G.; Cacciari, B.; Moro, S.; Spalluto, G.; Pastorin, G.; Da Ros, T.; Klotz, K. N.; Varani, K.; Gessi, S.; Borea, P. A. *J. Med. Chem.* **2002**, *45*, 770.
(633) Filizola, M.; Weinstein, H. *Biopolymers* **2002**, *66*, 317.
(634) Furukawa, H.; Hamada, T.; Hayashi, M. K.; Haga, T.; Muto, Y.; Hirota, H.; Yokoyama, S.; Nagasawa, K.; Ishiguro, M. *Mol. Pharmacol.* **2002**, *62*, 778.
(635) Gao, Z. G.; Chen, A.; Barak, D.; Kim, S. K.; Muller, C. E.; Jacobson, K. A. *J. Biol. Chem.* **2002**, *277*, 19056.
(636) Gao, Z. G.; Kim, S. K.; Biadatti, T.; Chen, W.; Lee, K.; Barak, D.; Kim, S. G.; Johnson, C. R.; Jacobson, K. A. *J. Med. Chem.* **2002**, *45*, 4471.
(637) Lequin, O.; Bolbach, G.; Frank, F.; Convert, O.; Girault-Lagrange, S.; Chassaing, G.; Lavielle, S.; Sagan, S. *J. Biol. Chem.* **2002**, *277*, 22386.
(638) Maconi, A.; Pastorin, G.; Da Ros, T.; Spalluto, G.; Gao, Z. G.; Jacobson, K. A.; Baraldi, P. G.; Cacciari, B.; Varani, K.; Moro, S.; Borea, P. A. *J. Med. Chem.* **2002**, *45*, 3579.
(639) Moro, S.; Jacobson, K. A. *Curr. Pharm. Des.* **2002**, *8*, 2401.
(640) Paterlini, M. G. *Biophys. J.* **2002**, *83*, 3012.
(641) Shin, N.; Coates, E.; Murgolo, N. J.; Morse, K. L.; Bayne, M.; Strader, C. D.; Monsma, F. J., Jr. *Mol. Pharmacol.* **2002**, *62*, 38.
(642) Ulfers, A. L.; Piserchio, A.; Mierke, D. F. *Biopolymers* **2002**, *66*, 339.
(643) Johren, K.; Holtje, H. D. *J. Comput.-Aided Mol. Des.* **2002**, *16*, 795.
(644) Anzini, M.; Canullo, L.; Braile, C.; Cappelli, A.; Gallelli, A.; Vomero, S.; Menziani, M. C.; De Benedetti, P. G.; Rizzo, M.; Collina, S.; Azzolina, O.; Sbacchi, M.; Ghelardini, C.; Galeotti, N. *J. Med. Chem.* **2003**, *46*, 3853.
(645) Berkhout, T. A.; Blaney, F. E.; Bridges, A. M.; Cooper, D. G.; Forbes, I. T.; Gribble, A. D.; Groot, P. H.; Hardy, A.; Ife, R. J.; Kaur, R.; Moores, K. E.; Shillito, H.; Willetts, J.; Witherington, J. *J. Med. Chem.* **2003**, *46*, 4070.
(646) Bissantz, C.; Bernard, P.; Hibert, M.; Rognan, D. *Proteins* **2003**, *50*, 5.
(647) Broer, B. M.; Gurrath, M.; Holtje, H. D. *J. Comput.-Aided Mol. Des.* **2003**, *17*, 739.
(648) Ebersole, B. J.; Visiers, I.; Weinstein, H.; Sealfon, S. C. *Mol. Pharmacol.* **2003**, *63*, 36.
(649) Gao, Z. G.; Kim, S. K.; Gross, A. S.; Chen, A.; Blaustein, J. B.; Jacobson, K. A. *Mol. Pharmacol.* **2003**, *63*, 1021.
(650) Kaltenbock, A.; Hibert, M.; Langer, T. *Recept. Channels* **2003**, *9*, 93.
(651) Kim, S. K.; Gao, Z. G.; Van Rompaey, P.; Gross, A. S.; Chen, A.; Van Calenbergh, S.; Jacobson, K. A. *J. Med. Chem.* **2003**, *46*, 4847.
(652) Tahtaoui, C.; Balestre, M. N.; Klotz, P.; Rognan, D.; Barberis, C.; Mouillac, B.; Hibert, M. *J. Biol. Chem.* **2003**, *278*, 40010.
(653) Trent, J. O.; Wang, Z. X.; Murray, J. L.; Shao, W.; Tamamura, H.; Fujii, N.; Peiper, S. C. *J. Biol. Chem.* **2003**, *278*, 47136.
(654) Xie, X. Q.; Chen, J. Z.; Billings, E. M. *Proteins* **2003**, *53*, 307.
(655) Gieldon, A.; Kazmierkiewicz, R.; Slusarz, R.; Pasenkiewicz-Gierula, M.; Ciarkowski, J. *J. Mol. Model. (Online)* **2003**, *9*, 372.
(656) Munshi, U. M.; Pogozheva, I. D.; Menon, K. M. *Biochemistry* **2003**, *42*, 3708.
(657) Shim, J. Y.; Welsh, W. J.; Howlett, A. C. *Biopolymers* **2003**, *71*, 169.

(658) Lopez-Rodriguez, M. L.; Porras, E.; Morcillo, M. J.; Benhamu, B.; Soto, L. J.; Lavandera, J. L.; Ramos, J. A.; Olivella, M.; Campillo, M.; Pardo, L. *J. Med. Chem.* **2003**, *46*, 5638.
(659) Aburi, M.; Smith, P. E. *Protein Sci.* **2004**, *13*, 1997.
(660) Bhogal, N.; Blaney, F. E.; Ingley, P. M.; Rees, J.; Findlay, J. B. *Biochemistry* **2004**, *43*, 3027.
(661) Bondensgaard, K.; Ankersen, M.; Thogersen, H.; Hansen, B. S.; Wulff, B. S.; Bywater, R. P. *J. Med. Chem.* **2004**, *47*, 888.
(662) Cappelli, A.; Pericot Mohr, Gl, G.; Gallelli, A.; Rizzo, M.; Anzini, M.; Vomero, S.; Mennuni, L.; Ferrari, F.; Makovec, F.; Menziani, M. C.; De Benedetti, P. G.; Giorgi, G. *J. Med. Chem.* **2004**, *47*, 2574.
(663) Colotta, V.; Catarzi, D.; Varano, F.; Calabri, F. R.; Lenzi, O.; Filacchioni, G.; Martini, C.; Trincavelli, L.; Deflorian, F.; Moro, S. *J. Med. Chem.* **2004**, *47*, 3580.
(664) Costanzi, S.; Mamedova, L.; Gao, Z. G.; Jacobson, K. A. *J. Med. Chem.* **2004**, *47*, 5393.
(665) Giragossian, C.; Schaschke, N.; Moroder, L.; Mierke, D. F. *Biochemistry* **2004**, *43*, 2724.
(666) Gutierrez-de-Teran, H.; Centeno, N. B.; Pastor, M.; Sanz, F. *Proteins* **2004**, *54*, 705.
(667) Gutierrez-de-Teran, H.; Pastor, M.; Centeno, N. B.; Aqvist, J.; Sanz, F. *ChemBioChem* **2004**, *5*, 841.
(668) Leonardi, A.; Barlocco, D.; Montesano, F.; Cignarella, G.; Motta, G.; Testa, R.; Poggesi, E.; Seeber, M.; De Benedetti, P. G.; Fanelli, F. *J. Med. Chem.* **2004**, *47*, 1900.
(669) Rosenkilde, M. M.; Gerlach, L. O.; Jakobsen, J. S.; Skerlj, R. T.; Bridger, G. J.; Schwartz, T. W. *J. Biol. Chem.* **2004**, *279*, 3033.
(670) Wilczynski, A.; Wang, X. S.; Bauzo, R. M.; Xiang, Z.; Shaw, A. M.; Millard, W. J.; Richards, N. G.; Edison, A. S.; Haskell-Luevano, C. *J. Med. Chem.* **2004**, *47*, 5662.
(671) Wilczynski, A.; Wang, X. S.; Joseph, C. G.; Xiang, Z.; Bauzo, R. M.; Scott, J. W.; Sorensen, N. B.; Shaw, A. M.; Millard, W. J.; Richards, N. G.; Haskell-Luevano, C. *J. Med. Chem.* **2004**, *47*, 2194.
(672) Evers, A.; Klebe, G. *J. Med. Chem.* **2004**, *47*, 5381.
(673) Fowler, C. B.; Pogozheva, I. D.; LeVine, H., III; Mosberg, H. I. *Biochemistry* **2004**, *43*, 8700.
(674) Han, S. J.; Hamdan, F. F.; Kim, S. K.; Jacobson, K. A.; Brichta, L.; Bloodworth, L. M.; Li, J. H.; Wess, J. *J. Biol. Chem.* **2005**, *280*, 24870.
(675) Kinsella, G. K.; Rozas, I.; Watson, G. W. *Biochem. Biophys. Res. Commun.* **2004**, *324*, 916.
(676) Kiss, R.; Kovari, Z.; Keseru, G. M. *Eur. J. Med. Chem.* **2004**, *39*, 959.
(677) Major, D. T.; Fischer, B. *J. Med. Chem.* **2004**, *47*, 4391.
(678) Mazna, P.; Obsilova, V.; Jelinkova, I.; Balik, A.; Berka, K.; Sovova, Z.; Ettrich, R.; Svoboda, P.; Obsil, T.; Teisinger, J. *J. Neurochem.* **2004**, *91*, 836.
(679) Salo, O. M.; Lahtela-Kakkonen, M.; Gynther, J.; Jarvinen, T.; Poso, A. *J. Med. Chem.* **2004**, *47*, 3048.
(680) Santos, E. L.; Pesquero, J. B.; Oliveira, L.; Paiva, A. C.; Costa-Neto, C. M. *Regul. Pept.* **2004**, *119*, 183.
(681) Xu, Y.; Liu, H.; Niu, C.; Luo, C.; Luo, X.; Shen, J.; Chen, K.; Jiang, H. *Bioorg. Med. Chem.* **2004**, *12*, 6193.
(682) Zhang, Y.; Sham, Y. Y.; Rajamani, R.; Gao, J.; Portoghese, P. S. *ChemBioChem* **2005**, *6*, 853.
(683) Allegretti, M.; Bertini, R.; Cesta, M. C.; Bizzarri, C.; Di Bitondo, R.; Di Cioccio, V.; Galliera, E.; Berdini, V.; Topai, A.; Zampella, G.; Russo, V.; Di Bello, N.; Nano, G.; Nicolini, L.; Locati, M.; Fantucci, P.; Florio, S.; Colotta, F. *J. Med. Chem.* **2005**, *48*, 4312.
(684) Ambrosio, C.; Molinari, P.; Fanelli, F.; Chuman, Y.; Sbraccia, M.; Ugur, O.; Costa, T. *J. Biol. Chem.* **2005**, *280*, 23464.
(685) Boeckler, F.; Lanig, H.; Gmeiner, P. *J. Med. Chem.* **2005**, *48*, 694.
(686) Cappellacci, L.; Franchetti, P.; Pasqualini, M.; Petrelli, R.; Vita, P.; Lavecchia, A.; Novellino, E.; Costa, B.; Martini, C.; Klotz, K. N.; Grifantini, M. *J. Med. Chem.* **2005**, *48*, 1550.
(687) Catarzi, D.; Colotta, V.; Varano, F.; Calabri, F. R.; Lenzi, O.; Filacchioni, G.; Trincavelli, L.; Martini, C.; Tralli, A.; Montopoli, C.; Moro, S. *Bioorg. Med. Chem.* **2005**, *13*, 705.
(688) Chai, B. X.; Pogozheva, I. D.; Lai, Y. M.; Li, J. Y.; Neubig, R. R.; Mosberg, H. I.; Gantz, I. *Biochemistry* **2005**, *44*, 3418.
(689) Ha, S. N.; Hey, P. J.; Ransom, R. W.; Harrell, C. M., Jr.; Murphy, K. L.; Chang, R.; Chen, T. B.; Su, D. S.; Markowitz, M. K.; Bock, M. G.; Freidinger, R. M.; Hess, F. J. *Biochem. Biophys. Res. Commun.* **2005**, *331*, 159.
(690) Hjerde, E.; Dahl, S. G.; Sylte, I. *Eur. J. Med. Chem.* **2005**, *40*, 185.
(691) Johren, K.; Holtje, H. D. *Arch. Pharm. (Weinheim, Germany)* **2005**, *338*, 260.
(692) Jongejan, A.; Bruysters, M.; Ballesteros, J.; Haaksma, E.; Bakker, R. A.; Pardo, L.; Leurs, R. *Nature Chem. Biol.* **2005**, *1*, 98.
(693) Jongejan, A.; Leurs, R. *Arch. Pharm. (Weinheim, Germany)* **2005**, *338*, 248.
(694) Lavecchia, A.; Cosconati, S.; Novellino, E. *J. Med. Chem.* **2005**, *48*, 2480.
(695) Lopez-Rodriguez, M. L.; Benhamu, B.; de la Fuente, T.; Sanz, A.; Pardo, L.; Campillo, M. *J. Med. Chem.* **2005**, *48*, 4216.
(696) Lopez-Rodriguez, M. L.; Morcillo, M. J.; Fernandez, E.; Benhamu, B.; Tejada, I.; Ayala, D.; Viso, A.; Campillo, M.; Pardo, L.; Delgado, M.; Manzanares, J.; Fuentes, J. A. *J. Med. Chem.* **2005**, *48*, 2548.
(697) Moro, S.; Braiuca, P.; Deflorian, F.; Ferrari, C.; Pastorin, G.; Cacciari, B.; Baraldi, P. G.; Varani, K.; Borea, P. A.; Spalluto, G. *J. Med. Chem.* **2005**, *48*, 152.
(698) Rivara, S.; Lorenzi, S.; Mor, M.; Plazzi, P. V.; Spadoni, G.; Bedini, A.; Tarzia, G. *J. Med. Chem.* **2005**, *48*, 4049.
(699) Soderhall, J. A.; Polymeropoulos, E. E.; Paulini, K.; Gunther, E.; Kuhne, R. *Biochem. Biophys. Res. Commun.* **2005**, *333*, 568.
(700) Urizar, E.; Montanelli, L.; Loy, T.; Bonomi, M.; Swillens, S.; Gales, C.; Bouvier, M.; Smits, G.; Vassart, G.; Costagliola, S. *EMBO J.* **2005**, *24*, 1954.
(701) Xhaard, H.; Nyronen, T.; Rantanen, V. V.; Ruuskanen, J. O.; Laurila, J.; Salminen, T.; Scheinin, M.; Johnson, M. S. *J. Struct. Biol.* **2005**, *150*, 126.
(702) Montero, C.; Campillo, N. E.; Goya, P.; Paez, J. A. *Eur. J. Med. Chem.* **2005**, *40*, 75.
(703) Jardon-Valadez, E.; Ulloa-Aguirre, A.; Pineiro, A. *J. Phys. Chem. B* **2008**, *112*, 10704.
(704) Punta, M.; Forrest, L. R.; Bigelow, H.; Kernytsky, A.; Liu, J.; Rost, B. *Methods* **2007**, *41*, 460.
(705) Costanzi, S. *J. Med. Chem.* **2008**, *51*, 2907.
(706) Kenakin, T. *FASEB J.* **2001**, *15*, 598.
(707) Leach, K.; Sexton, P. M.; Christopoulos, A. *Trends Pharmacol. Sci.* **2007**, *28*, 382.
(708) Gao, Z. G.; Jacobson, K. A. *Drug Discovery Today* **2006**, *11*, 191.
(709) May, L. T.; Leach, K.; Sexton, P. M.; Christopoulos, A. *Annu. Rev. Pharmacol. Toxicol.* **2007**, *47*, 1.
(710) Raddatz, R.; Schaffhauser, H.; Marino, M. J. *Biochem. Pharmacol.* **2007**, *74*, 383.
(711) Bridges, T. M.; Lindsley, C. W. *ACS Chem. Biol.* **2008**, *3*, 530.
(712) Conn, P. J.; Christopoulos, A.; Lindsley, C. W. *Nature Rev. Drug Discovery* **2009**, *8*, 41.
(713) Goblyos, A.; Ijzerman, A. P. *Biochim. Biophys. Acta* **2011**, *1808*, 1309.
(714) Keov, P.; Sexton, P. M.; Christopoulos, A. *Neuropharmacology* **2010**, *60*, 24.
(715) May, L. T.; Self, T. J.; Briddon, S. J.; Hill, S. J. *Mol. Pharmacol.* **2010**, *78*, 511.
(716) Smith, N. J.; Bennett, K. A.; Milligan, G. *Mol. Cell. Endocrinol.* **2010**, *331*, 241.
(717) Urwyler, S. *Pharmacol. Rev.* **2011**, *63*, 59.
(718) Valant, C.; Sexton, P. M.; Christopoulos, A. *Mol. Interventions* **2009**, *9*, 125.
(719) Kenakin, T. *Nature Rev. Drug Discovery* **2002**, *1*, 103.
(720) De Lean, A.; Stadel, J. M.; Lefkowitz, R. J. *J. Biol. Chem.* **1980**, *255*, 7108.
(721) Costa, T.; Ogino, Y.; Munson, P. J.; Onaran, H. O.; Rodbard, D. *Mol. Pharmacol.* **1992**, *41*, 549.

(722) Samama, P.; Cotecchia, S.; Costa, T.; Lefkowitz, R. J. *J. Biol. Chem.* **1993**, *268*, 4625.
(723) Weiss, J. M.; Morgan, P. H.; Lutz, M. W.; Kenakin, T. *J. Theor. Biol.* **1996**, *178*, 151.
(724) Weiss, J. M.; Morgan, P. H.; Lutz, M. W.; Kenakin, T. *J. Theor. Biol.* **1996**, *178*, 169.
(725) Weiss, J. M.; Morgan, P. H.; Lutz, M. W.; Kenakin, T. *J. Theor. Biol.* **1996**, *181*, 381.
(726) Costa, T.; Herz, A. *Proc. Natl. Acad. Sci. U.S.A.* **1989**, *86*, 7321.
(727) Tian, W. N.; Duzic, E.; Lanier, S. M.; Deth, R. C. *Mol. Pharmacol.* **1994**, *45*, 524.
(728) Agnati, L. F.; Fuxe, K.; Ferre, S. *Trends Biochem. Sci.* **2005**, *30*, 188.
(729) Durroux, T. *Trends Pharmacol. Sci.* **2005**, *26*, 376.
(730) Perez, D. M.; Karnik, S. S. *Pharmacol. Rev.* **2005**, *57*, 147.
(731) Kenakin, T. *Mol. Pharmacol.* **2007**, *72*, 1393.
(732) Urban, J. D.; Clarke, W. P.; von Zastrow, M.; Nichols, D. E.; Kobilka, B.; Weinstein, H.; Javitch, J. A.; Roth, B. L.; Christopoulos, A.; Sexton, P. M.; Miller, K. J.; Spedding, M.; Mailman, R. B. *J. Pharmacol. Exp. Ther.* **2007**, *320*, 1.
(733) Kenakin, T. *Trends Pharmacol. Sci.* **2007**, *28*, 407.
(734) Hoffmann, C.; Zurn, A.; Bunemann, M.; Lohse, M. J. *Br. J. Pharmacol.* **2008**, *153* (Suppl 1), S358.
(735) Rajagopal, S.; Rajagopal, K.; Lefkowitz, R. J. *Nature Rev. Drug Discovery* **2010**, *9*, 373.
(736) Zheng, H.; Loh, H. H.; Law, P. Y. *IUBMB Life* **2010**, *62*, 112.
(737) Vaidehi, N.; Kenakin, T. *Curr. Opin. Pharmacol.* **2010**, *10*, 775.
(738) Onaran, H. O.; Costa, T. *Ann. N.Y. Acad. Sci.* **1997**, *812*, 98.
(739) Onaran, H. O.; Scheer, A.; Cotecchia, S.; Costa, T. In *Handbook of Experimental Pharmacology*; Kenakin, T., Angus, J., Eds.; Springer: Heidelberg, 2000; Vol. 148.
(740) Gether, U.; Lin, S.; Kobilka, B. K. *J. Biol. Chem.* **1995**, *270*, 28268.
(741) Ghanouni, P.; Gryczynski, Z.; Steenhuis, J. J.; Lee, T. W.; Farrens, D. L.; Lakowicz, J. R.; Kobilka, B. K. *J. Biol. Chem.* **2001**, *276*, 24433.
(742) Ghanouni, P.; Steenhuis, J. J.; Farrens, D. L.; Kobilka, B. K. *Proc. Natl. Acad. Sci. U.S.A.* **2001**, *98*, 5997.
(743) Baneres, J. L.; Martin, A.; Hullot, P.; Girard, J. P.; Rossi, J. C.; Parello, J. *J. Mol. Biol.* **2003**, *329*, 801.
(744) Kobilka, B. K.; Deupi, X. *Trends Pharmacol. Sci.* **2007**, *28*, 397.
(745) Deupi, X.; Kobilka, B. K. *Physiology (Bethesda)* **2010**, *25*, 293.
(746) Kobilka, B. *Mol. Pharmacol.* **2004**, *65*, 1060.
(747) Swaminath, G.; Xiang, Y.; Lee, T. W.; Steenhuis, J.; Parnot, C.; Kobilka, B. K. *J. Biol. Chem.* **2004**, *279*, 686.
(748) Dell'Orco, D.; Schmidt, H.; Mariani, S.; Fanelli, F. *Mol. Biosyst.* **2009**, *5*, 1232.
(749) Heitzler, D.; Crepieux, P.; Poupon, A.; Clement, F.; Fages, F.; Reiter, E. *C. R. Biol.* **2009**, *332*, 947.
(750) Linderman, J. J. *J. Biol. Chem.* **2009**, *284*, 5427.
(751) Dell'Orco, D.; Koch, K. *Biochem. J.* **2011**, *440*, 263.
(752) Fanelli, F.; Themmen, A. P.; Puett, D. *IUBMB Life* **2001**, *51*, 149.
(753) Shinozaki, H.; Fanelli, F.; Liu, X.; Jaquette, J.; Nakamura, K.; Segaloff, D. L. *Mol. Endocrinol.* **2001**, *15*, 972.
(754) Angelova, K.; Felline, A.; Puett, D.; Lee, M.; Patel, M.; Fanelli, F. *Cell. Mol. Life Sci.* **2010**, *68*, 1227.
(755) Farrens, D. L.; Altenbach, C.; Yang, K.; Hubbell, W. L.; Khorana, H. G. *Science* **1996**, *274*, 768.
(756) Kjelsberg, M. A.; Cotecchia, S.; Ostrowski, J.; Caron, M. G.; Lefkowitz, R. J. *J. Biol. Chem.* **1992**, *267*, 1430.
(757) Periole, X.; Ceruso, M. A.; Mehler, E. L. *Biochemistry* **2004**, *43*, 6858.
(758) Huang, P.; Li, J.; Chen, C.; Visiers, I.; Weinstein, H.; Liu-Chen, L. Y. *Biochemistry* **2001**, *40*, 13501.
(759) Vogel, R.; Mahalingam, M.; Ludeke, S.; Huber, T.; Siebert, F.; Sakmar, T. P. *J. Mol. Biol.* **2008**, *380*, 648.
(760) Capra, V.; Veltri, A.; Foglia, C.; Crimaldi, L.; Habib, A.; Parenti, M.; Rovati, G. E. *Mol. Pharmacol.* **2004**, *66*, 880.
(761) Jones, D. T. *Curr. Opin. Struct. Biol.* **1997**, *7*, 377.
(762) Lazaridis, T. *Proteins* **2003**, *52*, 176.
(763) Im, W.; Feig, M.; Brooks, C. L., III *Biophys. J.* **2003**, *85*, 2900.
(764) Bakker, R. A.; Jongejan, A.; Sansuk, K.; Hacksell, U.; Timmerman, H.; Brann, M. R.; Weiner, D. M.; Pardo, L.; Leurs, R. *Mol. Pharmacol.* **2008**, *73*, 94.
(765) Xu, W.; Sanz, A.; Pardo, L.; Liu-Chen, L. Y. *Biochemistry* **2008**, *47*, 10576.
(766) Pellissier, L. P.; Sallander, J.; Campillo, M.; Gaven, F.; Queffeulou, E.; Pillot, M.; Dumuis, A.; Claeysen, S.; Bockaert, J.; Pardo, L. *Mol. Pharmacol.* **2009**, *75*, 982.
(767) Kleinau, G.; Hoyer, I.; Kreuchwig, A.; Haas, A. K.; Rutz, C.; Furkert, J.; Worth, C. L.; Krause, G.; Schulein, R. *J. Biol. Chem.* **2011**, *286*, 25859.
(768) Floquet, N.; M'Kadmi, C.; Perahia, D.; Gagne, D.; Berge, G.; Marie, J.; Baneres, J. L.; Galleyrand, J. C.; Fehrentz, J. A.; Martinez, J. *J. Mol. Biol.* **2010**, *395*, 769.
(769) Deflorian, F.; Engel, S.; Colson, A. O.; Raaka, B. M.; Gershengorn, M. C.; Costanzi, S. *Proteins* **2008**, *71*, 783.
(770) Bikker, J. A.; Trumpp-Kallmeyer, S.; Humblet, C. *J. Med. Chem.* **1998**, *41*, 2911.
(771) Gershengorn, M. C.; Osman, R. *Endocrinology* **2001**, *142*, 2.
(772) Klabunde, T.; Hessler, G. *ChemBioChem* **2002**, *3*, 928.
(773) Moro, S.; Deflorian, F.; Spalluto, G.; Pastorin, G.; Cacciari, B.; Kim, S. K.; Jacobson, K. A. *Chem. Commun. (Cambridge)* **2003**, *24*, 2949.
(774) Bywater, R. P. *J. Mol. Recognit.* **2005**, *18*, 60.
(775) Dahl, S. G.; Sylte, I. *Basic Clin. Pharmacol. Toxicol.* **2005**, *96*, 151.
(776) Moro, S.; Spalluto, G.; Jacobson, K. A. *Trends Pharmacol. Sci.* **2005**, *26*, 44.
(777) Moro, S.; Bacilieri, M.; Deflorian, F.; Spalluto, G. *New J. Chem.* **2006**, *30*, 301.
(778) Schlyer, S.; Horuk, R. *Drug Discovery Today* **2006**, *11*, 481.
(779) Tuccinardi, T.; Martinelli, A. *Curr. Med. Chem.* **2007**, *14*, 3105.
(780) Martinelli, A.; Tuccinardi, T. *Med. Res. Rev.* **2008**, *28*, 247.
(781) Carter, P. H.; Tebben, A. J. *Methods Enzymol.* **2009**, *461*, 249.
(782) Li, Y. Y.; Hou, T. J.; Goddard, W. A., III *Curr. Med. Chem.* **2010**, *17*, 1167.
(783) Strzelczyk, A. A.; Jaronczyk, M.; Chilmonczyk, Z.; Mazurek, A. P.; Chojnacka-Wojcik, E.; Sylte, I. *Biochem. Pharmacol.* **2004**, *67*, 2219.
(784) Hallmen, C.; Wiese, M. *J. Comput.-Aided Mol. Des.* **2006**, *20*, 673.
(785) Paillasse, M. R.; Deraeve, C.; de Medina, P.; Mhamdi, L.; Favre, G.; Poirot, M.; Silvente-Poirot, S. *Mol. Pharmacol.* **2006**, *70*, 1935.
(786) Marco, E.; Foucaud, M.; Langer, I.; Escrieut, C.; Tikhonova, I. G.; Fourmy, D. *J. Biol. Chem.* **2007**, *282*, 28779.
(787) Strasser, A.; Wittmann, H. J. *J. Comput.-Aided Mol. Des.* **2007**, *21*, 499.
(788) Chipot, C. *J. Chem. Theory Comput.* **2008**, *4*, 2150.
(789) Jojart, B.; Kiss, R.; Viskolcz, B.; Keseru, G. M. *J. Chem. Inf. Model.* **2008**, *48*, 1199.
(790) Yasuda, N.; Miura, S.; Akazawa, H.; Tanaka, T.; Qin, Y.; Kiya, Y.; Imaizumi, S.; Fujino, M.; Ito, K.; Zou, Y.; Fukuhara, S.; Kunimoto, S.; Fukuzaki, K.; Sato, T.; Ge, J.; Mochizuki, N.; Nakaya, H.; Saku, K.; Komuro, I. *EMBO Rep.* **2008**, *9*, 179.
(791) Katritch, V.; Reynolds, K. A.; Cherezov, V.; Hanson, M. A.; Roth, C. B.; Yeager, M.; Abagyan, R. *J. Mol. Recognit.* **2009**, *22*, 307.
(792) Bokoch, M. P.; Zou, Y.; Rasmussen, S. G.; Liu, C. W.; Nygaard, R.; Rosenbaum, D. M.; Fung, J. J.; Choi, H. J.; Thian, F. S.; Kobilka, T. S.; Puglisi, J. D.; Weis, W. I.; Pardo, L.; Prosser, R. S.; Mueller, L.; Kobilka, B. K. *Nature* **2010**, *463*, 108.
(793) Kolinski, M.; Filipek, S. *J. Mol. Model.* **2010**, *16*, 1567.
(794) Kamiya, Y.; Reynolds, C. A. *J. Mol. Struct. (THEOCHEM)* **1999**, *469*, 229.

(795) Hurst, D. P.; Grossfield, A.; Lynch, D. L.; Feller, S.; Romo, T. D.; Gawrisch, K.; Pitman, M. C.; Reggio, P. H. *J. Biol. Chem.* **2010**, *285*, 17954.
(796) Strasser, A.; Wittmann, H. J. *J. Comput.-Aided Mol. Des.* **2010**, *24*, 759.
(797) Wang, T.; Duan, Y. *J. Mol. Biol.* **2009**, *392*, 1102.
(798) Filizola, M.; Carteni-Farina, M.; Perez, J. J. *J. Comput.-Aided Mol. Des.* **1999**, *13*, 397.
(799) Freddolino, P. L.; Kalani, M. Y.; Vaidehi, N.; Floriano, W. B.; Hall, S. E.; Trabanino, R. J.; Kam, V. W.; Goddard, W. A., III *Proc. Natl. Acad. Sci. U.S.A.* **2004**, *101*, 2736.
(800) Kalani, M. Y.; Vaidehi, N.; Hall, S. E.; Trabanino, R. J.; Freddolino, P. L.; Kalani, M. A.; Floriano, W. B.; Kam, V. W.; Goddard, W. A., III *Proc. Natl. Acad. Sci. U.S.A.* **2004**, *101*, 3815.
(801) Floriano, W. B.; Hall, S.; Vaidehi, N.; Kim, U.; Drayna, D.; Goddard, W. A., III *J. Mol. Model.* **2006**, *12*, 931.
(802) Peng, J. Y.; Vaidehi, N.; Hall, S. E.; Goddard, W. A., III *ChemMedChem* **2006**, *1*, 878.
(803) Spijker, P.; Vaidehi, N.; Freddolino, P. L.; Hilbers, P. A.; Goddard, W. A., III *Proc. Natl. Acad. Sci. U.S.A.* **2006**, *103*, 4882.
(804) Bray, J. K.; Goddard, W. A., III *J. Mol. Graphics Modell.* **2008**, *27*, 66.
(805) Hedberg, M. H.; Jansen, J. M.; Nordvall, G.; Hjorth, S.; Unelius, L.; Johansson, A. M. *J. Med. Chem.* **1996**, *39*, 3491.
(806) Hedberg, M. H.; Linnanen, T.; Jansen, J. M.; Nordvall, G.; Hjorth, S.; Unelius, L.; Johansson, A. M. *J. Med. Chem.* **1996**, *39*, 3503.
(807) Kask, K.; Berthold, M.; Kahl, U.; Nordvall, G.; Bartfai, T. *EMBO J.* **1996**, *15*, 236.
(808) Nordvall, G.; Nilsson, B. M.; Sundquist, S.; Johansson, G.; Glas, G.; Nilvebrant, L.; Hacksell, U. *Prog. Brain Res.* **1996**, *109*, 141.
(809) Nordvall, G.; Sundquist, S.; Johansson, G.; Glas, G.; Nilvebrant, L.; Hacksell, U. *J. Med. Chem.* **1996**, *39*, 3269.
(810) Archer-Lahlou, E.; Escrieut, C.; Clerc, P.; Martinez, J.; Moroder, L.; Logsdon, C.; Kopin, A.; Seva, C.; Dufresne, M.; Pradayrol, L.; Maigret, B.; Fourmy, D. *J. Biol. Chem.* **2005**, *280*, 10664.
(811) Archer-Lahlou, E.; Tikhonova, I.; Escrieut, C.; Dufresne, M.; Seva, C.; Pradayrol, L.; Moroder, L.; Maigret, B.; Fourmy, D. *J. Med. Chem.* **2005**, *48*, 180.
(812) Foucaud, M.; Tikhonova, I. G.; Langer, I.; Escrieut, C.; Dufresne, M.; Seva, C.; Maigret, B.; Fourmy, D. *Mol. Pharmacol.* **2006**, *69*, 680.
(813) Henin, J.; Maigret, B.; Tarek, M.; Escrieut, C.; Fourmy, D.; Chipot, C. *Biophys. J.* **2006**, *90*, 1232.
(814) Langer, I.; Tikhonova, I. G.; Travers, M. A.; Archer-Lahlou, E.; Escrieut, C.; Maigret, B.; Fourmy, D. *J. Biol. Chem.* **2005**, *280*, 22198.
(815) Lopez-Rodriguez, M. L.; Murcia, M.; Benhamu, B.; Viso, A.; Campillo, M.; Pardo, L. *J. Med. Chem.* **2002**, *45*, 4806.
(816) McAllister, S. D.; Rizvi, G.; Anavi-Goffer, S.; Hurst, D. P.; Barnett-Norris, J.; Lynch, D. L.; Reggio, P. H.; Abood, M. E. *J. Med. Chem.* **2003**, *46*, 5139.
(817) Lopez-Rodriguez, M. L.; Benhamu, B.; Murcia, M.; Alvaro, E.; Campillo, M.; Pardo, L. *J. Comput.-Aided Mol. Des.* **2003**, *17*, 515.
(818) Lopez-Rodriguez, M. L.; Morcillo, M. J.; Fernandez, E.; Benhamu, B.; Tejada, I.; Ayala, D.; Viso, A.; Olivella, M.; Pardo, L.; Delgado, M.; Manzanares, J.; Fuentes, J. A. *Bioorg. Med. Chem. Lett.* **2003**, *13*, 1429.
(819) Fowler, C. B.; Pogozheva, I. D.; Lomize, A. L.; LeVine, H., III; Mosberg, H. I. *Biochemistry* **2004**, *43*, 15796.
(820) Hiramoto, T.; Nonaka, Y.; Inoue, K.; Yamamoto, T.; Omatsu-Kanbe, M.; Matsuura, H.; Gohda, K.; Fujita, N. *J. Pharmacol. Sci.* **2004**, *95*, 81.
(821) Jung, K. Y.; Kim, S. K.; Gao, Z. G.; Gross, A. S.; Melman, N.; Jacobson, K. A.; Kim, Y. C. *Bioorg. Med. Chem.* **2004**, *12*, 613.
(822) Major, D. T.; Nahum, V.; Wang, Y.; Reiser, G.; Fischer, B. *J. Med. Chem.* **2004**, *47*, 4405.
(823) Tchilibon, S.; Kim, S. K.; Gao, Z. G.; Harris, B. A.; Blaustein, J. B.; Gross, A. S.; Duong, H. T.; Melman, N.; Jacobson, K. A. *Bioorg. Med. Chem.* **2004**, *12*, 2021.
(824) Evers, A.; Klabunde, T. *J. Med. Chem.* **2005**, *48*, 1088.
(825) Boeckler, F.; Ohnmacht, U.; Lehmann, T.; Utz, W.; Hubner, H.; Gmeiner, P. *J. Med. Chem.* **2005**, *48*, 2493.
(826) Przydzial, M. J.; Pogozheva, I. D.; Bosse, K. E.; Andrews, S. M.; Tharp, T. A.; Traynor, J. R.; Mosberg, H. I. *J. Pept. Res.* **2005**, *65*, 333.
(827) Costanzi, S.; Joshi, B. V.; Maddileti, S.; Mamedova, L.; Gonzalez-Moa, M. J.; Marquez, V. E.; Harden, T. K.; Jacobson, K. A. *J. Med. Chem.* **2005**, *48*, 8108.
(828) Yan, F.; Mosier, P. D.; Westkaemper, R. B.; Stewart, J.; Zjawiony, J. K.; Vortherms, T. A.; Sheffler, D. J.; Roth, B. L. *Biochemistry* **2005**, *44*, 8643.
(829) Han, S. J.; Hamdan, F. F.; Kim, S. K.; Jacobson, K. A.; Bloodworth, L. M.; Li, B.; Wess, J. *J. Biol. Chem.* **2005**, *280*, 34849.
(830) Besada, P.; Shin, D. H.; Costanzi, S.; Ko, H.; Mathe, C.; Gagneron, J.; Gosselin, G.; Maddileti, S.; Harden, T. K.; Jacobson, K. A. *J. Med. Chem.* **2006**, *49*, 5532.
(831) Cosyn, L.; Palaniappan, K. K.; Kim, S. K.; Duong, H. T.; Gao, Z. G.; Jacobson, K. A.; Van Calenbergh, S. *J. Med. Chem.* **2006**, *49*, 7373.
(832) Ivanov, A. A.; Costanzi, S.; Jacobson, K. A. *J. Comput.-Aided Mol. Des.* **2006**, *20*, 417.
(833) Lenzi, O.; Colotta, V.; Catarzi, D.; Varano, F.; Filacchioni, G.; Martini, C.; Trincavelli, L.; Ciampi, O.; Varani, K.; Marighetti, F.; Morizzo, E.; Moro, S. *J. Med. Chem.* **2006**, *49*, 3916.
(834) Pastorin, G.; Da Ros, T.; Bolcato, C.; Montopoli, C.; Moro, S.; Cacciari, B.; Baraldi, P. G.; Varani, K.; Borea, P. A.; Spalluto, G. *J. Med. Chem.* **2006**, *49*, 1720.
(835) Jaschke, H.; Neumann, S.; Moore, S.; Thomas, C. J.; Colson, A. O.; Costanzi, S.; Kleinau, G.; Jiang, J. K.; Paschke, R.; Raaka, B. M.; Krause, G.; Gershengorn, M. C. *J. Biol. Chem.* **2006**, *281*, 9841.
(836) Moore, S.; Jaeschke, H.; Kleinau, G.; Neumann, S.; Costanzi, S.; Jiang, J. K.; Childress, J.; Raaka, B. M.; Colson, A.; Paschke, R.; Krause, G.; Thomas, C. J.; Gershengorn, M. C. *J. Med. Chem.* **2006**, *49*, 3888.
(837) Tafi, A.; Bernardini, C.; Botta, M.; Corelli, F.; Andreini, M.; Martinelli, A.; Ortore, G.; Baraldi, P. G.; Fruttarolo, F.; Borea, P. A.; Tuccinardi, T. *J. Med. Chem.* **2006**, *49*, 4085.
(838) Baleanu-Gogonea, C.; Karnik, S. *J. Mol. Model.* **2006**, *12*, 325.
(839) Fano, A.; Ritchie, D. W.; Carrieri, A. *J. Chem. Inf. Model.* **2006**, *46*, 1223.
(840) Patny, A.; Desai, P. V.; Avery, M. A. *Proteins* **2006**, *65*, 824.
(841) Singh, N.; Cheve, G.; Ferguson, D. M.; McCurdy, C. R. *J. Comput.-Aided Mol. Des.* **2006**, *20*, 471.
(842) Slusarz, M. J.; Sikorska, E.; Slusarz, R.; Ciarkowski, J. *J. Med. Chem.* **2006**, *49*, 2463.
(843) Tuccinardi, T.; Calderone, V.; Rapposelli, S.; Martinelli, A. *J. Med. Chem.* **2006**, *49*, 4305.
(844) Vabeno, J.; Nikiforovich, G. V.; Marshall, G. R. *Chem. Biol. Drug Des.* **2006**, *67*, 346.
(845) Axe, F. U.; Bembenek, S. D.; Szalma, S. *J. Mol. Graphics Modell.* **2006**, *24*, 456.
(846) Kolaczkowski, M.; Nowak, M.; Pawlowski, M.; Bojarski, A. J. *J. Med. Chem.* **2006**, *49*, 6732.
(847) Krystek, S. R., Jr.; Kimura, S. R.; Tebben, A. J. *J. Comput.-Aided Mol. Des.* **2006**, *20*, 463.
(848) MacDougall, I. J.; Griffith, R. *J. Mol. Graphics Modell.* **2006**, *25*, 146.
(849) Nowak, M.; Kolaczkowski, M.; Pawlowski, M.; Bojarski, A. J. *J. Med. Chem.* **2006**, *49*, 205.
(850) Ortore, G.; Tuccinardi, T.; Bertini, S.; Martinelli, A. *J. Med. Chem.* **2006**, *49*, 1397.
(851) Pedretti, A.; Vistoli, G.; Marconi, C.; Testa, B. *Chem. Biodiversity* **2006**, *3*, 481.
(852) Chugunov, A. O.; Farce, A.; Chavatte, P.; Efremov, R. G. *J. Biomol. Struct. Dyn.* **2006**, *24*, 91.
(853) Manera, C.; Benetti, V.; Castelli, M. P.; Cavallini, T.; Lazzarotti, S.; Pibiri, F.; Saccomanni, G.; Tuccinardi, T.; Vannacci, A.; Martinelli, A.; Ferrarini, P. L. *J. Med. Chem.* **2006**, *49*, 5947.
(854) Miguet, L.; Zhang, Z.; Grigorov, M. G. *J. Recept. Signal Transduction Res.* **2006**, *26*, 611.

(855) Tuccinardi, T.; Ferrarini, P. L.; Manera, C.; Ortore, G.; Saccomanni, G.; Martinelli, A. *J. Med. Chem.* **2006**, *49*, 984.
(856) Adachi, H.; Palaniappan, K. K.; Ivanov, A. A.; Bergman, N.; Gao, Z. G.; Jacobson, K. A. *J. Med. Chem.* **2007**, *50*, 1810.
(857) Colotta, V.; Catarzi, D.; Varano, F.; Capelli, F.; Lenzi, O.; Filacchioni, G.; Martini, C.; Trincavelli, L.; Ciampi, O.; Pugliese, A. M.; Pedata, F.; Schiesaro, A.; Morizzo, E.; Moro, S. *J. Med. Chem.* **2007**, *50*, 4061.
(858) Costanzi, S.; Tikhonova, I. G.; Ohno, M.; Roh, E. J.; Joshi, B. V.; Colson, A. O.; Houston, D.; Maddileti, S.; Harden, T. K.; Jacobson, K. A. *J. Med. Chem.* **2007**, *50*, 3229.
(859) Ivanov, A. A.; Ko, H.; Cosyn, L.; Maddileti, S.; Besada, P.; Fricks, I.; Costanzi, S.; Harden, T. K.; Calenbergh, S. V.; Jacobson, K. A. *J. Med. Chem.* **2007**, *50*, 1166.
(860) Ko, H.; Fricks, I.; Ivanov, A. A.; Harden, T. K.; Jacobson, K. A. *J. Med. Chem.* **2007**, *50*, 2030.
(861) Morizzo, E.; Capelli, F.; Lenzi, O.; Catarzi, D.; Varano, F.; Filacchioni, G.; Vincenzi, F.; Varani, K.; Borea, P. A.; Colotta, V.; Moro, S. *J. Med. Chem.* **2007**, *50*, 6596.
(862) Palaniappan, K. K.; Gao, Z. G.; Ivanov, A. A.; Greaves, R.; Adachi, H.; Besada, P.; Kim, H. O.; Kim, A. Y.; Choe, S. A.; Jeong, L. S.; Jacobson, K. A. *Biochemistry* **2007**, *46*, 7437.
(863) Tikhonova, I. G.; Sum, C. S.; Neumann, S.; Thomas, C. J.; Raaka, B. M.; Costanzi, S.; Gershengorn, M. C. *J. Med. Chem.* **2007**, *50*, 2981.
(864) Witt, M.; Ciarkowski, J.; Czaplewski, C. *Protein Pept. Lett.* **2007**, *14*, 381.
(865) Zylberg, J.; Ecke, D.; Fischer, B.; Reiser, G. *Biochem. J.* **2007**, *405*, 277.
(866) Ivanov, A. A.; Palyulin, V. A.; Zefirov, N. S. *J. Mol. Graphics Modell.* **2007**, *25*, 740.
(867) Sum, C. S.; Tikhonova, I. G.; Neumann, S.; Engel, S.; Raaka, B. M.; Costanzi, S.; Gershengorn, M. C. *J. Biol. Chem.* **2007**, *282*, 29248.
(868) Volpini, R.; Dal Ben, D.; Lambertucci, C.; Taffi, S.; Vittori, S.; Klotz, K. N.; Cristalli, G. *J. Med. Chem.* **2007**, *50*, 1222.
(869) Zhan, C.; Yang, J.; Dong, X. C.; Wang, Y. L. *J. Mol. Graphics Modell.* **2007**, *26*, 20.
(870) Dong, M.; Ding, X. Q.; Thomas, S. E.; Gao, F.; Lam, P. C.; Abagyan, R.; Miller, L. J. *Biochemistry* **2007**, *46*, 4522.
(871) Napier, K. B.; Wang, Z. X.; Peiper, S. C.; Trent, J. O. *J. Mol. Model.* **2007**, *13*, 29.
(872) Rodrigo, J.; Pena, A.; Murat, B.; Trueba, M.; Durroux, T.; Guillon, G.; Rognan, D. *Mol. Endocrinol.* **2007**, *21*, 512.
(873) Singh, S.; Malik, B. K.; Sharma, D. K. *Chem. Biol. Drug Des.* **2007**, *69*, 191.
(874) Zoffmann, S.; Bertrand, S.; Do, Q. T.; Bertrand, D.; Rognan, D.; Hibert, M.; Galzi, J. L. *J. Neurochem.* **2007**, *101*, 506.
(875) Asher, W. B.; Hoskins, S. N.; Slasor, L. A.; Morris, D. H.; Cook, E. M.; Bautista, D. L. *J. Chem. Inf. Model.* **2007**, *47*, 1906.
(876) Balogh, B.; Hetenyi, C.; Keseru, M. G.; Matyus, P. *ChemMedChem* **2007**, *2*, 801.
(877) Schlegel, B.; Laggner, C.; Meier, R.; Langer, T.; Schnell, D.; Seifert, R.; Stark, H.; Holtje, H. D.; Sippl, W. *J. Comput.-Aided Mol. Des.* **2007**, *21*, 437.
(878) Deng, Q.; Clemas, J. A.; Chrebet, G.; Fischer, P.; Hale, J. J.; Li, Z.; Mills, S. G.; Bergstrom, J.; Mandala, S.; Mosley, R.; Parent, S. A. *Mol. Pharmacol.* **2007**, *71*, 724.
(879) Gui, C.; Zhu, W.; Chen, G.; Luo, X.; Liew, O. W.; Puah, C. M.; Chen, K.; Jiang, H. *Proteins* **2007**, *67*, 41.
(880) Malde, A. K.; Srivastava, S. S.; Coutinho, E. C. *J. Pept. Sci.* **2007**, *13*, 287.
(881) Chen, J. Z.; Wang, J.; Xie, X. Q. *J. Chem. Inf. Model.* **2007**, *47*, 1626.
(882) Kellenberger, E.; Springael, J. Y.; Parmentier, M.; Hachet-Haas, M.; Galzi, J. L.; Rognan, D. *J. Med. Chem.* **2007**, *50*, 1294.
(883) Lu, Z. L.; Coetsee, M.; White, C. D.; Millar, R. P. *J. Biol. Chem.* **2007**, *282*, 17921.
(884) Colotta, V.; Catarzi, D.; Varano, F.; Lenzi, O.; Filacchioni, G.; Martini, C.; Trincavelli, L.; Ciampi, O.; Traini, C.; Pugliese, A. M.; Pedata, F.; Morizzo, E.; Moro, S. *Bioorg. Med. Chem.* **2008**, *16*, 6086.
(885) Ivanov, A. A.; Wang, B.; Klutz, A. M.; Chen, V. L.; Gao, Z. G.; Jacobson, K. A. *J. Med. Chem.* **2008**, *51*, 2088.
(886) Michielan, L.; Bacilieri, M.; Schiesaro, A.; Bolcato, C.; Pastorin, G.; Spalluto, G.; Cacciari, B.; Klotz, K. N.; Kaseda, C.; Moro, S. *J. Chem. Inf. Model.* **2008**, *48*, 350.
(887) Parravicini, C.; Ranghino, G.; Abbracchio, M. P.; Fantucci, P. *BMC Bioinf.* **2008**, *9*, 263.
(888) Tuccinardi, T.; Schenone, S.; Bondavalli, F.; Brullo, C.; Bruno, O.; Mosti, L.; Zizzari, A. T.; Tintori, C.; Manetti, F.; Ciampi, O.; Trincavelli, M. L.; Martini, C.; Martinelli, A.; Botta, M. *ChemMedChem* **2008**, *3*, 898.
(889) Deng, Q.; Frie, J. L.; Marley, D. M.; Beresis, R. T.; Ren, N.; Cai, T. Q.; Taggart, A. K.; Cheng, K.; Carballo-Jane, E.; Wang, J.; Tong, X.; Waters, M. G.; Tata, J. R.; Colletti, S. L. *Bioorg. Med. Chem. Lett.* **2008**, *18*, 4963.
(890) Lescot, E.; Sopkova-de Oliveira Santos, J.; Colloc'h, N.; Rodrigo, J.; Milazzo-Segalas, I.; Bureau, R.; Rault, S. *Proteins* **2008**, *73*, 173.
(891) Lindner, D.; van Dieck, J.; Merten, N.; Morl, K.; Gunther, R.; Hofmann, H. J.; Beck-Sickinger, A. G. *Biochemistry* **2008**, *47*, 5905.
(892) Nikiforovich, G. V.; Marshall, G. R.; Baranski, T. J. *Biochemistry* **2008**, *47*, 3117.
(893) Perez-Nueno, V. I.; Ritchie, D. W.; Rabal, O.; Pascual, R.; Borrell, J. I.; Teixido, J. *J. Chem. Inf. Model.* **2008**, *48*, 509.
(894) Skold, C.; Nikiforovich, G.; Karlen, A. *J. Mol. Graphics Modell.* **2008**, *26*, 991.
(895) Singh, P.; Wang, B.; Maeda, T.; Palczewski, K.; Tesmer, J. J. *J. Biol. Chem.* **2008**, *283*, 14053.
(896) Gieldon, A.; Lopez, J. J.; Glaubitz, C.; Schwalbe, H. *ChemBioChem* **2008**, *9*, 2487.
(897) Dastmalchi, S.; Hamzeh-Mivehroud, M.; Ghafourian, T.; Hamzeiy, H. *J. Mol. Graphics Modell.* **2008**, *26*, 834.
(898) Dukat, M.; Mosier, P. D.; Kolanos, R.; Roth, B. L.; Glennon, R. A. *J. Med. Chem.* **2008**, *51*, 603.
(899) Kiss, R.; Noszal, B.; Racz, A.; Falus, A.; Eros, D.; Keseru, G. M. *Eur. J. Med. Chem.* **2008**, *43*, 1059.
(900) Tan, E. S.; Groban, E. S.; Jacobson, M. P.; Scanlan, T. S. *Chem. Biol.* **2008**, *15*, 343.
(901) Fells, J. I.; Tsukahara, R.; Fujiwara, Y.; Liu, J.; Perygin, D. H.; Osborne, D. A.; Tigyi, G.; Parrill, A. L. *Bioorg. Med. Chem.* **2008**, *16*, 6207.
(902) Hirashima, A.; Huang, H. *Comput. Biol. Chem.* **2008**, *32*, 185.
(903) Pei, Y.; Mercier, R. W.; Anday, J. K.; Thakur, G. A.; Zvonok, A. M.; Hurst, D.; Reggio, P. H.; Janero, D. R.; Makriyannis, A. *Chem. Biol.* **2008**, *15*, 1207.
(904) Poso, A.; Huffman, J. W. *Br. J. Pharmacol.* **2008**, *153*, 335.
(905) Wolf, S.; Bockmann, M.; Howeler, U.; Schlitter, J.; Gerwert, K. *FEBS Lett.* **2008**, *582*, 3335.
(906) Cavasotto, C. N.; Orry, A. J.; Murgolo, N. J.; Czarniecki, M. F.; Kocsi, S. A.; Hawes, B. E.; O'Neill, K. A.; Hine, H.; Burton, M. S.; Voigt, J. H.; Abagyan, R. A.; Bayne, M. L.; Monsma, F. J., Jr. *J. Med. Chem.* **2008**, *51*, 581.
(907) Engel, S.; Skoumbourdis, A. P.; Childress, J.; Neumann, S.; Deschamps, J. R.; Thomas, C. J.; Colson, A. O.; Costanzi, S.; Gershengorn, M. C. *J. Am. Chem. Soc.* **2008**, *130*, 5115.
(908) Kiss, R.; Kiss, B.; Konczol, A.; Szalai, F.; Jelinek, I.; Laszlo, V.; Noszal, B.; Falus, A.; Keseru, G. M. *J. Med. Chem.* **2008**, *51*, 3145.
(909) Tikhonova, I. G.; Sum, C. S.; Neumann, S.; Engel, S.; Raaka, B. M.; Costanzi, S.; Gershengorn, M. C. *J. Med. Chem.* **2008**, *51*, 625.
(910) Colotta, V.; Lenzi, O.; Catarzi, D.; Varano, F.; Filacchioni, G.; Martini, C.; Trincavelli, L.; Ciampi, O.; Pugliese, A. M.; Traini, C.; Pedata, F.; Morizzo, E.; Moro, S. *J. Med. Chem.* **2009**, *52*, 2407.
(911) Hillmann, P.; Ko, G. Y.; Spinrath, A.; Raulf, A.; von Kugelgen, I.; Wolff, S. C.; Nicholas, R. A.; Kostenis, E.; Holtje, H. D.; Muller, C. E. *J. Med. Chem.* **2009**, *52*, 2762.
(912) Lenzi, O.; Colotta, V.; Catarzi, D.; Varano, F.; Poli, D.; Filacchioni, G.; Varani, K.; Vincenzi, F.; Borea, P. A.; Paoletta, S.; Morizzo, E.; Moro, S. *J. Med. Chem.* **2009**, *52*, 7640.
(913) Liu, X.; Kai, M.; Jin, L.; Wang, R. *Bioorg. Med. Chem. Lett.* **2009**, *19*, 5387.

(914) Yan, F.; Bikbulatov, R. V.; Mocanu, V.; Dicheva, N.; Parker, C. E.; Wetsel, W. C.; Mosier, P. D.; Westkaemper, R. B.; Allen, J. A.; Zjawiony, J. K.; Roth, B. L. *Biochemistry* **2009**, *48*, 6898.
(915) Balogh, B.; Szilagyi, A.; Gyires, K.; Bylund, D. B.; Matyus, P. *Neurochem. Int.* **2009**, *55*, 355.
(916) Li, G.; Mosier, P. D.; Fang, X.; Zhang, Y. *J. Mol. Graphics Modell.* **2009**, *28*, 70.
(917) Maruoka, H.; Barrett, M. O.; Ko, H.; Tosh, D. K.; Melman, A.; Burianek, L. E.; Balasubramanian, R.; Berk, B.; Costanzi, S.; Harden, T. K.; Jacobson, K. A. *J. Med. Chem.* **2010**, *53*, 4488.
(918) Parravicini, C.; Abbracchio, M. P.; Fantucci, P.; Ranghino, G. *BMC Struct. Biol.* **2010**, *10*, 8.
(919) Agelis, G.; Roumelioti, P.; Resvani, A.; Durdagi, S.; Androutsou, M. E.; Kelaidonis, K.; Vlahakos, D.; Mavromoustakos, T.; Matsoukas, J. *J. Comput.-Aided Mol. Des.* **2010**, *24*, 749.
(920) Dal Ben, D.; Antonini, I.; Buccioni, M.; Lambertucci, C.; Marucci, G.; Vittori, S.; Volpini, R.; Cristalli, G. *ChemMedChem* **2010**, *5*, 371.
(921) Adhikari, N.; Maiti, M. K.; Jha, T. *Eur. J. Med. Chem.* **2010**, *45*, 1119.
(922) Pecic, S.; Makkar, P.; Chaudhary, S.; Reddy, B. V.; Navarro, H. A.; Harding, W. W. *Bioorg. Med. Chem.* **2010**, *18*, 5562.
(923) Durdagi, S.; Papadopoulos, M. G.; Zoumpoulakis, P. G.; Koukoulitsa, C.; Mavromoustakos, T. *Mol. Diversity* **2010**, *14*, 257.
(924) Soriano, A.; Ventura, R.; Molero, A.; Hoen, R.; Casado, V.; Cortes, A.; Fanelli, F.; Albericio, F.; Lluis, C.; Franco, R.; Royo, M. *J. Med. Chem.* **2009**, *52*, 5590.
(925) Cirauqui, N.; Schrey, A. K.; Galiano, S.; Ceras, J.; Perez-Silanes, S.; Aldana, I.; Monge, A.; Kuhne, R. *Bioorg. Med. Chem.* **2010**, *18*, 7365.
(926) Helal, M. A.; Chittiboyina, A. G.; Avery, M. A. *J. Chem. Inf. Model* **2011**, *51*, 635.
(927) Shahlaei, M.; Madadkar-Sobhani, A.; Mahnam, K.; Fassihi, A.; Saghaie, L.; Mansourian, M. *Biochim. Biophys. Acta* **2011**, *1808*, 802.
(928) Marquer, C.; Fruchart-Gaillard, C.; Letellier, G.; Marcon, E.; Mourier, G.; Zinn-Justin, S.; Menez, A.; Servent, D.; Gilquin, B. *J. Biol. Chem.* **2011**, *286*, 31661.
(929) Gigoux, V.; Escrieut, C.; Fehrentz, J. A.; Poirot, S.; Maigret, B.; Moroder, L.; Gully, D.; Martinez, J.; Vaysse, N.; Fourmy, D. *J. Biol. Chem.* **1999**, *274*, 20457.
(930) Gigoux, V.; Maigret, B.; Escrieut, C.; Silvente-Poirot, S.; Bouisson, M.; Fehrentz, J. A.; Moroder, L.; Gully, D.; Martinez, J.; Vaysse, N.; Fourmy, A. D. *Protein Sci.* **1999**, *8*, 2347.
(931) Baker, J. G.; Proudman, R. G.; Hawley, N. C.; Fischer, P. M.; Hill, S. J. *Mol. Pharmacol.* **2008**, *74*, 1246.
(932) Neumann, S.; Kleinau, G.; Costanzi, S.; Moore, S.; Jiang, J. K.; Raaka, B. M.; Thomas, C. J.; Krause, G.; Gershengorn, M. C. *Endocrinology* **2008**, *149*, 5945.
(933) Selent, J.; Lopez, L.; Sanz, F.; Pastor, M. *ChemMedChem* **2008**, *3*, 1194.
(934) Dainese, E.; Oddi, S.; Maccarrone, M. *Cell. Mol. Life Sci.* **2008**, *65*, 2277.
(935) Ericksen, S. S.; Cummings, D. F.; Weinstein, H.; Schetz, J. A. *J. Pharmacol. Exp. Ther.* **2009**, *328*, 40.
(936) Kanagarajadurai, K.; Malini, M.; Bhattacharya, A.; Panicker, M. M.; Sowdhamini, R. *Mol. Biosyst.* **2009**, *5*, 1877.
(937) Klabunde, T.; Giegerich, C.; Evers, A. *J. Med. Chem.* **2009**, *52*, 2923.
(938) Neumann, S.; Huang, W.; Titus, S.; Krause, G.; Kleinau, G.; Alberobello, A. T.; Zheng, W.; Southall, N. T.; Inglese, J.; Austin, C. P.; Celi, F. S.; Gavrilova, O.; Thomas, C. J.; Raaka, B. M.; Gershengorn, M. C. *Proc. Natl. Acad. Sci. U.S.A.* **2009**, *106*, 12471.
(939) Tosh, D. K.; Chinn, M.; Ivanov, A. A.; Klutz, A. M.; Gao, Z. G.; Jacobson, K. A. *J. Med. Chem.* **2009**, *52*, 7580.
(940) Langham, J. J.; Cleves, A. E.; Spitzer, R.; Kirshner, D.; Jain, A. N. *J. Med. Chem.* **2009**, *52*, 6107.
(941) Cheong, S. L.; Dolzhenko, A.; Kachler, S.; Paoletta, S.; Federico, S.; Cacciari, B.; Klotz, K. N.; Moro, S.; Spalluto, G.; Pastorin, G. *J. Med. Chem.* **2010**, *53*, 3361.
(942) Du, L.; Li, M. *Curr. Comput.-Aided Drug Des.* **2010**, *6*, 165.
(943) Pastorin, G.; Federico, S.; Paoletta, S.; Corradino, M.; Cateni, F.; Cacciari, B.; Klotz, K. N.; Gao, Z. G.; Jacobson, K. A.; Spalluto, G.; Moro, S. *Bioorg. Med. Chem.* **2010**, *18*, 2524.
(944) Wang, X.; Yang, Q.; Li, M.; Yin, D.; You, Q. *J. Mol. Model.* **2010**, *16*, 1529.
(945) Zhao, Y.; Lu, X.; Yang, C. Y.; Huang, Z.; Fu, W.; Hou, T.; Zhang, J. *J. Chem. Inf. Model.* **2010**, *50*, 1633.
(946) McRobb, F. M.; Capuano, B.; Crosby, I. T.; Chalmers, D. K.; Yuriev, E. *J. Chem. Inf. Model.* **2010**, *50*, 626.
(947) Wang, Q.; Mach, R. H.; Luedtke, R. R.; Reichert, D. E. *J. Chem. Inf. Model.* **2010**, *50*, 1970.
(948) Sum, C. S.; Tikhonova, I. G.; Costanzi, S.; Gershengorn, M. C. *J. Biol. Chem.* **2009**, *284*, 3529.
(949) Bera, I.; Laskar, A.; Ghoshal, N. *J. Mol. Model.* **2011**, *17*, 1207.
(950) Runesson, J.; Sollenberg, U. E.; Jurkowski, W.; Yazdi, S.; Eriksson, E. E.; Elofsson, A.; Langel, U. *Neurochem. Int.* **2010**, *57*, 804.
(951) Sansuk, K.; Deupi, X.; Torrecillas, I.; Jongejan, A.; Nijmeijer, S.; Bakker, R.; Pardo, L.; Leurs, R. *Mol. Pharmacol.* **2010**, *79*, 262.
(952) Obiol-Pardo, C.; Lopez, L.; Pastor, M.; Selent, J. *Proteins* **2011**, *79*, 1695.
(953) Arakawa, M.; Yanamala, N.; Upadhyaya, J.; Halayko, A.; Klein-Seetharaman, J.; Chelikani, P. *Protein Sci.* **2010**, *19*, 85.
(954) Deflorian, F.; Jacobson, K. A. *J. Comput.-Aided Mol. Des.* **2011**, *25*, 329.
(955) Eberini, I.; Daniele, S.; Parravicini, C.; Sensi, C.; Trincavelli, M. L.; Martini, C.; Abbracchio, M. P. *J. Comput.-Aided Mol. Des.* **2011**, *25*, 743.
(956) Federico, S.; Paoletta, S.; Cheong, S. L.; Pastorin, G.; Cacciari, B.; Stragliotto, S.; Klotz, K. N.; Siegel, J.; Gao, Z. G.; Jacobson, K. A.; Moro, S.; Spalluto, G. *J. Med. Chem.* **2011**, *54*, 877.
(957) Kim, J. H.Lim, J. W.Lee, S. W.Kim, K.No, K. T. *J. Mol. Model.* **2011**, *17*, 2707.
(958) Latek, D.; Kolinski, M.; Ghoshdastider, U.; Debinski, A.; Bombolewski, R.; Plazinska, A.; Jozwiak, K.; Filipek, S. *J. Mol. Model.* **2011**, *17*, 2353.
(959) Maruoka, H.; Jayasekara, M. P.; Barrett, M. O.; Franklin, D. A.; de Castro, S.; Kim, N.; Costanzi, S.; Harden, T. K.; Jacobson, K. A. *J. Med. Chem.* **2011**, *54*, 4018.
(960) Isberg, V.; Balle, T.; Sander, T.; Jorgensen, F. S.; Gloriam, D. E. *J. Chem. Inf. Model* **2011**, *51*, 315.
(961) Simpson, L. M.; Wall, I. D.; Blaney, F. E.; Reynolds, C. A. *Proteins* **2011**, *79*, 1441.
(962) Sansuk, K.; Deupi, X.; Torrecillas, I. R.; Jongejan, A.; Nijmeijer, S.; Bakker, R. A.; Pardo, L.; Leurs, R. *Mol. Pharmacol.* **2011**, *79*, 262.
(963) Janovick, J. A.; Pogozheva, I. D.; Mosberg, H. I.; Conn, P. M. *J. Pharmacol. Exp. Ther.* **2011**, *338*, 430.
(964) Shim, J. Y.; Bertalovitz, A. C.; Kendall, D. A. *J. Biol. Chem.* **2011**, *286*, 33422.
(965) Shim, J. Y. *Biophys. J.* **2009**, *96*, 3251.
(966) Sabio, M.; Jones, K.; Topiol, S. *Bioorg. Med. Chem. Lett.* **2008**, *18*, 5391.
(967) Topiol, S.; Sabio, M. *Bioorg. Med. Chem. Lett.* **2008**, *18*, 1598.
(968) Kolb, P.; Rosenbaum, D. M.; Irwin, J. J.; Fung, J. J.; Kobilka, B. K.; Shoichet, B. K. *Proc. Natl. Acad. Sci. U.S.A.* **2009**, *106*, 6843.
(969) Gloriam, D. E.; Foord, S. M.; Blaney, F. E.; Garland, S. L. *J. Med. Chem.* **2009**, *52*, 4429.
(970) Carlsson, J.; Yoo, L.; Gao, Z. G.; Irwin, J. J.; Shoichet, B. K.; Jacobson, K. A. *J. Med. Chem.* **2010**, *53*, 3748.
(971) Kaszuba, K.; Rog, T.; Bryl, K.; Vattulainen, I.; Karttunen, M. *J. Phys. Chem. B* **2010**, *114*, 8374.
(972) Katritch, V.; Jaakola, V. P.; Lane, J. R.; Lin, J.; Ijzerman, A. P.; Yeager, M.; Kufareva, I.; Stevens, R. C.; Abagyan, R. *J. Med. Chem.* **2010**, *53*, 1799.
(973) Katritch, V.; Kufareva, I.; Abagyan, R. *Neuropharmacology* **2010**, *60*, 108.
(974) Soriano-Ursua, M. A.; Trujillo-Ferrara, J. G.; Alvarez-Cedillo, J.; Correa-Basurto, J. *J. Mol. Model.* **2010**, *16*, 401.

(975) Vilar, S.; Karpiak, J.; Costanzi, S. *J. Comput. Chem.* **2010**, *31*, 707.
(976) Ivetac, A.; Andrew McCammon, J. *Chem. Biol. Drug Des.* **2010**, *76*, 201.
(977) Balaraman, G. S.; Bhattacharya, S.; Vaidehi, N. *Biophys. J.* **2010**, *99*, 568.
(978) Soriano-Ursua, M. A.; Trujillo-Ferrara, J. G.; Correa-Basurto, J. *J. Med. Chem.* **2010**, *53*, 923.
(979) Vilar, S.; Karpiak, J.; Berk, B.; Costanzi, S. *J. Mol. Graphics Modell.* **2011**, *29*, 809.
(980) Gouldson, P. R.; Bywater, R. P.; Reynolds, C. A. *Biochem. Soc. Trans.* **1997**, *25*, 529S.
(981) Govaerts, C.; Lefort, A.; Costagliola, S.; Wodak, S. J.; Ballesteros, J. A.; Van Sande, J.; Pardo, L.; Vassart, G. *J. Biol. Chem.* **2001**, *276*, 22991.
(982) Urizar, E.; Claeysen, S.; Deupi, X.; Govaerts, C.; Costagliola, S.; Vassart, G.; Pardo, L. *J. Biol. Chem.* **2005**, *280*, 17135.
(983) Grossfield, A. *Biochim. Biophys. Acta* **2011**, *1808*, 1868.
(984) Chollet, A.; Turcatti, G. *J. Comput.-Aided Mol. Des.* **1999**, *13*, 209.
(985) Breton, C.; Chellil, H.; Kabbaj-Benmansour, M.; Carnazzi, E.; Seyer, R.; Phalipou, S.; Morin, D.; Durroux, T.; Zingg, H.; Barberis, C.; Mouillac, B. *J. Biol. Chem.* **2001**, *276*, 26931.
(986) Jaakola, V. P.; Ijzerman, A. P. *Curr. Opin. Struct. Biol.* **2010**, *20*, 401.
(987) Ananthan, S.; Zhang, W.; Hobrath, J. V. *Am. Assoc. Pharm. Sci. J.* **2009**, *11*, 178.
(988) Kolb, P.; Ferreira, R. S.; Irwin, J. J.; Shoichet, B. K. *Curr. Opin. Biotechnol.* **2009**, *20*, 429.
(989) Congreve, M.; Marshall, F. *Br. J. Pharmacol.* **2010**, *159*, 986.
(990) Audet, M.; Bouvier, M. *Nature Chem. Biol.* **2008**, *4*, 397.
(991) Yeagle, P. L.; Alderfer, J. L.; Albert, A. D. *Biochemistry* **1995**, *34*, 14621.
(992) Yeagle, P. L.; Alderfer, J. L.; Albert, A. D. *Nature Struct. Biol.* **1995**, *2*, 832.
(993) Yeagle, P. L.; Alderfer, J. L.; Salloum, A. C.; Ali, L.; Albert, A. D. *Biochemistry* **1997**, *36*, 3864.
(994) Yeagle, P. L.; Alderfer, J. L.; Albert, A. D. *Biochemistry* **1997**, *36*, 9649.
(995) Jimonet, P.; Jager, R. *Curr. Opin. Drug Discovery Dev.* **2004**, *7*, 325.
(996) De Benedetti, P. G.; Fanelli, F. *Curr. Protein Pept. Sci.* **2009**, *10*, 186.
(997) De Benedetti, P. G.; Fanelli, F. *Drug Discovery Today* **2010**, *15*, 859.
(998) Fanelli, F.; De Benedetti, P. G. In *Antitargets*; Vaz, R. J., Klabunde, T., Eds.; WILEY-VCH: Weinheim, Germany, 2008, 155.
(999) Fanelli, F.; Menziani, M. C.; Carotti, A.; De Benedetti, P. G. *J. Mol. Struct. (THEOCHEM)* **1993**, *283*, 63.
(1000) Montorsi, M.; Menziani, M. C.; Cocchi, M.; Fanelli, F.; De Benedetti, P. G. *Methods* **1998**, *14*, 239.
(1001) De Benedetti, P. G.; Fanelli, F.; Menziani, M. C.; Cocchi, M. *J. Mol. Struct. (THEOCHEM)* **2000**, *503*, 1.
(1002) Barlocco, D.; Cignarella, G.; Piaz, V. D.; Giovannoni, M. P.; De Benedetti, P. G.; Fanelli, F.; Montesano, F.; Poggesi, E.; Leonardi, A. *J. Med. Chem.* **2001**, *44*, 2403.
(1003) De Benedetti, P. G.; Menziani, M. C.; Cocchi, M.; Fanelli, F. *J. Mol. Struct. (THEOCHEM)* **1995**, *333*, 1.
(1004) Hiramoto, T.; Nemoto, W.; Kikuchi, T.; Fujita, N. *J. Protein Chem.* **2002**, *21*, 537.
(1005) Becker, O. M.; Marantz, Y.; Shacham, S.; Inbal, B.; Heifetz, A.; Kalid, O.; Bar-Haim, S.; Warshaviak, D.; Fichman, M.; Noiman, S. *Proc. Natl. Acad. Sci. U.S.A.* **2004**, *101*, 11304.
(1006) Ewing, T. J.; Makino, S.; Skillman, A. G.; Kuntz, I. D. *J. Comput.-Aided Mol. Des.* **2001**, *15*, 411.
(1007) Evers, A.; Klebe, G. *Angew. Chem., Int. Ed. Engl.* **2004**, *43*, 248.
(1008) Klabunde, T.; Evers, A. *ChemBioChem* **2005**, *6*, 876.
(1009) Verdonk, M. L.; Cole, J. C.; Hartshorn, M. J.; Murray, C. W.; Taylor, R. D. *Proteins* **2003**, *52*, 609.
(1010) Jain, A. N. *J. Med. Chem.* **2003**, *46*, 499.
(1011) Cavasotto, C. N.; Orry, A. J.; Abagyan, R. A. *Proteins* **2003**, *51*, 423.
(1012) Friesner, R. A.; Murphy, R. B.; Repasky, M. P.; Frye, L. L.; Greenwood, J. R.; Halgren, T. A.; Sanschagrin, P. C.; Mainz, D. T. *J. Med. Chem.* **2006**, *49*, 6177.
(1013) Noorwez, S. M.; Ostrov, D. A.; McDowell, J. H.; Krebs, M. P.; Kaushal, S. *Invest. Ophthalmol. Vis. Sci.* **2008**, *49*, 3224.
(1014) Vilar, S.; Ferino, G.; Phatak, S. S.; Berk, B.; Cavasotto, C. N.; Costanzi, S. *J. Mol. Graphics Modell.* **2011**, *29*, 614.
(1015) Raimondi, F.; Seeber, M.; Benedetti, P. G.; Fanelli, F. *J. Am. Chem. Soc.* **2008**, *130*, 4310.
(1016) Luo, X.; Zhang, D.; Weinstein, H. *Protein Eng.* **1994**, *7*, 1441.
(1017) Oliveira, L.; Paiva, A. C.; Sander, C.; Vriend, G. *Trends Pharmacol. Sci.* **1994**, *15*, 170.
(1018) Nygaard, R.; Frimurer, T. M.; Holst, B.; Rosenkilde, M. M.; Schwartz, T. W. *Trends Pharmacol. Sci.* **2009**, *30*, 249.
(1019) Schwartz, T. W.; Frimurer, T. M.; Holst, B.; Rosenkilde, M. M.; Elling, C. E. *Annu. Rev. Pharmacol. Toxicol.* **2006**, *46*, 481.
(1020) Porter, J. E.; Hwa, J.; Perez, D. M. *J. Biol. Chem.* **1996**, *271*, 28318.
(1021) Niesen, M. J.; Bhattacharya, S.; Vaidehi, N. *J. Am. Chem. Soc.* **2011**, *133*, 13197.
(1022) Tapaneeyakorn, S.; Goddard, A. D.; Oates, J.; Willis, C. L.; Watts, A. *Biochim. Biophys. Acta, Biomembr.* **2010**, *1808*, 1462.
(1023) Li, J. H.; Han, S. J.; Hamdan, F. F.; Kim, S. K.; Jacobson, K. A.; Bloodworth, L. M.; Zhang, X.; Wess, J. *J. Biol. Chem.* **2007**, *282*, 26284.
(1024) Wess, J.; Han, S. J.; Kim, S. K.; Jacobson, K. A.; Li, J. H. *Trends Pharmacol. Sci.* **2008**, *29*, 616.
(1025) Csermely, P.; Palotai, R.; Nussinov, R. *Trends Biochem. Sci.* **2010**, *35*, 539.
(1026) Maggio, R.; Vogel, Z.; Wess, J. *Proc. Natl. Acad. Sci. U.S.A.* **1993**, *90*, 3103.
(1027) Maggio, R.; Barbier, P.; Fornai, F.; Corsini, G. U. *J. Biol. Chem.* **1996**, *271*, 31055.
(1028) Rivero-Muller, A.; Chou, Y. Y.; Ji, I.; Lajic, S.; Hanyaloglu, A. C.; Jonas, K.; Rahman, N.; Ji, T. H.; Huhtaniemi, I. *Proc. Natl. Acad. Sci. U.S.A.* **2010**, *107*, 2319.
(1029) Persani, L.; Calebiro, D.; Bonomi, M. *Nature Clin. Pract. Endocrinol. Metab.* **2007**, *3*, 180.
(1030) Rives, M. L.; Vol, C.; Fukazawa, Y.; Tinel, N.; Trinquet, E.; Ayoub, M. A.; Shigemoto, R.; Pin, J. P.; Prezeau, L. *EMBO J.* **2009**, *28*, 2195.
(1031) Ferre, S.; Baler, R.; Bouvier, M.; Caron, M. G.; Devi, L. A.; Durroux, T.; Fuxe, K.; George, S. R.; Javitch, J. A.; Lohse, M. J.; Mackie, K.; Milligan, G.; Pfleger, K. D.; Pin, J. P.; Volkow, N. D.; Waldhoer, M.; Woods, A. S.; Franco, R. *Nature Chem. Biol.* **2009**, *5*, 131.
(1032) Franco, R. *Br. J. Pharmacol.* **2009**, *158*, 23.
(1033) Maggio, R.; Aloisi, G.; Silvano, E.; Rossi, M.; Millan, M. J. *Parkinsonism Relat. Disord.* **2009**, *15* (Suppl 4), S2.
(1034) Dorsch, S.; Klotz, K. N.; Engelhardt, S.; Lohse, M. J.; Bunemann, M. *Nature Methods* **2009**, *6*, 225.
(1035) Harding, P. J.; Attrill, H.; Boehringer, J.; Ross, S.; Wadhams, G. H.; Smith, E.; Armitage, J. P.; Watts, A. *Biophys. J.* **2009**, *96*, 964.
(1036) Ambrosio, M.; Lohse, M. *J. Nat. Chem. Biol.* **2010**, *6*, 570.
(1037) Cottet, M.; Albizu, L.; Perkovska, S.; Jean-Alphonse, F.; Rahmeh, R.; Orcel, H.; Mejean, C.; Granier, S.; Mendre, C.; Mouillac, B.; Durroux, T. *Curr. Opin. Pharmacol .* **2010**, *10*, 59.
(1038) van Rijn, R. M.; Whistler, J. L.; Waldhoer, M. *Curr. Opin. Pharmacol.* **2010**, *10*, 73.
(1039) Zhang, M.; Feng, X.; Guan, R.; Hebert, T. E.; Segaloff, D. L. *Cell. Signalling* **2009**, *21*, 1663.
(1040) Hwang, J. R.; Baek, M. W.; Sim, J.; Choi, H. S.; Han, J. M.; Kim, Y. L.; Hwang, J. I.; Kwon, H. B.; Beaudet, N.; Sarret, P.; Seong, J. Y. *Biochem. Biophys. Res. Commun.* **2010**, *391*, 1007.

(1041) Szidonya, L.; Cserzo, M.; Hunyady, L. *J. Endocrinol.* **2008**, *196*, 435.
(1042) Pin, J. P.; Comps-Agrar, L.; Maurel, D.; Monnier, C.; Rives, M. L.; Trinquet, E.; Kniazeff, J.; Rondard, P.; Prezeau, L. *J. Physiol.* **2009**, *587*, 5337.
(1043) White, J. H.; Wise, A.; Main, M. J.; Green, A.; Fraser, N. J.; Disney, G. H.; Barnes, A. A.; Emson, P.; Foord, S. M.; Marshall, F. H. *Nature* **1998**, *396*, 679.
(1044) Kaupmann, K.; Malitschek, B.; Schuler, V.; Heid, J.; Froestl, W.; Beck, P.; Mosbacher, J.; Bischoff, S.; Kulik, A.; Shigemoto, R.; Karschin, A.; Bettler, B. *Nature* **1998**, *396*, 683.
(1045) Marshall, F. H.; Jones, K. A.; Kaupmann, K.; Bettler, B. *Trends Pharmacol. Sci.* **1999**, *20*, 396.
(1046) Mohler, H.; Fritschy, J. M. *Trends Pharmacol. Sci.* **1999**, *20*, 87.
(1047) Margeta-Mitrovic, M.; Jan, Y. N.; Jan, L. Y. *Neuron* **2000**, *27*, 97.
(1048) Kunishima, N.; Shimada, Y.; Tsuji, Y.; Sato, T.; Yamamoto, M.; Kumasaka, T.; Nakanishi, S.; Jingami, H.; Morikawa, K. *Nature* **2000**, *407*, 971.
(1049) Zhu, X.; Wess, J. *Biochemistry* **1998**, *37*, 15773.
(1050) Morello, J. P.; Salahpour, A.; Laperriere, A.; Bernier, V.; Arthus, M. F.; Lonergan, M.; Petaja-Repo, U.; Angers, S.; Morin, D.; Bichet, D. G.; Bouvier, M. *J. Clin. Invest.* **2000**, *105*, 887.
(1051) Benkirane, M.; Jin, D. Y.; Chun, R. F.; Koup, R. A.; Jeang, K. T. *J. Biol. Chem.* **1997**, *272*, 30603.
(1052) Herrick-Davis, K.; Weaver, B. A.; Grinde, E.; Mazurkiewicz, J. E. *J. Biol. Chem.* **2006**, *281*, 27109.
(1053) Maurel, D.; Comps-Agrar, L.; Brock, C.; Rives, M. L.; Bourrier, E.; Ayoub, M. A.; Bazin, H.; Tinel, N.; Durroux, T.; Prezeau, L.; Trinquet, E.; Pin, J. P. *Nature Methods* **2008**, *5*, 561.
(1054) Ciruela, F.; Vilardaga, J. P.; Fernandez-Duenas, V. *Trends Biotechnol.* **2010**, *28*, 407.
(1055) Pisterzi, L. F.; Jansma, D. B.; Georgiou, J.; Woodside, M. J.; Chou, J. T.; Angers, S.; Raicu, V.; Wells, J. W. *J. Biol. Chem.* **2010**, *285*, 16723.
(1056) Ilien, B.; Glasser, N.; Clamme, J. P.; Didier, P.; Piemont, E.; Chinnappan, R.; Daval, S. B.; Galzi, J. L.; Mely, Y. *J. Biol. Chem.* **2009**, *284*, 19533.
(1057) Alvarez-Curto, E.; Ward, R. J.; Pediani, J. D.; Milligan, G. *J. Biol. Chem.* **2010**, *285*, 23318.
(1058) Vidi, P. A.; Watts, V. J. *Mol. Pharmacol.* **2009**, *75*, 733.
(1059) Vidi, P. A.; Chemel, B. R.; Hu, C. D.; Watts, V. J. *Mol. Pharmacol.* **2008**, *74*, 544.
(1060) Vidi, P. A.; Chen, J.; Irudayaraj, J. M.; Watts, V. J. *FEBS Lett.* **2008**, *582*, 3985.
(1061) Dean, M. K.; Higgs, C.; Smith, R. E.; Bywater, R. P.; Snell, C. R.; Scott, P. D.; Upton, G. J.; Howe, T. J.; Reynolds, C. A. *J. Med. Chem.* **2001**, *44*, 4595.
(1062) Filipek, S.; Krzysko, K. A.; Fotiadis, D.; Liang, Y.; Saperstein, D. A.; Engel, A.; Palczewski, K. *Photochem. Photobiol. Sci.* **2004**, *3*, 628.
(1063) Hamm, H. E. *Proc. Natl. Acad. Sci. U.S.A.* **2001**, *98*, 4819.
(1064) Baneres, J. L.; Parello, J. *J. Mol. Biol.* **2003**, *329*, 815.
(1065) Damian, M.; Mary, S.; Martin, A.; Pin, J. P.; Baneres, J. L. *J. Biol. Chem.* **2008**, *283*, 21084.
(1066) Grant, M.; Kumar, U. *Regul. Pept.* **2006**, *159*, 3.
(1067) Bayburt, T. H.; Vishnivetskiy, S. A.; McLean, M. A.; Morizumi, T.; Huang, C. C.; Tesmer, J. J.; Ernst, O. P.; Sligar, S. G.; Gurevich, V. V. *J. Biol. Chem.* **2010**, *286*, 1420.
(1068) Ernst, O. P.; Gramse, V.; Kolbe, M.; Hofmann, K. P.; Heck, M. *Proc. Natl. Acad. Sci. U.S.A.* **2007**, *104*, 10859.
(1069) Whorton, M. R.; Bokoch, M. P.; Rasmussen, S. G.; Huang, B.; Zare, R. N.; Kobilka, B.; Sunahara, R. K. *Proc. Natl. Acad. Sci. U.S.A.* **2007**, *104*, 7682.
(1070) Meyer, B. H.; Segura, J. M.; Martinez, K. L.; Hovius, R.; George, N.; Johnsson, K.; Vogel, H. *Proc. Natl. Acad. Sci. U.S.A.* **2006**, *103*, 2138.
(1071) White, J. F.; Grodnitzky, J.; Louis, J. M.; Trinh, L. B.; Shiloach, J.; Gutierrez, J.; Northup, J. K.; Grisshammer, R. *Proc. Natl. Acad. Sci. U.S.A.* **2007**, *104*, 12199.
(1072) Arcemisbehere, L.; Sen, T.; Boudier, L.; Balestre, M. N.; Gaibelet, G.; Detouillon, E.; Orcel, H.; Mendre, C.; Rahmeh, R.; Granier, S.; Vives, C.; Fieschi, F.; Damian, M.; Durroux, T.; Baneres, J. L.; Mouillac, B. *J. Biol. Chem.* **2010**, *285*, 6337.
(1073) Pellissier, L. P.; Barthet, G.; Gaven, F.; Cassier, E.; Trinquet, E.; Pin, J. P.; Marin, P.; Dumuis, A.; Bockaert, J.; Baneres, J. L.; Claeysen, S. *J. Biol. Chem.* **2011**, *286*, 9985.
(1074) Park, P. S.; Palczewski, K. *Proc. Natl. Acad. Sci. U.S.A.* **2005**, *102*, 8793.
(1075) Sakai, T.; Aoyama, M.; Kusakabe, T.; Tsuda, M.; Satake, H. *Mol. Biol. Evol.* **2010**, *27*, 1097.
(1076) Jordan, B. A.; Cvejic, S.; Devi, L. A. *Neuropsychopharmacology* **2000**, *23*, S5.
(1077) Levac, B. A.; O'Dowd, B. F.; George, S. R. *Curr. Opin. Pharmacol.* **2002**, *2*, 76.
(1078) Waldhoer, M.; Fong, J.; Jones, R. M.; Lunzer, M. M.; Sharma, S. K.; Kostenis, E.; Portoghese, P. S.; Whistler, J. L. *Proc. Natl. Acad. Sci. U.S.A.* **2005**, *102*, 9050.
(1079) Jordan, B. A.; Devi, L. A. *Nature* **1999**, *399*, 697.
(1080) George, S. R.; Fan, T.; Xie, Z.; Tse, R.; Tam, V.; Varghese, G.; O'Dowd, B. F. *J. Biol. Chem.* **2000**, *275*, 26128.
(1081) Golebiewska, U.; Johnston, J. M.; Devi, L.; Filizola, M.; Scarlata, S. *Biochemistry* **2011**, *50*, 2829.
(1082) Smith, N. J.; Milligan, G. *Pharmacol. Rev.* **2010**, *62*, 701.
(1083) Birdsall, N. J. *Trends Pharmacol. Sci.* **2010**, *31*, 499.
(1084) Springael, J. Y.; Urizar, E.; Costagliola, S.; Vassart, G.; Parmentier, M. *Pharmacol. Ther.* **2007**, *115*, 410.
(1085) Maurice, P.; Kamal, M.; Jockers, R. *Trends Pharmacol. Sci.* **2011**, *32*, 514.
(1086) Damian, M.; Martin, A.; Mesnier, D.; Pin, J. P.; Baneres, J. L. *EMBO J.* **2006**, *25*, 5693.
(1087) Novi, F.; Scarselli, M.; Corsini, G. U.; Maggio, R. *J. Biol. Chem.* **2004**, *279*, 7476.
(1088) Novi, F.; Stanasila, L.; Giorgi, F.; Corsini, G. U.; Cotecchia, S.; Maggio, R. *J. Biol. Chem.* **2005**, *280*, 19768.
(1089) Bohn, L. M.; Lefkowitz, R. J.; Gainetdinov, R. R.; Peppel, K.; Caron, M. G.; Lin, F. T. *Science* **1999**, *286*, 2495.
(1090) Bohn, L. M.; Gainetdinov, R. R.; Lin, F. T.; Lefkowitz, R. J.; Caron, M. G. *Nature* **2000**, *408*, 720.
(1091) Jastrzebska, B.; Tsybovsky, Y.; Palczewski, K. *Biochem. J.* **2010**, *428*, 1.
(1092) Maggio, R.; Innamorati, G.; Parenti, M. *J. Neurochem.* **2007**, *103*, 1741.
(1093) Govardovskii, V. I.; Korenyak, D. A.; Shukolyukov, S. A.; Zueva, L. V. *Mol. Vis.* **2009**, *15*, 1717.
(1094) Maurice, P.; Daulat, A. M.; Turecek, R.; Ivankova-Susankova, K.; Zamponi, F.; Kamal, M.; Clement, N.; Guillaume, J. L.; Bettler, B.; Gales, C.; Delagrange, P.; Jockers, R. *EMBO J.* **2010**, *29*, 3646.
(1095) Fonseca, J. M.; Lambert, N. A. *Mol. Pharmacol.* **2009**, *75*, 1296.
(1096) Hern, J. A.; Baig, A. H.; Mashanov, G. I.; Birdsall, B.; Corrie, J. E.; Lazareno, S.; Molloy, J. E.; Birdsall, N. J. *Proc. Natl. Acad. Sci. U.S.A.* **2010**, *107*, 2693.
(1097) Lambert, N. A. *Sci. Signal.* **2010**, *3*, pe12.
(1098) Kasai, R. S.; Suzuki, K. G.; Prossnitz, E. R.; Koyama-Honda, I.; Nakada, C.; Fujiwara, T. K.; Kusumi, A. *J. Cell Biol.* **2011**, *192*, 463.
(1099) Hebert, T. E.; Moffett, S.; Morello, J. P.; Loisel, T. P.; Bichet, D. G.; Barret, C.; Bouvier, M. *J. Biol. Chem.* **1996**, *271*, 16384.
(1100) Ng, G. Y.; O'Dowd, B. F.; Lee, S. P.; Chung, H. T.; Brann, M. R.; Seeman, P.; George, S. R. *Biochem. Biophys. Res. Commun.* **1996**, *227*, 200.
(1101) Guo, W.; Shi, L.; Javitch, J. A. *J. Biol. Chem.* **2003**, *278*, 4385.
(1102) Guo, W.; Filizola, M.; Weinstein, H.; Javitch, J. A. *Proc. Natl. Acad. Sci. U.S.A* **2005**, *102*, 17495.
(1103) Guo, W.; Urizar, E.; Kralikova, M.; Mobarec, J. C.; Shi, L.; Filizola, M.; Javitch, J. A. *EMBO J.* **2008**, *27*, 2293.
(1104) Lee, S. P.; O'Dowd, B. F.; Rajaram, R. D.; Nguyen, T.; George, S. R. *Biochemistry* **2003**, *42*, 11023.

(1105) Johnston, J. M.; Aburi, M.; Provasi, D.; Bortolato, A.; Urizar, E.; Lambert, N. A.; Javitch, J. A.; Filizola, M. *Biochemistry* **2011**, *50*, 1682.
(1106) Fung, J. J.; Deupi, X.; Pardo, L.; Yao, X. J.; Velez-Ruiz, G. A.; Devree, B. T.; Sunahara, R. K.; Kobilka, B. K. *EMBO J.* **2009**, *28*, 3315.
(1107) Mancia, F.; Assur, Z.; Herman, A. G.; Siegel, R.; Hendrickson, W. A. *EMBO Rep.* **2008**, *9*, 363.
(1108) Kim, H.; Lee, B. K.; Naider, F.; Becker, J. M. *Biochemistry* **2009**, *48*, 10976.
(1109) Wang, H. X.; Konopka, J. B. *Biochemistry* **2009**, *48*, 7132.
(1110) Hernanz-Falcon, P.; Rodriguez-Frade, J. M.; Serrano, A.; Juan, D.; del Sol, A.; Soriano, S. F.; Roncal, F.; Gomez, L.; Valencia, A.; Martinez, A. C.; Mellado, M. *Nature Immunol.* **2004**, *5*, 216.
(1111) Lemay, J.; Marullo, S.; Jockers, R.; Alizon, M.; Brelot, A. *Nature Immunol.* **2005**, *6*, 535author reply 535.
(1112) Stanasila, L.; Perez, J. B.; Vogel, H.; Cotecchia, S. *J. Biol. Chem.* **2003**, *278*, 40239.
(1113) Milligan, G.; Pediani, J. D.; Canals, M.; Lopez-Gimenez, J. F. *Vis. Res.* **2006**, *46*, 4434.
(1114) Zeng, F.; Wess, J. *Neuropsychopharmacology* **2000**, *23*, S19.
(1115) Tanaka, T.; Nomura, W.; Narumi, T.; Masuda, A.; Tamamura, H. *J. Am. Chem. Soc.* **2010**, *132*, 15899.
(1116) Navarro, G.; Ferre, S.; Cordomi, A.; Moreno, E.; Mallol, J.; Casado, V.; Cortes, A.; Hoffmann, H.; Ortiz, J.; Canela, E. I.; Lluis, C.; Pardo, L.; Franco, R.; Woods, A. S. *J. Biol. Chem.* **2010**, *285*, 27346.
(1117) Parker, M. S.; Sah, R.; Park, E. A.; Sweatman, T.; Balasubramaniam, A.; Sallee, F. R.; Parker, S. L. *Mini-Rev. Med. Chem.* **2009**, *9*, 329.
(1118) McMillin, S. M.; Heusel, M.; Liu, T.; Costanzi, S.; Wess, J. *J. Biol. Chem.* **2011**, *286*, 28584.
(1119) Nemoto, W.; Toh, H. *Curr. Protein Pept. Sci.* **2006**, *7*, 561.
(1120) Vohra, S.; Chintapalli, S. V.; Illingworth, C. J.; Reeves, P. J.; Mullineaux, P. M.; Clark, H. S.; Dean, M. K.; Upton, G. J.; Reynolds, C. A. *Biochem. Soc. Trans.* **2007**, *35*, 749.
(1121) Filizola, M. *Life Sci* **2010**, *86*, 590.
(1122) Simpson, L. M.; Taddese, B.; Wall, I. D.; Reynolds, C. A. *Curr. Opin. Pharmacol.* **2010**, *10*, 30.
(1123) Guidolin, D.; Ciruela, F.; Genedani, S.; Guescini, M.; Tortorella, C.; Albertin, G.; Fuxe, K.; Agnati, L. F. *Biochim. Biophys. Acta* **2011**, *1080*, 1267.
(1124) Gouldson, P. R.; Higgs, C.; Smith, R. E.; Dean, M. K.; Gkoutos, G. V.; Reynolds, C. A. *Neuropsychopharmacology* **2000**, *23*, S60.
(1125) Gouldson, P. R.; Snell, C. R.; Bywater, R. P.; Higgs, C.; Reynolds, C. A. *Protein Eng.* **1998**, *11*, 1181.
(1126) Pazos, F.; Helmer-Citterich, M.; Ausiello, G.; Valencia, A. *J. Mol. Biol.* **1997**, *271*, 511.
(1127) Lichtarge, O.; Bourne, H. R.; Cohen, F. E. *J. Mol. Biol.* **1996**, *257*, 342.
(1128) Madabushi, S.; Gross, A. K.; Philippi, A.; Meng, E. C.; Wensel, T. G.; Lichtarge, O. *J. Biol. Chem.* **2004**, *279*, 8126.
(1129) Schulz, A.; Grosse, R.; Schultz, G.; Gudermann, T.; Schoneberg, T. *J. Biol. Chem.* **2000**, *275*, 2381.
(1130) Bakker, R. A.; Dees, G.; Carrillo, J. J.; Booth, R. G.; Lopez-Gimenez, J. F.; Milligan, G.; Strange, P. G.; Leurs, R. *J. Pharmacol. Exp. Ther.* **2004**, *311*, 131.
(1131) Thummer, R. P.; Campbell, M. P.; Dean, M. K.; Frusher, M. J.; Scott, P. D.; Reynolds, C. A. *J. Mol. Neurosci.* **2005**, *26*, 113.
(1132) Filizola, M.; Olmea, O.; Weinstein, H. *Protein Eng.* **2002**, *15*, 881.
(1133) Gomes, I.; Jordan, B. A.; Gupta, A.; Trapaidze, N.; Nagy, V.; Devi, L. A. *J. Neurosci.* **2000**, *20*, RC110.
(1134) Cvejic, S.; Devi, L. A. *J. Biol. Chem.* **1997**, *272*, 26959.
(1135) del Sol Mesa, A.; Pazos, F.; Valencia, A. *J. Mol. Biol.* **2003**, *326*, 1289.
(1136) Soyer, O. S.; Dimmic, M. W.; Neubig, R. R.; Goldstein, R. A. *Biochemistry* **2003**, *42*, 14522.
(1137) Nemoto, W.; Toh, H. *Proteins* **2005**, *58*, 644.
(1138) de Juan, D.; Mellado, M.; Rodriguez-Frade, J. M.; Hernanz-Falcon, P.; Serrano, A.; del Sol, A.; Valencia, A.; Martinez, A. C.; Rojas, A. M. *Bioinformatics* **2005**, *21* (Suppl 2), ii13.
(1139) Filizola, M.; Weinstein, H. *FEBS J.* **2005**, *272*, 2926.
(1140) Casciari, D.; Seeber, M.; Fanelli, F. *BMC Bioinf.* **2006**, *7*, 340.
(1141) Chen, R.; Li, L.; Weng, Z. *Proteins* **2003**, *52*, 80.
(1142) Doyle, D. A.; Morais Cabral, J.; Pfuetzner, R. A.; Kuo, A.; Gulbis, J. M.; Cohen, S. L.; Chait, B. T.; MacKinnon, R. *Science* **1998**, *280*, 69.
(1143) Chang, G.; Spencer, R. H.; Lee, A. T.; Barclay, M. T.; Rees, D. C. *Science* **1998**, *282*, 2220.
(1144) Bass, R. B.; Strop, P.; Barclay, M.; Rees, D. C. *Science* **2002**, *298*, 1582.
(1145) Fanelli, F. *Mol. Cell. Endocrinol.* **2007**, *260*−*262*, 59.
(1146) Casciari, D.; Dell'Orco, D.; Fanelli, F. *J. Chem. Inf. Model.* **2008**, *48*, 1669.
(1147) Fanelli, F.; Mauri, M.; Capra, V.; Raimondi, F.; Guzzi, F.; Ambrosio, M.; Rovati, G. E.; Parenti, M. *Cell. Mol. Life Sci.* **2011**, *68*, 3109.
(1148) Dell'Orco, D.; Casciari, D.; Fanelli, F. *J. Struct. Biol.* **2008**, *163*, 155.
(1149) Ciruela, F.; Burgueno, J.; Casado, V.; Canals, M.; Marcellino, D.; Goldberg, S. R.; Bader, M.; Fuxe, K.; Agnati, L. F.; Lluis, C.; Franco, R.; Ferre, S.; Woods, A. S. *Anal. Chem.* **2004**, *76*, 5354.
(1150) Canals, M.; Burgueno, J.; Marcellino, D.; Cabello, N.; Canela, E. I.; Mallol, J.; Agnati, L.; Ferre, S.; Bouvier, M.; Fuxe, K.; Ciruela, F.; Lluis, C.; Franco, R. *J. Neurochem.* **2004**, *88*, 726.
(1151) Dell'Orco, D.; De Benedetti, P. G.; Fanelli, F. *J. Phys. Chem. B* **2007**, *111*, 9114.
(1152) Liu, X.; Kai, M.; Jin, L.; Wang, R. *J. Comput.-Aided Mol. Des.* **2009**, *23*, 321.
(1153) Bruno, A.; Guadix, A. E.; Costantino, G. *J. Chem. Inf. Model.* **2009**, *49*, 1602.
(1154) Gray, J. J.; Moughon, S.; Wang, C.; Schueler-Furman, O.; Kuhlman, B.; Rohl, C. A.; Baker, D. *J. Mol. Biol.* **2003**, *331*, 281.
(1155) Gray, J. J.; Moughon, S. E.; Kortemme, T.; Schueler-Furman, O.; Misura, K. M.; Morozov, A. V.; Baker, D. *Proteins* **2003**, *52*, 118.
(1156) Kim, S. K.; Jacobson, K. A. *J. Mol. Graphics Modell.* **2006**, *25*, 549.
(1157) Witt, M.; Slusarz, M. J.; Ciarkowski, J. *QSAR Comb. Sci.* **2008**, *27*, 684.
(1158) Provasi, D.; Johnston, J. M.; Filizola, M. *Biochemistry* **2010**, *49*, 6771.
(1159) Russo, O.; Berthouze, M.; Giner, M.; Soulier, J. L.; Rivail, L.; Sicsic, S.; Lezoualc'h, F.; Jockers, R.; Berque-Bestel, I. *J. Med. Chem.* **2007**, *50*, 4482.
(1160) Woolf, P. J.; Linderman, J. J. *J. Theor. Biol.* **2004**, *229*, 157.
(1161) Woolf, P. J.; Linderman, J. *J. Biophys. Chem.* **2003**, *104*, 217.
(1162) Fallahi-Sichani, M.; Linderman, J. J. *PLoS One* **2009**, *4*, e6604.
(1163) Clapham, D. E. *Nature* **1996**, *379*, 297.
(1164) Coleman, D. E.; Sprang, S. R. *Trends Biochem. Sci.* **1996**, *21*, 41.
(1165) Hamm, H. E.; Gilchrist, A. *Curr. Opin. Cell. Biol.* **1996**, *8*, 189.
(1166) Bunemann, M.; Frank, M.; Lohse, M. J. *Proc. Natl. Acad. Sci. U.S.A.* **2003**, *100*, 16077.
(1167) Klein, S.; Reuveni, H.; Levitzki, A. *Proc. Natl. Acad. Sci. U.S.A.* **2000**, *97*, 3219.
(1168) Bohm, A.; Gaudet, R.; Sigler, P. B. *Curr. Opin. Biotechnol.* **1997**, *8*, 480.
(1169) Sunahara, R. K.; Tesmer, J. J.; Gilman, A. G.; Sprang, S. R. *Science* **1997**, *278*, 1943.
(1170) Chen, Z.; Singer, W. D.; Sternweis, P. C.; Sprang, S. R. *Nature Struct. Mol. Biol.* **2005**, *12*, 191.
(1171) Nishimura, A.; Kitano, K.; Takasaki, J.; Taniguchi, M.; Mizuno, N.; Tago, K.; Hakoshima, T.; Itoh, H. *Proc. Natl. Acad. Sci. U.S.A.* **2010**, *107*, 13666.

(1172) Wall, M. A.; Coleman, D. E.; Lee, E.; Iniguez-Lluhi, J. A.; Posner, B. A.; Gilman, A. G.; Sprang, S. R. *Cell* **1995**, *83*, 1047.
(1173) Lambright, D. G.; Sondek, J.; Bohm, A.; Skiba, N. P.; Hamm, H. E.; Sigler, P. B. *Nature* **1996**, *379*, 311.
(1174) Smrcka, A. V.; Kichik, N.; Tarrago, T.; Burroughs, M.; Park, M. S.; Itoga, N. K.; Stern, H. A.; Willardson, B. M.; Giralt, E. *Proc. Natl. Acad. Sci. U.S.A.* **2010**, *107*, 639.
(1175) Kosloff, M.; Alexov, E.; Arshavsky, V. Y.; Honig, B. *J. Biol. Chem.* **2008**, *283*, 31197.
(1176) Medkova, M.; Preininger, A. M.; Yu, N. J.; Hubbell, W. L.; Hamm, H. E. *Biochemistry* **2002**, *41*, 9962.
(1177) Kisselev, O. G.; Kao, J.; Ponder, J. W.; Fann, Y. C.; Gautam, N.; Marshall, G. R. *Proc. Natl. Acad. Sci. U.S.A.* **1998**, *95*, 4270.
(1178) Koenig, B. W.; Kontaxis, G.; Mitchell, D. C.; Louis, J. M.; Litman, B. J.; Bax, A. *J. Mol. Biol.* **2002**, *322*, 441.
(1179) Kisselev, O. G.; Downs, M. A. *Structure (Cambridge, UK)* **2003**, *11*, 367.
(1180) Kisselev, O. G.; Downs, M. A. *Biochemistry* **2006**, *45*, 9386.
(1181) Fanelli, F.; Dell'Orco, D. *Biochemistry* **2005**, *44*, 14695.
(1182) Bourne, H. R. *Curr. Opin. Cell. Biol.* **1997**, *9*, 134.
(1183) Franke, R. R.; Sakmar, T. P.; Graham, R. M.; Khorana, H. G. *J. Biol. Chem.* **1992**, *267*, 14767.
(1184) Klein-Seetharaman, J.; Hwa, J.; Cai, K.; Altenbach, C.; Hubbell, W. L.; Khorana, H. G. *Biochemistry* **1999**, *38*, 7938.
(1185) Natochin, M.; Barren, B.; Ahmad, S. T.; O'Tousa, J. E.; Artemyev, N. O. *Vis. Res.* **2006**, *46*, 4575.
(1186) Wess, J. *FASEB J.* **1997**, *11*, 346.
(1187) Burstein, E. S.; Spalding, T. A.; Brann, M. R. *J. Biol. Chem.* **1998**, *273*, 24322.
(1188) Burstein, E. S.; Spalding, T. A.; Brann, M. R. *Biochemistry* **1998**, *37*, 4052.
(1189) Kushwaha, N.; Harwood, S. C.; Wilson, A. M.; Berger, M.; Tecott, L. H.; Roth, B. L.; Albert, P. R. *Mol. Pharmacol.* **2006**, *69*, 1518.
(1190) Ulloa-Aguirre, A.; Uribe, A.; Zarinan, T.; Bustos-Jaimes, I.; Perez-Solis, M. A.; Dias, J. A. *Mol. Cell. Endocrinol.* **2007**, *260−262*, 153.
(1191) Matsumoto, M. L.; Narzinski, K.; Kiser, P. D.; Nikiforovich, G. V.; Baranski, T. J. *J. Biol. Chem.* **2007**, *282*, 3105.
(1192) Matsumoto, M. L.; Narzinski, K.; Nikiforovich, G. V.; Baranski, T. J. *J. Biol. Chem.* **2007**, *282*, 3122.
(1193) Natochin, M.; Gasimov, K. G.; Moussaif, M.; Artemyev, N. O. *J. Biol. Chem.* **2003**, *278*, 37574.
(1194) Franke, R. R.; Konig, B.; Sakmar, T. P.; Khorana, H. G.; Hofmann, K. P. *Science* **1990**, *250*, 123.
(1195) Acharya, S.; Saad, Y.; Karnik, S. S. *J. Biol. Chem.* **1997**, *272*, 6519.
(1196) Yamashita, T.; Terakita, A.; Shichida, Y. *J. Biol. Chem.* **2000**, *275*, 34272.
(1197) Terakita, A.; Yamashita, T.; Nimbari, N.; Kojima, D.; Shichida, Y. *J. Biol. Chem.* **2002**, *277*, 40.
(1198) Vogel, R.; Martell, S.; Mahalingam, M.; Engelhard, M.; Siebert, F. *J. Mol. Biol.* **2007**, *366*, 1580.
(1199) Kleinau, G.; Jaeschke, H.; Worth, C. L.; Mueller, S.; Gonzalez, J.; Paschke, R.; Krause, G. *PLoS One* **2010**, *5*, e9745.
(1200) Gilchrist, A.; Mazzoni, M. R.; Dineen, B.; Dice, A.; Linden, J.; Proctor, W. R.; Lupica, C. R.; Dunwiddie, T. V.; Hamm, H. E. *J. Biol. Chem.* **1998**, *273*, 14912.
(1201) Rasenick, M. M.; Watanabe, M.; Lazarevic, M. B.; Hatta, S.; Hamm, H. E. *J. Biol. Chem.* **1994**, *269*, 21519.
(1202) Garcia, P. D.; Onrust, R.; Bell, S. M.; Sakmar, T. P.; Bourne, H. R. *EMBO J.* **1995**, *14*, 4460.
(1203) Neer, E. J. *Cell* **1995**, *80*, 249.
(1204) Osawa, S.; Weiss, E. R. *J. Biol. Chem.* **1995**, *270*, 31052.
(1205) Blahos, J., II; Mary, S.; Perroy, J.; de Colle, C.; Brabet, I.; Bockaert, J.; Pin, J. P. *J. Biol. Chem.* **1998**, *273*, 25765.
(1206) Hamm, H. E.; Deretic, D.; Arendt, A.; Hargrave, P. A.; Koenig, B.; Hofmann, K. P. *Science* **1988**, *241*, 832.
(1207) Nishimura, S.; Kandori, H.; Maeda, A. *Biochemistry* **1998**, *37*, 15816.
(1208) Martin, E. L.; Rens-Domiano, S.; Schatz, P. J.; Hamm, H. E. *J. Biol. Chem.* **1996**, *271*, 361.
(1209) Aris, L.; Gilchrist, A.; Rens-Domiano, S.; Meyer, C.; Schatz, P. J.; Dratz, E. A.; Hamm, H. E. *J. Biol. Chem.* **2001**, *276*, 2333.
(1210) Mazzoni, M. R.; Hamm, H. E. *J. Biol. Chem.* **1996**, *271*, 30034.
(1211) Bae, H.; Anderson, K.; Flood, L. A.; Skiba, N. P.; Hamm, H. E.; Graber, S. G. *J. Biol. Chem.* **1997**, *272*, 32071.
(1212) Onrust, R.; Herzmark, P.; Chi, P.; Garcia, P. D.; Lichtarge, O.; Kingsley, C.; Bourne, H. R. *Science* **1997**, *275*, 381.
(1213) Natochin, M.; Granovsky, A. E.; Muradov, K. G.; Artemyev, N. O. *J. Biol. Chem.* **1999**, *274*, 7865.
(1214) Cai, K.; Itoh, Y.; Khorana, H. G. *Proc. Natl. Acad. Sci. U.S.A.* **2001**, *98*, 4877.
(1215) Itoh, Y.; Cai, K.; Khorana, H. G. *Proc. Natl. Acad. Sci. U.S.A.* **2001**, *98*, 4883.
(1216) Ernst, O. P.; Meyer, C. K.; Marin, E. P.; Henklein, P.; Fu, W. Y.; Sakmar, T. P.; Hofmann, K. P. *J. Biol. Chem.* **2000**, *275*, 1937.
(1217) Marin, E. P.; Krishna, A. G.; Zvyaga, T. A.; Isele, J.; Siebert, F.; Sakmar, T. P. *J. Biol. Chem.* **2000**, *275*, 1930.
(1218) Herrmann, R.; Heck, M.; Henklein, P.; Kleuss, C.; Hofmann, K. P.; Ernst, O. P. *J. Biol. Chem.* **2004**, *279*, 24283.
(1219) Herrmann, R.; Heck, M.; Henklein, P.; Hofmann, K. P.; Ernst, O. P. *J. Biol. Chem.* **2006**, *281*, 30234.
(1220) Wang, X.; Kim, S. H.; Ablonczy, Z.; Crouch, R. K.; Knapp, D. R. *Biochemistry* **2004**, *43*, 11153.
(1221) Hamm, H. E.; Deretic, D.; Hofmann, K. P.; Schleicher, A.; Kohl, B. *J. Biol. Chem.* **1987**, *262*, 10831.
(1222) Iiri, T.; Farfel, Z.; Bourne, H. R. *Nature* **1998**, *394*, 35.
(1223) Rondard, P.; Iiri, T.; Srinivasan, S.; Meng, E.; Fujita, T.; Bourne, H. R. *Proc. Natl. Acad. Sci. U.S.A.* **2001**, *98*, 6150.
(1224) Johnston, C. A.; Willard, F. S.; Jezyk, M. R.; Fredericks, Z.; Bodor, E. T.; Jones, M. B.; Blaesius, R.; Watts, V. J.; Harden, T. K.; Sondek, J.; Ramer, J. K.; Siderovski, D. P. *Structure* **2005**, *13*, 1069.
(1225) Cherfils, J.; Chabre, M. *Trends Biochem. Sci.* **2003**, *28*, 13.
(1226) Marin, E. P.; Krishna, A. G.; Sakmar, T. P. *J. Biol. Chem.* **2001**, *276*, 27400.
(1227) Marin, E. P.; Krishna, A. G.; Sakmar, T. P. *Biochemistry* **2002**, *41*, 6988.
(1228) Oldham, W. M.; Van Eps, N.; Preininger, A. M.; Hubbell, W. L.; Hamm, H. E. *Nature Struct. Mol. Biol.* **2006**, *13*, 772.
(1229) Oldham, W. M.; Van Eps, N.; Preininger, A. M.; Hubbell, W. L.; Hamm, H. E. *Proc. Natl. Acad. Sci. U.S.A.* **2007**, *104*, 7927.
(1230) Van Eps, N.; Oldham, W. M.; Hamm, H. E.; Hubbell, W. L. *Proc. Natl. Acad. Sci. U.S.A.* **2006**, *103*, 16194.
(1231) Van Eps, N.; Preininger, A. M.; Alexander, N.; Kaya, A. I.; Meier, S.; Meiler, J.; Hamm, H. E.; Hubbell, W. L. *Proc. Natl. Acad. Sci. U.S.A.* **2011**, *108*, 9420.
(1232) Johnston, C. A.; Siderovski, D. P. *Proc. Natl. Acad. Sci. U.S.A.* **2007**, *104*, 2001.
(1233) Johnston, C. A.; Siderovski, D. P. *Mol. Pharmacol.* **2007**, *72*, 219.
(1234) Kapoor, N.; Menon, S. T.; Chauhan, R.; Sachdev, P.; Sakmar, T. P. *J. Mol. Biol.* **2009**, *393*, 882.
(1235) Abdulaev, N. G.; Ngo, T.; Zhang, C.; Dinh, A.; Brabazon, D. M.; Ridge, K. D.; Marino, J. P. *J. Biol. Chem.* **2005**, *280*, 38071.
(1236) Abdulaev, N. G.; Ngo, T.; Ramon, E.; Brabazon, D. M.; Marino, J. P.; Ridge, K. D. *Biochemistry* **2006**, *45*, 12986.
(1237) Ridge, K. D.; Abdulaev, N. G.; Zhang, C.; Ngo, T.; Brabazon, D. M.; Marino, J. P. *J. Biol. Chem.* **2006**, *281*, 7635.
(1238) Ridge, K. D.; Marino, J. P.; Ngo, T.; Ramon, E.; Brabazon, D. M.; Abdulaev, N. G. *Vis. Res.* **2006**, *46*, 4482.
(1239) Lichtarge, O.; Bourne, H. R.; Cohen, F. E. *Proc. Natl. Acad. Sci. U.S.A.* **1996**, *93*, 7507.
(1240) Tesmer, J. J.; Berman, D. M.; Gilman, A. G.; Sprang, S. R. *Cell* **1997**, *89*, 251.
(1241) Oliveira, L.; Paiva, A. C.; Vriend, G. *Protein Eng.* **1999**, *12*, 1087.
(1242) Mahmoudian, M. *J. Mol. Graphics* **1994**, *12*, 22.

(1243) Sutcliffe, M. J.; Haneef, I.; Carney, D.; Blundell, T. L. *Protein Eng.* **1987**, *1*, 377.
(1244) Sutcliffe, M. J.; Hayes, F. R.; Blundell, T. L. *Protein Eng.* **1987**, *1*, 385.
(1245) Ausiello, G.; Cesareni, G.; Helmer-Citterich, M. *Proteins* **1997**, *28*, 556.
(1246) Krzysko, K. A.; Kolinski, M.; Filipek, S. *J. Phys.: Condens. Matter* **2007**, 19.
(1247) Slusarz, R.; Ciarkowski, J. *Acta Biochim. Pol.* **2004**, *51*, 129.
(1248) Slusarz, M. J.; Gieldon, A.; Slusarz, R.; Ciarkowski, J. *J. Pept. Sci.* **2006**, *12*, 180.
(1249) Slusarz, M. J.; Slusarz, R.; Ciarkowski, J. *J. Pept. Sci.* **2006**, *12*, 171.
(1250) Nikiforovich, G. V.; Taylor, C. M.; Marshall, G. R. *Biochemistry* **2007**, *46*, 4734.
(1251) Anderson, M. A.; Ogbay, B.; Arimoto, R.; Sha, W.; Kisselev, O. G.; Cistola, D. P.; Marshall, G. R. *J. Am. Chem. Soc.* **2006**, *128*, 7531.
(1252) Anderson, M. A.; Ogbay, B.; Kisselev, O. G.; Cistola, D. P.; Marshall, G. R. *Chem. Biol. Drug Des.* **2006**, *68*, 295.
(1253) Taylor, C. M.; Nikiforovich, G. V.; Marshall, G. R. *Biophys. J.* **2007**, *92*, 4325.
(1254) Dell'Orco, D.; Seeber, M.; Fanelli, F. *FEBS Lett.* **2007**, *581*, 944.
(1255) Sgourakis, N. G.; Garcia, A. E. *J. Mol. Biol.* **2010**, *398*, 161.
(1256) Fanelli, F.; Dell'Orco, D. *FEBS Lett.* **2008**, *582*, 991.
(1257) Dell'Orco, D.; Schmidt, H. *J. Phys. Chem. B* **2008**, *112*, 4419.
(1258) Scheerer, P.; Heck, M.; Goede, A.; Park, J. H.; Choe, H. W.; Ernst, O. P.; Hofmann, K. P.; Hildebrand, P. W. *Proc. Natl. Acad. Sci. U.S.A.* **2009**, *106*, 10660.
(1259) Chou, K. C. *J. Proteome Res.* **2005**, *4*, 1681.
(1260) Strasser, A.; Wittmann, H. J. *J. Mol. Model.* **2010**, *16*, 1307.
(1261) Ambrosio, M.; Fanelli, F.; Brocchetti, S.; Raimondi, F.; Mauri, M.; Rovati, G. E.; Capra, V. *Cell. Mol. Life Sci.* **2010**, *67*, 2979.
(1262) Freire, E. *Proc. Natl. Acad. Sci. U.S.A.* **2000**, *97*, 11680.
(1263) Huber, T.; Sakmar, T. P. *Trends Pharmacol. Sci.* **2011**, *32*, 410.
(1264) Laughlin, R. B.; Pines, D.; Schmalian, J.; Stoikovic, B. P.; Wolynes, P. *Proc. Natl. Acad. Sci. U.S.A.* **2000**, *97*, 32.

EDITOR'S COMMENTS

This manuscript was originally published August 25, 2005 with a typographical error in the penultimate paragraph of section 5.2, and an incorrect reference number in the caption to Figure 15. The correct version of this manuscript was published September 1, 2005.